Western Australia School of Mines
Department of Exploration Geophysics

Modelling borehole wave signatures in elastic and poroelastic media with spectral method

Florian Karpfinger

This thesis is presented for the Degree of
Doctor of Philosophy
of
Curtin University of Technology

June 2009

Declaration

To the best of my knowledge and belief this thesis contains no material previously published by any other person except where due acknowledgment has been made.

This thesis contains no material which has been accepted for the award of any other degree or diploma in any university.

Signature:
Date:

Dedicated to my wife Kate

Abstract

Borehole sonic measurements are an important tool to characterize formation and completion properties of hydrocarbon or water reservoirs. Such measurements can provide direct information about rock physical parameters such as permeability or elastic moduli. These properties are obtained from guided waves propagating along boreholes. The so called tube wave or Stoneley wave is a symmetric mode which compresses the fluid column leading to a piston like motion. If the medium around the borehole wall is permeable, the radial expansion of the fluid column will result in fluid flow across the borehole wall. This results in a sensitivity of the tube wave signature to the permeability of the surrounding formation which manifests itself in a characteristic dispersion and attenuation of the tube wave. Information about the permeability of the surrounding formation provides essential knowledge for reservoir characterization.

In addition to the traditional method of using tube wave signatures for formation permeability estimations, the same approach may be used for production monitoring. In sand reservoirs a complicated borehole completion is installed during the production phase for the purpose of con-

trolling sand production. In such a setup highly permeable layers such as a sand screen or a gravel pack are used to prevent sand production.

The problem with such completions is that they are very expensive to install and susceptible to plugging or corrosion. No permanent surveillance tool exists to date which allows diagnosis of problems in sand-screened deepwater completions. However, the recently proposed Real-Time Completion Monitoring (RTCM) uses the signature of tube waves to identify permeability changes: the increase of the tube wave velocity can indicate a decrease of permeability and vice versa. Therefore, RTCM has potential to identify problems in sand-screened deepwater completions .

In order to understand the acoustic response of such deepwater completions, the dispersion and attenuation of tube waves in this complicated setup needs to be studied. To this end I have developed a modelling algorithm based on a spectral method. The developed algorithm computes the dispersion and attenuation of borehole modes propagating in a cylindrically layered structure with an arbitrary number of fluid, elastic and poroelastic layers. The numerical algorithm discretizes the medium along the radial axis using Chebyshev interpolation points derived from Chebyshev polynomials. The differential operators are discretized using spectral differentiation matrices. Thus, for any number of layers, the corresponding equations can be expressed as a generalized algebraic eigenvalue problem. For a given frequency, the eigenvalues correspond to the wavenumbers of different modes. The eigenvectors, computed along with the eigenvalues, correspond to the displacement potentials. They can be used to obtain the variation of displacement and stress components along the radius of the structure.

In this thesis the spectral method was first developed for structures with an arbitrary number of fluid and elastic layers. Subsequently, the algorithm was extended for poroelasticity. The results produced by the modelling program are benchmarked against analytical solutions. Such ana-

lytical solutions are known for elastic and poroelastic cylinders as well as fluid filled tubes. The tube wave dispersion in a fluid-filled borehole surrounded by an elastic or poroelastic formation obtained with the spectral method was compared to the analytical low-frequency solution.

I obtained the dispersion of the two tube waves propagating in a four layer completion model: fluid – permeable sand-screen – fluid – elastic casing. Varying the permeability of the sand-screen layer allowed me to account for the effect of fluid flow across this layer. Being able to obtain the acoustic response can help to identify broken fluid communication which increases the tube wave velocity. A corroded sand-screen has an extremely attenuated tube wave signature.

Furthermore, I have implemented the more complex model of a borehole surrounded by an altered zone in the algorithm. Due to drilling damage the altered zone is an area of reduced permeability. In order to account for the effect of the altered zone on the tube wave signature, up to ten layers were used with stepwise increase of permeability from the borehole towards the formation. Overall, the spectral method proved to be a valuable algorithm to model wave propagation in cylindrical structures.

Using borehole modes to evaluate the physical properties of the formation or completions is an important application. However, in borehole seismic modelling, such as crosshole or VSP, it is also important to account for the effect of boreholes and the associated modes. Since the borehole radius is a thousand times smaller then the investigated volume it would require a prohibitively small grid size to explicitly model the borehole. However, it is possible to effectively represent a borehole as a superposition of point sources. This mimics the presence of borehole modes. In order to implement this technique for poroelasticity, it is necessary to model source signatures in poroelastic media. To this end I have analyzed the radiation characteristics and moment tensor solutions for various source types. Together with the spectral method these point source representations can be

used to model the effect of boreholes. This will pave the way for more efficient poroelastic seismic modelling in various fluid-filled boreholes and completions.

Acknowledgements

First of all I would like to thank my supervisor Boris Gurevich for all the time he spent with me in the last three years debugging codes, editing my manuscripts (I know this was the least fun) and teaching me a lot about the world of rock physics and borehole geophysics. Thank you very much Boris!!! The supervision I received over the last years was amazing and I would have not achieved what I did without it.

I would also like to thank Andrey Bakulin for initiating the project, giving us the motivation for it and for all his help and support. In particular, his help with editing the manuscripts improved all of our publications significantly. In connection, I am of course extremely grateful to Shell E & P in Houston for the financial support of my PhD project.

In addition, Schlumberger–Doll research must be heartily thanked for making my Summer Internship in Boston possible. Here I would like to especially mention the invaluable contribution of Henri-Pierre Valero who put a lot of time and effort into helping me. Furthermore, I would like to extend my thanks to Bikash Sinha and David L. Johnson for all the useful

and interesting discussions we had during the internship.

To my colleagues and office mates at Curtin I would also like to say thank you for your advice, support and friendship throughout my PhD. Additionally, Deirdre and Rusta deserve my sincere thanks.

List of Publications included as part of this thesis

1. **Karpfinger, F.**, Gurevich B. and Bakulin A.(2008),*Computation of Wave Propagation Along Cylindrical Structures Using the Spectral Method*, The Journal of the Acoustical Society of America, 124(2), 859-865, http://dx.doi.org/10.1121/1.2940577.

2. **Karpfinger, F.**, Gurevich, B. and Bakulin, A.(2008), *Modelling of axisymmetric wave modes in a poroelastic cylinder using spectral method*, The Journal of the Acoustical Society of America, 124(4), EL230-EL235, http://dx.doi.org/10.1121/1.2968303.

3. Bakulin, A., **Karpfinger, F.** and Gurevich, B.(2008), *Understanding acoustic response of deepwater completions*, The Leading Edge, 27(12), 260-267, http://dx.doi.org/10.11 90/1.3036969.

4. **Karpfinger, F.**, Mueller, T., and Gurevich, B.(2009), *Green's functions and radiation patterns in poroelastic solids revisited*, Geophy. J. Int, **178**(1), 327-337.

5. **Karpfinger, F.**, Gurevich, B. and Bakulin, A., (2009), Axisymmetric

waves in fluid saturated porous structures, Poromechanics IV, 625-630, DEStech Publications.

Statement of candidate about the contribution of others

Of all the publications included as a part of this thesis (except paper 3) I am the lead author. For paper 3, I am the second author but the corresponding author. These papers were each based on work in which I was the principal investigator, but which included collaboration with my co-authors. I wrote these papers myself, having discussions with and technical review from my co-authors. See comments of my co-authors in Appendix 1.

List of additional publications by the candidate relevant
to the thesis but not forming part of it

Manuscripts in revision

1. **Karpfinger, F.**, Valero, H.-P., Gurevich, B., Bakulin, A. and Sinha, B. (2009), *Spectral method algorithm for modelling dispersion of acoustic modes in elastic cylindrical structures*, for Geopysics.

2. **Karpfinger, F.**, Gurevich, B., Valero, H.-P., Bakulin, A. and Sinha, B. (2009),*Tube wave signatures in cylindrically layered poroelastic media computed with spectral method*, for Geophy. J. Int.

These two papers are currently in revision and thus not included in the main part of the thesis. The manuscripts in their current form are attached to the thesis in the Appendices C and D.

Conference proceedings and abstracts

1. **Karpfinger, F.**, Gurevich B. and Bakulin A. (2007), Computing borehole modes with spectral method, 77th Ann. Mtg. Society of Exploration Geophysicists, San Antonio, Extended Abstracts, BG1: Acoustics Session.

2. **Karpfinger, F.**, Gurevich B. and Bakulin A.(2007), Modelling of borehole modes using the spectral method, 69th EAGE Conference, London, Extended Abstracts, P095, 2007.

3. **Karpfinger, F.**, Gurevich B. and Bakulin A. (2009), Spectral method for modelling the acoustic response of deepwater completions, 157th Meeting of the Acoustical Society of America, Portland , Oregon, 1pPA, General Physical Acoustics Session.

4. **Karpfinger, F.**, Gurevich, B., Valero, H.-P., and Bakulin, A. (2009), Spectral method for modelling waves in cylindrical poroelastic structures, 157th Meeting of the Acoustical Society of America, Portland , Oregon, 1pPA, General Physical Acoustics Session.

5. **Karpfinger, F.**, Bakulin, A. and Gurevich, B., (2009) Modeling acoustic response of deepwater completions using spectral method 79th Ann. Mtg. Society of Exploration Geophysicists, Houston, Extended Abstracts, BG1: Sonic Logging Session.

Contents

Part I

Introduction and Overview

CHAPTER 1

Background and motivation

Acoustic waves have a vast array of applications in mechanical engineering as well as reservoir geophysics. In mechanical engineering, acoustic waves are used for non-destructive testing (NDT) (Workman and Kishoni, 2007). Industrial machine parts require non-destructive testing methods during their lifetime in order to detect material damage such as cracks. Ultrasonic measurement is one technique used in NDT to detect flaws and to characterize materials.

One special class of waves used in ultrasonic NDT are guided waves. The energy in wave guides is trapped between two interfaces so the wave energy propagates over long distances parallel to the interfaces. Various structures such as free plates, beams, cylinders etc. are elastic wave guides. These waves are utilised to detect damage such as micro cracks or corrosion in pipelines, railroad tracks, concrete or rock bolts, storage tanks etc. The velocity dispersion and attenuation of the guided waves are used to
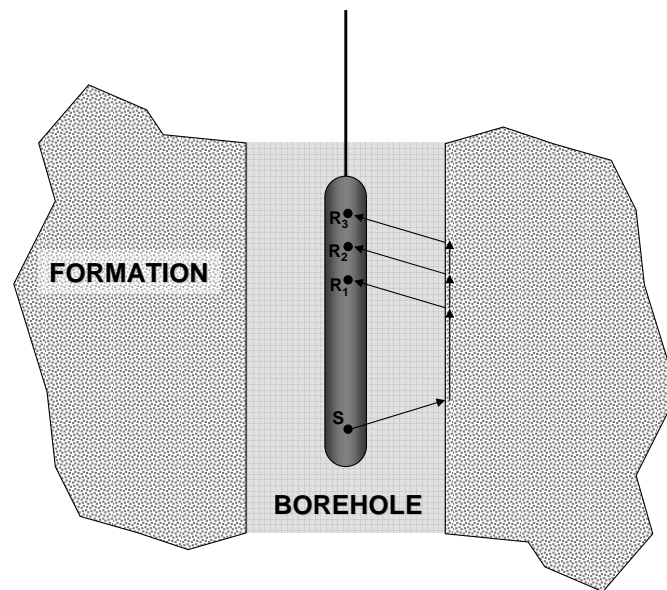
Figure 1.1: Schematic crossection of a borehole with a sonic tool in the center.

characterize the elastic material properties as well as the geometry.

Another field where acoustic wave propagation is utilised is oil and gas exploration. In a similar manner to NDT, acoustic waves are used to characterize oil reservoirs. Boreholes are drilled to produce oil and gas but at the same time they are used to perform measurements. So called wireline measurements give direct information about the formation lithology, porosity and permeability. The borehole can be thought of as a waveguide. It is, in the most simplified approximation, a cylindrical fluid column surrounded by a formation. In Fig. 1.1 a schematic crossection of a borehole with a sonic tool in the center is illustrated. Borehole radii vary between 10 and 15 cm while tool radii are about 5 cm. A varying number of sources and receivers can be arranged along a sonic tool and the typical frequency range of sonic tools is between 10 and 20 kHz.

Various modes can be excited by sources in a borehole. Fig. 1.2 illustrates
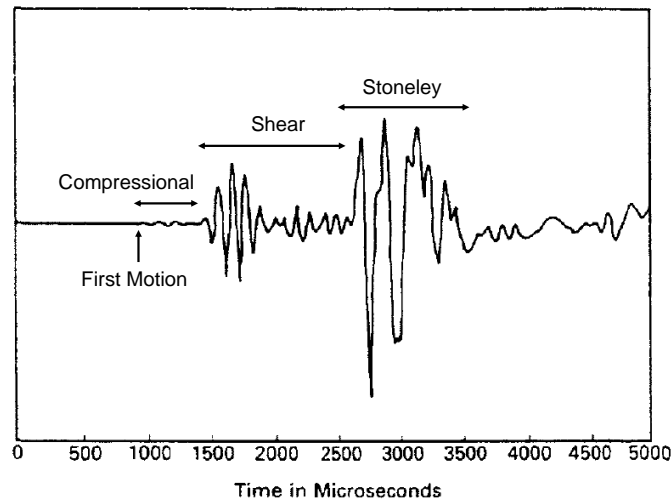
Figure 1.2: Typical waveform, recorded by an acoustic tool due to a monopole source (Ellis, 1987).

a typical waveform from a monopole source, recorded by an acoustic tool. The first two arrivals are the compressional and shear head waves which are used to measure P-and S-wave velocities. The last arrival is the Stoneley wave or tube wave. The Stoneley wave or tube wave is a guided borehole mode propagating in the fluid column. For low frequencies the propagation is characterized by the compression of the fluid column which leads to a piston-like motion. If the formation is permeable, radial fluid flow occurs across the borehole wall. Thus, the tube wave dispersion is sensitive to the permeability of the formation. This allows us to estimate formation permeability from the tube wave dispersion. This effect has been considered by various authors (Rosenbaum, 1974; Chang et al., 1988; Schmitt et al., 1988; Winkler et al., 1989).

The effect of the flow across the borehole wall is generally reduced by the presence of a so called mudcake between the borehole fluid and the formation. The mudcake is a thin layer built up by clay particles in the drillling fluid. These seal the borehole wall over time, forming an imper-

meable membrane layer whose low stiffness allows partial flexing into the pores. This partial flexing reduces, but does not eliminate, the formation permeability effect on the tube waves (Liu and Johnson, 1997).

For the estimation of the shear velocity of the surrounding formation dipole and multipole sources are used (Schmitt, 1993; Sinha and Asvadurov, 2004; Sinha et al., 2006). A comprehensive overview of all techniques for and concepts about acoustic borehole logging can be found in White (1983), Paillet and Cheng (1991) and Tang and Cheng (2004).

Traditionally, in exploration wells, tube wave signatures of fluid-filled boreholes surrounded by a permeable formation are used to obtain formation characteristics. For a closed interface between the borehole and the poroelastic formation, no fluid flow occurs and the tube wave is only sensitive to the rigidity of the formation: elastic case. The open borehole case is considered if the fluid can flow freely across the borehole wall. In this case the tube wave dispersion is sensitive to the formation permeability. For production monitoring the acoustic response of borehole completions has to be considered. Such completions are systems with a number of cylindrical layers within the borehole. Typical deepwater completions are built of additional layers such as sand screens, gravel packs and perforated casings, which make them quite different from a fluid-filled open or closed exploration borehole.

Recently, a concept called Real-Time Completion Monitoring (RTCM) was proposed which utilises tube waves to monitor permeability changes along deepwater borehole completions (Bakulin et al., 2008c,a, 2009). Monitoring changes in flow properties across the completion is crucial because impairment of permeability in any of these layers could cause reduced well productivity.

In order to understand wave propagation in cylindrical structures, typical of open boreholes or borehole completions, the velocity dispersion and attenuation needs to be studied. In addition, understanding of the

dispersion of borehole modes is crucial for the interpretation of acoustic borehole measurements. The traditional way of calculating the frequency dependence of borehole modes is the so called *root-finding* approach (Ewing, 1957). A general solution to the wave equations is sought in the form of a linear combination of Bessel functions of different order. Substituting the solution into the boundary conditions yields a homogeneous system of linear algebraic equations. In order for this system to have nontrivial solutions, the determinant of its matrix M must be equal to zero, $\det M(\omega, k_z) = 0$, with ω being the angular frequency and k_z being the axial wavenumber. This is called the frequency equation. The roots of this equation yield the dispersion relation $\omega(k_z)$. This concept has been utilised to compute the dispersion for simple models such as open boreholes surrounded by an elastic or poroelastic formation (Paillet and Cheng, 1991) and even some more complicated structures (Schmitt, 1988; Rao and Vandiver, 1997; Wisse et al., 2007). However, for structures with more complicated radial layering this method becomes a cumbersome task. Solving the frequency equation gets even more complicated in the case of leaky modes or lossy structures where solutions of the dispersion relation should be found in the complex plane.

In this thesis, I present a new numerical approach based on spectral methods which allows us to bypass the difficulties of *root-finding*. Spectral methods are efficient and accurate algorithms for solving partial differential equations. These methods have been widely used in numerical fluid dynamics (Canuto et al., 1988) as well as in seismic forward modelling (Fornberg, 1987; Carcione et al., 2002; Kosloff et al., 1990).

Adamou and Craster (2004) introduced an algorithm based on a spectral Chebyshev scheme, which computes the dispersion of circumferential waves in an elastic annulus. The spectral method used in their work discretizes the underlying equations with Chebyshev collocation points and differentiation matrices leading to a set of linear algebraic equations.

The corresponding system is then solved as a generalised eigenvalue prob-
lem. The computed eigenvalues obtained at a given frequency correspond
to the slownesses of different modes. The advantages compared to *root-
finding* are clearly highlighted by Adamou and Craster (2004). They point
out that the coding effort and the computational time is small compared
to root-finding. Furthermore, extension to viscoelastic media with com-
plex moduli adds to the computational time very little. Another benefit
is that the spectral method can be applied to situations where *root-finding*
completely fails such as radial inhomogeneities or nonseparable geome-
tries. These advantages made the method appealing for me to extend it
for axisymmetric wave propagation in elastic and poroelastic radially lay-
ered structures. I have successfully extended this approach to model wave
propagation in such structures and present my findings in this thesis as a
series of published papers.

Using the spectral method, wave propagation in fluid-filled boreholes sur-
rounded by an elastic or poroelastic formation can be simulated. For seis-
mic modelling on a larger scale, such as crosshole seismic, VSP or single-
wave imaging, the explicit modelling of the borehole requires a prohibitively
fine grid size. We can overcome this problem by approximating the bore-
hole as a series of point sources as discussed by Kurkjian (1985). With-
out adding extra computational cost this method mimics the presence of
a borehole at seismic frequencies. This technique simulates the effect of
dispersive tube waves, head waves as well as secondary sources on in-
terfaces. This approach requires the computation of the point source re-
sponse in a medium. A similar approach for poroelasticity could take
into account the hydraulic interaction between borehole and formation.
Knowledge of the point source response in poroelastic media is required.
In the last paper of the thesis Green's functions in poroelastic media were
studied including the analysis of the radiation pattern and moment tensor
representation of various source types.

CHAPTER 2

Thesis objectives and outline

The overall objective of this thesis is to develop a 1-D modelling algorithm for wave propagation in complicated cylindrical structures. This algorithm is based on spectral methods, which enables easy computation of the velocity dispersion and attenuation of modes propagating in structures built of an arbitrary number of fluid, elastic and poroelastic cylindrical layers. In spectral method schemas orthogonal polynomials of high degree are used as global interpolants to approximate the unknown functions of the considered differential equations. The discretization of the differential operators can be based on Chebyshev, Fourier, Hermite or other interpolants, which can be differentiated exactly. We use Chebychev interpolation points and differentiation matrices to discretize the underlying equations along the radial coordinate. A Matlab routine is provided by Weideman and Reddy (2000) which computes such Chebychev points and differentiation matrices.

The interpolation points, which discretize the medium in the radial direction, are chosen to be the maxima of the Chebychev polynomials. The differential operators are approximated by a differentiation matrix. They result from the fact that any function ϕ evaluated at N Chebychev interpolation points is connected to its first derivative ϕ' by a matrix vector product. This discrete matrix operator, which approximates the differential operator, is called a differentiation matrix. If the exact expression for ϕ and its derivative ϕ' at all interpolation points is known, the exact expression for the differentiation matrix can be obtained (Trefethen, 2000).

I combine the discretized differential operators of the Helmholtz equations with the stress and displacement components defining the boundary conditions (Karpfinger et al., 2008a, 2009). Thus, the problem is formulated and solved as a generalised algebraic eigenvalue problem. For a given frequency, the eigenvalues correspond to the axial slownesses of different modes and the eigenvectors to the radial distribution of the displacement potentials. They can be used to obtain the distribution of the stress and displacement components along the radial coordinate.

The spectral method modelling algorithm has the advantage of providing results relatively quickly and easily, even for complicated structures. It is possible to apply this algorithm in various fields such as borehole acoustics, production monitoring or laboratory measurements. Initially the algorithm was developed within the project which proposed the concept of Real-Time Completion Monitoring (Bakulin et al., 2008c,a, 2009). In order to understand wave propagation in complicated structures involving casing, a sand screen and a gravel pack, it was necessary to quickly obtain the dispersion for such systems. The spectral method was used in this context for parameter studies (Bakulin et al., 2008c) as well as to investigate the effects of sand screen permeability (Bakulin et al., 2008b).

Beyond the scope of production monitoring, the spectral method is used to model typical borehole acoustical setups. Due to the fact that the spectral

method is more flexible than other approaches, a more detailed model of a borehole can be computed, including a model with a radial change of the permeability around the borehole. Furthermore, the spectral method can be used to analyze laboratory measurements of cylindrical samples.

For seismic forward modelling on a larger scale, the explicit modelling of the borehole requires a prohibitively fine grid size. We can overcome this problem by approximating the borehole as a series of point sources as discussed by Kurkjian (1985). This approach mimics the presence of borehole modes while adding no extra computational time. In order to extend this method for poroelastic media, Green's functions in poroelastic media were studied, including the analysis of the radiation pattern and moment tensor representation of various source types.

The overall work accomplished in this thesis can be divided into the following areas:

- development of a spectral method code for obtaining tube wave dispersion in structures with an arbitrary number of fluid and elastic layers.

- extension of the approach to a free poroelastic cylinder.

- extension to a code which allows the computation of the mode dispersion and attenuation in structures involving an arbitrary number of fluid, elastic and poroelastic layers.

- evaluation of permeability effects of a sand screen in the setup for Real-Time Completion Monitoring.

- modelling of complicated borehole acoustical setups which involve a damaged zone with a radial change in permeability.

- analysis of Green's function solutions for poroelastic media and analysis of radiation patterns and moment tensor representations for different sources.

CHAPTER 3

Thesis publications and their relation to the thesis topic

The thesis is presented as a series of five papers in peer reviewed techni-
cal journals. An overview of all articles is presented in this chapter which
highlights their relevance to the topic and how each of them are inter-
linked. The papers cover three different aspects: theoretical implementa-
tion of spectral method for borehole acoustical problems, computational
aspects of the spectral method algorithm and computation of synthetic ex-
amples for various real scenarios.

The overall aim of the thesis was to develop a numerical modelling code,
based on a spectral method, which allows me to obtain the dispersion and
attenuation of tube waves propagating in cylindrically layered structures
composed of fluid, elastic and poroelastic layers. In this approach the dif-
ferential equations are discretized using Chebychev interpolation points
and differentiation matrices. The problem can then be formulated for any

number of layers as a generalised eigenvalue problem where the eigenvalues correspond to the phase velocities. This modelling algorithm can be useful to characterize fluid communication in complicated borehole completions.

Paper 1:

Karpfinger, F., Gurevich B. and Bakulin A.,Computation of Wave Propagation Along Cylindrical Structures Using the Spectral Method, The Journal of the Acoustical Society of America, 124(2), 859-865, 2008.

A lot of research has been done over the past decades on wave propagation in elastic cylindrical structures using the traditional *root–finding* approach (Kolsky, 1963; Del Grosso and McGill, 1968; Rao and Vandiver, 1997). In Paper 1 I introduce an alternative to the traditional method, called spectral method, to obtain the velocity dispersion of modes propagating in structures with an arbitrary number of fluid and elastic layers. This alternative approach is based on the work done by Adamou and Craster (2004) who used the spectral method to compute the dispersion of circumferential waves in an elastic annulus. The underlying differential equations are discretized using spectral differentiation matrices which allows us to formulate and solve the problem as a generalised eigenvalue problem.

Paper 1 presents the underlying equations for axisymmetric wave propagation along the cylindrical structures as well as their discretization and implementation for the spectral method. The algorithm was benchmarked by reproducing some known results from literature (Kolsky, 1963; Del Grosso and McGill, 1968). Paper 1 also gives an overview on the theoretical background and the formulation of the generalised eigenvalue problem using the spectral method for multi layered cylindrical structures.

> **Paper 2:**
>
> **Karpfinger, F.**, Gurevich, B. and Bakulin, A., Modelling of axisymmetric wave modes in a poroelastic cylinder using spectral method, Journal of the Acoustical Society of America, 124(4), EL230-EL235, 2008.

In Paper 2 I extended the spectral method approach to a poroelastic cylinder. The equations in cylindrical coordinates for a fluid-saturated poroelastic medium were derived on the basis of Biot's theory (Biot, 1962). The generalised eigenvalue problem was constructed and solved for a poroelastic cylinder with open and closed pore boundary conditions imposed on the surface of the cylinder.

I compared the mode dispersion obtained with the spectral method to *root-finding* results. These results are discussed in context of the results from Berryman (1983). I showed that my results help to give a complete physical understanding of the fundamental modes propagating in a poroelastic cylinder. In addition, I have shown that the spectral method is approximately three orders of magnitude faster than the *root-finding* technique which I developed for this purpose.

> **Paper 3:**
>
> **Karpfinger, F.**, Gurevich, B. and Bakulin, A., (2009), Axisymmetric waves in fluid saturated porous structures, Poromechanics IV, 625-630, DEStech Publications.

After studying a free poroelastic cylinder the next logical step was to study multilayered structures with an arbitrary number of cylindrical fluid, elastic and poroelastic layers. In order to achieve this, interface boundary conditions had to be introduced for poroelastic/fluid, poroelastic/solid and poroelastic/poroelastic interfaces.

In Paper 3 the generalised eigenvalue problem for a borehole surrounded by a poroelastic formation is constructed. The classical result for a fluid-

filled borehole surrounded with a poroelastic formation is reproduced. The dispersion is then compared to the low-frequency approximation from Chang et al. (1988). Results for the effect of an altered zone with reduced permeability are presented.

Paper 4:

Bakulin, A., **Karpfinger, F.** and Gurevich, B., Understanding acoustic response of deepwater completions, The Leading Edge, 27(12), 260-267, 2008.

After the theoretical framework for the computation of the dispersion and attenuation in poroelastic structures was formulated, I used the method in Paper 4 to compute the acoustic response of deepwater completions. Of particular interest is the effect of the fluid–flow across layers such as a sand screen on the tube wave signature . Based on the four layer model (fluid – sand screen – fluid – casing) discussed by Bakulin et al. (2008c) we have computed the dispersion of the four fundamental modes propagating in such a system. The presence of two fluid-like columns supports the propagation of two tube waves: fast and slow. There are also two plate waves propagating in the system: one in the sand screen and one in the casing. Neither are sensitive to the screen permeability. For the case of a non-permeable sand screen the dispersion can be straightforwardly computed using the elastic theory. In the case when one layer (sand screen) is poroelastic, both tube waves become very dispersive due to the fluid exchange across the screen. For this case the dispersion and attenuation as well as the stress and displacement profiles were computed for various permeabilities. The study qualitatively verifies the results observed in the laboratory experiments by Bakulin et al. (2009).

Paper 5:

Karpfinger, F., Mueller, T., and Gurevich, B., Green's functions and radiation patterns in poroelastic solids revisited, Geophy. J. Int., 2009.

The spectral method allows us to simulate wave propagation in fluid-filled boreholes surrounded by an elastic or poroelastic formation. For seismic modelling on a larger scale, such as crosshole seismic, VSP or single-wave imaging, the explicit modelling of the borehole requires a prohibitively fine grid size. This problem can be overcome by approximating the borehole as a series of point sources as suggested by Kurkjian (1985). This method mimics the presence of a borehole at seismic frequencies without adding extra computational cost. This technique simulates the effect of dispersive tube waves, head waves as well as secondary sources on interfaces. This approach requires the computation of the point source response in a medium. To take into account hydraulic interaction between borehole and formation it would be desirable to implement a similar approach for poroelasticity. Knowledge of the point source response in poroelastic media is required. To this end Green's functions in poroelastic media were studied including the analysis of the radiation pattern and moment tensor representation of various source types.

Together these five papers form an in depth analysis of wave propagation in cylindrical structures composed of fluid, elastic and poroelastic layers. With the help of the spectral method, scenarios are investigated for which traditional methods would be very difficult to implement. The examples discussed have a wide variety of applications from laboratory experiments to production monitoring and conventional borehole acoustics. Together with a better understanding of sources in poroelastic media the way is paved for various applications in seismic modelling.

Manuscripts in revision

In addition to the five published papers, two manuscripts which are currently in revision add to the context of the thesis. The manuscripts are included in Appendices C and D of the thesis.

Manuscript 1:

Karpfinger, F., Valero, H.-P., Gurevich, B., Bakulin, A. and Sinha, B., Spectral method algorithm for modelling dispersion of acoustic modes in elastic cylindrical structures, for Geopysics.

As a follow up to the theoretical paper (Paper 1) I submitted a paper which discusses in detail the spectral method algorithm and its implementation in Matlab. This paper was submitted to the Software & Algorithm section of *GEOPHYSICS* which required the publication of the code in addition to the paper. Manuscript 1 discusses the workflow of the code for fluid and elastic layers. Two examples are used to illustrate the results in the form of dispersion curves as well as modeshapes. Reproducing these results using the computer code shows the ease of use and computational efficiency of the algorithm.

Manuscript 2:

Karpfinger, F., Gurevich, B., Valero, H.-P., Bakulin, A. and Sinha, B., Tube wave signatures in cylindrically layered poroelastic media computed with spectral method, for Geophy. J. Int.

Manuscript 2 expands the poroelastic algorithm briefly summarized in Paper 3. The eigenvalue problem for an arbitrary number of poroelastic layers is formulated. Three examples are discussed. First the classic case of a borehole for which the dispersion and attenuation are computed for a series of permeabilities. The second example discusses the effect of the thickness of a layer sandwiched between the borehole fluid and the poroelastic

formation. Finally, the effect of an altered zone on the tube wave signature is discussed considering a radial change of the formation permeability.

Discussion, conclusions and outlook

Discussion

The five peer reviewed papers forming this thesis present a new method for obtaining dispersion of tube waves in cylindrical structures with an arbitrary number of fluid, elastic and poroelastic layers. The spectral method approach presented enables us to obtain the signatures of tube waves and other modes in complicated multi layered structures in a flexible, easy to use and fast manner.

The first publication discusses structures built of fluid and elastic layers. The theoretical framework is discussed in detail, where the equations used for the spectral method are provided as well as how the eigenvalue problem is constructed for an arbitrary number of fluid and elastic layers. The benchmark models discussed are in very good agreement with analytical solutions. In addition to the dispersion curves, displacement and stress

profiles are shown, which are obtained from the displacement potentials. The code as presented here is implemented for a finite structure. For borehole acoustical applications the outside radius can. However, the problem is that some modes such as pseudo-Rayleigh modes are not computed. In order to account for these modes, non-reflecting boundary conditions have to be introduced to mimic a infinite structure.

Subsequently, the spectral method was extended for poroelastic layers. I applied the approach to a free poroelastic cylinder with open and closed pore boundary conditions on the surface. The results are in very good agreement with the modes obtained by *root-finding*. For a free poroelastic cylinder the time efficiency of the spectral method was significant. The computational time of the spectral method to obtain the dispersion curves was two orders of magnitude faster than the *root-finding* approach for an approximately 20 times larger set of frequencies.

The spectral method approach was subsequently applied to more complicated structures involving poroelastic as well as fluid and elastic layers. As a benchmark model, a fluid-filled borehole surrounded with a poroelastic formation was used. The analytical low-frequency approximation was compared to our numerical results, which showed very good agreement. The next step was to apply the method to multi-layered structures built of up to ten layers. In particular the model with an altered zone is of great interest. In an altered zone the area around the borehole is mechanically damaged due to drilling which can result in a reduced permeability compared to the untouched formation. With the spectral method we are able to model the dispersion of tube waves in such a structure using a stepwise increase of the permeability in small intervals. The main problem I encountered for poroelasticity is for layers with very small permeability (less than $1mD$). In this case the number of collocation points must be increased by a factor of $4 - 5$ otherwise the results become numerically unstable.

The spectral method approach could now be applied to the four layer completion model with permeable sand screen. I obtained the dispersion and attenuation for both tube waves with varying permeability of the sand screen. Both tube wave signatures showed sensitivity to the permeability of the sand screen. It is important to mention that the slow tube wave gets extremely attenuated for very high permeabilities. The attenuation at low frequencies becomes bigger than $Q^{-1} = 2$. This means that the mode loses its energy within less than one wavelength. Overall the numerical study shows qualitatively similar features to the laboratory experiments. Quantitatively there is still a discrepancy between experiment and numerics. The permeability of the sand screen is estimated with 100 Darcy but the numerical simulation already predicts a complete dissipation of the slow tube wave at 10 Darcy for all frequencies of interest. In contrast to that the slow tube wave can be observed in the laboratory experiment with open screen. This suggests that the Biot theory does not sufficiently describe tube wave propagation supported by a sand screen. A better model of sand screens is required to reconcile this discrepancy.

In addition to the dispersion of borehole modes the radiation characteristics of sources in poroelastic media were studied. Two fundamental point source solutions in poroelastic media were reviewed. It is shown how a combination of both solutions can best describe wave radiation from sources in poroelastic solids. The two solutions were investigated due to their radiation characteristics using radiation patterns. With the help of the moment tensor concept, more complicated sources such as double couple or dipole were implemented. The understanding of these point source solutions can help in the future for various seismic modelling applications. In particular in borehole seismic, these sources can be used to mimic the presence of a borehole and its modes. This can be accomplished as a superposition of point sources (Kurkjian, 1985). The spectral method approach can be used to benchmark these results. This can be a further

development resulting from this thesis.

Conclusions

The main conclusions which can be drawn from the five publications forming this thesis are:

Mode dispersion in cylindrically layered fluid-elastic structures

- I extended and implemented the spectral method for propagation of axisymmetric modes in an elastic cylindrical bar and further generalized the algorithm to n–layered cylindrical fluid-solid structures.

- Traditional techniques require finding complex roots of nonlinear equations that involve special functions. In contrast, our spectral method demands only the solution of a generalized eigenvalue problem without involving special functions. This represents a great simplification that becomes particularly advantageous for complex rheologies like viscoelastic, anisotropic, and poroelastic structures.

- Creating an input file for multi-layered models is very straightforward and the results are very efficiently obtained. The algorithm is very fast due to the computational efficiency of the spectral method. The algorithm works for any number of layers and down to a layer thickness of 0.5 % relative to the thickness of the structure.

- The drawbacks are that for a increasing number of layers the computational time significantly increases and for very thin layers the accuracy decreases. However, for most models of interest the algorithm works very efficiently and is easy to use.

Mode dispersion in cylindrically layered poroelastic structures

- I have extended and implemented the spectral method for propagation of axisymmetric modes in a poroelastic cylindrical bar and have further generalized the method to n–layered cylindrical fluid- solid–poroelastic structures.

- The results of the spectral method are in very good agreement with the analytical results; one advantage of the spectral method is that, in contrast to traditional methods, it is easier to implement and faster by a factor of approximately 1000.

- The results for a single poroelastic cylinder show that the singularities of the dispersion curve for the fast extensional mode correspond to intersections with the high order slow extensional modes.

- As an example for a more complicated model I applied spectral method to a borehole in a permeable formation with an altered near-wellbore zone and show how this altered zone changes the dispersion of the Stoneley wave. Such more complicated models gives us a chance to obtain a more accurate description of realistic borehole conditions and thus achieve a better characterization of petrophysical properties of subsurface formations.

Acoustic response of deepwater completions

- I used the spectral method to model the acoustic response of a deepwater completion model without gravel pack and I assumed that the sand screen can be modeled as a poroelastic layer.

- Modeling with spectral method confirms the existence of a fast and a slow tube wave supported by casing and screen, respectively, as

well as a strong dependence of fast and slow tube wave signatures on the sand screen permeability.

- For the slow tube wave velocity decreases and attenuation increases with increasing screen permeability. Such behavior is caused by escalating fluid communication between two fluid columns and can be explained by opposite signs of axial fluid displacements on different sides of the screen.

- The fast tube wave experiences moderate attenuation at some characteristic frequency, which is controlled by screen permeability and thickness, whereas for small and large permeability the fast tube wave remains free of losses. At the limit of high permeability, the fast tube wave transforms into a regular tube wave as if the sand screen becomes part of the surrounding liquids.

- These modeling results are in a qualitative agreement with experimental observations in full-scale laboratory models of deepwater completions. The main discrepancy is related to the behavior of the slow tube wave. Simple calculation of static screen permeability suggests values larger than 100 Darcy, for which modeling predicts complete dissipation of the slow mode. A better model of sand screens is required to reconcile this discrepancy. Understanding the connection between static and dynamic or acoustic permeability for meso–scale structures such as sand screens and perforated casing is a key to such reconciliation.

Green's functions and radiation patterns in poroelastic solids

- A review and comparison of different formulations of Green's functions for dynamic poroelasticity is provided. In this review I can show that previously reported sets of Green's functions can be used

in a complementary sense such that all possible combinations of field variables and source types are included. The unified presentation of Greens functions resolves the apparent contradictions between existing formulations.

- As expected, the shape of the radiation patterns of the fast compressional and shear waves is identical to their elastodynamic counterparts and is complemented with the radiation pattern of Biot's slow wave. The relative magnitudes of the field variables shown in the radiation patterns can be very different for different source types. In particular, for any source acting in the fluid phase the pressure field is dominated by the Biot slow wave which has compressional wave polarization.

- I introduce the concept of moment tensors for dynamic poroelasticity that allows us to overcome the inconsistency in Green's function formulation with respect to point force sources in the fluid phase.

Outlook

The spectral method has great potential to be used for evaluating borehole acoustical measurements as well as laboratory experiments. In this thesis the main focus was on axisymmetric wave propagation. A next step would be to extend the method for non-symmetric modes, such as flexural waves. They have a major importance in borehole logging as they can give information on the formation shear rigidity, which is an important engineering parameter.

So far I have considered isotropic elastic and poroelastic layers. Many reservoir formations are anisotropic. In order to account for this effect the spectral method should be expanded to anisotropic media. It should be possible to do this for elastic as well as poroelastic media. Anisotropy

would be also of great importance to model ultrasonic measurements performed on cylindrical rock samples with anisotropic stress.

The modelling so far is performed in the frequency domain. A next step is to obtain the time domain response by applying the inverse Fourier transform. This would allow us to model the full waveform which represents the actual measurement obtained in borehole logging.

A big advantage of the spectral method is that the generalised eigenvalue problem is solved for the structure globally. This allows implementation of a gradual change of input parameters. For example heterogeneities can be considered by introducing a radial change of velocity or permeability in form of a function within one layer. This will save computational time, as the radial change happens within one layer and not as a superposition of layers with changing properties.

Overall, the spectral method can be used to obtain the dispersion of waves with complicated layering, which gives the possibility of modelling in greater detail the acoustic response of borehole structures with and without completion.

Another aspect which requires more detailed investigation is the dispersion and attenuation of tube waves in a four layer model with changing permeability of the sand screen. It is important to understand the nature of attenuation with $Q^{-1} > 2$.

Furthermore the effect of the gravel pack, as well as perforations in the casing, on the signature of the tube waves needs to be studied. For all these layers it is sufficient, for preliminary studies, to use Biot's theory of poroelasticity. However, in order to quantify the effects it would be important to develop new models for wave propagation in materials such as highly permeable sand screens. All this can pave the way to a greater understanding of the acoustic response of borehole completions, which is essential for the success of Real-Time Completion Monitoring.

The understanding of borehole waves propagating in a poroelastic formation together with the understanding of sources in poroelastic media will help to extend the method by Kurkjian (1985) to a poroelastic formation in the future.

Bibliography

Achenbach, J. D. (1973). *Wave propagation in elastic solids*. North Holland, Amsterdam.

Adamou, A. T. I. and Craster, R. V. (2004). Spectral methods for modelling guided waves in elastic media. *J. Acoust. Soc. Amer.*, 116(3):1524–1535.

Bakulin, A., Alexandrov, D., Sidorov, A., and Kashtan, B. (2009). Acoustic waves in sand-screened deepwater completions: Comparison of experiments and modeling. *Geophysics*, 74(1):E45–E56.

Bakulin, A., Jaaskelainen, M., Sidorov, A., and Kashtan, B. (2008a). Downhole acoustic surveillance of deepwater wells. *The Leading Edge*, 27(4):518–531.

Bakulin, A., Karpfinger, F., and Gurevich, B. (2008b). Understanding the acoustic response of deepwater completions. *The Leading Edge*, 27(12):1646–1653.

Bakulin, A., Sidorov, A., Kashtan, B., and Jaaskelainen, M. (2008c). Real-

time completion monitoring with acoustic waves. *Geophysics*, 73(1):E15–E33.

Bancroft, D. (1941). The velocity of longitudinal waves in cylindrical bars. *Physical Review*, 59(7):588–593.

Berryman, J. G. (1983). Dispersion of extensional waves in fluid-saturated porous cylinders at ultrasonic frequencies. *J. Acoust. Soc. Amer.*, 74(6):1805 – 1812.

Biot, M. A. (1962). Generalized theory of acoustic propagation in porous dissipative media. *J. Acoust. Soc. Amer.*, 34(5):1254 – 1264.

Canuto, C., Hussaini, M., Quarteroni, A., and Zang, T. (1988). *Spectral Methods in Fluid Dynamics*. Springer Series in Computational Physics. Springer.

Carcione, J. M., Herman, G. C., and ten Kroode, A. P. E. (2002). Seismic modeling. *Geophysics*, 67(4):1304–1325.

Chang, S. K., Liu, H. L., and Johnson, D. L. (1988). Low-frequency tube waves in permeable rocks. *Geophysics*, 53(4):519 – 527.

Chree, C. (1889). The equations of an isotropic elastic solid in polar and cylindrical coordinates, their solutions and applications. *Trans. Camb. Phil. Soc.*, 14:250.

Davies, R. M. (1948). A critical study of Hopkinson pressure bar. *Proc. Royal Soc. of London*, 240(821):375–457.

Del Grosso, V. A. and McGill, R. E. (1968). Remarks on "Axially symmetric vibrations of a thin cylindrical elastic shell filled with nonviscous fluid" by Ram Kumar, Acustica 17 [1968],218. *Acustica*, 20(5):313–314.

Ellis, D. (1987). *Well logging for earth scientists*. Elsevier Science Publisher.

Ewing, W. M. (1957). *Elastic Waves in Layered Media*. McGraw Hill.

Feng, S. and Johnson, D. L. (1983). High-frequency acoustic properties of a fluid/porous solid interface. i. new surface mode. *J. Acoust. Soc. Amer.*, 74(3):906–914.

Fornberg, B. (1987). The pseudospectral method: Comparisons with finite differences for the elastic wave equation. *Geophysics*, 52(4):483–501.

Gardner, G. H. F. (1962). Extensional waves in fluid-saturated porous cylinders. *J. Acoust. Soc. Amer.*, 34(1):36–39.

Gassmann, F. (1951). Über die elastizität poröser medien. *Viertel. Naturforsch. Ges. Zürich*, 96:1–23.

Gazis, D. C. (1959a). Three-dimensional investigation of the propagation of waves in hollow circular cylinders. I. Analytical foundation. *J. Acoust. Soc. Amer.*, 31(5):568–573.

Gazis, D. C. (1959b). Three-dimensional investigation of the propagation of waves in hollow circular cylinders. II. Numerical results. *J. Acoust. Soc. Amer.*, 31(5):573–578.

Karpfinger, F., Gurevich, B., and Bakulin, A. (2008a). Computation of wave propagation along cylindrical structures using the spectral method. *J. Acoust. Soc. Amer.*, 124(2):859–865.

Karpfinger, F., Gurevich, B., and Bakulin, A. (2008b). Modeling of axisymmetric wave modes in a poroelastic cylinder using spectral method. *J. Acoust. Soc. Amer.*, 124(4):EL230–EL235.

Karpfinger, F., Valero, H.-P., Gurevich, B., Bakulin, A., and Sinha, B. (2009). Spectral method algorithm for modelling dispersion of acoustic modes in elastic cylindrical structures. *Geophysics*.

Kolsky, H. (1963). *Stress waves in solids*. Dover, New York.

Kosloff, D., Kessler, D., Filho, A. Q., Tessmer, E., Behle, A., and Strahilevitz, R. (1990). Solution of the equations of dynamic elasticity by a Chebychev spectral method. *Geophysics*, 55(6):734–748.

Kurkjian, A. L. (1985). Numerical computation of individual far-field arrivals excited by an acoustic source in a borehole. *Geophysics*, 50(5):852 – 866.

Lin, T. and Morgan, G. (1956). Wave propagation through a fluid contained in a cylindrical, elastic shell. *J. Acoust. Soc. Amer.*, 28(6):1165–1176.

Liu, H.-L. and Johnson, D. L. (1997). Effects of an elastic membrane on tube waves in permeable formations. *The Journal of the Acoustical Society of America*, 101(6):3322–3329.

Love, A. E. H. (1944). *A treatise on the mathematical theory of elasticity*. Dover, New York.

McFadden, J. A. (1954). Radial vibrations of thick-walled hollow cylinders. *J. Acoust. Soc. Amer.*, 26(5):714–715.

Morgan, G. W. and Kiely, J. P. (1954). Wave propagation in a viscous liquid contained in a flexible tube. *J. Acoust. Soc. Amer.*, 26(3):323–328.

Paillet, F. L. and Cheng, C. H. (1991). *Acoustic waves in boreholes*. CRC Press.

Pochhammer, L. (1876). On the propagation velocities of small oscillations in an unlimited isotropic circular cylinder. *J. Reine Angew. Math.*, 81:324.

Rao, V. N. R. and Vandiver, J. K. (1997). Acoustics of fluid filled boreholes with pipe: Guided propagation and radiation. *J. Acoust. Soc. Amer.*, 105(6):3057–3066.

Rosenbaum, J. H. (1974). Synthetic microseismograms: Logging in porous formations. *Geophysics*, 39:14–32.

Rubinow, S. I. and Keller, J. B. (1971). Wave propagation in a fluid-filled tube. *J. Acoust. Soc. Amer.*, 50(1B):198–223.

Schmitt, D. P. (1988). Effects of radial layering when logging in saturated porous formations. *The Journal of the Acoustical Society of America*, 84(6):2200–2214.

Schmitt, D. P. (1993). Dipole logging in cased boreholes. *The Journal of the Acoustical Society of America*, 93(2):640–657.

Schmitt, D. P., Zhu, Y., and Cheng, C. H. (1988). Shear wave logging in semi-infinite saturated porous formations. *The Journal of the Acoustical Society of America*, 84(6):2230–2244.

Sinha, B. K. and Asvadurov, S. (2004). Dispersion and radial depth of investigation of borehole modes. *Geophysical Prospecting*, 52(4):271–286.

Sinha, B. K., Vissapragada, B., Renlie, L., and Tysse, S. (2006). Radial profiling of the three formation shear moduli and its application to well completions. *Geophysics*, 71(6):E65–E77.

Tang, X. and Cheng, A. (2004). *Quantitative Borehole Acoustic Methods*, volume 24 of *Handbook of Geophysical Exploration: Seismic Exploratio*. Pergamon.

Trefethen, L. N. (2000). *Spectral Methods in MATLAB*. SIAM, Philadelphia.

Weideman, J. A. C. and Reddy, S. C. (2000). A MATLAB differentiation matrix suite. *ACM Trans. Math. Softw.*, 26:465.

White, J. E. (1983). *Underground sound - Application of seismic waves*. Elsevier.

Winkler, K. W., Liu, H.-L., and Johnson, D. L. (1989). Permeability and borehole Stoneley: Comparison between experiment and theory. *Geophysics*, 54(1):66 – 75.

Wisse, C. J., Smeulders, D. M. J., Chao, G., and van Dongen, M. E. H. (2007). Guided wave modes in porous cylinders: Theory. *The Journal of the Acoustical Society of America*, 122(4):2049–2056.

Workman, G. L. and Kishoni, D. (2007). *Ultrasonic Testing*, volume 7 of *Nondestructive Testing Handbook*. ASNT.

Part II

Published papers

CHAPTER 1

Modeling of wave dispersion along cylindrical structures using the spectral method

Modeling of wave dispersion along cylindrical structures using the spectral method

Florian Karpfinger[a)] and Boris Gurevich[b)]
Department of Exploration Geophysics, Curtin University, GPO Box U1987, Perth, Western Australia 6845, Australia

Andrey Bakulin[c)]
WesternGeco, 10001 Richmond Ave., Houston, Texas 77042

Algorithm and code are presented that solve dispersion equations for cylindrically layered media consisting of an arbitrary number of elastic and fluid layers. The algorithm is based on the spectral method which discretizes the underlying wave equations with the help of spectral differentiation matrices and solves the corresponding equations as a generalized eigenvalue problem. For a given frequency the eigenvalues correspond to the wave numbers of different modes. The advantage of this technique is that it is easy to implement, especially for cases where traditional root-finding methods are strongly limited or hard to realize, i.e., for attenuative, anisotropic, and poroelastic media. The application of the new approach is illustrated using models of an elastic cylinder and a fluid-filled tube. The dispersion curves so produced are in good agreement with analytical results, which confirms the accuracy of the method. Particle displacement profiles of the fundamental mode in a free solid cylinder are computed for a range of frequencies.
© 2008 Acoustical Society of America. [DOI: 10.1121/1.2940577]

I. INTRODUCTION

Modeling different wave modes propagating along a cylindrical borehole is important for the understanding and quantitative interpretation of borehole sonic and seismic measurements. Numerous different modes such as head waves, trapped modes, and surface waves can be observed in these structures. All these modes are frequency dependent. In sonic-logging recordings these modes overlap and are often hard to identify. In order to separate different borehole modes it is useful to analyze their dispersive characteristics.

Traditionally, mode dispersion was studied by finding roots of analytical dispersion equations. The method has a long history. By the end of the 19th century Pochhammer[1] and Chree[2] investigated the wave propagation in free elastic rods. These solutions are presented in detail by Love (Ref. 3, Sec. 201) and Kolsky (Ref. 4, Chap. 3). Numerical solutions to the Pochhammer–Chree equation are presented, for example, by Bancroft.[5]

Another case which was investigated by different authors is that of a hollow[6–8] and fluid-filled[9–11] cylindrical shell.

The root-finding method, however, becomes difficult to implement when the number of cylindrical layers and/or modes of interest becomes large.[12] The separation of different roots in the complex plane becomes even more challenging when inelastic effects need to be taken into account, such as in the case of a cylinder filled with a viscoelastic fluid[13–15] or poroelastic structures.[16–18]

An alternative approach to model two-dimensional circular structures was recently introduced by Adamou and Craster[19] based on spectral methods. The idea of this method is to solve the underlying differential equations by numerical interpolation using orthogonal polynomials and spectral differentiation matrices (DMs). The advantage of this approach is that it is much faster and easier to implement than conventional root-finding methods, especially for attenuating, poroelastic, or anisotropic structures.

In this paper we extend the concept of the spectral method for wave propagation along circular cylindrical structures, and compare the results with known analytical solutions. In Sec. II, the underlying equations in cylindrical coordinates and the eigenvalue problem are formulated for a free solid cylinder. In Sec. III, the solution of the eigenvalue problem for an elastic cylinder is described using the spectral method. Numerical results are presented in the form of dispersion curves. In Sec. IV the approach is extended to multiple layers. The dispersion curves are displayed for the case of a fluid filled tube. In Sec. V, displacement profiles are computed for various frequencies of the fundamental mode propagating in the free solid cylinder.

II. THEORY

A. Equations of motion

We first introduce the spectral method for the simplest case of axisymmetric wave propagation along a free solid bar. The dynamics of the cylinder is analyzed in cylindrical

---
a)Electronic mail: florian.karpfinger@postgrad.curtin.edu.au
b)Electronic mail: boris.gurevich@geophy.curtin.edu.au. Also at CSIRO Petroleum, Bentley, Western Australia
c)Electronic mail: abakulin@slb.com

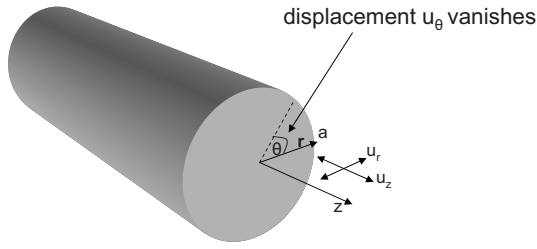FIG. 1. Geometry of a free solid bar, displaying the coordinate system which reduces to (r,z) and the displacement field (u_r, u_z) for axisymmetric wave propagation.

coordinates (r,θ,z) (Fig. 1). For axisymmetric motion the transverse component u_θ of the displacement field $\mathbf{u} = (u_r, u_\theta, u_z)$ is identically zero, while its radial and axial components u_r and u_z are independent of θ.

For the analysis of the wave propagation it is convenient to introduce displacement potentials

$$u_r = \partial_r \phi - \partial_z \psi_\theta, \tag{1}$$

$$u_z = \partial_z \phi + r^{-1} \partial_r (r \psi_\theta), \tag{2}$$

where ϕ is the scalar potential and ψ_θ is the transverse component of the vector potential $\boldsymbol{\psi}$, ∂_x is a shortcut for the partial derivative $\partial/\partial x$. For axisymmetric motion ψ_θ is the only nonzero component of $\boldsymbol{\psi}$:

$$\psi = (0, \psi_\theta, 0)^T, \tag{3}$$

where ψ_θ can in turn be written as

$$\psi_\theta = -\partial_r \eta, \tag{4}$$

so that

$$\boldsymbol{\psi} = \nabla \times (\eta \mathbf{e}_z), \tag{5}$$

where $\mathbf{e}_z$ is the unit vector in z direction.

The equations of axisymmetric motion can be written in the form (see Ref. 20, Sec. 2.13)

$$\nabla^2 \phi = \frac{1}{v_p^2} \partial_t^2 \phi, \tag{6}$$

$$\left(\nabla^2 - \frac{1}{r^2} \right) \psi_\theta = \frac{1}{v_p^2} \partial_t^2 \psi_\theta, \tag{7}$$

where v_p is the P-wave velocity, v_s is S-wave velocity, t is time, and ∇^2 is Laplace operator,

$$\nabla^2 = \partial_r^2 + r^{-1} \partial_r + \partial_z^2. \tag{8}$$

The motion of the cylinder can be found from the solution of Eqs. (6) and (7) subject to the boundary conditions on the displacements and stress tractions on the free surface of the cylinder. The displacements are given by Eqs. (1) and (2). The normal and tangential stress tractions are related to displacements using the Hooke's law,

$$\sigma_{rr} = \lambda \Delta + 2\mu \partial_r u_r, \tag{9}$$

and

$$\sigma_{rz} = \mu(\partial_z u_r + \partial_r u_z), \tag{10}$$

where $\Delta = \partial_r u_r + \partial_r r^{-1} + \partial_z u_z$ denotes the dilatation in cylindrical $r-z$ coordinates, λ and μ are the Lame parameters.

We consider the propagation of an infinite train of sinusoidal waves along the z axis of the cylinder, which is a harmonic function of z and t of the form

$$\phi = \Phi e^{i(k_z z - \omega t)}, \quad \psi_\theta = \Psi e^{i(k_z z - \omega t)}, \tag{11}$$

where ω is the angular frequency, k_z the axial wave number, and U and W are the amplitudes which are functions of r and θ. From Eq. (11) it follows that $\partial_t \phi = -\omega \phi$ and $\partial_z \phi = i k_z \phi$, etc.

B. Helmholtz equations

The two wave equations [Eqs. (6) and (7)] transformed into the $\omega - k_z$ domain by introducing Eq. (11) and dropping $e^{i(k_z z - \omega t)}$ become

$$\underbrace{\left(\partial_r^2 + r^{-1} \partial_r + \frac{\omega^2}{v_p^2} \right)}_{\mathcal{L}_{v_p}} \Phi = k_z^2 \Phi, \tag{12}$$

$$\underbrace{\left(\frac{\partial^2}{\partial r^2} + \frac{1}{r} \frac{\partial}{\partial r} - \frac{1}{r^2} + \frac{\omega^2}{v_s^2} \right)}_{\mathcal{L}_{v_s}} \Psi = k_z^2 \Psi. \tag{13}$$

Equations (12) and (13) are now ordinary differential equations containing derivatives with respect to r only and coefficients depending on frequency ω and axial wave number k_z. The aim is to find a relation between ω and k_z. This means finding a k_z for a given ω or vice versa. This can be done by solving Eqs. (12) and (13) as an eigenvalue problem so that the wave number k_z^2 represents the eigenvalue and the potentials $\Phi(r)$ and $\Psi(r)$ are the eigenvectors. Alternatively, we could rearrange Eqs. (12) and (13) so that the terms with k_z appear on the left-hand side and with ω on the right-hand side, which will give an eigenvalue problem for ω^2. For linear elasticity both approaches must give identical results.[19] However for more complicated media (say, viscoelastic or poroelastic) it is advantageous to look for k_z as a function of ω as coefficients of governing equations may themselves explicitly depend on ω.

C. Boundary conditions

The solution of Eqs. (12) and (13) should be solved subject to boundary conditions on the surface of the cylinder. In order to apply the boundary conditions, the displacements and stress components have to be expressed independent of the axial wave number k_z.

The radial and axial displacement components u_r and u_z can be expressed by substituting Eq. (11) into Eqs. (1) and (2),

$$u_r = \partial_r \Phi - \hat{\Psi}, \tag{14}$$

$$\hat{u}_z = -\underbrace{k_z^2 \Phi}_{\mathfrak{L}_{v_p}\Phi} + (\partial_r + r^{-1})\hat{\Psi},$$
(15)

where $\hat{\Psi} = ik_z\Psi$ and $\hat{u}_z = ik_zu_z$.

These expressions are used to make the stress components σ_{rr} and σ_{rz} [Eqs. (9) and (10)] solely dependent on the potentials Φ and $\hat{\Psi}$. This yields after some manipulations

$$\sigma_{rr} = \left[-\lambda\left(r^{-2} + \frac{\omega^2}{v_p^2} \right) + 2\mu\partial_r^2 \right]\Phi + 2\mu\partial_r\hat{\Psi},$$
(16)

$$\hat{\sigma}_{rz} = -2\mu\left(\partial_r^3 + r^{-1}\partial_r^2 - r^{-2}\partial_r + \frac{\omega^2}{v_p^2}\partial_r \right)\Phi + \mu\left(2\partial_r^2 \right.$$
$$\left. + 2r^{-1}\partial_r - 2r^{-2} + \frac{\omega^2}{v_s^2} \right)\hat{\Psi},$$
(17)

where $\hat{\sigma}_{rz} = ik_z\sigma_{rz}$. Equations (12)–(17) fully describe the problem of any vibrating cylindrical structures in the r–z plane.

The classical way to solve such problems would be the so-called *root-finding* approach. A general solution to Eqs. (12) and (13) is found, which is a combination of Bessel functions of different order. Substituting the solution into the boundary conditions yields a homogeneous system of linear algebraic equations. In order for this system to have non-trivial solutions, the determinant of its matrix M must be equal to zero, det $M(\omega, k_z) = 0$. This is called the frequency equation. The roots of this equation yield the dispersion relation $\omega(k_z)$. Since wave solutions in cylindrical coordinates contain various Bessel functions, it is often quite difficult to isolate and determine the various roots. Solving the frequency equation gets even more complicated in the case of leaky modes or lossy structures where solutions of the dispersion relation should be found in the complex plane.

In Sec. III an alternative approach, based on the spectral method, is presented.

III. SPECTRAL METHOD FOR AN ELASTIC CYLINDER

The spectral method bypasses the difficulties and solves the underlying Helmholtz equations numerically. For elastic wave propagation this was first implemented by Adamou and Craster,[19] who investigated circumferential waves in an elastic annulus (motion independent of r and z, see Fig. 1). In this study we extend the spectral method to axisymmetric longitudinal modes.

Subsequently the method is straightforwardly extended to the case of arbitrary n-layered fluid–solid media. The eigenvectors correspond to the potentials Φ and Ψ which are used to compute the mode shapes.

A. Polynomial interpolation

In order to solve the eigenvalue problem (12) and (13) numerically represent functions $\Phi(r)$ and $\Psi(r)$ by Chebychev polynomials. The advantage of this approach is that the derivatives of these polynomials can be computed exactly using so-called differentiation matrices. Consider a function

$f(r)$ evaluated at N interpolation points, which is represented by a vector $\mathbf{f}$ of length N. This interpolated function $\mathbf{f}^{(m)}$ is connected to its mth derivative $\mathbf{f}$ through

$$\begin{pmatrix} f_1^{(m)} \\ f_2^{(m)} \\ \vdots \\ f_N^{(m)} \end{pmatrix} \approx \underbrace{\begin{pmatrix} D_{11}^{(m)} & D_{12}^{(m)} & \cdots & D_{1N}^{(m)} \\ D_{21}^{(m)} & \ddots & & \vdots \\ \vdots & & \ddots & \vdots \\ D_{N1}^{(m)} & \cdots & \cdots & D_{NN}^{(m)} \end{pmatrix}}_{D^{(m)}} \cdot \begin{pmatrix} f_1 \\ f_2 \\ \vdots \\ f_N \end{pmatrix}.$$
(18)

This is, the mth derivative of $\mathbf{f}$ can be calculated by multiplying $\mathbf{f}$ with the $N \times N$ matrix $D^{(m)}$, which represents the DM. The N interpolation points, which are, in our case, evaluated along the radius r of the cylinder, are the N maxima of the Chebyshev polynomial of the Nth order. The Chebyshev DMs are calculated using the recursive formula for the derivatives of Chebyshev polynomials. The advantage of this approach is that the derivatives of the polynomials can be computed exactly.

The DMs may be generated using the MATLAB routine CHEBDIF.[21] The discretized $\mathbf{r}$ vector and the calculated DMs are now used to represent the differential operator $\mathfrak{L}_{vp}$ as an $N \times N$ matrix,

$$L_{v_p} = D^{(2)} + \text{diag}\left(\frac{1}{r} \right)D^{(1)} + \left(\frac{\omega^2}{v_p^2} \right)\mathbf{I},$$
(19)

where $\text{diag}(g(r))$ represents a matrix with the elements of a vector $\mathbf{g}(\mathbf{r})$ on the leading diagonal and zeros elsewhere. $\mathbf{I}$ is the identity tensor of size $N \times N$. In the same way matrix representations for all equations of motion as well as displacement and stress components are constructed.

B. Eigenvalue problem

The Helmholtz equations (12) and (13) can be combined as a matrix equation of the following form:

$$\underbrace{\begin{pmatrix} \mathfrak{L}_{v_p} & 0 \\ 0 & \mathfrak{L}_{v_s} \end{pmatrix}}_{\mathfrak{L}} \underbrace{\begin{pmatrix} \Phi \\ \hat{\Psi} \end{pmatrix}}_{\Theta} = k_z^2 \begin{pmatrix} \Phi \\ \hat{\Psi} \end{pmatrix}.$$
(20)

To solve Eq. (20) as an eigenvalue problem numerically, the differential operator matrix $\mathfrak{L}$ has to be discretized in analogy to Eq. (19). Equation (20) can now be expressed in terms of DMs where L now is a matrix of size $2N \times 2N$ matrix,

$$\underbrace{\begin{pmatrix} L_{v_p} & 0 \\ 0 & L_{v_s} \end{pmatrix}}_{L} \Theta = k_z^2 \Theta,$$
(21)

where

$$L_{vp} = D^{(2)} + \text{diag}\left(\frac{1}{r} \right)D^{(1)} + \left(\frac{\omega^2}{v_p^2} \right)\mathbf{I},$$
(22)

$$L_{vs} = D^{(2)} + \text{diag}\left(\frac{1}{r} \right)D^{(1)} - \left(\frac{1}{r^2} \right)\mathbf{I} + \left(\frac{\omega^2}{v_p^2} \right)\mathbf{I}.$$
(23)

Furthermore, the boundary conditions, also expressed in form of DMs have to be substituted. For a free solid bar, the

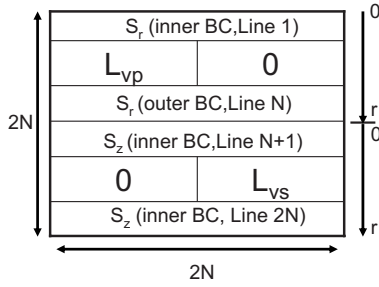FIG. 2. Structure of the $\widetilde{L}$ matrix for a cylinder.

stress-free boundary conditions are assumed at $r=a$, which means $\sigma_{rr}|_{r=a} = \sigma_{rr}|_{r=a} = 0$. σ_{rr} is the normal stress in radial direction and σ_{rz} is the radial shear stress acting in z direction.

The expressions for the stress components σ_{rr} [Eq. (16)] and σ_{rz} [Eq. (17)] can also be expressed using the DMs: The resulting equations can be written in a matrix form

$$\begin{pmatrix} \sigma_{rr} \\ \hat{\sigma}_{rz} \end{pmatrix} = \underbrace{\begin{pmatrix} S_{r\Phi} & S_{r\Psi} \\ S_{z\Phi} & S_{z\Psi} \end{pmatrix}}_{S} \begin{pmatrix} \Phi \\ \hat{\Psi} \end{pmatrix},$$

(24)

where submatrices $S_{r\Phi} S_{r\Psi} S_{z\Phi} S_{z\Psi}$ are

$$S_{r\Phi} = -\lambda[\operatorname{diag}(r^{-2}) + \omega^2/v_p^2] + 2\mu D^{(2)},$$ (25)

$$S_{z\Phi} = 2\mu D^{(1)},$$ (26)

$$S_{r\hat{\Psi}} = -2\mu\left[D^{(3)} + \operatorname{diag}\left(\frac{1}{r}\right)D^{(2)} \right.$$ (27)

$$\left. -\operatorname{diag}\left(\frac{1}{r^2}\right)D^{(1)} + (\omega^2/v_p^2)I \right],$$ (28)

$$S_{z\hat{\Psi}} = \mu\left[2D^{(2)} + 2\operatorname{diag}\left(\frac{1}{r}\right)D^{(1)} \right.$$ (29)

$$\left. -\operatorname{diag}\left(\frac{1}{r^2}\right) + (\omega^2/v_s^2)I \right].$$ (30)

The last step is to embed appropriate boundary conditions in the matrix representation and replace matrix L with matrix $\widetilde{L}$ as shown in Fig. 2. The lines in the L matrix in Eq. (21) corresponding to $r=a$ will be replaced by the corresponding lines of the S matrix. In order to fulfill the stress free boundary conditions, the corresponding values on the right-hand side have to be set equal to zero. In addition, for the lines at $r=0$ the same has to be done. The reason for that is that due to the singularities of the equations at $r=0$ we have to consider a hollow cylinder with a very small inner radius, which is a limiting case for a solid cylinder.

This can be done by introducing a matrix Q on the right-hand side of Eq. (21),

$$\widetilde{L}\Theta = k_z^2 Q\Theta,$$ (31)

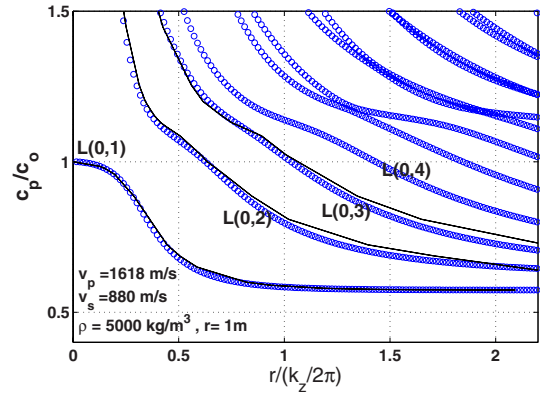which is a $2N \times 2N$ matrix and defined as follows:

FIG. 3. (Color online) Dispersion curves of an elastic cylinder (circles). x axis: Wave-number-radius product, y axis: Phase velocity $v_{ph} = \omega/k_z$ normalized by the bar velocity $v_0^2 = E/\rho$ where E is the Young's modulus and ρ is density [compare with Davies (Ref. 22, Sec. 11, Fig. 13, lines)].

$$Q = \begin{pmatrix} M & 0 \\ 0 & M \end{pmatrix}.$$ (32)

Here M is a diagonal matrix which has the following form:

$$M = \begin{pmatrix} 0 & & & & \\ & 1 & & & \\ & & \ddots & & \\ & & & 1 & \\ & & & & 0 \end{pmatrix}.$$ (33)

Equation (31) is a generalized eigenvalue problem, which means that we cannot find the inverse M^{-1} as $\det(M)=0$. But generalized eigenvalue problems can be solved using the MATLAB routine $\mathrm{EIG}(\widetilde{L},Q)$ for instance.

In the next section this approach can be extended to n arbitrary cylindrical fluid and solid layers.

C. Dispersion curves

Let us illustrate the results produced by this approach in the form of dispersion curves (Fig. 3). To compare with previous results obtained by root-finding techniques, we use a model presented by Davies.[22] In Fig. 3 the dispersion curves for a free solid bar are computed (circles) with the parameters shown in the picture. These curves are in good agreement (lines) with the dispersion curves provided in Davies,[22] (Fig. 4) which were calculated analytically using root-finding techniques. The fundamental mode $L(0,1)$ behaves like a pure extensional mode for low frequencies and propagates with the velocity $\sqrt{E/\rho}$ where E is the Young's modulus and ρ is density. For higher frequencies the mode propagates like a Rayleigh wave on the cylinder surface. The higher modes $(L(0,1)\ldots L(0,n))$ have cut-off frequencies, which means they do not exist below these frequencies. For very high frequencies they tend to propagate close to the Rayleigh velocity.

IV. MULTIPLE LAYERS

The above-described approach can be extended to n cylindrical fluid and solid layers (see Fig. 4). Each of the n
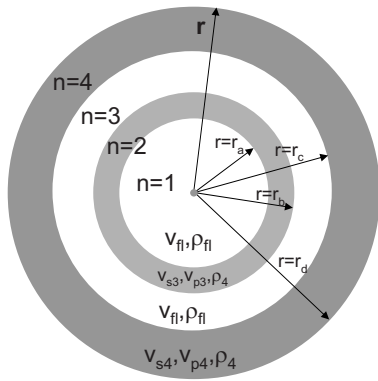
FIG. 4. Geometry of a model with four cylindrical layers. The layer index is $n=1-4$ numbered from the center to the surface of the bar. The layers are either nonviscous fluid (v_{fl}, ρ_{fl}) or elastic solid $(v_{pn}, v_{sn}, \rho_{fl})$.

FIG. 5. Structure of the matrix $\tilde{L}$ for n layers.

layers has P- and S-wave velocities $(v_{p_1}, \ldots, v_{p_n}, v_{s_1}, \ldots, v_{s_n})$ and densities $\rho_1, \ldots, \rho_n$. In this work we represent the fluid layers as solids with very small shear velocity. For each of the layers the matrix L_n is constructed in analogy to Eq. (21). These matrices are combined in a diagonal matrix of the size $n2N \times n2N$ which has the form

$$L = \begin{pmatrix} L_1 & 0 & 0 \\ 0 & \ddots & 0 \\ 0 & 0 & L_n \end{pmatrix}. \tag{34}$$

The same procedure has to be followed for the stress components S_n [see Eq. (24)] and for each layer n which are finally combined in a matrix S of same size as L. A similar matrix U is computed for the displacement components.

For the case of layering, additional conditions of continuity of displacements and stresses have to be introduced,

$$[\sigma_{rr}]|_{r=r_i} = [\sigma_{rz}]|_{r=r_i} = 0, \tag{35}$$

$$[u_r]|_{r=r_i} = [u_z]|_{r=r_i} = 0, \tag{36}$$

where r_i indicates the position of the interface of the nth layer with $i = a, b, \ldots$.

The interface conditions are introduced as the vanishing differences of the displacements and stresses of the corresponding layers. It is convenient to apply the conditions as illustrated in Fig. 5, which shows in which lines of the L matrix for n layers all boundary conditions have to be introduced. The stress-free boundary conditions on the inner and outer boundary are introduced in the L matrix the same way as for a free cylinder in the rows (1, $N+1$, $n2N-N$ and $n2N$).

This means that the elements of S and U representing the interpolation points of the inner and outer boundary and the interfaces replace the corresponding rows in the L matrix, which is now referred to as $\tilde{L}$. The eigenvalue problem can now be formulated analogous to Eq. (31) and solved using a generalized eigenvalue routine.

Dispersion curves: Fluid-filled cylinder. The second example (Fig. 6) is a two-layer model: A fluid-filled cylinder. The dispersion curves were originally calculated by Del Grosso and McGill.[9] Here the dispersion curves (lines) were computed by Sidorov using the *root-finding* technique analo-

gous to that of Ref. 9. Again we were able to reproduce these results accurately using the spectral method. The dispersion curves referred to as ETn are for stress free surface boundary conditions, while the Rn modes were computed for rigid surface boundary conditions.

In the case of a stress free surface there exist two fundamental modes starting from zero frequency: The first one (ET0) is commonly referred to as a tube wave or Stoneley wave, while the second (ET1) is an analog of a (longitudinal) plate or extensional wave. Mode ET1 only weakly depends on the fluid properties and disappears when the thickness of the cylinder wall increases to infinity or the outer boundary of the cylinder becomes rigid (Rn).
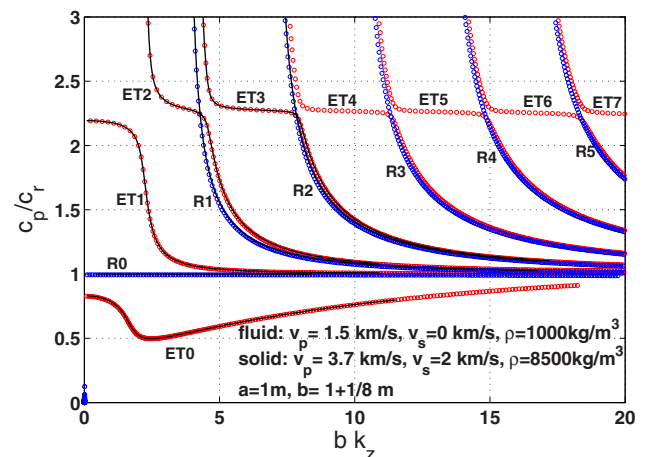

FIG. 6. (Color online) Dispersion curves for a hollow cylinder filled with nonviscous fluid. Thickness of the cylinder wall: 0.125 m. Modes in elastic tube with stress-free outer boundary: ET$_n$, whereas modes for pipe with rigid outer boundary: R_n. Phase velocity v_{ph} is normalized by the velocity of the fluid ($v_{p,fl}$) [compare with Del Grosso and McGill (Ref. 9), lines].
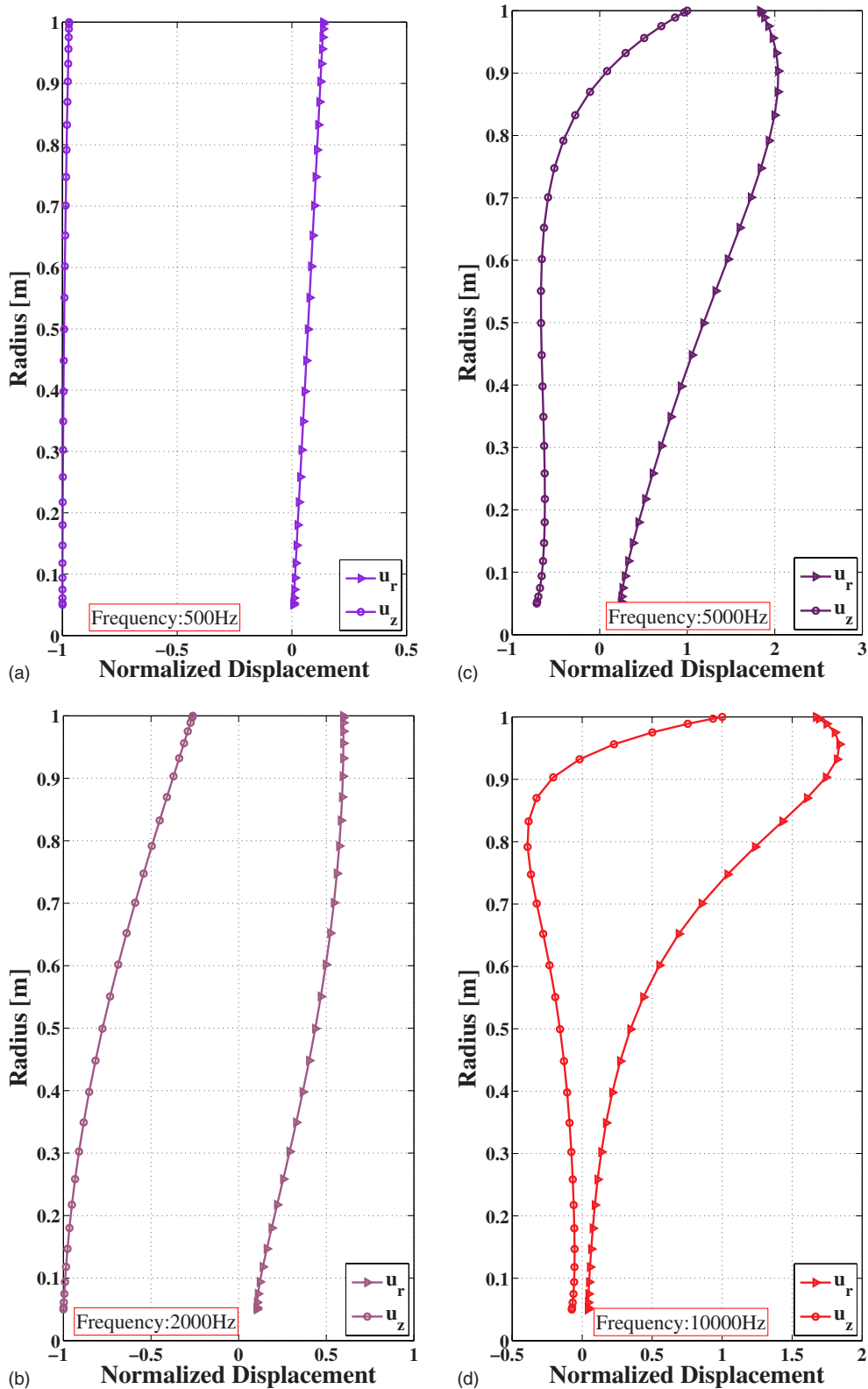
FIG. 7. (Color online) Particle displacement profiles of the fundamental longitudinal mode $L(0,1)$ for (a) 500 Hz, (b) 2000 Hz, (c) 5000 Hz, (d) 10 000 Hz. x axis: Normalized $u_r = |u_r|$ (triangle) and $u_z = i|u_z|$ (circle) displacement. y axis: Bar radius from 0 m (center of bar) to 1 m (surface of bar).

V. PARTICLE DISPLACEMENT PROFILES

In addition to eigenvalues representing dispersion curves, we also obtain eigenvectors representing the potentials Φ and Ψ. They allow the computation of the mode shapes, that is the distribution of field quantities for each

mode like displacements, stresses, power flow, etc., along the radius of the cylinder. Figure 7 shows the displacements (u_r, u_z) which can be easily computed using the eigenvectors and Eqs. (4) and (5). In order to display the particle displacement profiles u_r and u_z are calculated along the radius for a

certain frequency. These values are normalized by the maximum absolute value of the u_z displacement. Finally the radial displacement is plotted as $u_r = |u_r|$ and the longitudinal displacement as $u_z = \text{Im}|u_z|$.

For the illustration of the displacement profiles we have chosen the fundamental mode $L(0,1)$ propagating in a free solid cylinder (see Fig. 1). The particle motions u_r and u_z are computed for four different frequencies. Figures 7(a)–7(d) display the displacement profiles for u_r and u_z for the different frequencies.

For low frequencies (500 Hz) [Fig. 7(a)] the wave propagates like a longitudinal body wave. Consequently the particle motion is in the axial direction mainly and uniform throughout the radius of the cylinder. The radial displacement is very small.

In Fig. 7(b) we can see that for 2000 Hz the u_r displacement has already significantly increased all over the cross section. It only remains zero in the center of the cylinder. At the same time the u_z displacement decreases but keeps its maximum value in the center.

For a higher frequency [5000 Hz; Fig. 7(c)] it can be observed that the shape of the displacement profiles evolves slowly toward the typical pattern of Rayleigh modes. Close to the surface ($r = 0.85 - 1$ m) the motion is already Rayleigh-like. Only toward the center of the bar is the u_z component still relatively strong.

Finally in Fig. 7(d) we get the typical particle motion profile of Rayleigh waves. In contrast to Fig. 7(c) obviously the amplitudes of both displacement components decrease significantly for $r < 0.8$ m.

VI. CONCLUSIONS

We extended and implemented the spectral method for propagation of axisymmetric modes in a cylindrical bar. The method was also generalized to *n*-layered cylindrical fluid–solid structures. Numerical examples for a free solid cylinder and a fluid-filled tube were given in the form of dispersion curves and particle displacement profiles. Traditional techniques require finding complex roots of nonlinear equations that involve special functions. In contrast, spectral method demands only solving generalized eigenvalue problem without involving special functions. This represents a great simplification that becomes particularly advantageous for complex rheologies like viscoelastic, anisotropic, and poroelastic structures.

There are a lot of directions for further work. One scope is the extension to more complicated media like viscoleasticity and poroelasticity. The approach can also be extended for anisotropic and heterogeneous media. Of great importance will also be to allow unbounded structures, representing a borehole surrounded by infinite rock formation. Finally it would be of great importance to be able to compute the full wave form using the spectral method.

[1] L. Pochhammer, "On the propagation velocities of small oscillations in an unlimited isotropic circular cylinder," J. Reine Angew. Math. **81**, 324–336 (1876).

[2] C. Chree, "The equations of an isotropic elastic solid in polar and cylindrical coordinates, their solutions and applications," Trans. Cambridge Philos. Soc. **14**, 250–369 (1889).

[3] A. E. H. Love, *A Treatise on the Mathematical Theory of Elasticity* (Dover, New York, 1944).

[4] H. Kolsky, *Stress Waves in Solids* (Dover, New York, 1963).

[5] D. Bancroft, "The velocity of longitudinal waves in cylindrical bars," Phys. Rev. **59**, 588–593 (1941).

[6] D. C. Gazis, "Three-dimensional investigation of the propagation of waves in hollow circular cylinders. I. Analytical foundation," J. Acoust. Soc. Am. **31**, 568–573 (1959).

[7] D. C. Gazis, "Three-dimensional investigation of the propagation of waves in hollow circular cylinders. II. Numerical results," J. Acoust. Soc. Am. **31**, 573–578 (1959).

[8] J. A. McFadden, "Radial vibrations of thick-walled hollow cylinders," J. Acoust. Soc. Am. **26**, 714–715 (1954).

[9] V. A. Del Grosso and R. E. McGill, "Remarks on 'Axially symmetric vibrations of a thin cylindrical elastic shell filled with nonviscous fluid' by Ram Kumar, Acustica 17 [1968], 218," Acustica **20**, 313–314 (1968).

[10] T. Lin and G. Morgan, "Wave propagation through a fluid contained in a cylindrical, elastic shell," J. Acoust. Soc. Am. **28**, 1165–1176 (1956).

[11] S. I. Rubinow and J. B. Keller, "Wave propagation in a fluid-filled tube," J. Acoust. Soc. Am. **50**, 198–223 (1971).

[12] V. N. R. Rao and J. K. Vandiver, "Acoustics of fluid filled boreholes with pipe: Guided propagation and radiation," J. Acoust. Soc. Am. **105**, 3057–3066 (1997).

[13] G. W. Morgan and J. P. Kiely, "Wave propagation in a viscous liquid contained in a flexible tube," J. Acoust. Soc. Am. **26**, 323–328 (1954).

[14] J. Vollmann, R. Breu, and J. Dual, "High-resolution analysis of the complex wave spectrum in a cylindrical shell containing a viscoelastic medium. II. Experimental results versus theory," J. Acoust. Soc. Am. **102**, 909–920 (1997).

[15] J. Vollmann and J. Dual, "High-resolution analysis of the complex wave spectrum in a cylindrical shell containing a viscoelastic medium. I. Theory and numerical results," J. Acoust. Soc. Am. **102**, 896–908 (1997).

[16] J. G. Berryman, "Dispersion of extensional waves in fluid-saturated porous cylinders at ultrasonic frequencies," J. Acoust. Soc. Am. **74**, 1805–1812 (1983).

[17] G. H. F. Gardner, "Extensional waves in fluid-saturated porous cylinders," J. Acoust. Soc. Am. **34**, 36–39 (1962).

[18] C. J. Wisse, D. M. J. Smeulders, G. Chao, and M. E. H. van Dongen, "Guided wave modes in porous cylinders: Theory," J. Acoust. Soc. Am. **122**, 2049–2056 (2007).

[19] A. T. I. Adamou and R. V. Craster, "Spectral methods for modelling guided waves in elastic media," J. Acoust. Soc. Am. **116**, 1524–1535 (2004).

[20] J. D. Achenbach, *Wave Propagation in Elastic Solids* (North Holland, Amsterdam, 1973).

[21] J. A. C. Weideman and S. C. Reddy, "A MATLAB differentiation matrix suite," ACM Trans. Math. Softw. **26**, 465–519 (2000).

[22] R. M. Davies, "A critical study of Hopkinson pressure bar," Proc. R. Soc. London, Ser. A **240**, 375–457 (1948).

CHAPTER 2

Modeling of axisymmetric wave modes in a poroelastic
cylinder using spectral method

Modeling of axisymmetric wave modes in a poroelastic cylinder using spectral method

Florian Karpfinger and Boris Gurevich[a]
*Department of Exploration Geophysics, Curtin University of Technology, GPO Box U1987,
Perth, Western Australia 6845, Australia*
florian.karpfinger@postgrad.curtin.edu.au, B.Gurevich@curtin.edu.au

Andrey Bakulin[b]
WesternGeco, 10001 Richmond Ave., Houston, Texas 77042
abakulin@slb.com

Abstract: Algorithm and code are presented which solve the dispersion equation for cylindrical poroelastic structures. The algorithm is based on the spectral method, which discretizes the underlying wave equations with the help of spectral differentiation matrices and solves the corresponding equations as a generalized eigenvalue problem. The results are illustrated for the case of a fluid-saturated free cylinder with open- and closed-pore boundary conditions on its surface. The computed dispersion curves are in good agreement with analytical results, which confirms the accuracy of the method.
© 2008 Acoustical Society of America

1. Introduction

Modeling wave propagation modes in cylindrical structures is important for the understanding and quantitative interpretation of acoustic and seismic measurements in hydrocarbon wells, pipelines, as well as laboratory measurements. For porous materials these waves are affected by material permeability. These effects can be analyzed using Biot's equations of poroelasticity (Biot 1956a, b, 1962).

For a porous cylinder with open-pore boundary conditions on its surface this was first done by Gardner (1962), who derived the dispersion equation for extensional waves at low frequencies. For the full frequency range and closed boundary conditions the dispersion in a fluid-saturated cylinder was studied by Berryman (1983).

This was done for the first few modes because conventional *root finding* becomes challenging for poroelastic media. An alternative approach to modeling wave propagation in circular structures was recently introduced by Adamou and Craster (2004) based on the spectral method.

Karpfinger *et al.* (2008) extended the spectral method to axisymmetric waves for arbitrary fluid and solid layers. In this letter we extend the spectral method to cylindrical poroelastic structures.

2. Biot's thory of poroelasticity

Waves propagating in a poroelastic medium satisfy the following equations (Biot, 1962):

$$\boldsymbol{\nabla} \cdot \boldsymbol{\sigma} = - \omega^2 (\rho \mathbf{u} + \rho_f \mathbf{w}), \tag{1}$$

---

[a]Also at CSIRO Petroleum, ARRC, 26 Dick Perry Ave., Kensington, Perth, Western Australia 6151, Australia.
[b]Present address: Shell International Exploration & Production Inc., Houston, Texas.

$$\nabla p = \omega^2(\rho_f \mathbf{u} + q\mathbf{w}), \tag{2}$$

where the field variables are the solid $\mathbf{u}$ and the average solid–fluid displacement $\mathbf{w} = \phi(\mathbf{U} - \mathbf{u})$, ϕ is the porosity, and $\mathbf{U}$ is the fluid displacement. ρ and ρ_f are the densities of the porous material and the fluid, respectively. The frequency-dependent density term $q(\omega)$ is responsible for the viscous and inertial coupling between the solid and fluid phases (Biot, 1956b). The total stress tensor $\boldsymbol{\sigma}$ and the fluid pressure p are related to the field vectors by the constitutive equations

$$\boldsymbol{\sigma} = [(H - 2\mu)\, \boldsymbol{\nabla} \cdot \mathbf{u} + \alpha M \boldsymbol{\nabla} \cdot \mathbf{w}]\mathbf{I} + \mu[\boldsymbol{\nabla}\mathbf{u} + \boldsymbol{\nabla}\mathbf{u}^T], \tag{3}$$

$$p = -M \boldsymbol{\nabla} \cdot \mathbf{w} - \alpha M \boldsymbol{\nabla} \cdot \mathbf{u}. \tag{4}$$

The stress–strain relations, Eqs. (3) and (4), are defined in terms of the shear modulus of the skeleton μ and two poroelastic material constants M and H which are related to the bulk moduli of the fluid K_f, the grain material K_g, and the skeleton K. This relation is given by the Gassmann equations (Gassmann, 1951).

Substituting the constitutive relations, Eqs. (3) and (4), into Eqs. (1) and (2), we obtain two coupled wave equations. In order to decouple these equations into separate equations for the three bulk waves the displacements can be written in terms of potentials.

For time-harmonic oscillations this yields Helmholtz equations for the shear waves

$$(\nabla^2 + k_s^2)\boldsymbol{\beta} = 0, \quad \chi = -\frac{\rho_f}{q}\boldsymbol{\beta}, \tag{5}$$

and for the compressional waves

$$(\nabla^2 + k_\pm^2)A_\pm = 0. \tag{6}$$

Here $A_\pm$ is a linear combination of the scalar potentials Υ and ψ. $\boldsymbol{\beta}$ and χ are vector potentials, k_s is the wave number of the shear wave, and k_+ and k_- are the wave numbers of the fast and slow longitudinal waves, respectively. These wave numbers give the dispersion in an infinite poroelastic medium.

In order to distinguish between the torsional and extensional components of the wave field, the potential $\boldsymbol{\beta}$ is further decomposed as $\boldsymbol{\beta} = \hat{\mathbf{z}}\beta_1 + \boldsymbol{\nabla} \times (\hat{\mathbf{z}}\beta_2)$, where $\hat{\mathbf{z}}$ is the unit vector in z direction. For axisymmetric modes only β_2 is nonzero. Due to the symmetry of the system, Eqs. (3)–(6), expressed in cylindrical coordinates, describe the axisymmetric wave propagation in a poroelastic cylinder.

3. The Poroelastic eigenvalue problem

With the help of the *root-finding* technique, the velocity dispersion for a porous cylinder can be obtained, but can be very difficult to compute for a poroelastic medium (as it requires finding numerous complex roots of a cumbersome dispersion equation involving Bessel functions).

The spectral method bypasses these difficulties and solves the underlying Helmholtz equations numerically. For elastic wave propagation this was first implemented by Adamou and Craster (2004), who investigated circumferential waves in an elastic annulus. The problem is solved by numerical interpolation using spectral differentiation matrices (DM's). This approach is explained in detail for axisymmetric waves in cylindrical structures in Karpfinger *et al.* (2008).

To apply the spectral method to the cylindrical poroelastic problem, Eqs. (5) and (6) can be presented as the following eigenvalue problem

$$\underbrace{\begin{pmatrix} L_+ & 0 & 0 \\ 0 & L_{v_s} & 0 \\ 0 & 0 & L_- \end{pmatrix}}_{L} \underbrace{\begin{pmatrix} A_+ \\ \beta_2 \\ A_- \end{pmatrix}}_{\Theta} = k_z^2 \begin{pmatrix} A_+ \\ \beta_2 \\ A_- \end{pmatrix}. \tag{7}$$

The differential operators $L_\pm$ and L_s are discretized using DMs (Karpfinger *et al.*, 2008) and combined in a $3N \times 3N$ matrix. N is the number of Chebyshev points discretizing the cylinder along its radius.

In order to solve Eq. (7), appropriate boundary conditions have to be incorporated (Deresiewicz and Skalak, 1963). For a porous-vacuum interface two scenarios can be considered: open- or closed-pore boundary conditions. Open-pore boundary conditions on the free surface of the cylinder $r=a$ are

$$\sigma_{rr}|_{r=a} = \sigma_{rz}|_{r=a} = -p_f|_{r=a} = 0. \tag{8}$$

In addition to the zero stress, the fluid pressure is zero on the surface and fluid can thus flow across the interface. For a closed surface, the boundary conditions become

$$\sigma_{rr}|_{r=a} = \sigma_{rz}|_{r=a} = 0, \qquad w_r|_{r=a} = 0. \tag{9}$$

The pore pressure condition is replaced by the condition that relative motion of fluid with respect to solid is zero on the surface of the cylinder.

Such boundary conditions thus have to be set within Eq. (7). In order to achieve this, the stress components σ_{rr}, σ_{rz}, and $-p$ are grouped in a matrix of the same size

$$\begin{pmatrix} \sigma_{rr} \\ \sigma_{rz} \\ -p \end{pmatrix} = \underbrace{\begin{pmatrix} S_{rr}^+ & S_{rr}^s & S_{rr}^- \\ S_{rz}^+ & S_{rz}^s & S_{rz}^- \\ S_p^+ & S_p^s & S_p^- \end{pmatrix}}_{S} \cdot \begin{pmatrix} A_+ \\ \beta_2 \\ A_- \end{pmatrix}, \tag{10}$$

where the components of **S** are separated in terms of fast longitudinal wave, shear wave, and slow longitudinal wave.

A similar matrix can be introduced for the components of displacement

$$\begin{pmatrix} u_r \\ u_z \\ w_r \end{pmatrix} = \underbrace{\begin{pmatrix} T_{rr}^+ & T_{rr}^s & T_{rr}^- \\ T_{rz}^+ & T_{rz}^s & T_{rz}^- \\ T_p^+ & T_p^s & T_p^- \end{pmatrix}}_{T} \cdot \begin{pmatrix} A_+ \\ \beta_2 \\ A_- \end{pmatrix}, \tag{11}$$

where the components of the $3N \times 3N$ matrix **T** are arranged in analogy to **S**.

The last step is to combine these displacements and stress components with the equations of motion, in an appropriate way, in order to solve the problem for such boundary conditions. This means that the rows of **S** and/or **T** representing the points at the outer boundary (N, $2N$, and $3N$) replace the corresponding rows in the **L** matrix. The modified matrix is now denoted by $\tilde{\mathbf{L}}$. Boundary conditions are introduced by setting the corresponding rows to zero on the right-hand side. The eigenvalue problem can now be formulated in the form

$$\tilde{L}\Theta = k_z^2 Q\Theta, \tag{12}$$

where Q is a $3N \times 3N$ diagonal matrix with zeros elements in rows corresponding to the points on the surface and ones in all other diagonal elements. Equation (12) is a generalized eigenvalue
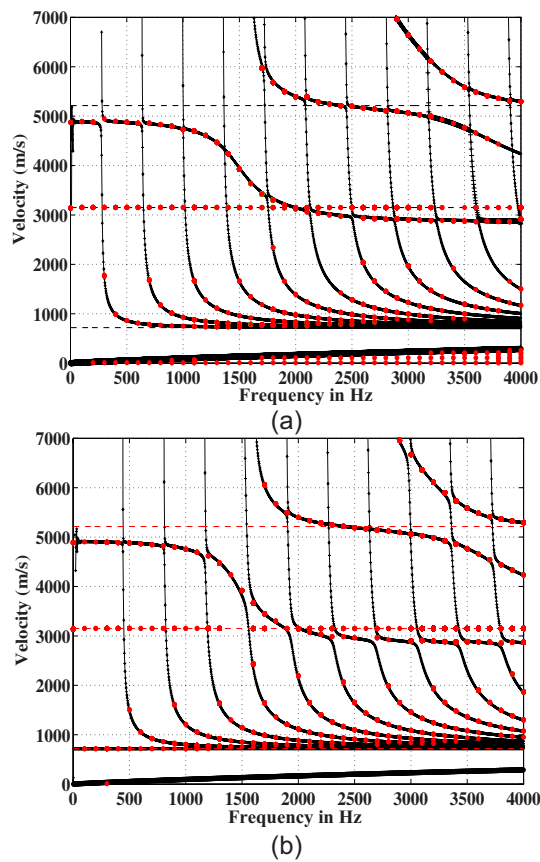
Fig. 1. (Color online) Dispersion curves for open-pore (a) and closed (b) boundary conditions; spectral method (positive signs); *root finding* (dots); and the dashes show explicitly the fast and slow *P* waves and the shear wave velocities.

problem, which means that we cannot find the inverse Q^{-1} as $\det(Q)=0$, but it can be solved with numerical eigenvalue routines.

4. Dispersion curves

Solution of Eq. (12) yields wave numbers k_z for a given frequency. Repeating this for various frequencies allows the computation of dispersion curves. To illustrate the results, in Figs. 1(a) and 1(b) dispersion curves are computed of a porous cylinder with open and closed boundary conditions, respectively. This is done for the case of high permeability which corresponds to the high frequency limit of Biot's theory where the slow *P* wave is propagatory. The parameters chosen are the same as in Berryman (1983).The permeability used in this study is $k_0=24.4$ darcy and the radius of the cylinder is 1 m. The positive sign (+) indicates the results computed with the spectral method. They are overlayed with the analytical solution obtained with *root-finding* method (dots). The dashed lines show the velocity of the fast *P* wave, the shear wave, and the slow *P* wave, respectively.

      In both cases the dispersion curves show a very good agreement between the results for spectral method (+) and the *root-finding* approach. Due to a very high computational effort of *root finding*, only a few points were computed. The spectral method is about 1000 times more efficient.

In the low and high frequency limit the extensional mode velocity agrees with the values calculated by Berryman (1983) for both types of boundary conditions. The extensional mode propagates for low frequencies with 4910 m/s, while for high frequencies the limit is the Rayleigh velocity 2890 m/s.

Figure 1(a) shows singularities in the main extensional mode. Berryman (1983) observed these singularities and discussed their connection to Biot's slow wave. Figure 1(a) shows that these singularities are connected to higher modes of Biot's slow wave. These higher modes propagate, for frequencies higher than the first cut-off frequency (~270 Hz), with the Biot slow wave velocity. At the cut-off frequencies they go to infinity and cross over with the extensional mode where the interaction between the two modes causes the distortion of the dispersion curve of the extensional mode. The nature of the higher modes can be explained using the analogy with waves along a water column. In the high frequency limit of Biot's theory, the fluid phase can be considered as an independent fluid column. Since a fluid has zero Young's modulus, at zero frequency no slow extensional mode exists (Rubinow and Keller, 1971).

Overall, the result for closed-pore boundary conditions [Fig. 1(b)] looks similar to that of open-pore boundary conditions. The major difference is that now the slow extensional mode can be observed down to zero frequency. This is in agreement with Feng and Johnson (1983), who showed that the extensional Biot slow wave becomes a propagating mode for a closed interface. The fast extensional mode is again distorted by the higher modes of the Biot slow wave at the cut-off frequencies. The cut-off frequencies are shifted toward higher frequencies. Such modes can be explained in the same way as for open boundary conditions. Due to the closed boundary conditions, the fluid phase is analogous to the fluid in a closed solid tube (Rubinow and Keller, 1971). Thus a tube wave exists down to zero frequency. For both boundary conditions the shear wave velocity is a root of the dispersion equation in agreement with Berryman (1983). This is not the case for the spectral method.

5. Conclusions

We conclude that the spectral method provides an efficient and precise tool for the analysis of wave dispersion in poroelastic cylindrical structures. The results of the spectral method are in very good agreement with the analytical results. The advantage of this approach is that, in contrast to traditional methods, it is easier to implement and faster by a factor of approximately 1000. For multilayered structures the advantages of the spectral method will be even more significant. The results for a single poroelastic cylinder show that the singularities of the dispersion curve for the fast extensional mode correspond to intersections with the high order slow extensional modes.

References and links

Adamou, A. T. I., and Craster, R., V. (**2004**). "Spectral methods for modelling guided waves in elastic media," J. Acoust. Soc. Am. **116**, 1524–1535.

Berryman, J. G. (**1983**). "Dispersion of extensional waves in fluid-saturated porous cylinders at ultrasonic frequencies," J. Acoust. Soc. Am. **74**, 1805–1812.

Biot, M. A. (**1956a**). "Theory of propagation of elastic waves in a fluid-saturated porous solid. I. Low-frequency range," J. Acoust. Soc. Am. **28**, 168–178.

Biot, M. A. (**1956b**). "Theory of propagation of elastic waves in a fluid-saturated porous solid. II. Higher frequency range," J. Acoust. Soc. Am. **28**, 179–191.

Biot, M. A. (**1962**). "Generalized theory of acoustic propagation in porous dissipative media," J. Acoust. Soc. Am. **34**, 1254–1264.

Deresiewicz, H., and Skalak, R. (**1963**). "On uniqueness in dynamic poroelasicity," Bull. Seismol. Soc. Am. **53**, 783–788.

Feng, S., and Johnson, D. L. (**1983**). "High-frequency acoustic properties of a fluid/porous solid interface. i. New surface mode," J. Acoust. Soc. Am. **74**, 906–914.

Gardner, G. H. F. (**1962**). "Extensional waves in fluid-saturated porous cylinders," J. Acoust. Soc. Am. **34**, 36–39.

Gassmann, F. (**1951**). "Über die elastizität poröser medien," Vierteljahrsschr. Natforsch. Ges. Zur. **96**, 1–23.

Karpfinger, F., Gurevich, B., and Bakulin, A. (**2008**). "Computation of wave propagation along cylindrical structures using the spectral method," J. Acoust. Soc. Am. **124**(2), 859–865.

Rubinow, S. I., and Keller, J. B. (**1971**). "Wave propagation in a fluid-filled tube," J. Acoust. Soc. Am. **50**, 198–223.

CHAPTER 3

Axisymmetric waves in fluid-saturated porous structures

Abstract

A new numerical approach for simulating wave propagation in cylindrically layered poroelastic structures is presented. Dispersion of free modes for an arbitrary number of fluid, elastic and poroelastic layers is computed. The algorithm is based on spectral method, meaning that the underlying equations are discretized using spectral differentiation matrices. Thus the problem can be formulated as a generalized algebraic eigenvalue problem. For a given frequency, the eigenvalues correspond to the axial wavenumbers of different modes. The advantage of this approach, compared to root-finding techniques, is that it can be more efficient as searching and separating the roots in the complex plane can be difficult task especially for poroelasticity. Dispersion curves for an open borehole in a poroelastic formation are presented and benchmarked by comparing the results to a low-frequency approximation. In addition, a more complicated model considering an altered zone of reduced permeability between the borehole and the formation is considered.

Introduction

In the petroleum industry, borehole acoustic measurements are performed in order to characterize subsurface formation properties. One very desirable quantity is the mobility (ratio of formation permeability and pore fluid viscosity). The mobility is one of the most valuable information for petroleum engineers as it defines how well petroleum reservoirs flow. The problem is that the direct measurement of mobility downhole is very difficult. Acoustic measurements are the only direct method to estimate permeability because Stoneley waves are sensitive to the mobility of the surrounding formation (Chang et al. [1]; Winkler et al. [2]). At low frequencies Stoneley wave dominates wave propagation in a borehole. It is characterized by compression of the fluid column resulting in a piston-like motion of fluid. If the formation is permeable this motion will cause the fluid to oscillate across the borehole

Florian Karpfinger, Curtin Uni. of Technology, GPO Box U1987, Perth, WA, Australia.
Boris Gurevich, Curtin University of Technology & CSIRO Petroleum, GPO Box U1987, Perth, WA, Australia.
Andrey Bakulin, WesternGeco , 10001 Richmond Ave., Houston, TX 77042, USA.

wall which changes the signature of the Stoneley: velocity decreases and attenuation increases with increasing mobility of the formation.

In practice clay particles present in the borehole mud may build a thin layer called mudcake. The mudcake can be described as a thin elastic layer. Membrane stiffness controls the flexing of the mudcake into the pores of the formation. Liu et al. [3] introduce new boundary condition that takes into account the mudcake and effect of a pressure gradient between the borehole and the poroelastic formation.

To study propagation if tube waves in boreholes, we applied a new approach. In contrast to the traditional root-finding approach, which needs to find the roots of the dispersion equation in the complex plane, we use spectral method that bypasses these difficulties by discretizing the underlying equations using Chebyshev differentiation matrices. This approach has been originally introduced by Adamou and Craster [4] for circumfential waves in an elastic annulus. It was recently developed for axisymmetric wave propagation in cylindrical elastic structures with fluid and solid layers by Karpfinger et al. [5] and later expanded for poroelastic layers (Karpfinger et al. [6]).

1. Biot's theory of poroelasticity

Waves propagating in a poroelastic medium satisfy the following equations (Biot [7]):

$$\nabla \cdot \boldsymbol{\sigma} = -\omega^2 \left(\rho \mathbf{u} + \rho_f \mathbf{w} \right) \tag{1.1}$$

$$\nabla p = \omega^2 \left(\rho_f \mathbf{u} + q\mathbf{w} \right) \tag{1.2}$$

where the field variables are the solid displacement $\mathbf{u}$ and the average solid-fluid displacement $\mathbf{w} = \phi(\mathbf{U} - \mathbf{u})$, ϕ is the porosity, $\mathbf{U}$ is the fluid displacement and ω is the angular frequency. ρ and ρ_f are the densities of the porous material and the fluid, respectively. The frequency-dependent density term q is responsible for the viscous and inertial coupling between the solid and fluid phases (Biot, [8]). The total stress tensor $\boldsymbol{\sigma}$ and the fluid pressure p are related to the field vectors by the following constitutive equations

$$\boldsymbol{\sigma} = \left[(H - 2\mu)\nabla \cdot \mathbf{u} + \alpha M \nabla \cdot \mathbf{w} \right] \mathbf{I} + \mu \left[\nabla \mathbf{u} + \nabla \mathbf{u}^T \right] \tag{1.3}$$

$$p = -M \nabla \cdot \mathbf{w} - \alpha M \nabla \cdot \mathbf{u} \tag{1.4}$$

The stress-strain relations, (1.3) and (1.4), are defined in terms of the shear modulus of the skeleton μ and two poroelastic material constants M and H which are related to the bulk moduli of the fluid K_f, the grain material K_g and the skeleton K (Gassmann, [9]).

Substituting the constitutive relations eqs. (1.3) and (1.4) into eqs. (1.1) and (1.2) we obtain two coupled wave equations. In order to decouple these equations into separate equations for the three bulk waves the displacements can be written in terms of potentials. For time-harmonic oscillations this yields Helmholtz equations for shear and compressional waves

$$\left(\nabla^2 + k_s^2 \right) \boldsymbol{\beta} = 0, \quad \boldsymbol{\chi} = -\frac{\rho_f}{q} \boldsymbol{\beta}, \quad \left(\nabla^2 + k_\pm^2 \right) A_\pm = 0, \tag{1.5}$$

where $A_\pm$ are the scalar potentials and $k_\pm$ are the wave numbers of the fast (+) and slow (-) longitudinal wave. $\boldsymbol{\beta}$ and $\boldsymbol{\chi}$ are vector potentials and k_s is the wave

number of the shear wave. These wave numbers provide dispersion in an infinite poroelastic medium. In order to distinguish between the torsional and extensional components of the wavefield, the potential $\boldsymbol{\beta}$ is further decomposed as $\boldsymbol{\beta} = \hat{\mathbf{z}}\beta_1 + \nabla \times (\hat{\mathbf{z}}\beta_2)$ where $\hat{\mathbf{z}}$ is the unit vector in z-direction. For axisymmetric modes only β_2 is non zero. Due to the symmetry of the system, eqs. (1.3)-(1.5), expressed in cylindrical coordinates, describe the axisymmetric wave propagation in a poroelastic cylinder.

2. Underlying equations in cylindrical coordinates

The wave equations (1.5) are expressed in the $\omega - k_z$ domain using a plane wave solution of the form $\left[A_{\pm}, \beta_2\right] = \left[a_{\pm}, \gamma_s\right]e^{i(k_z - \omega t)}$ and cylindrical coordinates as

$$\underbrace{\left(\partial_r^2 + \frac{1}{r}\partial_r + \frac{\omega^2}{v_{\pm}^2}\right)}_{L_{\pm}}a_{\pm} = k_z^2 a_{\pm}, \quad \underbrace{\left(\partial_r^2 + \frac{1}{r}\partial_r - \frac{1}{r^2} + \frac{\omega^2}{v_s^2}\right)}_{L_s}\tilde{\gamma}_s = k_z^2\tilde{\gamma}_s, \qquad (2.1)$$

where $\tilde{\gamma}_s = ik_z\gamma_s$. The three wave equations are now ordinary differential equations with derivatives with respect to r only. The other coefficients are the bulk velocities in a poroelastic medium: a fast (v_+) and a slow (v_-) P-wave as well as a shear wave (v_s). Starting from these equations we wish to find the relation between the angular frequency ω and the axial wave number k_z which will provide the dispersion by solving (2.1) as an eigenvalue problem.

Consequently the stress and displacement components required for the boundary conditions have to be expressed independently of the axial wave number k_z. The derivation of the displacement and stress components is done in a similar manner as is done in Karpfinger et al. [5]. The expression for the displacements are as follows:

$$u_r = \Gamma\partial_r a_+ - \Gamma\partial_r a_- - \tilde{\gamma}_s,$$
$$\tilde{u}_z = -\Gamma L_+ a_+ + \Gamma L_- a_- + \left(\partial_r + r^{-1}\right)\tilde{\gamma}_s, \qquad (2.2)$$
$$w_r = -\Gamma\Gamma_-\partial_r a_+ - \Gamma\Gamma_+\partial_r a_- + \frac{\rho_f}{q}\tilde{\gamma}_s,$$

where $\tilde{u}_z = ik_z u_z$. The definition of the amplitude coefficients $\Gamma_{\pm}$ can be found in Berryman [10] and $\Gamma = \left(\Gamma_+ - \Gamma_-\right)^{-1}$. The stress components expressed independently of the axial wave number have the following form:

$$\sigma_{rr} = \sum_{\pm}\pm\Gamma\left(2\mu\partial_r^2 + (C\Gamma_{\mp} - H + 2\mu)k_{\pm}^2\right)a_{\pm} - 2\mu\partial_r^2\tilde{\gamma}_s,$$
$$\bar{\sigma}_{rz} = \sum_{\pm}\mp 2\mu\Gamma\left(\partial_r^3 + \frac{1}{r}\partial_r^2 - \frac{1}{r^2}\partial_r + k_{\pm}^2\partial_r\right)a_{\pm} + \left(2\mu L_s - \mu k_s^2\right)\bar{\gamma}_s, \quad (2.3)$$
$$p = \sum_{\pm}\pm\Gamma k_{\pm}^2\left(M\Gamma_{\mp} - C\right)a_{\pm},$$

where $\bar{\sigma}_{rz} = ik_z \sigma_{rz}$ and $\sum_{\pm}$ indicates the summation over the terms a_+ and a_-. Eqs. (2.2)-(2.3) are now utilized to get all the possible interface and boundary conditions in case of porous layers.

3. Boundary Conditions

The general form of the boundary conditions between fluid and porous media can be given as (Liu et al [3]):

$$\sigma_{rr}\big|_{fl} = \sigma_{rr}\big|_{p}, (a) \qquad u_r\big|_{fl} = u_r\big|_{p} + w_r\big|_{p}, (b)$$

$$0 = \sigma_{rz}\big|_{p}, (c) \qquad -\sigma_{rr}\big|_{fl} = p\big|_{p} + W_{mc}\, w_r\big|_{p}, (d) \tag{3.1}$$

The radial stress (3.1-a) and displacement (3.1-b) are required to be continuous across the interface. The shear stress (3.1-c) in the porous layer vanishes on the boundary. The last condition (3.1-d) may describe conditions with open and, closed pores as well as accommodate intermediate case with the mudcake by varying parameter W_{mc} which is the mudcake membrane stiffness. If $W_{mc} = 0$ then (3.1-d) describes open-pore case. For a closed interface $W_{mc} \to \infty$ and eq. (1.1-d) is replaced by $0 = w_r\big|_{p}$. In the case of an interface between two porous media, all field quantities are continuous. Eqs. (2.1)-(2.3) are now solved for a given geometry considering the equations for fluid and solid layers and the boundary conditions (3.1) using the spectral method.

4. Spectral Method

Using Chebyshev collocation points to discretize the structure along its radius as well as differential operators, (2.1)-(2.3) can be transformed into algebraic matrix equations for each layer. The size of the matrices corresponds to the number of collocation points N_i chosen for each individual layer $i = 1...n$ multiplied by the number of wave equations. For a poroelastic layer the size of the matrix equation is $3N_i \times 3N_i$ due to the three wave equations.
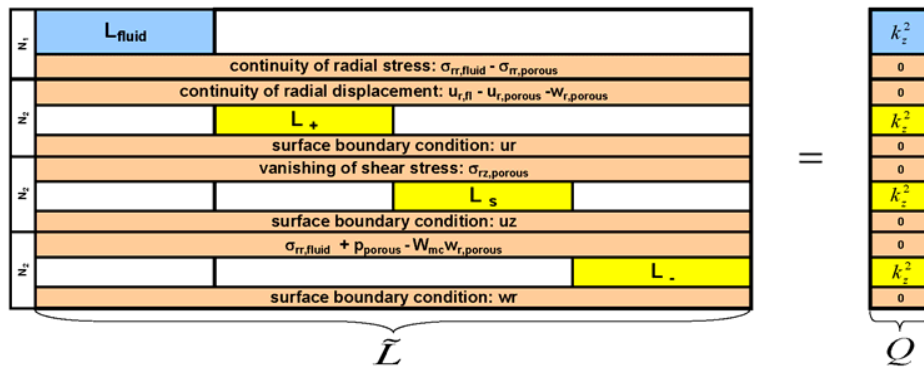

Figure 1: Structure of the matrix for a borehole surrounded by a porous formation. Orange lines: set boundary conditions on the interface and the surface of the structure.

After construction of the matrices the adequate boundary conditions have to be introduced. This is shown in Fig. 1 for the case of a fluid-porous interface using open

boundary conditions. The matrix $\tilde{L}$ combines all the wave equations and coefficients of the boundary conditions. The blue square is the matrix of the fluid equation while the yellow ones represent the three matrices of the poroelastic layer. The boundary conditions are set in the orange lines which are always either the first or the last line of each matrix representing either the inner or outer surface of the layers. The interface boundary conditions (3.1) are introduced and set to zero in the corresponding lines of the diagonal matrix Q, which has the same size as $\tilde{L}$. Also three boundary conditions are set on the surface of the structure. This is required as no absorbing boundary conditions have been implemented yet.

The matrices from Fig.1 can be expressed as an generalized eigenvalue problem

$$\tilde{L}\Theta = k_z^2 Q\Theta. \tag{4.1}$$

Solving this system with standard eigenvalue solvers yields for a given frequency the wavenumbers corresponding to the different modes. Repeating this operation for a range of frequencies allows construction of dispersion curves.
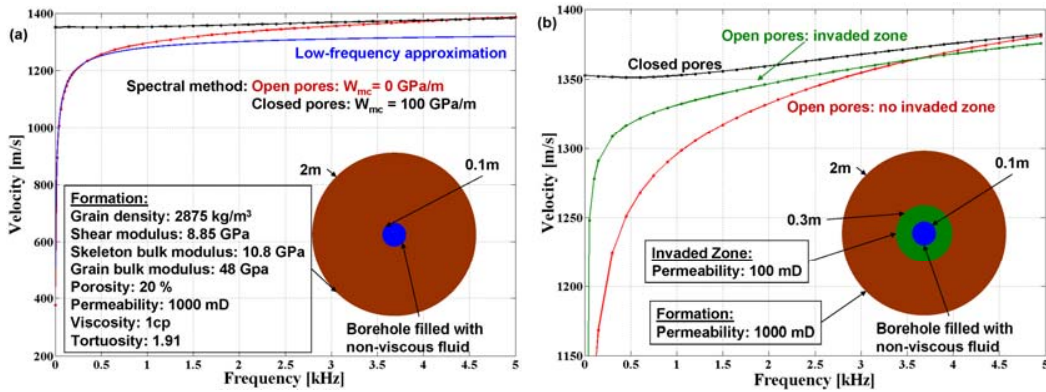
5. Numerical examples

Figure 2: a) Dispersion curves of Stoneley wave in a borehole surrounded by a poroelastic formation. b) Same model as in Fig.2-a but new layer, representing altered zone, is added between borehole and formation. This layer has same properties as the formation except its permeability is reduced by a factor of 10.

The first example (Fig.2-a) illustrates the dispersion of the Stoneley wave in a borehole surrounded by a poroelastic formation. The borehole dimensions and formation parameters are given in Fig 2-a. Open and closed boundary conditions are considered. Numerical results obtained with the spectral method for the case of open pores are benchmarked with the low-frequency approximation from Liu et al [3]. Excellent agreement between two approaches can be observed up to 0.5 kHz which is the range of validity of low-frequency approximation. For higher frequencies the full solution obtained by spectral method becomes faster then the equivalent elastic model (closed pores) and reaches the Rayleigh wave velocity for a poroelastic interface. The closed-pore case is compared with the equivalent elastic model obtained from spectral method. The agreement is good over the entire range of frequencies.

Drilling and completion processes often alter formation properties in the vicinity of the borehole. As a result altered zone of reduced permeability may occur near the wellbore which can have adverse effect on hydrocarbon production. In order to take into account effect of the altered zone we compute dispersion in a three-layer model.

The formation properties are the same as in Fig.-2a but for the altered zone (Fig.-2b) the permeability is reduced by a factor of ten. The green dispersion curve shows the dispersion in the presence of the altered zone. One can see that the reduction of the permeability around the borehole leads to a significant increase of the Stoneley wave up to 3 kHz compared to the case with no altered zone. In general dispersion curve in the presence of the altered zone lies in between cases of open and closed pores.

Conclusions

The spectral method is a simple and straightforward approach for modeling the dispersion of axisymmetric waves in cylindrical poroelastic formations. We apply it to study signatures of Stoneley waves in boreholes surrounded by permeable formations. For known cases the results are in good agreement with the analytical solutions. The advantage of the spectral method compared to traditional root-finding techniques is that it can be very easily implemented and extended for more complicated models such as a multilayered case. As an example we applied spectral method to describe more case of boreholes in a permeable formation with an altered near-wellbore zone and showed how it changes the dispersion of the Stoneley wave. This gives us a chance to obtain more accurate description of realistic borehole conditions and thus achieve a better characterization of petrophysical properties of subsurface formations.

ACKNOWLEDGEMENTS

REFERENCES

[1] Chang, S.K.,Liu,H.-L., and Johnson, D.L., 1988, Low-frequency tube waves in permeable rocks: Geophysics,**53**, 519-527.
[2] Winkler, K.W., Liu,H.-L., and Johnson, D.L., 1989, Permeability and borehole Stoneley waves: Comparison between experiment and theory: Geophysics ,**54**, 66-75.
[3] Liu,H.-L., and Johnson, D.L., 1996,Effects of an elastic membrane on tube waves in permeable formations: J. Acoust. Soc. Amer., **101**, 3322-3329.
[4] Adamou, A.T.I. and R.V. Craster, 2004, Spectral methods for modeling guided waves in elastic media: J. Acoust. Soc. Amer., **116**, 1524-1535.
[5] Karpfinger, F., B. Gurevich, and A.Bakulin, 2008a, Computation of wave propagation along cylindrical structures using the spectral method : J. Acoust. Soc. Amer., **124**, 859-865.
[6] Karpfinger, F., B. Gurevich, and A.Bakulin, 2008b, Modelling of axisymmetric wave modes in a poroelastic cylinder: J. Acoust. Soc. Amer. Express letters, **124**, 859-865.
[7] Biot, M. A., 1962, Mechanics of deformation and acoustic propagation in porous media: J.Appl. Phys.,**33**, 1482-1498.
[8] Biot, M. A., 1956, Theory of Propagation of Elastic Waves in a Fluid-saturated Porous solid II. Higher Frequency Range: J. Acoust. Soc. Amer.,**28**, 179-191.
[9] Gassmann, F., 1951, Über die elastizität poröser Medien: Viertel. Naturforsch. Ges. Zürich, **96**, 1–23.
[10] Berryman, J. G., 1983, Dispersion of extensional waves in fluid-saturated porous cylinders at ultrasonic frequencies: J. Acoust. Soc. Amer., **74**, 1805 – 1812.

CHAPTER 4

Understanding the acoustic response of deepwater completions

Understanding the acoustic response of deepwater completions

ANDREY BAKULIN, WesternGeco
FLORIAN KARPFINGER and BORIS GUREVICH, Curtin University of Technology

Deepwater production often hinges on the ability to safely complete and effectively draw down a small number of very challenging wells. Chances of success are greatly increased if surveillance tools are available to quickly diagnose downhole conditions and detect potential issues early on. Real-time completion monitoring with acoustic waves (RTCM) has great potential for diagnosing problems in sand-screened deepwater completions. RTCM uses tube waves to detect permeability changes and passive noises to characterize perforation flow. Interaction of a single tube wave with permeable formations in open boreholes is well explained by Biot's theory of poroelasticity. However, experimental studies in laboratory models of sand-screened completions reveal that fast- and slow-tube waves behave differently. Further progress in acoustic surveillance requires better understanding on how signatures of fast- and slow-tube waves depend on completion properties. To this end, we simulate the dispersion and attenuation of the two tube waves by examining the solutions of Biot's equations of poroelasticity in cylindrical structures using a spectral method.

Basic concept of evaluating permeability with acoustic waves

At low frequencies, wave propagation in an open borehole is dominated by tube (Stoneley) waves. Waves compress the fluid column and lead to a piston-like motion. When fluid is compressed, it expands radially and pushes against the formation or casing. In the presence of a permeable borehole wall, fluid movement across the interface leads to a slowdown in velocity and an increase in attenuation (Figure 1). These effects are well explained by Biot's theory and form the foundation for estimating near-wellbore permeability from an open-hole acoustic logging.

Sand-screened deepwater completion has a more complicated structure (Figure 2) due to multiple permeable layers. The sand screen represents an additional pipe with a very high permeability. The annulus between the casing and screen is filled with gravel sand or fluid, both of which possess negligible shear modulus. The sand screen and gravel pack prevent migration of reservoir sand into the wellbore and maintain the structure of the reservoir around the wellbore. The presence of two fluid-like columns in the completion gives birth to two tube waves: fast and slow. They have been observed in experiments with full-scale laboratory models of deepwater completion. The most basic task of RTCM is to monitor changes in the permeability of the sand screen and gravel-pack layer. Here we aim to examine the effect of sand-screen permeability on velocities and attenuation of two tube waves.

Experimental observations in models of sand-screened deepwater completions

Bakulin et al. (2008) described experiments in a full-scale
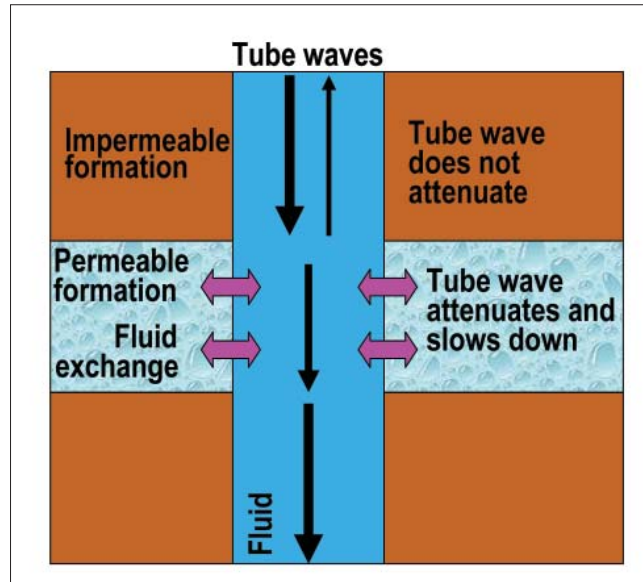
Figure 1. *Tube waves increase in attenuation and decrease in velocity when encountering a permeable interval where fluid exchange can occur between borehole and formation.*
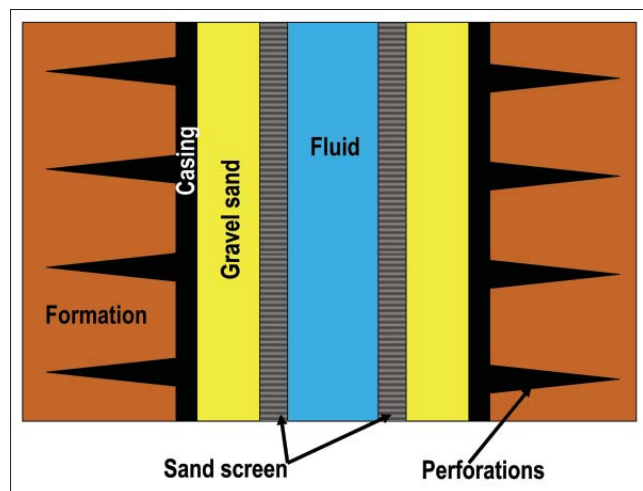
Figure 2. *Schematic representation of a cased deepwater well with sand-screened completion.*

laboratory model of idealized completion. Figure 3 shows schematics as well as actual photographs of the setup. Table 1 shows the geometry of the model. The outer pipe simulates the casing string, whereas the inner pipe represents the sand screen. The sand screen has aluminum base pipe and plastic wire wraps (Figure 3c). To simulate the impermeable or plugged sand screen, a blank pipe was used (Figure 3d). The casing was impermeable (closed perforations), and the experimental study focused on the effects of the screen permeability on the signatures of the fast- and slow-tube waves.
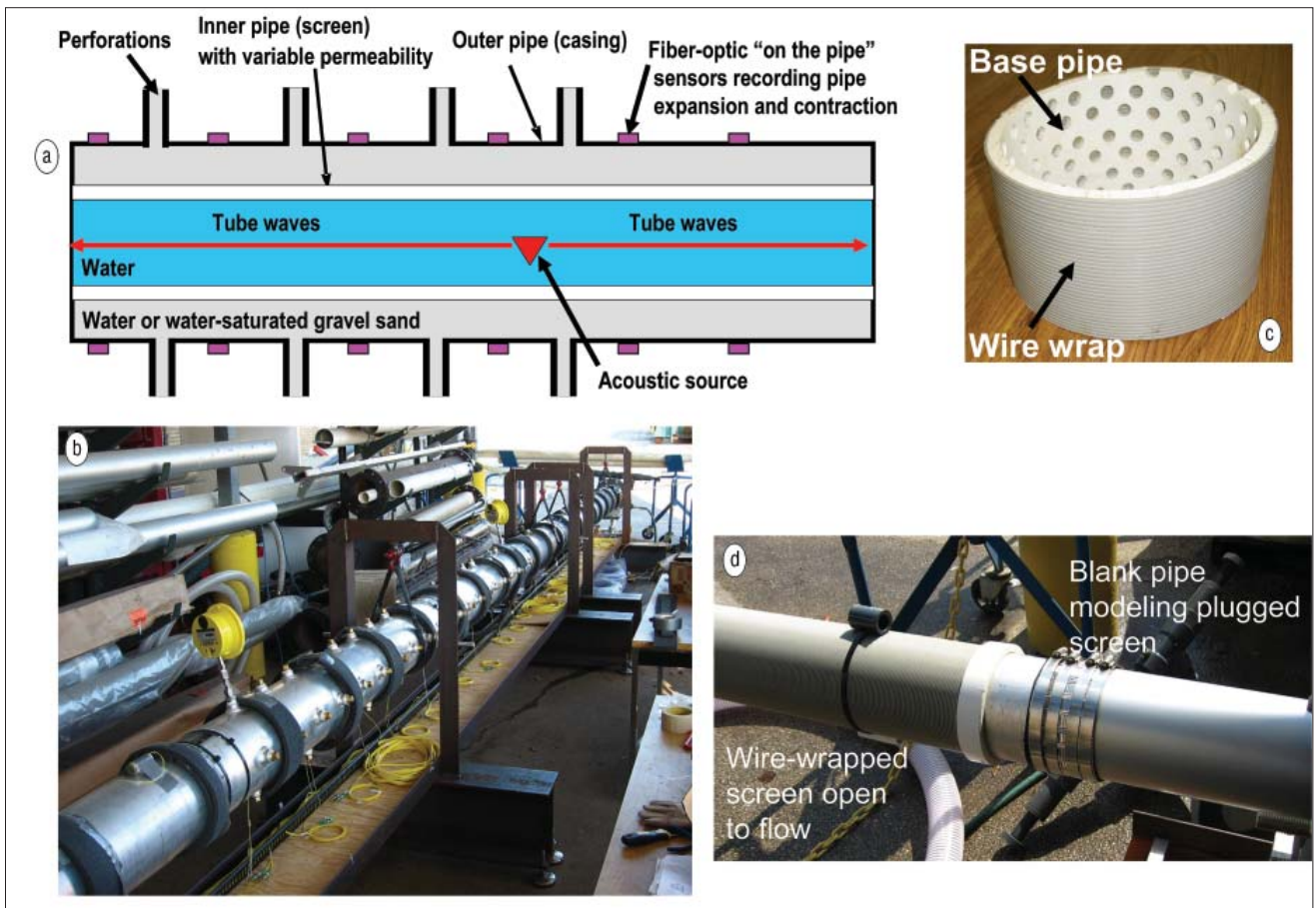
Figure 3. *Sketch (a) and photograph (b) of the full-scale laboratory setup used to simulate completed horizontal well; (c) cross-section of the screen showing wire wrap and base pipe (although plastic base pipe is shown, aluminum was used in the experiment); (d) wire-wrapped sand screen open to flow and blank pipe simulating plugged screen.*

If the sand screen is impermeable (blank pipe), then theory predicts four wave modes at low frequencies, all without attenuation (Figure 4): two tube waves and two plate (extensional) waves. Two tube waves exist because the completion contains two fluid columns: one inside the screen and the other in the annulus. The two plate waves are supported by the screen (inner pipe) and casing (outer pipe), respectively. If formation is added on the outside of the casing, then the casing-supported plate wave disappears, while all three other modes remain.

Experimental seismograms (Figure 5a) confirm the presence of fast- and slow-tube waves. The plate waves have smaller amplitudes and are visible only at higher amplifications. Since the plate waves are not sensitive to permeability, we concentrate on the analysis of the tube-wave signatures.

Figure 5b suggests that an open-to-flow sand screen leads to increased attenuation of both fast- and slow-tube waves. This attenuation is further increased when water in the annulus is replaced by gravel sand. Wave propagation in a completion model with impermeable screen is well understood and can be accomplished by a root-finding technique. However, to capture the effects of sand-screen permeability on wave propagation, we need to use more complex constitutive equations that pose substantial challenges for modeling borehole

Cylindrical layers	Material	Outer radius (m)
Layer 1	Water	0.0635
Layer 2	Aluminum sand screen	0.0667
Layer 3	Water	0.1032
Layer 4	Aluminum casing	0.1095

Table 1. *Geometry and material composition of the completion model.*

modes. Following Bakulin et al., we assume that, to the first approximation, sand screen can be modeled as a poroelastic Biot's layer and examine tube-wave signatures as a function of screen permeability. Such signatures are usually derived using an analytical root-finding technique (Paillet and White, 1982) that is difficult to implement for multilayered attenuative poroelastic structures. The spectral method is a new approach to bypass the difficulties of root-finding for fluid and elastic cylindrical structures and was recently extended to poroelastic cylindrical structures (Karpfinger et al., 2008). By directly discretizing the underlying differential equations in the radial direction, the spectral method handles such complicated cylindrical structures very effectively and gives phase velocities and attenuation of all modes as a function of frequency.

Effect of screen permeability on tube waves

Let us examine how velocities and attenuation of two tube waves depend on the screen permeability, and compare them with the behavior of these signatures for a single tube wave in the case of an open borehole surrounded by infinite fluid-saturated and permeable formation (Winkler et al., 1989). In the open-hole model at low frequencies, tube-wave velocity decreases and attenuation increases with increasing forma-tion permeability. In a completion model, we have two tube waves, and their behavior is different.

Figures 6 and 7 show modeled velocity and attenuation of fast- and slow-tube waves as a function of screen permeability. Let us first examine the fast-tube wave, which is mainly sup-ported by the casing. In the low-permeability limit, the screen behaves as an impermeable pipe, and the fast-tube wave ex-periences no loss as already shown in Figure 4. At the other extreme, when the screen is very perme-able, it provides almost no resistance to the radial fluid motion across the screen and behaves like a layer of liquid. There-fore we expect to have a single (fast) tube wave supported by casing, again without a loss. From this transition, we deduce that the fast-tube wave is mainly sup-ported by the casing. What would hap-pen for intermediate permeabilities?

For subdarcy permeabilities, attenua-tion of the fast-tube wave increases with increasing permeability. However, this elevated attenuation peaks at about 1.5 darcy and then decreases, returning to the state of virtually no attenuation at large permeability (Figure 6b). To a first order, the location of the attenuation maximum is controlled by screen permeability and thickness. Radial profiles of displace-ment provide an additional insight on a possible mechanism for this attenuation at intermediate permeabilities. For low permeabilities, axial displacements of the fast wave are of the same sign, but of different magnitudes (Figure 8a). When the screen becomes more permeable, the different rates of compression inside the two liquid columns lead to a fluid ex-change across the screen. This exchange particularly intensifies for permeabilities
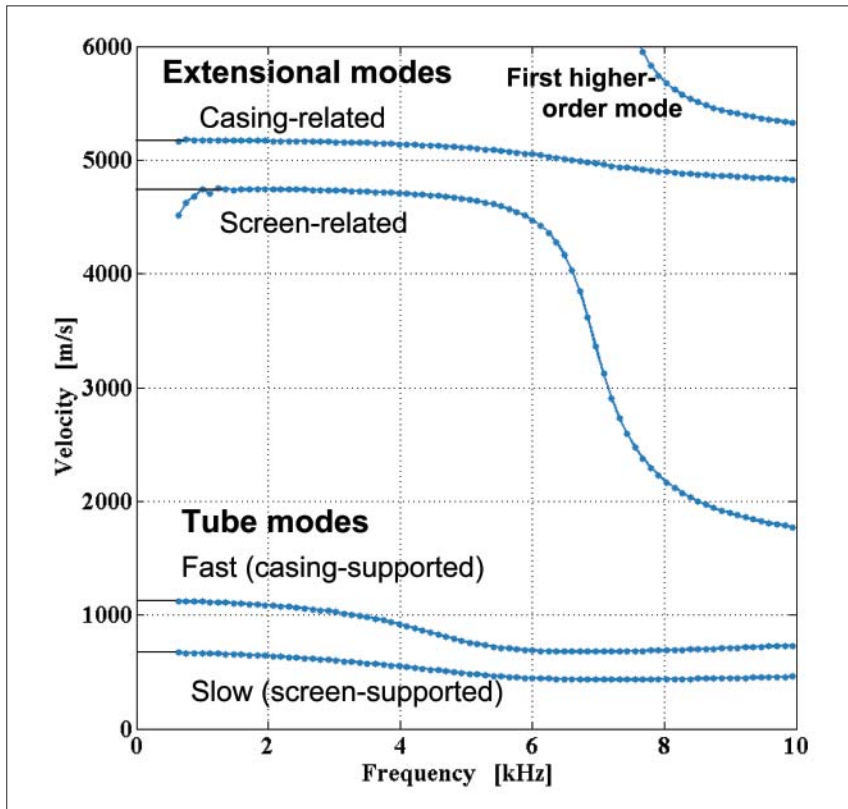
Figure 4. *Dispersion curves for an idealized completion model (water-impermeable screen-water-casing-vacuum) when sand screen has vanishing permeability. Note that all modes are completely lossless. Two slowest modes represent tube waves associated with the two fluid columns whereas two fastest modes represent plate (extensional) modes in screen and casing tubulars, respectively.*
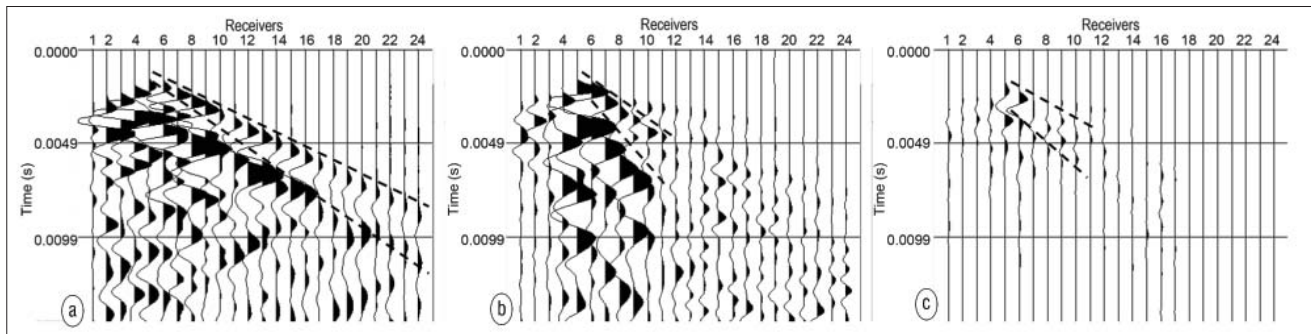
Figure 5. *Experimental seismograms in different completion models from the same source near receiver 5 shown with the identical magnification: (a) entire completion has impermeable screen (blank pipe) with no gravel sand; (b) blank pipe between receivers 1 and 12 is replaced by a section of open-to-flow wire-wrapped screen; (c) same as (b) but with gravel pack. Note that two arrivals of fast- and slow-tube waves are visible on both displays. For an impermeable screen without sand (a) velocities are ~1000 m/s and 700 m/s, but for an open screen with and without sand (b-c) they are slower (~700–800 m/s and 400–600 m/s, respectively). Observe increase in attenuation with introduction of screen section (b) and even larger increase when adding sand (c).*

Figure 6. *Velocity (a) and attenuation (b) of the fast-tube wave mode as a function of screen permeability in an idealized completion model (water-permeable screen-water-casing-vacuum). Dots denote computations by spectral method. Thin black lines show extrapolated behavior at low frequencies where current implementation of the spectral method is numerically unstable.*

and 3 darcy (Figure 6a). While one normally expects velocity slowdown with the increased attenuation, it is unusual to observe that velocity continues to decrease even when attenuation starts to drop between 1.5 and 10 darcy.

The slow-tube wave demonstrates a behavior that is more similar to that of a single tube wave in an open borehole surrounded by a permeable formation. Attenuation is increasing progressively with increasing permeability (Figure 7b). While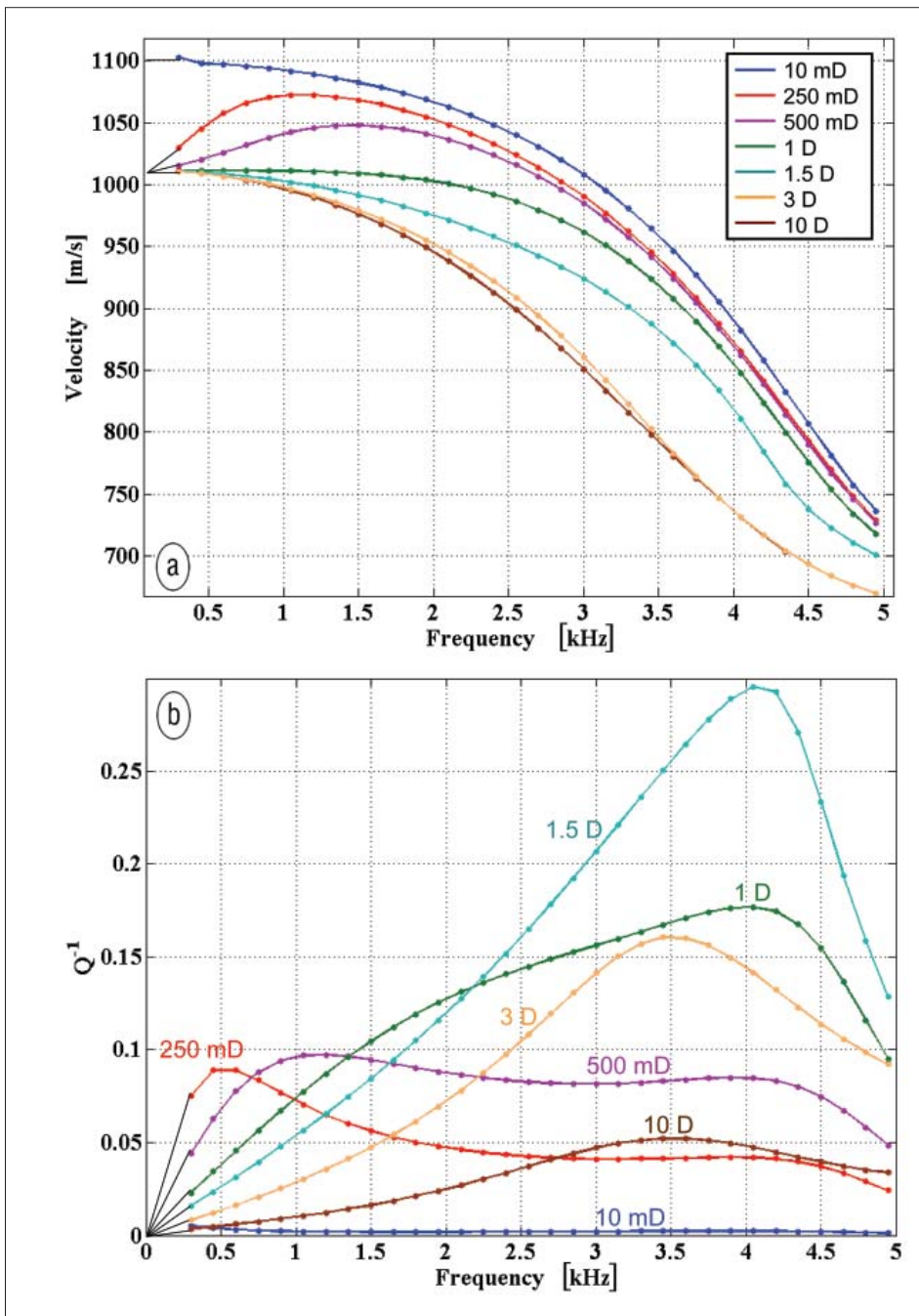 in open borehole, the tube wave always remains a propagating mode ($Q^{-1} \leq 2$, e.g., wave attenuates within more than one wavelength), in a completion the slow-tube wave may become nonpropagatory ($Q^{-1} > 2$) at a finite frequency and thus attenuates within less than a wavelength (Figure 7b). Such behavior of the slow mode can be readily explained by radial profiles of displacement (Figure 8). One can observe a piston-like motion with large axial displacement and small radial one. However, those pistons move in opposite directions in the inner and outer fluid columns, which are manifested by the opposite signs of the axial displacements in Figure 8. This distinct feature makes slow-tube mode analogous to a Biot's slow body wave. When the screen becomes permeable, this out-of-phase motion in the two columns naturally leads to an elevated fluid communication between two liquid columns. As a result, we observe rapid increase in attenuation (Figure 7b) and eventually a complete absorption of the slow mode at higher permeabilities. Despite amplitude decay of the slow wave, the character of the profile, and in particular, the opposite signs of the displacements remain stable at all permeabilities (compare Figure 8a and 8b).

In line with the increased attenuation at low frequencies, the velocity of the slow-tube wave drastically decreases (Figure 7a). One important observation is that at zero frequency, the slow-tube wave velocity approaches a positive value, where-

(~1.5 darcy) where the attenuation reaches maximum and is also manifested by rapid equalization of axial displacements occurring in this region. At higher permeabilities, the axial displacement levels off, while the radial displacement resembles the linear profile typical for a conventional tube wave in a fluid-filled cylinder with weak dispersion and no attenuation (Figure 8b).

As for the fast-tube wave velocity, it slows down progressively, with most changes occurring between 250 mdarcy
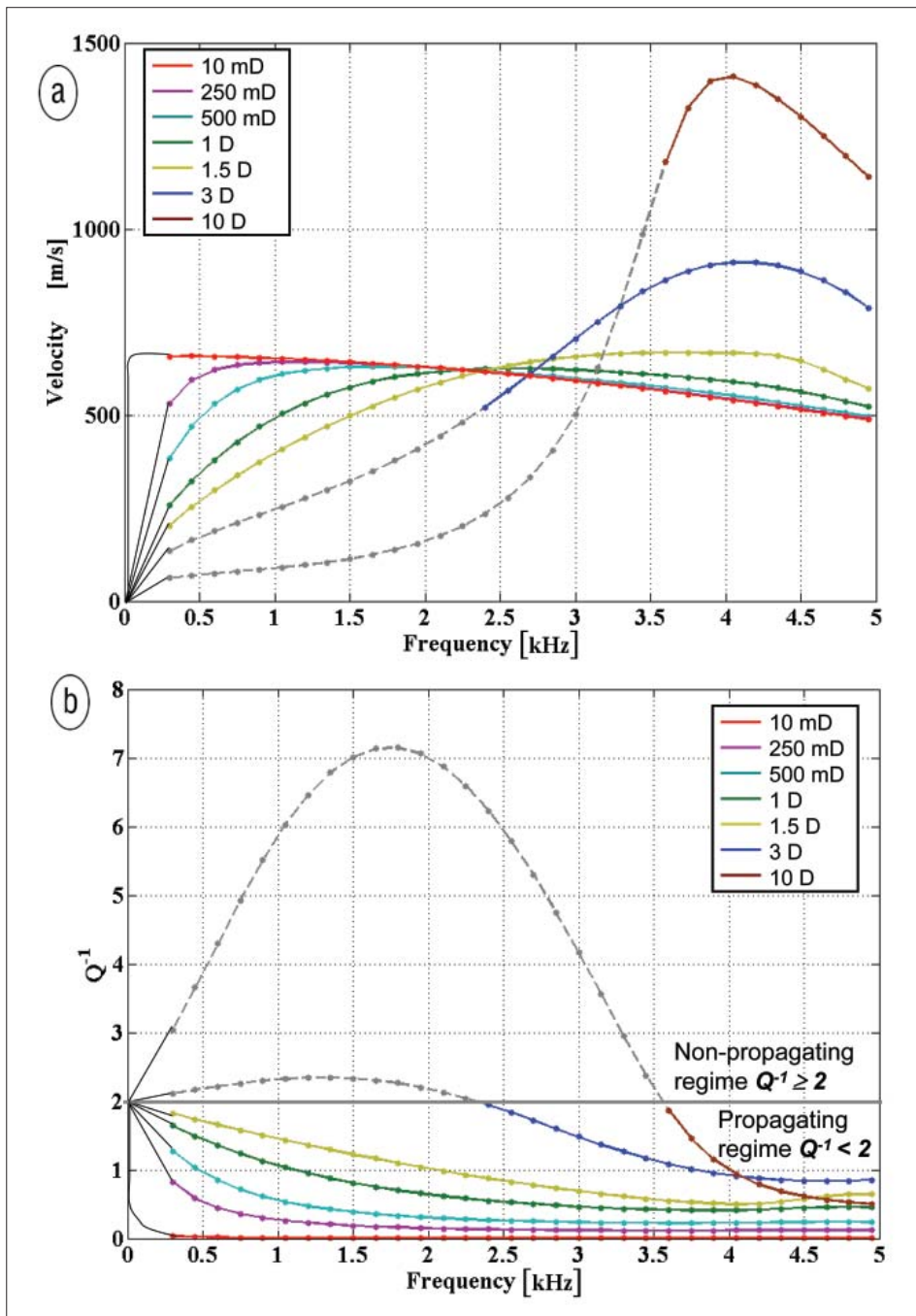
Figure 7. *Velocity (a) and attenuation (b) of slow-tube wave mode as a function of screen permeability in an idealized completion model (water-permeable screen-water-casing-vacuum). Notation is the same as in Figure 6. Horizontal gray line (Q⁻¹ = 2) separates nonpropagating (Q⁻¹ ≥ 2) and propagating regimes (Q⁻¹ < 2). In addition, curves are grayed out for frequencies where the slow mode becomes nonpropagating and attenuates within less than a wavelength.*

meable limit. This has been also observed for a simpler model of open borehole in fluid-saturated formation (Winkler and Johnson, 1989).

Discussion and conclusions

Modeling with spectral method confirms strong dependence of fast- and slow-tube wave signatures on the screen permeability. Therefore, an acoustic surveillance system installed in a deepwater completion has a great chance to detect sand-screen plugging in real time. Sand-screen plugging is a serious problem that can create high skin factor for a well and cause a substantial decrease in production rates and thus well underperformance. However, without surveillance, it is virtually impossible to identify the source of the well underperformance, since it may be caused by other completion problems such as perforation plugging, near-wellbore permeability reduction (formation damage), or large-scale issues such as reservoir compartmentalization. Real-time completion monitoring with acoustic waves may reveal, actual source of well underperfomance and thus lead to a safer and more prolific drawdown and production strategies. RTCM has the potential to revolutionize our ability to manage deepwater wells by understanding evolution of flow, drawdown, and impairment in real time.

To accomplish these ambitious goals, we need to have good understanding of how acoustic signatures of interest depend on permeability of various completion layers. In this study, we concentrated on the analysis of the simplest completion model without gravel pack, and assumed that the sand screen can be modeled as a poroelastic Biot's layer. We verified that in this case the wave propagation is dominated by fast- and slow-tube modes supported by casing and screen, respectively. We studied the effect of screen permeability on the velocity and attenuation of fast- and slow-tube waves. For the slow-tube wave, veloc-

as for a finite permeability, it is expected to vanish at zero frequency similarly to the tube wave in an open borehole. Current implementation of the spectral method (Karpfinger, 2008) becomes numerically unstable at very low frequencies, and therefore these conclusions are tentative and need to be verified by additional research. Interestingly, at higher frequencies, the velocity of the slow mode increases with permeability increase (Figure 7a) and may even exceed the imper-

Figure 8. *Radial variation of displacements at 1000 Hz in fast- and slow-tube wave modes for a model of sand-screened completion without gravel pack with different screen permeabilities: (top) 10 mdarcy, (bottom) 5 darcy. For a poroelastic screen, the displacement averaged over solid and fluid phase is shown that is continuous at the open interface with a fluid. Note that increasing permeability equalizes axial displacement of the fast wave in both fluid columns, and leads to a linear profile of radial displacement. In contrast, axial displacement in the slow wave maintains opposite signs in two fluid columns, which creates fluid communication and eventually leads to a complete dissipation of this mode at higher permeabilities.*

ity decreases and attenuation increases with increasing screen permeability. Such behavior is caused by escalating fluid communication between two fluid columns and can be explained by opposite signs of axial fluid displacements on different sides of the screen. In contrast, the fast-tube wave experiences moderate attenuation at some characteristic frequency, which is controlled by screen permeability and thickness, whereas for small and large permeability fast-tube wave remains free of losses. In the limit of high permeability, the fast-tube wave transforms into a regular tube wave as if the sand screen becomes part of the surrounding liquids.

These modeling results are in a qualitative agreement with experimental observations in full-scale laboratory models of deepwater completions. The main discrepancy is related to the behavior of the slow-tube wave. Simple calculation of static screen permeability suggests values larger than 100 darcy for which modeling predicts complete dissipation of the slow mode (Figure 7b). However experiments reveal that slow-tube waves are observed and survive even when water in the annulus is replaced by water-saturated gravel sand. Better model of sand screens is required to reconcile this discrepancy. Understanding the connection between static and "dynamic" or "acoustic" permeability for meso-scale structures such as sand screens and perforated casing is a key to such reconciliation.

Suggested reading. "Real-time completion monitoring with acoustic waves" by Bakulin et al. (GEOPHYSICS, 2008). "Acoustic waves in sand-screened deepwater completions: Comparison of experiments and modeling" by Bakulin et al. (GEOPHYSICS, 2008). "Downhole acoustic surveillance of deepwater wells" by Bakulin et al. (*TLE*, 2008). "Modeling of wave dispersion along cylindrical structures using the spectral method" by Karpfinger et al. (*Journal of Acoustical Society of America*, 2008). "Modeling of axisymmetric wave modes in a poroelastic cylinder using spectral method" by Karpfinger et al. (*Journal of the Acoustical Society of America Express Letters*, 2008). "Acoustic modes of propagation in the borehole and their relationship to rock properties" by Paillet and White (GEOPHYSICS, 1982). "Permeability and borehole Stoneley waves: Comparison between experiment and theory" by Winkler et al. (GEOPHYSICS, 1989). **T-LE**

Corresponding author: florian.karpfinger@postgrad.curtin.edu.au

CHAPTER 5

Greens functions and radiation patterns in poroelastic

solids revisited

Green's functions and radiation patterns in poroelastic solids revisited

Florian Karpfinger,[1] Tobias M. Müller[2] and Boris Gurevich[1]*

[1]*Department of Exploration Geophysics, Curtin University* GPO Box U1987, *Perth, Western Australia* 6845, *Australia.*
E-mails: florian.karpfinger@postgrad.curtin.edu.au; boris.gurevich@geophy.curtin.edu.au
[2]*CSIRO Petroleum, 26 Dick Perry Avenue, 6151 Kensington, WA, Australia. E-mail: tobias.mueller@csiro.au*

SUMMARY

A consistent and unified formulation of Green's functions for wave propagation in poroelastic solids based on Biot's theory is given. Over the last decades various authors have made the attempt to derive different Green's tensor representation for poroelastic solids. Due to the various possible combinations of field variables and source terms the different solutions differ significantly. The main solutions are reviewed and compared. It is shown that these previously reported representations of Green's tensors can be used in a complementary sense such that all possible combinations of field variables and source types are included. As a new element we introduce the concept of moment tensors for poroelasticity. This allows us to describe sources in poroelastic solids in a consistent manner. With the help of the moment tensor concept a pressure source acting on the fluid phase is introduced as well as dipole sources and double-couple sources. To visualize the results, radiation patterns for all the discussed sources are constructed. The shape of the radiation patterns of the fast compressional and shear wave is the same as in elastodynamics, however, the radiation characteristics of Biot's slow wave are superimposed. The relative magnitudes of the field variables shown in the radiation patterns can be very different for different source types. In particular, for any source acting in the fluid phase the pressure field is dominated by the Biot slow wave having compressional wave polarization.

Key words: Body waves; Theoretical seismology; Wave propagation.

GJI Seismology

1 INTRODUCTION

The equations for wave propagation in a fully fluid-saturated porous medium were first proposed by Biot 50 years ago Biot (1956a,b, 1962). Finding solutions of the two coupled poroelastic partial differential equations (PDE) in the presence of body force source terms is an important problem of wave mechanics in porous continua. In particular, if the source term is assumed to be a Dirac's delta function in time and space the solutions are referred to as Green's functions.

Green's functions have been obtained, under various assumptions, by various authors over the last decades. However, the Green's function differ since several combinations of field variables and source terms are possible in a poroelastic continuum. One set of field variables to represent the two PDEs are the solid displacement $\boldsymbol{u}$ and the relative solid-fluid displacement $\boldsymbol{w}$. Another representation is based on $\boldsymbol{u}$ and the fluid displacement $\boldsymbol{U}$. The third representation is a combination of a vector and a scalar variable, namely the solid

displacement $\boldsymbol{u}$ and the pore-fluid pressure p. Each of these sets of field variables allows different source terms to be introduced. It is therefore not surprising that these different representations lead to a number of publications on Green's function in poroelasticity which are apparently different.

The first authors who derived Green's function for the dynamic poroelastic problem were Burridge & Vargas (1979). Their solution is based on the representation of the poroelastic wave equations using the solid displacement $\boldsymbol{u}$ and the relative solid-fluid displacement $\boldsymbol{w}$ as field variables. Burridge & Vargas (1979) applied the method of potential decomposition in conjunction with the Laplace transform. Explicit solutions were given for the far-field using the saddle point method. As only one type of source, which is a single force vector, is acting on the bulk phase but none on the fluid phase this solution solves the problem only partly. Using the Fourier transform method Norris (1985) derived Green's function in terms of the field variables $(\boldsymbol{u}, \boldsymbol{U})$. In addition to a source acting on the bulk phase a source vector in the fluid phase was added. In this work no explicit expression of Green's functions including all source types were given. Using a similar approach, Green's functions for poroelasticity were derived by Philippacopoulos (1998)

*CSIRO Petroleum.

and Lu *et al.* (2008). Norris (1994) used a different approach based on integration over a closed surface to derive Green's functions for poroelasticity.

Another way to determine Green's function for the equations of poroelasticity is to exploit the analogy with the PDEs of thermoelasticity (Kupradze 1979). This is possible since the PDEs of thermoelasticity and poroelasticity are mathematically equivalent (Norris 1992). The PDEs of poroelasticity can be represented in terms of one vectorial and one scalar field (u, p) (Bonnet 1987). Using the method of Kupradze, the frequency-domain Green's functions were derived by Bonnet (1987) and Boutin (1991). The source term acting on the fluid phase is a volume source V while the source in the bulk composite is a vector force F. In addition to the 3-D space Green's function the solution for the 2-D Green's function was also presented. Bonnet (1987) and Boutin (1991) pointed out that a source vector acting on the fluid phase (as used in Norris 1985) is unphysical.

Green's functions for coupled problem of elastic and electromagnetic wave propagation in porous media were presented by Pride & Haartsen (1996). These solutions can be reduced to the poroelastic Green's functions by neglecting the electromagnetic coupling terms (Müller & Gurevich 2005). On the basis of the field variables (u, w) representation, these Green's functions are given in the frequency space domain and are analogous to those given by Norris (1985). The advantage of the solution presented by Pride & Haartsen (1996) is that Green's functions were presented in the most explicit form separated in far-field and near-field contributions.

All Green's functions described above are presented in the frequency domain. In the presence of the Darcy dissipation term (Biot 1956a,b) it is not possible to analytically transform the results back into time domain without any further assumptions. A closed-form time domain solution for the case without viscous dissipation was given by Norris (1985). Two authors obtained Green's functions in time domain including the viscous dissipation term. Chen (1994a,b) gives solutions for 2-D and 3-D space using the Laplace transform method, however introducing approximations in the Laplace domain. Another approach is presented by Schanz & Pryl (2004) also using inverse Laplace transform method.

The solutions discussed here can be used to implement point sources in a number of seismic forward modelling algorithms in porous media, such as reflectivity (Allard *et al.* 1986), finite differences (Wenzlau & Müller 2009). The analytical solutions obtained in the paper can be used to benchmark the results of these algorithms. Furthermore, even when the source is physically located in a non-porous region of the medium, such as a fluid-filled borehole, explicit modelling of such geometrical configuration may require a prohibitively small grid size. This problem can be overcome by approximating the borehole as a series of point sources (Kurkjian *et al.* 1994). This approach requires the computation of the point source response. Thus, the poroelastic point source solutions presented in this paper can also help model the effect of a borehole in a poroelastic formation (including the effect of flow between the reservoir and the borehole).

In this paper, we provide a consistent formulation of Green's functions in poroelastic solids. The similarities and differences between the approaches described above are highlighted. In Section 2, we present the equations of linear poroelasticity. We provide a comparative review of Green's function of poroelasticity in Section 3. Radiation patterns for various source types are illustrated in Section 4. The concept of moment tensors is introduced to describe consistent source mechanisms in poroelastic solids including fluid and solid dipole sources as well as double-couple sources. Their radiation characteristics are also illustrated with the help of radiation patterns.

2 EQUATIONS OF POROELASTICITY

A theory wave propagation in fully saturated porous media was developed by Biot (1956a,b, 1962). The wave equations of dynamic poroelasticity (Biot 1962) can be represented in the frequency domain as

$$\nabla \cdot \sigma = \omega^2 (\rho \mathbf{u} + \rho_f \mathbf{w}) \tag{1}$$

$$-\nabla p = \omega^2 \left(\frac{i}{\omega} \frac{\eta}{k(\omega)} \mathbf{w} + \rho_f \mathbf{u} \right) \tag{2}$$

where $\mathbf{w} = \phi(\mathbf{U} - \mathbf{u})$ is the relative fluid-solid displacement, ϕ is the porosity, $\mathbf{u}$ is the average bulk displacement, and $\mathbf{u}$ is the absolute fluid displacement. ρ and ρ_f are the densities of the bulk and the fluid phase where $\rho = \phi \rho_f + (1 - \phi)\rho_s$, with ρ_s being the density of the grain material.

The viscosity is denoted as η, and the permeability is k. The permeability is frequency dependent and we adopt the dynamic permeability model of Johnson *et al.* (1987):

$$k(\omega) = \frac{k_0}{\sqrt{\left(1 + i \frac{\omega}{\omega_t} \frac{4}{m}\right) + i \frac{\omega}{\omega_t}}},$$

$$\omega_t \equiv \frac{\phi}{a_\infty k_0} \frac{\eta}{\rho_f}, \quad m \equiv \frac{\phi}{a_\infty k_0} \Lambda^2, \tag{3}$$

where the transition frequency ω_t separates the regimes of low-frequency viscous flow and the high-frequency inertial resistance. According to Pride (1994), m is a dimensionless factor describing pore-space geometry, a_∞ is the tortuosity, k_0 is the hydraulic permeability, and Λ, which has the dimension of length, represents a weighted volume-to-surface ratio. m lies between $4 \leq m \leq 8$. In the low-frequency limit, expression (3) reduces to the hydraulic permeability k_0.

σ and p are the total stress tensor and fluid pressure, which are related to the displacement vectors via the constitutive relations

$$\sigma = [(H - 2\mu)\nabla \cdot \mathbf{u} + \alpha M \nabla \cdot \mathbf{w}]\mathbf{I} + \mu[\nabla \mathbf{u} + \nabla \mathbf{u}^T], \tag{4}$$

$$-p = \alpha M \nabla \cdot \mathbf{u} + M \nabla \mathbf{w}. \tag{5}$$

In eqs (4) and (5) μ is the shear modulus of the solid frame, $\alpha = 1 - K/K_g$ is the Biot–Willis coefficient (Biot & Willis 1957), $M^{-1} = \frac{\alpha - \phi}{K_g} + \frac{\phi}{K_f}$ is the so-called pore space modulus and the saturated P-wave modulus is defined by $H = K_{sat} + 4/3\mu$. K_{sat} is the bulk modulus of the saturated medium that is related to the bulk moduli of the fluid K_f, solid K_g, and dry skeleton K by the Gassmann (1951) equation

$$K_{sat} = K + \alpha^2 M. \tag{6}$$

Eqs (1)–(6) constitute the framework of wave propagation in fluid-saturated porous solids. To obtain Green's functions, appropriate source terms have to be introduced in eqs (1) and (2).

3 GREEN'S FUNCTIONS IN POROELASTICITY

In elastodynamics, the Green's function approach is commonly used. The representation theorem of elastodynamics relates the displacement field $\tilde{\mathbf{u}}$, excitation force $\tilde{\mathbf{F}}$, and Green's function $\tilde{\mathbf{G}}$ in

time domain (Aki & Richards 2002) in the form of a convolution

$$\tilde{\mathbf{u}}(r;t) = \tilde{\mathbf{F}} * \tilde{\mathbf{G}} = \int_{-\infty}^{\infty} \boldsymbol{F}(r;\tau)\boldsymbol{G}(r;t-\tau)d\tau. \tag{7}$$

This equation can be expressed in the frequency domain as

$$\boldsymbol{u}(\boldsymbol{r};\omega) = \boldsymbol{G}(\boldsymbol{r};\omega) \cdot \boldsymbol{F}(\boldsymbol{r};\omega). \tag{8}$$

Using eq. (8), it is possible to compute the displacement field for any point and any frequency for arbitrary excitation. For further properties of Green's function in elastodynamics, we refer to the textbook of Aki & Richards (2002).

A similar approach can be used to derive Green's function for poroelasticity. Eqs (1), (2), (4) and (5) can be represented as a pair of coupled wave equations by inserting the constitutive relations (4 and 5) into the equations of motion (1 and 2). However, depending on which of the three field variables ($\boldsymbol{u}$, $\boldsymbol{w}$ or p) is eliminated, the set of wave equations consists of either six or four wave equations. Choosing $\boldsymbol{u}$ and $\boldsymbol{w}$ as field variables, one obtains two vector wave equations, whereas choosing $\boldsymbol{u}$ and p one obtains one vector and one scalar wave equation. Introducing source terms into these sets of equations allows to derive Green's functions that are different for both sets of equations. These two different Green's functions are reproduced in the next section based on the work of Pride & Haartsen (1996) and Boutin (1987).

3.1 Solid and relative fluid-solid displacement representation

To obtain wave equations for the homogeneous and isotropic poroelastic wholespace including the solid and relative displacement ($\boldsymbol{u}$, $\boldsymbol{w}$) as field variables the stress tensor σ_{ij} and the pore pressure p have to be eliminated from the governing eqs (1) and (2). By substituting eq. (4) into eq. (1) and eq. (5) into eq. (2), we obtain the following matrix differential equation:

$$\boldsymbol{L}_{u,w} \cdot \begin{pmatrix} \boldsymbol{u} \\ \boldsymbol{w} \end{pmatrix} = \begin{pmatrix} -\boldsymbol{F} \\ -\boldsymbol{f} \end{pmatrix}, \tag{9}$$

where $\boldsymbol{L}_{u,w}$ is the matrix differential operator

$$\boldsymbol{L}_{u,w} = \begin{pmatrix} (H-\mu)\nabla\nabla + (\mu\nabla^2 + \omega^2\rho)\boldsymbol{I} & C\nabla\nabla + \omega^2\rho_f\boldsymbol{I} \\ C\nabla\nabla + \omega^2\rho_f\boldsymbol{I} & M\nabla\nabla + \omega^2\tilde{\rho}\boldsymbol{I} \end{pmatrix}. \tag{10}$$

In this equation $\tilde{\rho}$ is

$$\tilde{\rho}(\omega) = \frac{i\eta}{\omega k(\omega)} \tag{11}$$

and $\boldsymbol{I}$ is the identity tensor. Time dependence is assumed as $\exp(-i\omega t)$. Source terms in the form of body forces $\boldsymbol{F}$ and $\boldsymbol{f}$ are introduced on the right-hand side, which act on the bulk and the fluid phase, respectively. Assuming source terms in the form of Dirac delta functions

$$\boldsymbol{F} = \boldsymbol{F}_0\delta(\boldsymbol{r} - \boldsymbol{r}') \tag{12}$$

$$\boldsymbol{f} = \boldsymbol{f}_0\delta(\boldsymbol{r} - \boldsymbol{r}'), \tag{13}$$

where $\boldsymbol{r}'$ is the location vector pointing to the source position and $\boldsymbol{r}$ indicates the observation point, a solution of eq. (10) involving the corresponding Green's tensors can be expressed as

$$\begin{pmatrix} \boldsymbol{u} \\ \boldsymbol{w} \end{pmatrix} = \begin{pmatrix} \boldsymbol{G}^{F,u} & \boldsymbol{G}^{f,u} \\ \boldsymbol{G}^{F,w} & \boldsymbol{G}^{f,w} \end{pmatrix} \cdot \begin{pmatrix} \boldsymbol{F}_0 \\ \boldsymbol{f}_0 \end{pmatrix}. \tag{14}$$

Green's tensor $\boldsymbol{G}^{F,u}$ describes the solid displacement $\boldsymbol{u}$ response due to a bulk force $\boldsymbol{f}_0$ excitations. $\boldsymbol{G}^{f,w}$ describes the relative displacement $\boldsymbol{w}$ due to a force $\boldsymbol{F}_0$ acting on the fluid phase. The other Green's tensors can be interpreted in a similar way.

Explicit expressions for these Green's tensors can be obtained using the Fourier transform method. To do so, eq. (9) is transformed into the spatial wavenumber domain resulting into a system of six algebraic equations. This system of equations can be solved for Green's tensors in frequency-wavenumber domain. The spatial response can be obtained by applying the inverse Fourier transform in spherical $\boldsymbol{k}$ coordinates. This yields (Pride & Haartsen 1996):

$$\boldsymbol{G}^{\xi,\eta}(r|r') = T^{\xi}_{\eta,s_3}\frac{e^{i\omega s_3 r}}{4\pi r}(\boldsymbol{I} - \hat{\mathbf{r}}\hat{\mathbf{r}}) + \sum_{j=1}^{2} L^{\xi}_{\eta,s_j}\frac{e^{i\omega s_j r}}{4\pi r}\hat{\mathbf{r}}\hat{\mathbf{r}}$$

$$+ \left[T^{\xi}_{\eta,s_3}\left(\frac{i}{\omega s_3 r} - \frac{1}{(\omega s_3 r)^2}\right)\frac{e^{i\omega s_3 r}}{4\pi r} \right.$$

$$\left. - \sum_{j=1}^{2} L^{\xi}_{\eta,s_j}\left(\frac{i}{\omega s_j r} - \frac{1}{(\omega s_j r)^2}\right)\frac{e^{i\omega s_j r}}{4\pi r} \right](\boldsymbol{I} - 3\hat{\mathbf{r}}\hat{\mathbf{r}}). \tag{15}$$

In eq. (15), the Green tensors are separated in components with transverse ($\boldsymbol{I} - \hat{\mathbf{r}}\hat{\mathbf{r}}$), longitudinal ($\hat{\mathbf{r}}\hat{\mathbf{r}}$) and near-field ($\boldsymbol{I} - 3\hat{\mathbf{r}}\hat{\mathbf{r}}$) polarizations; $\hat{\mathbf{r}}$ is the unit direction vector pointing from the source to the observation point. T^{ξ}_{η,s_3} and L^{ξ}_{η,s_j} are the amplitudes of the transverse and longitudinal components. They are specified through the type of source indicated by $\xi = \{F, f\}$ and the type of field indicated by $\eta = \{u, w\}$ and the slownesses of the fast and slow compressional waves, s_1, s_2, and the shear wave, s_3. Explicit expression of these three wave slownesses is given in Appendix A. The expressions for the amplitudes T^{ξ}_{η,s_3} and L^{ξ}_{η,s_j} is given in Appendix B. Green's functions as defined in (14) and (15) can be easily reduced to the elastodynamic Green's function. In this case, only Green's function $\boldsymbol{G}^{F,u}$ exists since in an elastic solid only the solid displacement field $\boldsymbol{u}$ due to a body force vector $\boldsymbol{F}_0$ is excited. Then, in eqs (15) one has to set the slow P-wave slowness to zero.

Eqs (15) are equivalent to the fundamental solutions provided by Norris (1985). The solution from Norris (1985) was considered by Bonnet (1987) as overdetermined as a scalar source term is sufficient to describe sources in the fluid phase. Such a solution was derived by Boutin (1987) and is outlined in the next section.

3.2 Solid displacement and pore pressure representation

The correspondence between thermoelasticity and poroelasticity was pointed out by Norris (1992). In particular, the pore-fluid pressure is the poroelastic counterpart of the temperature as scalar field variable in thermoelasticity. Eliminating the stress tensor $\boldsymbol{\sigma}$ and the relative displacement vector $\boldsymbol{w}$ from eqs (1), (2), (4) and (5) results into a vector wave equation for the solid displacement vector $\boldsymbol{u}$ and into a scalar wave equation for the pore-fluid pressure

$$\boldsymbol{L}_{u,p} \cdot \begin{pmatrix} \boldsymbol{u} \\ p \end{pmatrix} = \begin{pmatrix} -\boldsymbol{F} \\ -V \end{pmatrix}, \tag{16}$$

with the matrix differential operator $\boldsymbol{L}_{u,p}$ defined as

$$\boldsymbol{L}_{u,p} = \begin{pmatrix} (P_{dry} - 2\mu)\nabla\nabla + (\mu\nabla^2 + \omega^2\rho_t)\boldsymbol{I} & -\hat{\alpha}\nabla\boldsymbol{I} \\ -(\tilde{\rho}^{-1}\nabla^2 + M^{-1})\boldsymbol{I} & -\hat{\alpha}\nabla \end{pmatrix}. \tag{17}$$

ρ_t and $\hat{\alpha}$ are defined as

$$\rho_t = \rho - \rho_f^2\tilde{\rho}^{-1},$$

$$\hat{\alpha} = \alpha - \rho_f\tilde{\rho}^{-1}. \tag{18}$$

The dry *P*-wave modulus is defined as $P_{\mathrm{dry}} = K + 4/3\ \mu$. In eq. (16), two source terms are introduced, where F is a body force acting on the bulk phase (the same as in eq. 8), while the scalar source term V corresponds to a volume injection applied within the fluid phase. Assuming that these sources have the form of Dirac delta pulses

$$F = F_0\delta(r - r'), \tag{19}$$

$$V = V_0\delta(r - r'), \tag{20}$$

eq. (16) can be represented with help of eq. (8) in terms of Green's functions

$$\begin{pmatrix} u \\ p \end{pmatrix} = \begin{pmatrix} G^{F,u} & G^{V,u} \\ G^{F,p} & G^{V,p} \end{pmatrix} \cdot \begin{pmatrix} F_0 \\ V_0 \end{pmatrix}. \tag{21}$$

As in eq. (14), four Green's tensors appear, however, their structure is different. The solid displacement response u due to a body force vector on the solid phase F_0 is a tensor of rank 2, $G^{F,u}$. The pressure response p due to the same force and the displacement response due to a volume injection source are vectors, $G^{F,p}$ and $G^{V,u}$. Finally, Green's function connecting the scalar source V to the fluid pressure p is of scalar nature, $G^{V,p}$.

The problem of determining Green's functions can be solved in analogy to thermoelasticity by using the method of Kupradze (1979, pp. 94). This method can be summarized as follows (a detailed outline of the method is also given in Sahay (2001, Section 4.1). The impulse response can be obtained by solving

$$G = L^{-1}\tau, \tag{22}$$

where L^{-1} is the inverse of the differential operator in eq. (17), which can be represented as $L^{-1} = \frac{(L^{\ddagger})^T}{\det(L)}$. $L^{\ddagger}$ is the cofactor matrix of L and τ is the solution of the scalar equation $\det(L\tau) + \delta = 0$.

The (u, F) response $G^{F,u}$ is identical to that of eq. (15). Due to the symmetry of eq. (21) Green's functions $G^{V,u}$ and $G^{F,p}$ are the same. This means that the displacement response u due to a volume source V and the pressure response p due to a single force vector F can be expressed as

$$G^{\xi,\eta}(r|r') = \sum_{j=1}^{2} L_{\eta,s_j}^{\xi} \frac{e^{is_j\omega r}}{4\pi r}\hat{\mathbf{r}} + \sum_{j=1}^{2} L_{\eta,s_j}^{\xi} \frac{i}{s_j\omega} \frac{e^{is_j\omega r}}{4\pi r^2}\hat{\mathbf{r}}, \tag{23}$$

where $\eta = \{u, p\}$ and $\xi = \{V, F\}$. The amplitudes L_{η,s_j}^{ξ} are given in the Appendix B. It is interesting to observe that the pressure field can be separated into a far-field term (first term proportional to $1/r$) and a near-field (first term proportional to $1/r^2$). The scalar Green's function describing the pressure response p due to a volume source V is

$$G^{V,p}(r|r') = \sum_{j=1}^{2} L_{p,s_j}^{V} \frac{e^{i\omega s_j r}}{4\pi r}, \tag{24}$$

where the amplitudes L_{p,s_j}^{V} are listed in the Appendix B.

Green's tensors (15), (23) and (24) fully describe a poroelastic medium as they provide solutions for all possible combinations of field variables (u, w, p) and for all possible forces (F, V). Note, however, that the single force in the fluid f is an unphysical source, as a fluid can only sustain hydrostatic pressure. This was already pointed out by Bonnet (1987).

Below we show that this inconsistency can be overcome by introducing the concept of moment tensor sources, thus replacing the single body force in the fluid phase by the body force equivalent of an explosive source.

4 RADIATION PATTERNS

The radiation characteristics of waves emanating from various sources in poroelastic continua have only been investigated by Molotkov & Bakulin (1998). However, their work is restricted to the high-frequency range of Biot's theory. We generalize this work by analysing radiation characteristics in the full frequency range for relevant source configurations. A useful way to present the radiation characteristics of sources in elastic continua is presented by Chapman (2004). Here we follow this approach to construct radiation patterns of sources in poroelastic continua.

Radiation patterns show the directional behaviour of the displacement magnitude $|u|$ generated by different source configurations. For a fluid-saturated porous medium the field variables can be either solid displacement u, relative displacement w or pore pressure p. Based on eq. (8) all Green's functions of poroelasticity can be represented in terms of field variables in the generic form

$$u^{P,S} \sim A^{L,T} \left\{ \begin{array}{c} \hat{\mathbf{r}}\hat{\mathbf{r}}, \quad I - \hat{\mathbf{r}}\hat{\mathbf{r}} \\ \hat{\mathbf{r}} \end{array} \right\} \cdot \left\{ \begin{array}{c} F \\ V \end{array} \right\}, \tag{25}$$

where $u^{P,S}$ represents the displacement of the longitudinal (*P*) or shear (*S*) waves. The right-hand side of eq. (25) consists of the scalar product of the source excitation (either body force F or injection volume V) and the polarization (one of $\hat{\mathbf{r}}\hat{\mathbf{r}}$, $I - \hat{\mathbf{r}}\hat{\mathbf{r}}$, $\hat{\mathbf{r}}$) multiplied by the corresponding amplitude

$$A^{L,T} = \left\{ L, \quad T \right\} \frac{e^{is\omega r}}{4\pi r}, \tag{26}$$

where L, T are defined in the Appendix B. Similarly, the scalar response p can be represented as

$$p \sim A^{L} \left\{ \begin{array}{c} \hat{\mathbf{r}} \cdot F \\ V \end{array} \right\}, \tag{27}$$

where

$$A^{L} = L\ \frac{e^{is\omega r}}{4\pi r}. \tag{28}$$

The right-hand side of eq. (27) represents the possible combinations of polarizations and source terms that produce a fluid-pore pressure field.

4.1 Point force source

4.1.1 Far-field

According to eq. (25) and Chapman (2004, Sec. 4.5.5.1) the *P*-wave radiation pattern is given by $A^{P}\hat{\mathbf{r}} \cdot F$. Using spherical coordinates, the unit vector $\hat{\mathbf{r}}$ can be expressed as

$$\hat{\mathbf{r}} = \begin{pmatrix} \sin\theta\cos\kappa \\ \sin\theta\sin\kappa \\ \cos\theta \end{pmatrix}, \tag{29}$$

where θ and κ are the angles from the z and x axes, respectively. The radiation pattern for the *P* wave is then

$$|A^{L}\hat{\mathbf{r}} \cdot F| = \left| A^{L}\hat{\mathbf{r}} \cdot (F_x, F_y, F_z)^{T} \right|$$
$$\left| A^{L} \right| |(F_x\cos\kappa + F_y\sin\kappa)\sin\theta + F_z\cos\theta|. \tag{30}$$

The *S*-wave radiation pattern is constructed as follows. The unit basis vectors $\hat{\mathbf{r}}, \hat{\kappa}, \hat{\theta}$ of the spherical coordinate system satisfy the identity

$$I = \hat{\mathbf{r}}\hat{\mathbf{r}} + \hat{\kappa}\hat{\kappa} + \hat{\theta}\hat{\theta}. \tag{31}$$
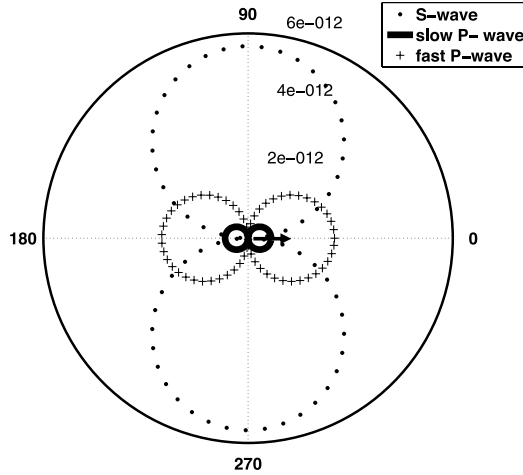
Figure 1. Radiation pattern of solid displacement $\boldsymbol{u}$ due to a point force; the numbers 2×10^{-12} to 6×10^{-12} denote the displacement in meters along the radial axis; the radiation pattern of the slow P wave is enhanced by the factor 1×10^{8}.

Thus, the S-wave polarization can be expressed as $\boldsymbol{I} - \hat{\mathbf{r}}\hat{\mathbf{r}} = \hat{\boldsymbol{\kappa}}\hat{\boldsymbol{\kappa}} + \hat{\boldsymbol{\theta}}\hat{\boldsymbol{\theta}}$. The polarization of the S wave is in the plane perpendicular to the propagation direction $\hat{\mathbf{r}}$. If the z-axis is vertical, and the $x - y$ plane is horizontal, it is common to introduce the notion of SH and SV waves. The horizontal component is

$$\hat{\kappa}_{SH} = \begin{pmatrix} -\sin(\kappa) \\ \cos(\kappa) \\ 0 \end{pmatrix}, \tag{32}$$

yielding the radiation pattern of a SH wave

$$|A^{T}\kappa_{\mathbf{sh}} \cdot \boldsymbol{F}| = |-F_{x}\cos\kappa + F_{y}\sin\kappa|. \tag{33}$$

The vertical component can be expressed as

$$\theta_{\mathbf{sv}} = \begin{pmatrix} \cos\theta\cos\kappa \\ \cos\theta\sin\kappa \\ -\sin\theta \end{pmatrix}. \tag{34}$$

From eq. (34) we get the radiation pattern of a SV wave as

$$|A^{T}\theta_{\mathbf{sv}} \cdot \boldsymbol{F}| = |(F_{x}\cos\kappa + F_{y}\sin\kappa)\cos\theta - F_{z}\sin\theta|. \tag{35}$$

Assuming a body force with z component only, i.e., $\boldsymbol{F} = (0, 0, F_z)^T$ acting on a poroelastic solid, the radiation patterns of the solid displacement $\boldsymbol{u}$ and relative solid-fluid displacement are illustrated in Figs 1–3 using the frequency of 100 Hz and the material parameters as specified in Table 1. It can be observed that the shape of the radiation patterns is identical to the elastodynamic case. The P-wave displacement is largest in the direction of the applied force, whereas the S-wave displacement is largest perpendicular to the direction of the force vector. The amplitude of the S wave is larger than that of the P wave. In addition, the radiation pattern of the slow P wave has the same shape as that of the fast P wave, however its amplitude is significantly smaller (its amplitude has been amplified by a factor 10^8 to make it visible in Fig. 1).

As a poroelastic medium is a two-phase system, the two P waves are differently manifested for different field variables. Comparing Figs 1 and 2(c) showing the solid and fluid displacement for 100 Hz, respectively a difference in magnitude of factor 4 from solid to fluid displacement can be observed. The slow P wave is easier to observe in terms of the fluid displacement especially for smaller frequencies

(Figs 2a and b). Here the contribution of the fast P wave and S wave becomes significantly smaller than the slow P-wave displacement.

In Fig. 3, the pressure response p due to a single force $\boldsymbol{F}$ acting in z-direction (compare eq. 23) is computed for various frequencies. In this case only the fast and slow compressional waves exist. The values computed are plotted on a logarithmic scale. For low frequencies, the slow P wave (1 – 10 Hz) has a bigger amplitude than the fast P wave. For higher frequencies, the slow P-wave amplitude decays rapidly. An analogous case is the pressure field due to a volume source (eq. 24). The difference is that the slow P-wave amplitudes are larger while the fast P-wave amplitudes are smaller. The low-frequency limit of this case was studied by Chandler & Johnson (1981), Rudnicki (1986) and Müller (2006).

4.1.2 The near-field

At distances smaller than one wavelength the near-field terms become noticeable (Wu & Ben-Menahem 1985). The polarization of the near-field is $\boldsymbol{I} - 3\hat{\mathbf{r}}\hat{\mathbf{r}}$ and the leading-order amplitude decays as $1/(\omega\, s_i r^2)$ (while the far-field decays with $1/r$). Using again identity (31), the near-field polarization can be expressed as

$$\boldsymbol{I} - 3\hat{\mathbf{r}}\hat{\mathbf{r}} = \hat{\boldsymbol{\kappa}}\hat{\boldsymbol{\kappa}} + \hat{\boldsymbol{\theta}}\hat{\boldsymbol{\theta}} - 2\hat{\mathbf{r}}\hat{\mathbf{r}}. \tag{36}$$

Assuming a force acting in z-direction and using eqs (29), (34) and (32) we find the near-field polarization

$$\left(\hat{\boldsymbol{\kappa}}\hat{\boldsymbol{\kappa}} + \hat{\boldsymbol{\theta}}\hat{\boldsymbol{\theta}} - 2\hat{\mathbf{r}}\hat{\mathbf{r}}\right) \cdot \begin{pmatrix} 0 \\ 0 \\ F_z \end{pmatrix} = (-2\cos\theta - \sin\theta)\, F_z. \tag{37}$$

The radiation pattern of the near-field is illustrated in Fig. 4. The form is the same for elastic and poroelastic media, only the amplitude differs. In source direction the amplitude is smaller than in perpendicular direction. This already indicates the difference in amplitude of P waves and S waves. Looking at eq. (23) it is obvious that the second term also decays like near-field terms but has the same polarization as the far-field. This means that for a pressure field due to a force vector (or displacement due to volume source) part of the energy decays with $1/r^2$ but with the same directivity as the far-field.

4.2 Moment tensor sources

Single body forces, as presented in the previous section are often not sufficient to describe real physical sources. For example, if a seismic vibrator or a hammer is used as a source acting on the surface of a poroelastic solid, a single body force representation is sufficient. However, as isolated forces cannot exist inside a closed system (e.g. the earth), it is necessary to introduce the concept of moment tensors (Backus & Mulcahy 1976a,b). The concept of moment tensors is widely acknowledged in elasticity (Aki & Richards 2002; Rudnicki & Freund 1981). In earthquake seismology they are used to describe dislocation type sources. Moment tensors are used as well to describe explosive/pressure sources and higher order type of sources such as dipoles. Such source types are mostly used in exploration seismology and borehole acoustics. The displacement field can be expressed in frequency domain as

$$u_i(\boldsymbol{r}; \omega) = M_{jk} G_{ij,k}. \tag{38}$$

This means that in the frequency domain the displacement field can be computed as a product of the spatial derivative of Green's function and the moment tensor M_{jk}. The components of the moment tensor
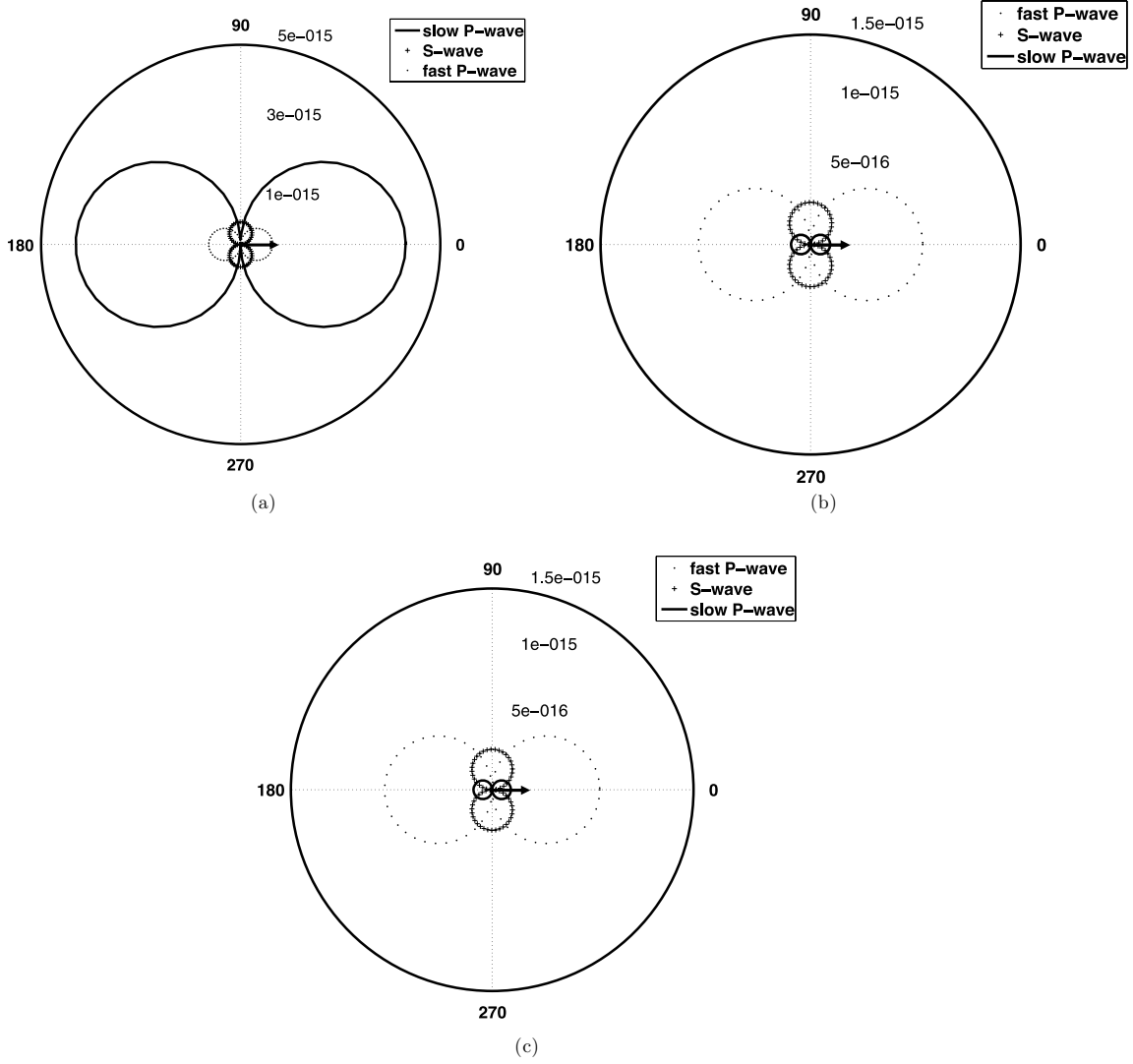
Figure 2. Radiation pattern of fluid displacement U due to single force for slow P wave, fast P wave and S wave, respectively; the numbers along the radial axis denote the displacement in meters; results are given for three different frequencies (a) 15 Hz, (b) 25 Hz, (c) 100 Hz.

in form of its equivalent body forces are illustrated in Fig. 5 (Aki & Richards 2002). A review on the use of moment tensors can be found in Jost & Herrmann (1989).

A similar approach can be used to study moment tensor sources in poroelastic media. To use moment tensor sources, expressions eqs (25) and (27) have to be modified accordingly

$$\boldsymbol{u}^{P,S} \sim s_j A^{P,S} \left\{ \begin{matrix} \hat{\boldsymbol{r}}\hat{\boldsymbol{r}}, & \boldsymbol{I} - \hat{\boldsymbol{r}}\hat{\boldsymbol{r}} \\ \hat{\boldsymbol{r}} \end{matrix} \right\} \cdot \boldsymbol{M}, \qquad (39)$$

where an additional multiplication with the slowness s_j appears as a consequence of the spatial derivative in eq. (38). On the left-hand side, the field quantity can be either a displacement ($\boldsymbol{u}$, $\boldsymbol{w}$) or the pressure p. The components of the moment tensor are

$$\boldsymbol{M} = \begin{pmatrix} M_{xx} & M_{xy} & M_{xz} \\ M_{yx} & M_{yy} & M_{yz} \\ M_{zx} & M_{zy} & M_{zz} \end{pmatrix}. \qquad (40)$$

From eq. (40) and Chapman (2004, Sec. 4.6.2), we deduce that the radiation pattern of moment tensor sources for P waves is

$|s_j A\hat{\boldsymbol{r}} \cdot \boldsymbol{M} \cdot \hat{\boldsymbol{r}}|$. Introducing spherical coordinates yields

$$\hat{\boldsymbol{r}} \cdot \boldsymbol{M} \cdot \hat{\boldsymbol{r}} = (M_{xx} \cos^2 \kappa + M_{yy} \sin^2 \kappa + M_{xy} \sin 2\kappa) \sin^2 \theta$$
$$+ M_{zz} \cos^2 \theta + (M_{zx} \cos \kappa + M_{yz} \sin \kappa) \sin 2\theta. \qquad (41)$$

In analogy to the body force source we obtain the *SV* radiation pattern by substituting eq. (34) into $|s_j A\hat{\boldsymbol{\theta}} \cdot \boldsymbol{M} \cdot \hat{\boldsymbol{r}}|$ yielding

$$\hat{\theta}_{sv} \cdot \boldsymbol{M} \cdot \hat{\boldsymbol{r}} = \frac{1}{2}(M_{xx} \cos^2 \kappa + M_{yy} \sin^2 \kappa - M_{zz} + M_{xy} \sin 2\kappa)$$
$$\cdot \sin 2\theta (M_{zx} \cos \kappa + M_{yz} \sin \kappa) \cos 2\theta. \qquad (42)$$

The radiation pattern for *SH* waves ($|s_j A\hat{\boldsymbol{\kappa}} \cdot \boldsymbol{M} \cdot \hat{\boldsymbol{r}}|$) is using eq. (32)

$$\hat{\boldsymbol{\kappa}}_{sh} \cdot \boldsymbol{M} \cdot \hat{\boldsymbol{r}} = \left[\frac{1}{2}(M_{yy} - M_{xx}) \sin 2\kappa + M_{xy} \cos 2\kappa\right] \sin \theta$$
$$+ (M_{yz} \cos \kappa - M_{zx} \sin \kappa) \cos 2\theta. \qquad (43)$$

These expressions allow to construct various moment tensor sources such as explosive, dipole and double-couple sources as exemplified next.
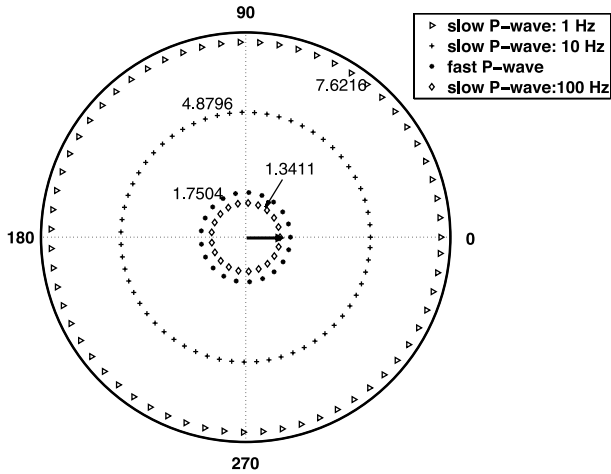
Figure 3. Pressure field p due to a single force $\boldsymbol{F}$ for the slow and the fast P wave; the numbers 1.7504–7.6216 denote the pressure in Pascal along the radial axis; The slow P-wave dispersion is illustrated for three frequencies: 1 Hz, 10 Hz and 100 Hz.

Table 1. Material parameters of a typical sandstone used for the computations.

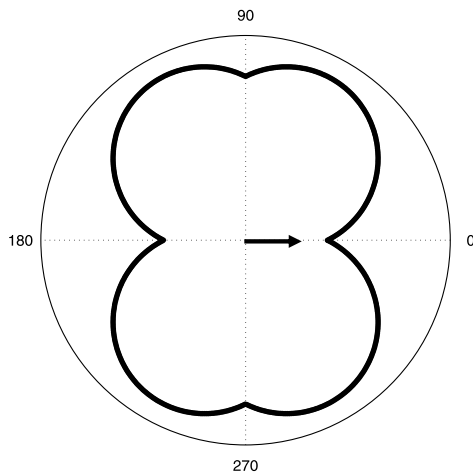|	
Permeability	$k_0 = 100 \, mD$
Viscosity	$\eta = 1 \, \mathrm{m\,Pa\,s}$
Tortuosity	$a_\infty = 1.75$
Pore space geometry factor	$m = 6$
Fluid density	$\rho_f = 1000 \, \mathrm{kg\,m^{-3}}$
Porosity	$\phi = 0.26$
Grain Density	$\rho_s = 2650 \, \mathrm{kg\,m^{-3}}$
Shear modulus	$\mu = 10 \, \mathrm{GPa}$
drained bulk modulus	$K = 6.7 \, \mathrm{GPa}$
grain modulus	$K_s = 30 \, \mathrm{GPa}$
fluid bulk modulus	$K_f = 1 \, \mathrm{GPa}$
fast P-wave slowness	$s_1 = 316 \, \mu \, \mathrm{s/m}$
S-wave slowness	$s_3 = 471 \, \mu \, \mathrm{s/m}$
Biot critical frequency	$\omega_t = 1.49 \, \mathrm{MHz}$

Figure 4. The radiation characteristics of the near-field. Only the geometry is illustrated without rock parameters.
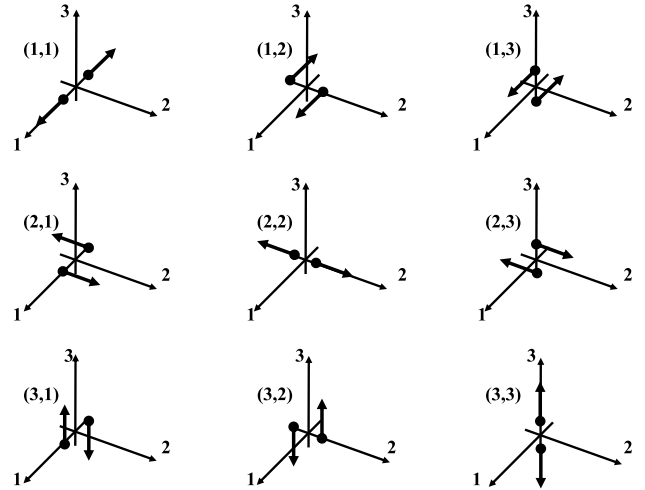
Figure 5. Body force equivalents of the moment tensor components (after Aki & Richards 2002).

4.2.1 Monopole source

An explosion source can be represented by an isotropic moment tensor of the form

$$\boldsymbol{M}_0 = M_0 \boldsymbol{I} = \begin{pmatrix} M_0 & 0 & 0 \\ 0 & M_0 & 0 \\ 0 & 0 & M_0 \end{pmatrix}. \tag{44}$$

Introducing eq. (44) into eq. (14) allows to generate physically realizable sources in the fluid phase. The fluid phase cannot sustain a single force vector $\boldsymbol{f}$, however, substituting the isotropic moment tensor $M_{ij} = M^f_0 \delta_{ij}$ into eq. (14) yields

$$u_k = M_{ij}^F \cdot G_{ki,j}^{F,u} + M_0^f \cdot G_{kj,j}^{f,u}, \tag{45}$$

$$w_k = M_{ij}^F \cdot G_{ki,j}^{F,w} + M_0^f \cdot G_{kj,j}^{f,w}. \tag{46}$$

The two terms including sources acting on the solid phase $\boldsymbol{G}^{F,u}$ and $\boldsymbol{G}^{F,w}$ support the full moment tensor while those terms containing source vectors in the fluid phase ($\boldsymbol{G}^{F,w}$ and $\boldsymbol{G}^{F,u}$) only support an explosive source with magnitude M^f_0. In other words, due to the use of moment tensors a physical meaning is given to Green's functions (14), which support force vectors in the fluid phase.

4.2.2 Dipole source

A dipole source can be realized either in the solid or in the fluid phase. In the solid phase, it can be thought of as tensile stress on a fault surface. Assuming the fault surface to be the $x - y$ plane, yields a momentless force couple acting along the z-axis expressed in terms of moment tensors as (Chapman 2004)

$$\boldsymbol{M}_{\mathrm{dipole}} = 2 \begin{pmatrix} 0 & 0 & 0 \\ 0 & 0 & 0 \\ 0 & 0 & M_{zz} \end{pmatrix}. \tag{47}$$

The P-wave radiation pattern is then obtained by setting corresponding terms in eq. (41) equal to zero. We obtain for the P-wave radiation pattern

$$\hat{\mathbf{r}} \cdot \boldsymbol{M}_{\mathrm{dipole}} \cdot \hat{\mathbf{r}} = 2M_{zz} \cos^2 \theta \tag{48}$$

and for the SV wave using eq. (42)

$$\hat{\theta} \cdot \boldsymbol{M}_{\mathrm{dipole}} \cdot \hat{\boldsymbol{r}} = -M_{zz} \sin 2\theta \,. \tag{49}$$
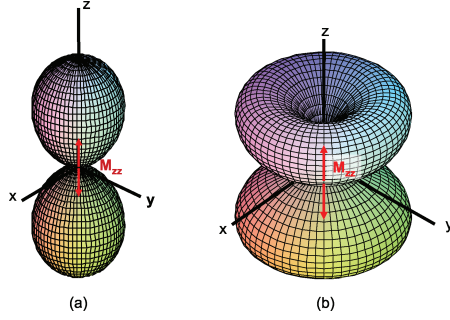
Figure 6. (colour online) Geometry of a 3-D radiation pattern for a dipole source acting on the solid phase; (a) P wave (b) S wave.
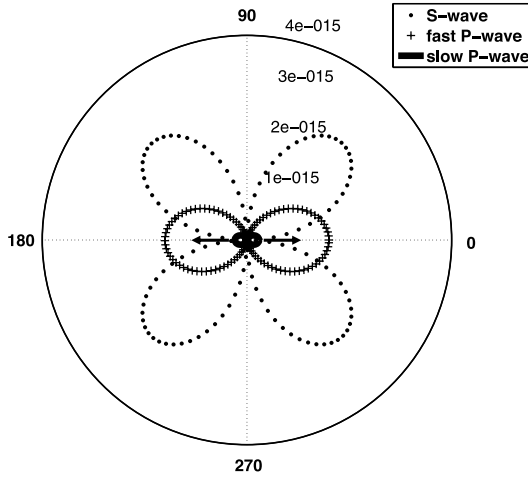

Figure 7. Dipole radiation pattern for solid displacement $\boldsymbol{u}$; the numbers 1×10^{-15} to 4×10^{-15} denote the displacement in meters along the radial axis; Cross-section perpendicular to the x–y plane; the slow *P*-wave radiation pattern is amplified by factor 3×10^5.

The radiation patterns for a dipole source acting on the bulk are illustrated in Figs 6–9. Fig. 6 gives a qualitative impression how a dipole source radiates into 3-D space. The *P*-wave radiation pattern in Fig. 6(a) has a similar form to its equivalent for a single force vector, however, its cones are more directionally shaped. The *S*-wave radiation in Fig. 6(b) of a dipole source are two doughnuts with zero radiation in axial direction. Both radiation patterns are symmetric with respect to the force direction.

Figs 7–9 give a quantitative interpretation of a dipole source acting on a poroelastic medium. The responses for a medium described by the parameters in Table 1 are computed in terms of the solid displacement $\boldsymbol{u}$, the relative displacement $\boldsymbol{w}$ and the pore pressure p. Similar to the single force case it can be observed that the solid displacement response is stronger by a factor of 5 compared to the relative displacement. The slow *P* wave is amplified by a factor of 3×10^5 for the solid displacement while it is not amplified for the relative displacement. Obviously, the slow *P* wave is stronger emphasized for $\boldsymbol{w}$ even though the overall magnitude is smaller. The strongest response for both *P* waves can be observed in the pressure field. The slow *P* wave is amplified by a factor of 3×10^5 but still has a significantly larger amplitude than for $\boldsymbol{u}$ and $\boldsymbol{w}$.
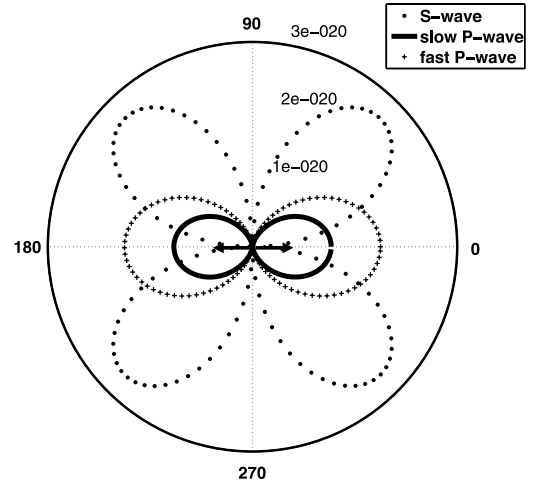
Figure 8. Dipole radiation pattern for the relative displacement $\boldsymbol{w}$; the numbers 1×10^{-20} to 3×10^{-20} denote the displacement in meters along the radial axis; Cross-section perpendicular to the x–y plane.
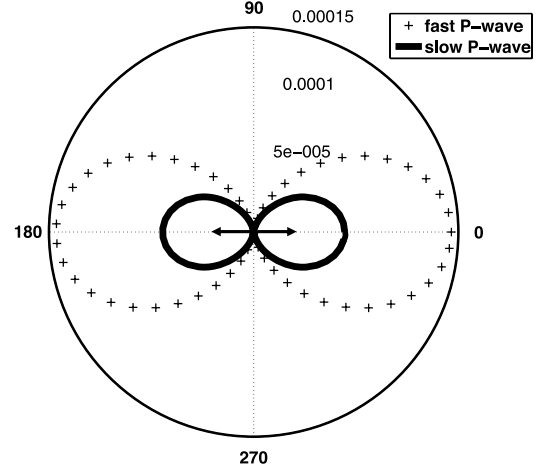
Figure 9. Dipole radiation pattern: pore pressure p; Cross-section perpendicular to the x–y plane; the numbers 5×10^{-5} to 0.00015 denote the pressure in Pascal along the radial axis; the slow *P*-wave displacement is amplified by factor 2×10^2; no shear wave is radiating in the fluid phase.

4.2.3 Fluid dipole source

As a source in the fluid phase can only consist of a volume source that can be either a volume injection V or an explosion, the fluid dipole source cannot be represented by the moment tensor concept. To overcome this difficulty, we use the concept introduced by Wang (2000) (section 5.8). A dipole source acting on the fluid phase can be thought of as a fluid sink distribution and a fluid source distribution displaced by vector $\boldsymbol{d}$. The pressure field can be expressed as

$$p^{\mathrm{dipol}} = -\nabla p \cdot \boldsymbol{d}. \tag{50}$$

This means that the pressure field of a dipole is the negative directional derivative of a pressure field due to a volume point source multiplied by the distance of the source and the sink. Using eq. (21) the pressure field (50) can be written as

$$p^{\mathrm{dipol}} = -V \nabla G^{V,p} \cdot \boldsymbol{d}. \tag{51}$$

Computing the gradient of both sides of eq. (24) yields the pressure field for a fluid dipole due to a pair of volume source and sink.
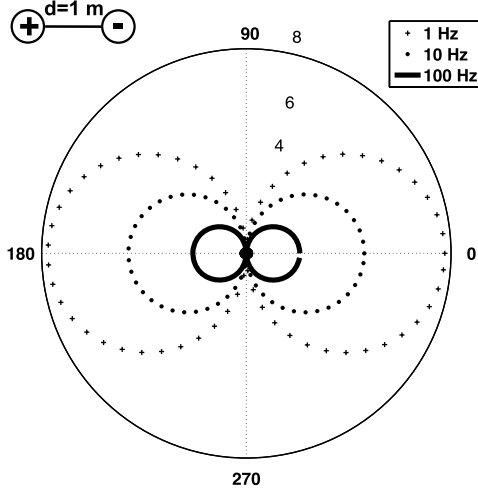
Figure 10. Fluid dipole radiation pattern: logarithm of the pore pressure p of the slow P wave for three frequencies; the numbers $4 - 8$ denote the pressure in Pascal along the radial axis; point in the centre is the fast P wave that is negligibly small compared to the slow P wave.

Using the parameters from Table 1, the radiation pattern of such a dipole is illustrated in Fig. 10. The distance is assumed as $|\boldsymbol{d}| = 1$ m and the orientation of the dipole is along the z-axis.

4.2.4 Double-couple source

Another source type that can be described using moment tensors is a double-couple source. For a fault in the $x - z$ plane with slip in x-direction the moment tensor is reduced to its off-diagonal components

$$\boldsymbol{M}_{DC} = \begin{pmatrix} 0 & M_{yx} & 0 \\ M_{xy} & 0 & 0 \\ 0 & 0 & 0 \end{pmatrix}. \tag{52}$$

Eq (41) for the P-wave radiation pattern reduces then to

$$\hat{\boldsymbol{r}} \cdot \boldsymbol{M}_{DC} \cdot \hat{\boldsymbol{r}} = M_{xy} \sin 2\kappa \sin^2 \theta . \tag{53}$$

Its 3-D radiation is qualitatively illustrated in Fig. 11. It has the form of a four-leaved clover with maximum energy radiated in the $x - y$ directions and zero energy in the direction of the coordinate axes. Two diagonal lobes are rotationally symmetric with respect to $x = y$.

The SH-radiation pattern in the $x - y$ plane is

$$\hat{\boldsymbol{\kappa}}_{SH} \cdot \boldsymbol{M}_{DC} \cdot \hat{\boldsymbol{r}} = M_{xy} \cos 2\kappa \sin \theta . \tag{54}$$
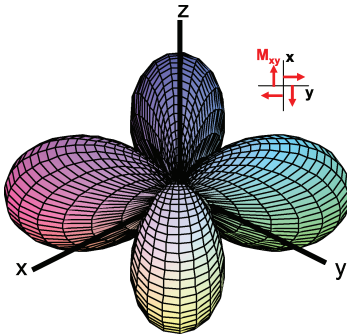
Figure 11. (colour online) 3-D P-wave radiation pattern of a double-couple source.
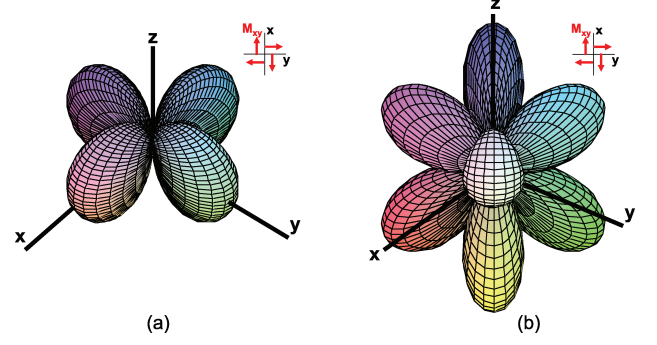
Figure 12. (colour online) 3-D radiation pattern of a double-couple source; (a) *SH* wave (b) *SV* wave.
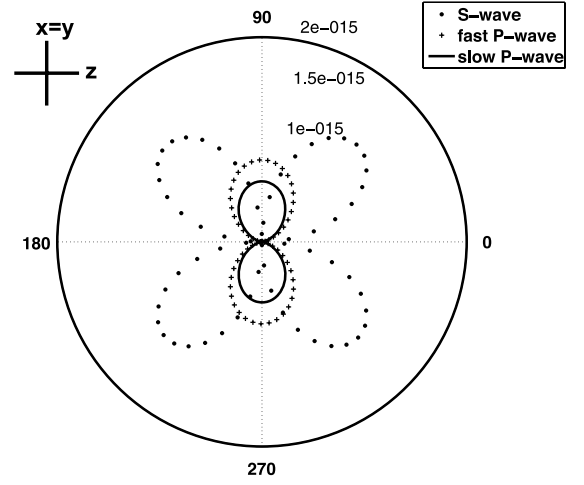
Figure 13. Double-couple radiation pattern: solid displacement $\boldsymbol{u}$; the numbers 1×10^{-15} to 2×10^{-15} denote the displacement in meters along the radial axis; the slow P wave displacement is amplified by 5×10^5.

The 3-D radiation pattern (Fig. 12a) is again a four-leaved clover but it is rotated by $45°$ with respect to the z-axes. For the SV wave, the radiation pattern is given by

$$\boldsymbol{\theta}_{SV} \cdot \boldsymbol{M}_{DC} \cdot \hat{\boldsymbol{r}} = \frac{1}{2} M_{xy} \sin 2\kappa \sin 2\theta, \tag{55}$$

and is illustrated in Fig. 12(b). It has eight lobes, one in each quadrant radiating maximum energy in the diagonal direction. The radiation patterns of a double-couple source are also illustrated in Figs 13–15.

5 CONCLUSIONS

A review and comparison of different formulations of Green's functions for dynamic poroelasticity is provided. We conclude that previously reported sets of Green's functions can be used in a complementary sense such that all possible combinations of field variables and source types are included. We think that the unified presentation of Green's functions resolves the apparent contradictions between existing formulations. As expected, the shape of the radiation patterns of the fast compressional and shear wave is identical to their elastodynamic counterparts, however, complemented with the radiation pattern of Biot's slow wave. The relative magnitudes of the field variables shown in the radiation patterns can be very different for different source types. In particular, for any source acting
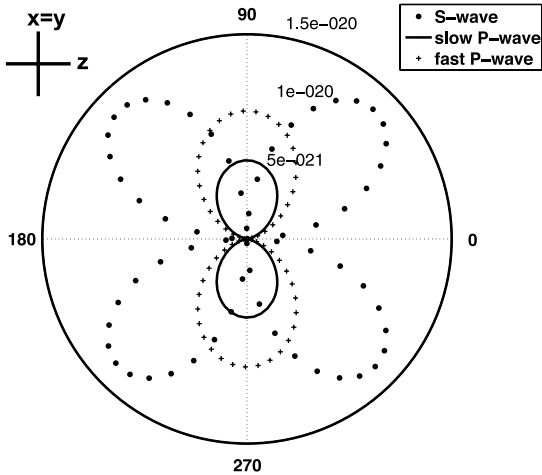
Figure 14. Double-couple radiation pattern: relative displacement w; the numbers 5×10^{-21} to 1.5×10^{-20} denote the displacement in meters along the radial axis.
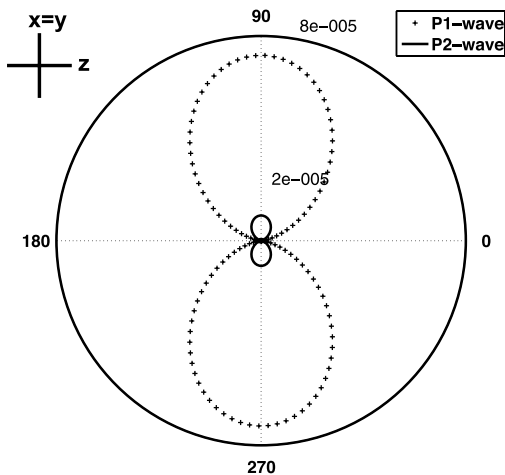
Figure 15. Double-couple radiation pattern: pore pressure p; the numbers 2×10^{-5} to 8×10^{-5} denote the pressure in Pascal along the radial axis; the slow *P*-wave radiation pattern is amplified by 1×10^5.

in the fluid phase the pressure field is dominated by the Biot slow wave having compressional wave polarization. We introduce the concept of moment tensors for dynamic poroelasticity that allows us to overcome the inconsistency in Green's function formulation with respect to point force sources in the fluid phase.

ACKNOWLEDGMENTS

REFERENCES

Aki, K. & Richards, P.G., 2002. *Quantitative Seismology,* University Science Books Sausalito, California.

Allard, J.-F., Bourdier, R. & Depollier, C., 1986. Biot waves in layered media, *J. appl. Phys.,* **60**(6), 1926–1929.

Backus, G. & Mulcahy, M., 1976a. Moment tensors and other phenomenological descriptions of seismic sources; i. continuous displacements, *Geophys. J. Int.,* **46**(2), 341–361.

Backus, G. & Mulcahy, M., 1976b. Moment tensors and other phenomenological descriptions of seismic sources; ii. discontinuous displacements, *Geophys. J. Int.,* **47**(2), 301–329.

Biot, M., 1956a. Theory of propagation of elastic waves in a fluid saturated porous solid. i-low frequency range, *J. acoust. Soc. Am.,* **28,** 168–178.

Biot, M., 1956b. Theory of propagation of elastic waves in a fluid saturated porous solid. ii-high frequency range, *J. acoust. Soc. Am.,* **28,** 179–191.

Biot, M., 1962. Mechanics of deformation and acoustic propagation in porous solids, *J. appl. Phys.,* **33,** 1482–1498.

Biot, M. & Willis, D., 1957. The elastic coefficients of the theory of consolidation, *J. appl. Mech.,* **24,** 594–601.

Bonnet, G., 1987. Basic singular solutions for a poroelastic medium in the dynamic range, *J. acoust. Soc. Am.,* **82**(5), 1758–1762.

Boutin, C., 1987. Green functions and associated sources in infinite and stratified poroelastic media, *Geophys. J. R. astr. Soc.,* **90,** 521–550.

Boutin, C., 1991. Integral representation and sources in isotropic poroelastic media, in *Transport Processes in Porous Media,* pp. 521–538, Kluwer Academic Publishers.

Burridge, R. & Vargas, C., 1979. The fundamental solutions in dynamic poroelasticity, *Geophys. J. R. astr. Soc,* **58,** 61–90.

Chandler, R.N. & Johnson, D.L., 1981. The equivalence of quasistatic flow in fluid-saturated porous media and Biot's slow wave in the limit of zero frequency, *J. appl. Phys.,* **52**(5), 3391–3395.

Chapman, C., 2004. *Fundamentals of Seismic Wave Propagation,* Cambridge University Press.

Chen, J., 1994a. Time domain fundamental solution to Biot's complete equations of dynamic poroelasticity. part i: Two-dimensional solution., *Int. J. Solids Struct.,* **31**(10), 1447–1490.

Chen, J., 1994b. Time domain fundamental solution to Biot's complete equations of dynamic poroelasticity. part ii: Three-dimensional solution., *Int. J. Solids Struct.,* **31**(2), 169–202.

Gassmann, F., 1951. Über die Elastizität poröser Medien, *Viertel. Naturforsch. Ges. Zürich,* **96**(1), 1–23.

Johnson, D.L., Koplik, J. & Dashen, R., 1987. Theory of dynamic permeability and tortuosity in fluid-saturated porous media, *J. Fluid Mech.,* **176,** 379–402.

Jost, M. & Herrmann, R., 1989. A student's guide to and review of moment tensors, *Seismol. Res. Lett.,* **60,** 37–57.

Kupradze, V., 1979. *Three-dimensional Problems of the Mathmatical Theory of Elasticity and Thermoelasticity,* North-Holland, Amsterdam.

Kurkjian, A.L., Coates, R.T., White, J.E. & Schmidt, H., 1994. Finite-difference and frequency-wavenumber modeling of seismic monopole sources and receivers in fluid-filled boreholes, *Geophysics,* **59**(7), 1053–1064.

Lu, J.-F., Jeng, D.-S. & Williams, S., 2008. A 2.5-d dynamic model for a saturated porous medium: Part i. Green's function, *Int. J. Solids Struct.,* **45**(2), 378–391.

Molotkov, L.A. & Bakulin, A., 1998. Internal point sources in poroelastic Biot medium, in *Amplitude-Preserving Seismic Reflection Imaging, Seismic application series,* **Vol. 2,** pp. 73–88, ed. Hubral, P., Geophysical Press.

Müller, T.M., 2006. Spatiotemporal pore pressure evolution due to fluid-mass point sources in dynamic poroelasticity, *Geophys. J. Int.,* **165**(3), 906–912.

Müller, T.M. & Gurevich, B., 2005. A first-order statistical smoothing approximation for the coherent wave field in random porous media, *J. acoust. Soc. Am.,* **117**(4), 1796–1805.

Norris, A.N., 1985. Radiation from a point source and scattering theory in a fluid-saturated porous solid, *J. acoust. Soc. Am.,* **77**(6), 2012–2023.

Norris, A.N., 1992. On the correspondence between poroelasticity and thermoelasticity, *J. appl. Phys.,* **71**(3), 1138–1141.

Norris, A.N., 1994. Dynamic Green's functions in anisotropic piezoelectric, thermoelastic and poroelastic solids, *Proc. R. Soc. Lond.,* **447,** 175–188.

Philippacopoulos, A., 1998. Spectral Green's dyadic for point sources in poroelastic media, *J. Eng. Mech.,* **124**(1), 24–30.

Pride, S.R., 1994. Governing equations for the coupled electromagnetics and acoustics of porous media, *Phys.Rev. B,* **50,** 15 678–15 696.

Pride, S.R. & Haartsen, M.W., 1996. Electroseismic wave properties, *J. acoust. Soc. Am.,* **100**(3), 1301–1315.

Rudnicki, J.W., 1986. Fluid mass sources and point forces in linear elastic diffusive solids, *Mech. Mat.,* **5,** 383–393.

Rudnicki, J.W. & Freund, L., 1981. On energy radiation from seismic sources, *Bull. seism. Soc. Am.,* **71,** 583–595.

Sahay, P., 2001. DynamicGreen's function for homogeneous and isotropic porous media, *Geophys. J. Int.,* (147), 622–629.

Schanz, A. & Pryl, D., 2004. Dynamic fundamental solutions for compressible and incompressible modeled poroelastic continua, *Int. J. Solids Struct.,* **41,** 4047–4073.

Wang, H., 2000. *Theory of Linear Poroelasticity with Applications to Geomechanics and Hydrogeology,* Princeton University Press.

Wenzlau, F. & Müller, T., 2009. Finite-difference modeling of wave propagation and diffusion in poroelastic media, *Geophysics,* in press.

Wu, R.-S. & Ben-Menahem, A., 1985. The elastodynamic near field, *Geophys. J. Int.,* **81**(3), 609–621.

APPENDIX A: BIOT BULK WAVE SLOWNESSES

The bulk wave slowness in a poroelastic medium is given by

$$2s_1^2 = \gamma - \sqrt{\gamma^2 - \frac{4\tilde{\rho}\rho_t}{MH - C^2}} \quad ,$$
$$2s_2^2 = \gamma + \sqrt{\gamma^2 - \frac{4\tilde{\rho}\rho_t}{MH - C^2}} \quad ,$$
$$s_3^2 = \frac{\rho_t}{\mu}, \tag{A1}$$

where s_1, s_2 and s_3 are fast, slow compressional and shear slowness respectively and $C = \alpha M$. The coefficient γ is defined as

$$\gamma = \frac{\rho M + \tilde{\rho} H - 2\rho_f C}{HM - C^2}. \tag{A2}$$

APPENDIX B: AMPLITUDES OF GREEN'S FUNCTIONS

The amplitudes appearing in the expression for the Green tensors (15), (23) and (24) are given by

$$T_{u,s_3}^F = \frac{1}{\mu}$$

$$T_{w,s_3}^F = T_{u,s_3}^f = -\frac{\rho_f}{\tilde{\rho}\mu}$$

$$T_{w,s_3}^f = -\frac{s_3^2 - \frac{\rho}{\mu}}{\omega^2 \tilde{\rho}}$$

$$L_{u,s_1}^F = \left(\frac{M}{MH - C^2}\right)\left(\frac{s_2^2 - \frac{\tilde{\rho}}{M}}{s_1^2 - s_2^2}\right)$$

$$L_{w,s_1}^F = L_{u,s_1}^f = -\left(\frac{C}{MH - C^2}\right)\left(\frac{s_1^2 - \frac{\rho_f}{C}}{s_1^2 - s_2^2}\right)$$

$$L_{w,s_1}^f = \left(\frac{H}{MH - C^2}\right)\left(\frac{s_1^2 - \frac{\rho}{H}}{s_1^2 - s_2^2}\right)$$

$$L_{u,s_2}^F = \left(\frac{M}{MH - C^2}\right)\left(\frac{s_2^2 - \frac{\tilde{\rho}}{M}}{s_1^2 - s_2^2}\right)$$

$$L_{w,s_2}^F = L_{u,s_2}^f = \left(\frac{C}{MH - C^2}\right)\left(\frac{s_2^2 - \frac{\rho_f}{C}}{s_1^2 - s_2^2}\right)$$

$$L_{w,s_2}^f = \left(\frac{H}{MH - C^2}\right)\left(\frac{s_2^2 - \frac{\rho}{H}}{s_1^2 - s_2^2}\right)$$

$$L_{p,s_1}^F = L_{u,s_1}^V = -is_1\omega\frac{P_{\text{dry}}}{\tilde{\rho}\hat{\alpha}}\left(s_2^2 - s_1^2\right)$$

$$L_{p,s_2}^F = L_{u,s_2}^V = is_2\omega\frac{P_{\text{dry}}}{\tilde{\rho}\hat{\alpha}}\left(s_2^2 - s_1^2\right)$$

$$L_{p,s_1}^V = \frac{\omega^2 \tilde{\rho}}{T_{u,s_3}^F}L_{u,s_1}^F\frac{s_3^2}{s_1^2}$$

$$L_{p,s_2}^V = \frac{\omega^2 \tilde{\rho}}{T_{u,s_3}^F}L_{u,s_2}^F\frac{s_3^2}{s_2^2} \quad . \tag{B1}$$

Bibliography

Achenbach, J. D. (1973). *Wave propagation in elastic solids*. North Holland, Amsterdam.

Adamou, A. T. I. and Craster, R. V. (2004). Spectral methods for modelling guided waves in elastic media. *J. Acoust. Soc. Amer.*, 116(3):1524–1535.

Aki, K. and Richards, P. G. (2002). *Quantitative Seismology*. University Science Books.

Allard, J.-F., Bourdier, R., and Depollier, C. (1986). Biot waves in layered media. *Journal of Applied Physics*, 60(6):1926–1929.

Backus, G. and Mulcahy, M. (1976a). Moment tensors and other phenomenological descriptions of seismic sources;i. continuous displacements. *Geophysical Journal International*, 46(2):341–361.

Backus, G. and Mulcahy, M. (1976b). Moment tensors and other phenomenological descriptions of seismic sources;ii. discontinuous displacements. *Geophysical Journal International*, 47(2):301–329.

Bakulin, A., Jaaskelainen, M., Sidorov, A., and Kashtan, B. (2008a). Downhole acoustic surveillance of deepwater wells. *The Leading Edge*, 27(4):518–531.

Bakulin, A., Sidorov, A., Kashtan, B., and Jaaskelainen, M. (2008b). Real-time completion monitoring with acoustic waves. *Geophysics*, 73(1):E15–E33.

Bancroft, D. (1941). The velocity of longitudinal waves in cylindrical bars. *Physical Review*, 59(7):588–593.

Berryman, J. G. (1983). Dispersion of extensional waves in fluid-saturated porous cylinders at ultrasonic frequencies. *J. Acoust. Soc. Amer.*, 74(6):1805 – 1812.

Biot, M. A. (1956a). Theory of propagation of elastic waves in a fluid-saturated porous solid. I. Low-frequency range. *J. Acoust. Soc. Amer.*, 28:168–178.

Biot, M. A. (1956b). Theory of propagation of elastic waves in a fluid-saturated porous solid. II. Higher frequency range. *J. Acoust. Soc. Amer.*, 28:179–191.

Biot, M. A. (1962). Generalized theory of acoustic propagation in porous dissipative media. *J. Acoust. Soc. Amer.*, 34(5):1254 – 1264.

Bonnet, G. (1987). Basic singular solutions for a poroelastic medium in the dynamic range. *J.Acoust.Soc.Am.*, 82(5):1758–1762.

Boutin, C. (1987). Green functions and associated sources in infinite and stratified poroelastic media. *Geophys.J.R.astr.Soc.*, 90:521–550.

Boutin, C. (1991). Transport processes in porous media: Integral representation and sources in isotropic poroelastic media. pages 521–538. Kluwer Academic Publishers.

Burridge, R. and Vargas, C. A. (1979). The fundamental solutions in dynamic poroelasticity. *Geophys. J. Roy. Astr. Soc*, 58:61–90.

Chang, S. K., Liu, H. L., and Johnson, D. L. (1988). Low-frequency tube waves in permeable rocks. *Geophysics*, 53(4):519 – 527.

Chapman, C. (2004). *Fundamentals of Seismic Wave Propagation*. Cambridge University Press.

Chen, J. (1994a). Time domain fundamental solution to biot?s complete equations of dynamic poroelasticity. part i: Two-dimensional solution. *International Journal of Solids and Structures*, 31(10):1447–1490.

Chen, J. (1994b). Time domain fundamental solution to biot?s complete equations of dynamic poroelasticity. part ii: Three-dimensional solution. *International Journal of Solids and Structures*, 31(2):169–202.

Chree, C. (1889). The equations of an isotropic elastic solid in polar and cylindrical coordinates, their solutions and applications. *Trans. Camb. Phil. Soc.*, 14:250.

Davies, R. M. (1948). A critical study of Hopkinson pressure bar. *Proc. Royal Soc. of London*, 240(821):375–457.

Del Grosso, V. A. and McGill, R. E. (1968). Remarks on "Axially symmetric vibrations of a thin cylindrical elastic shell filled with nonviscous fluid" by Ram Kumar, Acustica 17 [1968],218. *Acustica*, 20(5):313–314.

Deresiewicz, H. and Skalak, R. (1963). On uniqueness in dynamic poroelasicity. *Bull. Seismol. Soc. Amer.*, 53:783–788.

Feng, S. and Johnson, D. L. (1983). High-frequency acoustic properties of a fluid/porous solid interface. i. new surface mode. *J. Acoust. Soc. Amer.*, 74(3):906–914.

Gardner, G. H. F. (1962). Extensional waves in fluid-saturated porous cylinders. *J. Acoust. Soc. Amer.*, 34(1):36–39.

Gassmann, F. (1951). Über die elastizität poröser medien. *Viertel. Naturforsch. Ges. Zürich*, 96:1–23.

Gazis, D. C. (1959a). Three-dimensional investigation of the propagation of waves in hollow circular cylinders. I. Analytical foundation. *J. Acoust. Soc. Amer.*, 31(5):568–573.

Gazis, D. C. (1959b). Three-dimensional investigation of the propagation of waves in hollow circular cylinders. II. Numerical results. *J. Acoust. Soc. Amer.*, 31(5):573–578.

Johnson, D. L., Koplik, J., and Dashen, R. (1987). Theory of dynamic permeability and tortuosity in fluid-saturated porous media. *Journal of Fluid Mechanics*, 176:379–402.

Jost, M. and Herrmann, R. (1989). A student's guide to and review of moment tensors. *Seismological Research Letters*, 60:37–57.

Karpfinger, F., Gurevich, B., and Bakulin, A. (2008a). Computation of wave propagation along cylindrical structures using the spectral method. *J. Acoust. Soc. Amer.*, 124(2):859–865.

Karpfinger, F., Gurevich, B., and Bakulin, A. (2008b). Modeling of axisymmetric wave modes in a poroelastic cylinder using spectral method. *J. Acoust. Soc. Amer.*, 124(4):EL230–EL235.

Kolsky, H. (1963). *Stress waves in solids*. Dover, New York.

Kupradze, V. D. (1979). *Three-dimensional problems of the mathmatical theory of elasticity and thermoelasticity*. North-Holland,Amsterdam.

Kurkjian, A. L., Coates, R. T., White, J. E., and Schmidt, H. (1994). Finite-difference and frequency-wavenumber modeling of seismic monopole

sources and receivers in fluid-filled boreholes. *Geophysics*, 59(7):1053–1064.

Lin, T. and Morgan, G. (1956). Wave propagation through a fluid contained in a cylindrical, elastic shell. *J. Acoust. Soc. Amer.*, 28(6):1165–1176.

Liu, H.-L. and Johnson, D. L. (1997). Effects of an elastic membrane on tube waves in permeable formations. *The Journal of the Acoustical Society of America*, 101(6):3322–3329.

Love, A. E. H. (1944). *A treatise on the mathematical theory of elasticity*. Dover, New York.

Lu, J.-F., Jeng, D.-S., and Williams, S. (2008). A 2.5-d dynamic model for a saturated porous medium: Part i. green's function. *International Journal of Solids and Structures*, 45(2):378–391.

McFadden, J. A. (1954). Radial vibrations of thick-walled hollow cylinders. *J. Acoust. Soc. Amer.*, 26(5):714–715.

Molotkov, L. A. and Bakulin, A. V. (1998). Internal point sources in poroelastic biot medium. In Hubral, P., editor, *Amplitude-Preserving Seismic Reflection Imaging, Seismic application series*, volume 2, pages 73–88. Geophysical Press.

Morgan, G. W. and Kiely, J. P. (1954). Wave propagation in a viscous liquid contained in a flexible tube. *J. Acoust. Soc. Amer.*, 26(3):323–328.

Müller, T. M. (2006). Spatiotemporal pore pressure evolution due to fluid-mass point sources in dynamic poroelasticity. *Geophysical Journal International*, 165(3):906–912.

Müller, T. M. and Gurevich, B. (2005). A first-order statistical smoothing approximation for the coherent wave field in random porous media". *J. Acoust. Soc. Am.*", 117 ":4, 1796–1805.

Norris, A. N. (1985). Radiation from a point source and scattering theory in a fluid-saturated porous solid. *J.Acoust.Soc.Am.*, 77(6):2012–2023.

Norris, A. N. (1992). On the correspondence between poroelasticity and thermoelasticity. *Journal of Applied Physics*, 71(3):1138–1141.

Norris, A. N. (1994). Dynamic green's functions in anisotropic piezoelectric, thermoelastic and poroelastic solids. *Proc. R. Soc. Lond*, 447:175–188.

Paillet, F. L. and White, J. E. (1982). Acoustic modes of propagation in the borehole and their relationship to rock properties. *Geophysics*, 47(8):1215–1228.

Philippacopoulos, A. (1998). Spectral green's dyadic for point sources in poroelastic media. *Journal of engineering mechanics*, 124(1):24–30.

Pochhammer, L. (1876). On the propagation velocities of small oscillations in an unlimited isotropic circular cylinder. *J. Reine Angew. Math.*, 81:324.

Pride, S. R. (1994). Governing equations for the coupled electromagnetics and acoustics of porous media. *Physical Review B*, 50:15678–15696.

Pride, S. R. and Haartsen, M. W. (1996). Electroseismic wave properties. *J. Acoustic. Soc. Am.*, 100(3):1301–1315.

Rao, V. N. R. and Vandiver, J. K. (1997). Acoustics of fluid filled boreholes with pipe: Guided propagation and radiation. *J. Acoust. Soc. Amer.*, 105(6):3057–3066.

Richard N. Chandler and David Linton Johnson (1981). The equivalence of quasistatic flow in fluid-saturated porous media and biot's slow wave in the limit of zero frequency. *Journal of Applied Physics*, 52(5):3391–3395.

Rubinow, S. I. and Keller, J. B. (1971). Wave propagation in a fluid-filled tube. *J. Acoust. Soc. Amer.*, 50(1B):198–223.

Rudnicki, J. W. (1986). Fluid mass sources and point forces in linear elastic diffusive solids. *Mechanics of Materials*, 5:383–393.

Rudnicki, J. W. and Freund, L. B. (1981). On energy radiation from seismic sources. *Bulletin of the Seismological Society of America*, 71:583–595.

Sahay, P. N. (2001). Dynamic green's function for homogeneous and isotropic porous media. *Geophys. J. Int.*, (147):622–629.

Schanz, A. and Pryl, D. (2004). Dynamic fundamental solutions for compressible and incompressible modeled poroelastic continua. *International Journal of Solids and Structures*, 41:4047–4073.

Vollmann, J., Breu, R., and Dual, J. (1997). High-resolution analysis of the complex wave spectrum in a cylindrical shell containing a viscoelastic medium. part ii. experimental results versus theory. *The Journal of the Acoustical Society of America*, 102(2):909–920.

Vollmann, J. and Dual, J. (1997). High-resolution analysis of the complex wave spectrum in a cylindrical shell containing a viscoelastic medium. part i. theory and numerical results. *The Journal of the Acoustical Society of America*, 102(2):896–908.

Wang, H. F. (2000). *Theory of linear poroelasticity with applications to geomechanics and hydrogeology*. Princeton University Press.

Weideman, J. A. C. and Reddy, S. C. (2000). A MATLAB differentiation matrix suite. *ACM Trans. Math. Softw.*, 26:465.

Wenzlau, F. and Müller, T. M. (accepted). Finite-difference modeling of wave propagation and diffusion in poroelastic media. *Geophysics*.

Winkler, K. W., Liu, H.-L., and Johnson, D. L. (1989). Permeability and borehole Stoneley: Comparison between experiment and theory. *Geophysics*, 54(1):66 – 75.

Wisse, C. J., Smeulders, D. M. J., Chao, G., and van Dongen, M. E. H. (2007). Guided wave modes in porous cylinders: Theory. *The Journal of the Acoustical Society of America*, 122(4):2049–2056.

Wu, R.-S. and Ben-Menahem, A. (1985). The elastodynamic near field. *Geophysical Journal International*, 81(3):609–621.

APPENDIX A

Statements of co-authors

Co-Author 1: Boris Gurevich

To whom it may concern,

To the publication by

Karpfinger, F., <u>Gurevich B.</u> and Bakulin A., Computation of Wave Propagation Along Cylindrical Structures Using the Spectral Method (2008), The Journal of the Acoustical Society of America, **124**(2), 859-865.

my contribution consisted in supervision of the research work and editing of the manuscript. The bulk of the research and all of the programming, computations and writing was done by Florian Karpfinger.

Boris Gurevich

To whom it may concern,

To the publication by

Karpfinger, F., <u>Gurevich, B.</u> and Bakulin, A. (2008), Modeling of axisymmetric wave modes in a poroelastic cylinder using spectral method, Journal of the Acoustical Society of America, **124**(4), EL230-EL235.

my contribution consisted in supervision of the research work and editing of the manuscript. The bulk of the research and all of the programming, computations and writing was done by Florian Karpfinger.

Boris Gurevich

To whom it may concern,

To the publication by

Bakulin, A., **Karpfinger, F.** and <u>Gurevich, B.</u> (2008), Understanding acoustic response of deepwater completions, The Leading Edge, **27**(12), 260-267.

my contribution consisted in supervision of the research work and editing of the manuscript. The bulk of the research and all of the programming and computations was done by Florian Karpfinger.

Boris Gurevich

To whom it may concern,

To the publication by

Karpfinger, F., Mueller, T., and <u>Gurevich, B.</u> (2009), Green's functions and radiation patterns in poroelastic solids revisited, Geophy. J. Int, DOI: 10.1111/j.1365-246X.2009.04116.x.

my contribution consisted in posing the problem, technical advice and discussion. The bulk of the research and all of the programming, computations and writing was done by Florian Karpfinger.

Boris Gurevich

To whom it may concern,

To the publication by

Karpfinger, F., <u>Gurevich, B.</u> and Bakulin, A. (2009), Axisymmetric waves in fluid saturated porous structures, 4th Biot Conference.

my contribution consisted in supervision of the research work and editing of the manuscript. The bulk of the research and all of the programming, computations and writing was done by Florian Karpfinger.

Boris Gurevich

To whom it may concern,

To the manuscript by

Karpfinger, F., Valero, H.-P., <u>Gurevich, B.</u>, Bakulin, A. and Sinha, B. (2009), Spectral method algorithm for modeling dispersion of acoustic modes in elastic cylindrical structures, Geophysics.

my contribution consisted in supervision of the research work and editing of the manuscript. The bulk of the research and all of the programming, computations and writing was done by Florian Karpfinger.

Boris Gurevich

Co-Author 2: Andrey Bakulin

To whom it may concern,

To the publication by

Karpfinger, F., Gurevich B. and <u>Bakulin A.</u>, Computation of Wave Propagation Along Cylindrical Structures Using the Spectral Method (2008), The Journal of the Acoustical Society of America, **124**(2), 859-865, ,

my contribution consisted in posing the problem, motivating practical examples and editing of the manuscript. The bulk of the research and all of the programming, computations and writing was done by Florian Karpfinger.

Andrey Bakulin

To whom it may concern,

To the publication by

Karpfinger, F., Gurevich, B. and <u>Bakulin, A.</u> (2008), Modeling of axisymmetric wave modes in a poroelastic cylinder using spectral method, Journal of the Acoustical Society of America, **124**(4), EL230-EL235.

my contribution consisted in posing the problem, motivating practical examples and editing of the manuscript. The bulk of the research and all of the programming, computations and writing was done by Florian Karpfinger.

Andrey Bakulin

To whom it may concern,

To the publication by

<u>Bakulin, A.,</u> **Karpfinger, F.** and Gurevich, B. (2008), Understanding acoustic response of deepwater completions, The Leading Edge, **27**(12), 260-267.

my contribution consisted in posing the problem, motivating practical examples and editing of the manuscript. The bulk of the research and all of the programming, computations and writing was done by Florian Karpfinger.

Andrey Bakulin

To whom it may concern,

To the publication by

Karpfinger, F., Gurevich, B. and <u>Bakulin, A.</u> (2009), Axisymmetric waves in fluid saturated porous structures, 4th Biot Conference.

my contribution consisted in posing the problem, motivating practical examples and editing of the manuscript. The bulk of the research and all of the programming, computations and writing was done by Florian Karpfinger.

Andrey Bakulin

To whom it may concern,

To the manuscript by

Karpfinger, F., Valero, H.-P., Gurevich, B., <u>Bakulin, A.</u> and Sinha, B. (2009), Spectral method algorithm for modeling dispersion of acoustic modes in elastic cylindrical structures, Geophysics.

my contribution consisted in posing the problem, motivating practical examples and editing of the manuscript. The bulk of the research and all of the programming, computations and writing was done by Florian Karpfinger.

Andrey Bakulin

Co-Author 3: Tobias Müller

To whom it may concern,

I, Dr. Tobias Müller, contributed to the publication entitled

Karpfinger, F., Müller, T., and <u>Gurevich, B.</u> (2009), Green's functions and radiation patterns in poroelastic solids revisited, Geophy. J. Int. (in press)

in the following way:

I supervised the research and revised the manuscript.

Sincerely,

Tobias Müller

Co-Author 4: Henri-Pierre Valero

To whom it may concern,

To the manuscript by

Karpfinger, F., Valero, H.-P., Gurevich, B., Bakulin, A. and Sinha, B. (2009), Spectral method algorithm for modeling dispersion of acoustic modes in elastic cylindrical structures, Geophysics.

My contribution consisted in supervision of the programming and computations. The bulk of the research and all of the implementation of the method together with the documentation and the redaction of the paper have been done by Florian Karpfinger.

Henri-Pierre Valero

Co-Author 5: Bikash Sinha

To whom it may concern,

To the manuscript by

Karpfinger, F., Valero, H.-P., Gurevich, B., Bakulin, A. and Sinha, B. (2009), Spectral method algorithm for modeling dispersion of acoustic modes in elastic cylindrical structures, Geophysics.

My contribution consists of supervising Florian Karpfinger's work while he was a Summer Intern at Schlumberger-Doll Research; and providing him with the borehole modal dispersions for a radially homogeneous and isotropic formation obtained by a root-search method of a boundary-condition determinant. Most of the work in this paper has been performed by Florian Karpfinger.

Bikash Sinha

APPENDIX B

Permission letters for copyright release

Paper 1:

Karpfinger, F., Gurevich B. and Bakulin A.(2008),Computation of Wave Propagation Along Cylindrical Structures Using the Spectral Method, The Journal of the Acoustical Society of America, 124(2), 859-865, http://dx.doi.org/10.1121/1.2940577.

Paper 2:

Karpfinger, F., Gurevich, B. and Bakulin, A.(2008), Modelling of axisymmetric wave modes in a poroelastic cylinder using spectral method, Journal of the Acoustical Society of America, 124(4), EL230-EL235, http://dx.doi.org/10.1121/1.2968303.

Florian Karpfinger

From:	RIGHTS [Rights@aip.org]
Sent:	Thursday, 26 February 2009 2:58 AM
To:	Florian Karpfinger
Subject:	Re: Using publication in Thesis

Dear Dr. Karpfinger:

Thank you for requesting permission to reproduce material from Acoustical Society of America publications.

Permission is granted – subject to the conditions outlined below – for the following:

Karpfinger, F., Gurevich, B. and Bakulin, A., Modeling of axisymmetric wave modes in a poroelastic cylinder using spectral method, Journal of the Acoustical Society of America, 124(4), EL230-EL235, 2008.

Karpfinger, F., Gurevich, B. and Bakulin, A., Computation of Wave Propagation Along Cylindrical Structures Using the Spectral Method, Journal of the Acoustical Society of America, 124(2), 859-865, 2008.

To be used in the following manner:

Reproduced as part of your PhD thesis for submission to the University of Australia.

1. The Acoustical Society of America grants you the right to reproduce the material indicated above on a one-time, non-exclusive basis, solely for the purpose described. Permission must be requested separately for any future or additional use.

2. This permission pertains only to print use and its electronic equivalent, including CD-ROM or DVD.

3. The following copyright notice must appear with the material (please fill in the information indicated by capital letters): "Reprinted with permission from [FULL CITATION]. Copyright [PUBLICATION YEAR], Acoustical Society of America."
Full citation format is as follows: Author names, journal title, Vol. #, Issue #, Page #, Year of publication.
For an article, the copyright notice must be printed on the first page of the article or book chapter. For figures, photographs, covers, or tables, the notice may appear with the material, in a footnote, or in the reference list.

4. This permission does not apply to any materials credited to sources other than the copyright holder.

Please let us know if you have any questions.

Sincerely,
Susann Brailey

~~~~~~~~~~
Office of the Publisher, Journals and Technical Publications Rights & Permissions American Institute of Physics Suite 1NO1
2 Huntington Quadrangle
Melville, NY 11747-4502
516-576-2268   TEL
516-576-2450   FAX

Paper 3:

Bakulin, A., **Karpfinger, F.** and Gurevich, B.(2008), Understanding acoustic response of deepwater completions, The Leading Edge, 27(12), 260-267, http://dx.doi.org/10.11 90/1.3036969.

Florian Karpfinger

From: Ted Bakamjian [Tbakamjian@seg.org]
Sent: Wednesday, 11 February 2009 2:21 AM
To: florian.karpfinger@postgrad.curtin.edu.au
Cc: Dean Clark
Subject: Permission request

Greetings Florian,

You have permission to republish the work in your thesis. Please provide acknowledgement of SEG copyright and a complete citiation, and please also provide the permalink so that the online publication of the article can be viewed by readers in the context within which it was published.

The permalink: http://dx.doi.org/10.1190/1.3036969

I just tested the permissions@seg.org e-mail and found it works. If the problem is that you sent a message to it earlier and did not get a response, please accept my apologies.

Best of luck iv>

Ted Bakamjian
Director, Publications
Society of Exploration Geophysicists
P. O. Box 702740, Tulsa, OK 74170-2740 USA
Shipping: 8801 S. Yale Ave., Tulsa, OK 74137
Phone: (918) 497-5506; Fax v style="margin-top: 0px; margin-right: 0px; margin-bottom: 0px; margin-left: 0px; ">E-mail: tbakamjian@seg.org; Web: http://www.seg.org/

From: Florian Karpfinger [mailto:florian.karpfinger@postgrad.curtin.edu.au]
Sent: Tuesday, February 10, 2009 1:12 AM
To: Dean Clark
Subject: Re-publishing of article for thesis

To whom it may concern,

I am a PhD student at C Australia and I am planning to submit my thesis by publication.
I have published the following article in TLE:

Bakulin, A., **Karpfinger, F.** and Gurevich, B., *Understanding acoustic response of deepwater completions*, The Leading Edge, **27**(12), 260-267, 2008.

Paper 4:

Karpfinger, F., Mueller, T., and Gurevich, B.(2009), Green's functions and radiation patterns in poroelastic solids revisited, Geophy. J. Int, DOI:10.1111/j.1365-246X.2009.04116.x.

Florian Karpfinger

From:	Mothersole, Laura - Oxford [lmothersole@wiley.com] on behalf of Permission Requests - UK [permreq@wiley.com]
Sent:	Wednesday, 18 February 2009 8:40 PM
To:	Florian Karpfinger
Subject:	RE:

Dear Florian Karpfinger

Thank you for your email request. Permission is granted for you to use the material below for your thesis/dissertation subject to the usual acknowledgements and on the understanding that you will reapply for permission if you wish to distribute or publish your thesis/dissertation commercially.

Best wishes,

Laura Mothersole

Permissions Assistant
Wiley-Blackwell
9600 Garsington Road
Oxford OX4 2DQ
UK
Tel: +44 (0) 1865 476160
Fax: +44 (0) 1865 471158
Email: laura.mothersole@wiley.com

From: Florian Karpfinger [mailto:florian.karpfinger@postgrad.curtin.edu.au]
Sent: 10 February 2009 06:49
To: Permission Requests - UK
Subject:

To whom it may concern,

I am a PhD student at Curtin Univeristy in Australia and I am planning to submit my thesis by publication.
I have published (accepted but not published) the following article in GJI:

Karpfinger, F., Mueller, T., and Gurevich, B., *Green's functions and radiation patterns in poroelastic solids revisited*, Geophy. J. Int., 2009.

In order to be able to include this publication in my thesis I ask you herby for permission to do so.

If you have any further questions please do not hesitate to ask me.

Best regards

Florian Karpfinger

Paper 5:

Karpfinger, F., Gurevich, B. and Bakulin, A.(2009), Axisymmetric waves in fluid saturated porous structures, 4th Biot Conference, DEStech Publications, Inc., PA.

Florian Karpfinger

From: Fourth Biot Conference 2009 [biot@civil.columbia.edu]
Sent: Thursday, 30 April 2009 10:01 PM
To: Florian Karpfinger
Subject: RE: Copyright Release

Florian, I have confirmed that you can use it for your thesis without restriction.

Hoe

Quoting Florian Karpfinger
<florian.karpfinger@postgrad.curtin.edu.au>:

> Hoe,
>
> Sorry for not explaining correctly. In order to include the Biot paper
> in my thesis I need permission from the publisher to do so. Because by
> putting the paper in my thesis I basically re-publish it. I just need
> a contact at the publisher who can provide me with such a permission.
>
> The other question was if there is a version of the paper in its final
> form as it will appear in the book in electronic form.
> And I have one more question: can you let me know how long the talk
> will be.
>
> Thank you very much I appreciate your help.
>
> Best regards,
>
> Florian
>
> -----Original Message-----
> From: Fourth Biot Conference 2009
> [mailto:biot@civil.columbia.edu]
> Sent: Thursday, 30 April 2009 8:24 AM
> To: Florian Karpfinger
> Subject: Re: Copyright Release
>
> Florian, I can't follow your message correctly.
>
> You would sign a copyright release and send it to me (for the
> publisher). Is my interpretation right?
>
> Thanks
> Hoe
>
> Quoting Florian Karpfinger
> <florian.karpfinger@postgrad.curtin.edu.au>:
>
> > To whom it may concern,
> >
> >
> > My contribution to the Biot Conference is entitled:
> >
> > Axisymmetric waves in fluid-saturated porous Structures by

> > Florian Karpfinger, Boris Gurevich & Andrey Bakulin
> >
> >
> >
> >
> > I need a copyright release for this publication as it will be part
> > of my PhD thesis. Can you please advise me who to contact from the
> > Publisher. Can you also tell me if there is or will be a final
> > electronic version
> of
> > the paper
> > available.
> >
> > Thank you very much for your help!!!
> >
> >
> > Best regards,
> >
> >
> > Florian Karpfinger
> >
> >
> >
> >
> >
> >

APPENDIX C

Spectral method algorithm for modeling dispersion of acoustic modes in elastic cylindrical structures

Spectral method algorithm for modeling dispersion of acoustic modes in elastic cylindrical structures

Florian Karpfinger*, Henri-Pierre Valero‡, Boris Gurevich†, Andrey Bakulin§ and Bikash Sinha‡ *

ABSTRACT

This paper introduces a new spectral method algorithm which can be used to study wave propagation in cylindrically layered fluid and elastic structures. The cylindrical structure is discretized with Chebyshev points in the radial direction, whereas differentiation matrices are used to approximate the differential operators. We express the problem of determining modal dispersions as a generalized eigenvalue problem that can be readily solved for all eigenvalues corresponding to various axial wavenumbers. Modal dispersions of various guided modes can then be expressed interms of axial wavenumbers as a function of frequency. The associated eigenvectors are related to the displacement potentials that can be used to calculate radial distributions of modal amplitudes as well as stress components at a given frequency. This paper describes the overall workflow that includes input parameters, construction of differentiation matrices and boundary conditions that yield the generalized eigenvalue problem. Results from this algorithm for a fluid-filled borehole surrounded by an elastic formation agree very well with those from a root-finding search routine. Computational efficiency of this spectral method algorithm is illustrated in terms of a four-layer completion model used in a hydrocarbon producing well. Even though the algorithm is numerically unstable at very low frequencies, it produces reliable and accurate results for multilayered cylindrical structures at moderate frequencies that are of interest in the estimation of formation properties using modal dispersions.

INTRODUCTION

Modeling various wave modes propagating along a cylindrical borehole is of importance to understand and allow quantitative interpretation of borehole sonic and seismic measurements. Various modes and headwaves propagate in a fluid filled borehole (Sinha and Zeroug, 1997). Most notably this includes compressional and shear headwaves in addition to the flexural, Stoneley, pseudo-Rayleigh, and leaky modes. The recognition of these headwaves and modes further enhances sonic log quality and validates the use of dispersion curves in related applications. In order to fully understand and analyze the various modes/headwaves present in recorded waveforms, it is of interest to be able to properly model their characteristics as a function of formation, fluid parameters and geometry.

The classic way to solve such problems is to use a root-finding technique to solve the frequency equation. While this is not a significant problem for simple structures, such as solid cylinders (Zemanek, 1972; Gazis, 1959b,a), it becomes more complicated for multi-layered structures due to the fact that the separation of the different roots in the complex plane can be a challenging task.

An alternative approach to modeling mode dispersion is to use spectral collocation methods, that are efficient and accurate tools for solving partial differential equations. These methods have been widely used in numerical fluid dynamics (Canuto et al., 1988), as well as in geophysical modeling (Fornberg, 1987; Carcione et al., 2002; Kosloff et al., 1990).

Adamou and Craster (2004) introduced an algorithm, based on a spectral Chebyshev scheme which computes the dispersion of circumferential waves in an elastic annulus. Based on this work, Karpfinger et al. (2008a) developed an algorithm for axissymmetric modes propagating in cylindrical structures with an arbitrary number of fluid and solid layers. This algorithm allows the efficient computation of dispersion and radial profiles of various modes propagating in such structures.

The spectral method, which we introduce in this paper, discretizes the underlying equations with Chebyshev collocation points and differentiation matrices leading to a set of linear equations. We then solve the correspond-

ing system of linear equation as a generalized eigenvalue problem. Note that the eigenvalues we obtain for a given frequency correspond to the slownesses of the different modes.

The purpose of this paper is to describe the algorithm and its MATLAB implementation to compute propagating modes in cylindrical structures with arbitrary solid and fluid layers. We briefly discuss the underlying equations as well as the basic principles of spectral collocation methods. Next, we present in detail the workflow for the MATLAB code implementation is presented. Following this we discuss the solution of the generalized eigenvalue problem, which yields eigenvalues and eigenvectors. In addition we show how we separate the eigenvalues associated with the propagating modes from the non-propagating modes and spurious eigenvalues. Subsequently we illustrate how related dispersion curves are computed. Furthermore, we show how eigenvectors, which correspond to the displacement potentials, allow computation of the distribution of the stress and displacement components along the radius. Finally, we illustrate the results of the spectral method algorithm using examples from borehole acoustics involving two and four layers.

THEORY

We developed the theory to compute dispersion curves in cylindrical structures with arbitrary fluid and solid layers using the spectral approach in Karpfinger et al. (2008a). The underlying equations used for the numerical scheme are provided in Appendix A. Equations for an elastic solid and an in-viscous fluid are respectively presented in eqs. (A-1)-(A-6) and eqs. (A-7)-(A-10).
For each layer of the considered structure we compute the differential operator of the fluid $\mathfrak{L}_{fl}$ (eq. A-7) or solid layer. The elastic solid matrix consists of two differential operators due to the two differential equations: $\mathfrak{L}_p$ (eq. A-1) is the P-wave and $\mathfrak{L}_s$ (eq. A-2) is the S-wave differential operator. These differential operators are combined in a diagonal block matrix $\mathfrak{L}$. In the case of a fluid-solid structure (i.e. two-layer system, see Figure 2), the $\mathfrak{L}$ matrix has the following form

$$\mathfrak{L} = \left(\begin{array}{ccc} \mathfrak{L}_{fl} & 0 & 0 \\ 0 & \mathfrak{L}_p & 0 \\ 0 & 0 & \mathfrak{L}_s \end{array} \right) \qquad (1)$$

After discretizing all constitutive equations and introducing related boundary conditions, the problem can be expressed as an algebraic generalized eigenvalue problem:

$$\tilde{L}\boldsymbol{\Theta} = k_z^2 M \boldsymbol{\Theta} \qquad (2)$$

where $\tilde{L}$ is given by eq. (1) combined with the stress and displacement components of the boundary conditions. In the diagonal unit matrix M, the stress and displacement components introduced in $\tilde{L}$ are set to zero. This introduces the boundary conditions into the matrix eigenvalue problem. Solving this eigenvalue problem yields the un-
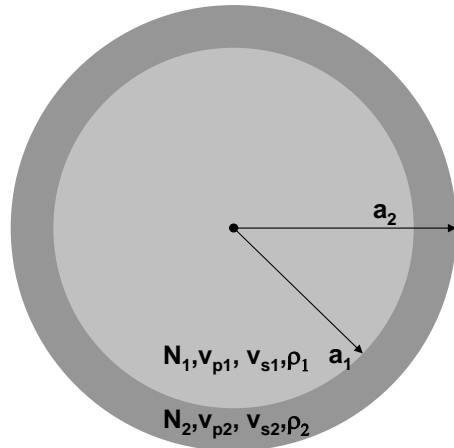

Figure 1: Input parameters for a fluid-filled tube: two-layer system; for each layer i the P-wave velocities (v_{pi}), S-wave (v_{si}) velocities, densities ρ_i, number of collocation points N_i and the radii a_i have to be known.

known squared axial wavenumber k_z^2. The axial wavenumber k_z is used to compute the phase velocity of the different modes propagating in the structure, while the displacement potential vector $\boldsymbol{\Theta}$ gives the potential for each collocation point along the radial direction, and allows computation of stress and displacement components along the radius. For a detailed description of how the eigenvalue problem is formulated and how the $\tilde{L}$ matrix is constructed (see Karpfinger et al., 2008a).

There are two main differences between our implementation of the spectral method in Karpfinger et al. (2008a) and the implementation described in this paper. First, in this paper we describe fluid layers using the acoustic equation of motion (eqs. A-7-A-10) rather than the limiting case of the elastic equations. Secondly, we have now discarded the boundary conditions in the center of the structure. It is shown in Boyd (2001,Chap.18.3) that no boundary conditions have to be set in the center of the structure, as for spectral methods this boundary condition is automatically fulfilled.

SPECTRAL METHOD

Differential equations can be very efficiently solved with spectral collocation methods. Orthogonal polynomials of high degree are used as global interpolants to approximate the unknown functions of the considered differential equations. The discrete matrix operator which approximates the differential operator is called a differentiation matrix. The computation of differentiation matrices can be based on Chebyshev, Fourier, Hermite or other interpolants, which can be differentiated exactly. Here we use the Chebyshev differentiation matrices, provided by Weideman and Reddy (2000). The global interpolant evaluated at N interpolation points is connected to its first derivative by a matrix vector product.

Functions interpolated by orthogonal polynomials in evenly spaced points fail to converge for $N \rightarrow \infty$. This is known as the Runge phenomenon which can be avoided by using unevenly spaced points (Trefethen, 2000). In order to avoid this effect, Chebyshev points are used to interpolate unknown functions as follows:

$$x_j = \cos\left(\frac{(i-1)\pi}{N-1}\right), \quad j = 1...N. \quad (3)$$

The N interpolation points x_j are the extrema of the Chebyshev polynomials computed on the interval $[-1, 1]$. The collocation points cluster at both ends of the interval.

Chebyshev points used to discretize an unknown function $f(x)$ interpolated at N nodes $f(x_k)$ can be approximated using interpolant polynomials $\phi_k(x)$

$$f(x) \approx \sum_{k=1}^{N+1} f(x_k)\phi_k(x). \quad (4)$$

Thus the l-th derivative of $f(x)$ can be obtained by

$$f(x_j)^{(l)} = \sum_{k=1}^{N+1} \frac{d^l}{dx^l}(\phi_k(x_j))f(x_k) \quad (5)$$

If the exact expression of the interpolant polynomial is known, its derivative is obtained exactly. This results in an $N \times N$ differentiation matrix

$$DM_{jk}^{(l)} = \frac{d^l}{dx^l}(\phi_k(x_j)). \quad (6)$$

Eq. (6) is used to approximate differential operators and therefore can serve to discretize differential equations. Entries of the matrix D_{jk} and the related code are provided in Trefethen (2000). The n-th derivative is computed by n matrix multiplications of the first derivative differentiation matrix. The differentiation matrix can be computed with very high spectral accuracy. Nevertheless, round-off errors can be a problem for an increasing number of collocation points. A discussion on how to minimize such errors can be found, for example, in Baltensperger and Trummer (2002).

In the following sections we show how Chebyshev collocation points and differentiation matrices are used to compute dispersion and radial profiles of waves propagating in cylindrical structures.

STRUCTURE AND ORGANIZATION OF THE CODE

The computation of dispersion curves in cylindrical structures with arbitrary fluid and solid layers requires various steps. They are illustrated in Figure. 1. Each step is related to its corresponding MATLAB subroutine.

The input parameters of the considered model are set in an input file called *DefineModelParams.m* [1]. All frequency independent quantities such as differentiation matrices, geometry etc. are subsequently computed in the subroutine *StructureParameters.m* [2]. Parameters set in previous subroutines are the inputs of the subroutine *matrices.m* [3]. This function computes and constructs the matrices for Helmholtz equations L, stress components S and the displacement components T. After construction of these matrices, the related boundary conditions are set using the function *eigen.m* [4]. This eigenvalue problem is solved using the standard MATLAB eigenvalue solver *eig*. Outputs [5] of this computation are the squared eigenvalues and eigenvectors, i.e., k_z^2 and θ for each frequency.

By repeating this workflow (*ComputeDispersion.m*) for a chosen interval of frequencies, dispersion curves are constructed and plotted in [6] via *PlotDispersion.m*. For a single frequency, eigenvectors are utilized to construct and plot radial profiles (*radialprofile.m* [7]) as a function of the radius's structure. In the following sections the various steps are described in detail and it is shown how they are implemented in the final program.

Figure 2: Workflow of the code for the computation of dispersion and radial profiles; on the left hand side it is displayed how the matrices which define the generalized eigenvalue problem are constructed from the input parameters; each step is related to its corresponding MATLAB routine on the right hand side.

Input file

The first step is to set parameters for a certain model. All input parameters are defined in a file called *DefineModelParams.m*. For each layer we define the material parameters which are the P-wave v_p and S-wave v_s velocity as well as the density ρ. The geometry of the model is represented by the outer radii a_i of the layers. The number of Chebyshev points N for the computation of differential

operators are individually defined for each layer. In addition to these elastic and geometric parameters, we need to define the minimum, maximum and step frequency as `wmin`, `wmax` and `wstep` respectively.

Furthermore, some additional parameters must be set. In order to account either for an elastic or a rigid structure, the surface boundary conditions of the structure are set as stress free `s=0` or rigid `s=1`. Limits for the highest, i.e., `SelectmaxVel=maxvel` and lowest, i.e., `SelectminVel =minvel` phase velocity can be set to choose a velocity interval of interest.

All these parameters are entered into a MATLAB structure for code clarity. For a model composed of j-layers the parameter structure will have the following form:

```
Par.N=[N1..Nj]; %Number of collocation points in each layer
Par.vp=[vp1..vpj]; %P-wave velocity of each layer
Par.vs=[vs1..vsj]; %S-wave velocity of each layer
Par.rho=[rho1..rhoj]; %density of each layer
Par.a=[1e-4,a1..aj]; % center radius of each layer
Par.wmin= wmin;  Par.wstep= wstep; Par.wmax= wmax;
Par.s= 0 or 1;
Par.SelectmaxVel = maxvel;
Par.SelectminVel = minvel;
```

All corresponding parameters are set in a vector whose length corresponds to the number of layers, where the elements of this vector are sorted from the center to the surface of the structure. Due to the singularity of the Laplace operator in cylindrical coordinates, the inner radius of the structure must be different from zero. An initial radius with a value of 0.01% of the outside radius of the structure turned out to be appropriate for most cases.

Chebyshev points and differentiation matrices

The routine *chebdif.m* produces interpolation points and differentiation matrices for the interval $[-1, 1]$. For the case of cylindrical structures, which is considered here, we have to transform the interpolation points and differentiation matrices for the minimum and maximum radii of each layer. Each component of the vector $Par.N_j$ corresponds to the number of interpolation points in each layer. All inner and outer radii of the structure are contained in the vector $Par.a_{j+1}$. Both quantities are used to compute the Chebyshev points and differentiation matrices for each layer of the input model. We transform the interpolation points x_i calculated in eq. (3) into radial points r_i for each layer j by

$$r_i^j = -\frac{(a_{j+1} - a_j)x_i + a_j + a_{j+1}}{2}. \qquad (7)$$

We do the same for the differentiation matrices produced by the function `chebdif` which approximates the m-th derivative $\frac{d^m}{dx^m}$ and can be transformed into a radial dependence $\frac{d^m}{dr^m}$ as

$$D_r^m = -\left(\frac{2}{Par.a_{j+1} - Par.a_j}\right)^m D_x^m. \qquad (8)$$

The radius vector, like the differentiation matrices, is frequency independent and thus computed in *SetStructureParameters.m* like all other non-frequency dependent parameters.

Construction of matrices

The underlying equations describing axisymmetric wave propagation in solid and fluid media are provided in Appendix A. A detailed derivation of the equation for solids is given in Karpfinger et al. (2008a).

The equations of motion (A-1, A-2 and A-7) are ordinary differential equations containing derivatives with respect to r only and coefficients depending on frequency ω and axial wave number k_z. The aim is to find a relation between ω and k_z. This means finding a k_z for a given ω or vice versa. This can be done by solving the equations of motion (A-1, A-2 and A-7) as an eigenvalue problem so that the wave number k_z^2 represents the eigenvalue. Alternatively, we could formulate the problem as a generalized eigenvalue problem in ω^2. To do so we have to rearrange the eqs. (A-1, A-2 and A-7) so that the terms with k_z appear on the left-hand side only. For linear elasticity both approaches must give identical results. However for more complicated media (say, viscoelastic or poroelastic) it is advantageous to look for k_z as a function of ω as coefficients of governing equations may themselves explicitly depend on ω.

The wave equations as well as the stress and displacement components, being independent of k_z on the left hand side, are discretized for each layer using Chebyshev interpolation points and differentiation matrices. The matrices of each layer are finally combined in three bigger diagonal block matrices in the subroutine *matrices.m*.

Helmholtz equation matrix L

Eq. (A-7) is the Helmholtz equation for a fluid while eqs. (A-1)-(A-2) represent P-wave and S-wave equations for a solid. The differential operators $\mathfrak{L}_{fl}$, $\mathfrak{L}_p$ and $\mathfrak{L}_s$ are discretized using the differentiation matrices, the radial collocation points r_i and the material parameters. This results for fluid layers in an $N \times N$ matrix L_{fl} while for solid layers P-wave and S-wave operators are combined in a $2N \times 2N$ matrix

$$L_s = \begin{pmatrix} L_{vp} & 0 \\ 0 & L_{vs} \end{pmatrix}. \qquad (9)$$

Finally, all matrices, L_{fl} and L_s, of all layers are combined in one matrix. In the case of a fluid-filled tube the size of the final matrix L is $3N \times 3N$ and has the following form

$$L = \begin{pmatrix} L_{fl} & 0 \\ 0 & L_s \end{pmatrix}. \qquad (10)$$

Matrices with stress and displacement components

After we have built the matrix L representing the differential operators of Helmholtz equations, it is necessary to perform the same operation for the stress and displacement equations. These equations are given in Appendix A. For a solid layer the displacement components are eqs. (A-3)-(A-4) while the stress components are eqs. (A-5)-(A-6). The fluid displacement components are eqs. (A-8)-(A-9) and the radial stress in the fluid is given by eq. (A-10). The matrices for the displacement and stress components are constructed in a similar manner to the L matrix (eq. 10). Stress components for a solid layer can be expressed as

$$\begin{pmatrix} \sigma_{rr} \\ \hat{\sigma}_{rz} \end{pmatrix} = \underbrace{\begin{pmatrix} S_{r\Phi} & S_{r\Psi} \\ S_{z\Phi} & S_{z\Psi} \end{pmatrix}}_{SS} \begin{pmatrix} \Phi \\ \hat{\Psi} \end{pmatrix} \quad , \qquad (11)$$

while displacement components are

$$\begin{pmatrix} u_r \\ \hat{u}_z \end{pmatrix} = \underbrace{\begin{pmatrix} T_{r\Phi} & T_{r\Psi} \\ T_{z\Phi} & T_{z\Psi} \end{pmatrix}}_{TT} \begin{pmatrix} \Phi \\ \hat{\Psi} \end{pmatrix} \quad . \qquad (12)$$

Similarly to the L matrix, a $3N \times 3N$ matrix SS combining all stress coefficients of all layers is constructed.

$$S_S = \begin{pmatrix} S_{fl} & 0 \\ 0 & S_s \end{pmatrix} \quad . \qquad (13)$$

Likewise, the corresponding displacement coefficient matrix TT can be written as:

$$TT = \begin{pmatrix} T_{fl} & 0 \\ 0 & T_s \end{pmatrix} \quad . \qquad (14)$$

Both, S_S and T_S are a $2N \times 2N$ matrix (see eqs 11-12). Each matrix, i.e., L, SS and TT is normalized by the absolute value of its largest element.

Implementing boundary conditions

While formulating an eigenvalue problem, we have to set boundary conditions on the interfaces between layers and on the free surface of the cylinder. The surface and interface boundary conditions are discussed by Karpfinger et al. (2008a). The main emphasis here is to illustrate the implementation of various boundary conditions in the code. The row indices of the matrix $\boldsymbol{L}$ in which the boundary conditions are introduced are independent of frequency. Thus we compute these indices in the subroutine *SetStructureParameters.m*. The addition of the boundary conditions into the L matrix for each individual interface is performed in *eigen.m*. This results in the matrix $\tilde{L}$.

Figure 3 presents the indexing for a n-layered system. The interface of interest is between the layers number j and $j+1$ which have $Par.N_j$ and $Par.N_{j+1}$ interpolation points. In the following equations we discard $Par.$ for simplicity. In order to compute the indices of the matrix

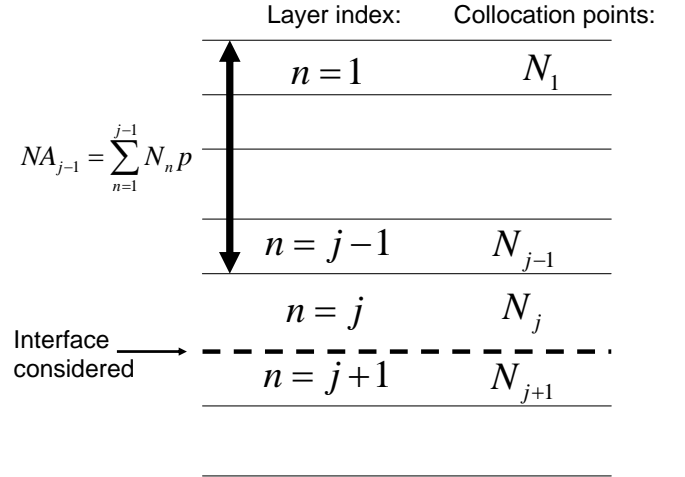Figure 3: Computation of indices for an interface between layer $n = j$ and $n = j+1$: in order to be able to introduce the interface conditions at these layers the size of the matrix from layer $n = 1$ up to $n = j - 1$ needs to be known: NA_{j-1}.

elements where we want to enter the boundary conditions, we have to know the quantity NA_{j-1}. NA_{j-1} is the size of the matrix up to the last interface between the layers $j - 1$ and j. It is computed as

$$NA_{j-1} = \sum_{n=1}^{j-1} N_n p, \qquad (15)$$

where p is a vector of length $j - 1$. By convention, components of p are either 1 if the layer is fluid or 2 if the layer is solid. Knowing NA_{j-1} for each interface we are able to set the boundary conditions for any combination of solid and fluid layers for the interface between the layer j and $j+1$. Subsequently, we describe how the boundary conditions are introduced for the different interfaces.

For a fluid/fluid interface the required boundary conditions are the continuity of radial stress and displacement. They are introduced in the following rows

$$\sigma_{rr}|_{j,j+1} : NA_{j-1} \quad + \quad N_j, \qquad (16)$$
$$u_r|_{j,j+1} : NA_{j-1} \quad + \quad N_j + 1. \qquad (17)$$

For a fluid/solid interface, in addition to the continuity of radial stress and displacement, the shear stress vanishes in the fluid. The three indices for such an interface are

$$\sigma_{rr}|_{j,j+1} : NA_{j-1} \quad + \quad N_j, \qquad (18)$$
$$u_r|_{j,j+1} : NA_{j-1} \quad + \quad N_j + 1, \qquad (19)$$
$$\sigma_{rz}|_{j,j+1} : NA_{j-1} \quad + \quad N_j + N_{j+1} + 1. \qquad (20)$$

For a solid/fluid interface the same interface conditions

are considered but the indices change to

$$\sigma_{rr}|_{j,j+1} : NA_{j-1} \quad + \quad N_j, \tag{21}$$
$$u_r|_{j,j+1} : NA_{j-1} \quad + \quad 2N_j, \tag{22}$$
$$\sigma_{rz}|_{j,j+1} : NA_{j-1} \quad + \quad 2N_j + 1. \tag{23}$$

For a solid/solid interface the following field quantities are continuous: axial and radial displacement as well as normal and shear stress. The indices for such an interface are

$$\sigma_{rr}|_{j,j+1} : NA_{j-1} \quad + \quad N_j, \tag{24}$$
$$u_r|_{j,j+1} : NA_{j-1} \quad + \quad 2N_j, \tag{25}$$
$$u_z|_{j,j+1} : NA_{j-1} \quad + \quad 2N_j + 1, \tag{26}$$
$$\sigma_{rz}|_{j,j+1} : NA_{j-1} \quad + \quad 2N_j + N_{j+1} + 1. \tag{27}$$

Figure 4 illustrates an example of a fluid-solid interface. The interface is indicated with a red horizontal line. The matrix of the fluid (blue) is interpolated by N_1 points while the matrix of the solid (yellow) is of size $2N_2 \times 2N_2$. As discussed above, three interface conditions are required for this boundary: continuity of radial stress and displacement as well as the vanishing of the shear stress. The boundary conditions are represented by the orange color in Figure 4. In order to compute the correct indices for such boundary conditions we use, eq. (18-20) where $j = 1$ for the fluid and $j = 2$ for the solid layer. We can compute the indices of the interface boundary conditions with $NA = 0$. The components of the displacement and stress components are thus introduced as illustrated in Figure 4.

In order to set the boundary condition, we built an identity matrix M of the same size as $\tilde{L}$. This matrix is normalized with the same value as L is normalized. In rows where the stress and displacement components are introduced in the matrix L the value of the M matrix is set equal to zero. In a similar manner we set boundary conditions for all possible interfaces (fluid/fluid, fluid/solid, solid/fluid and solid/solid).

After all the interface conditions are introduced, it only remains to consider conditions for the surface of the structure. Surface conditions can be selected in the *DefineModelParams.m* file either as stress free ($\sigma_{rr} = 0$ and $\sigma_{rz} = 0$) or rigid ($u_r = 0$ and $u_z = 0$) . These conditions are then set in the rows corresponding to the interpolation points of the surface of the structure. We refer now to the matrix containing all the coefficients for the boundary conditions as $\tilde{L}$ (see Figure 4).

Eigenvalue problem

After we have set the boundary conditions, we need to solve a generalized eigenvalue problem of the following form

$$\tilde{L}\boldsymbol{\Theta} = k_z^2 M \boldsymbol{\Theta} \quad . \tag{28}$$

We are using the eigenvalue solver provided by MAT-LAB: `eig`. For each frequency ω, the eigenvalues correspond to the squared axial wavenumber k_z^2. The number of obtained eigenvalues corresponds to the size of the matrix $\tilde{L}$. It is not straightforward to separate the values of interest from spurious values. The non-propagating modes, which are not spurious but also not of interest in this study, are excluded by deleting those eigenvalues whose real part is either negative or smaller than the imaginary part. The remaining spurious eigenvalues are easy to distinguish from the desired values as they are usually significantly smaller in the phase velocity domain. Solving the eigenvalue problem for an interval of frequencies gives the dispersion curves of all obtained modes. These curves are constructed and plotted in *PlotDispersion.m*.

Solving the eigenvalue problem provides also the eigenvectors corresponding to the displacement potentials Θ. They can be used to compute the radial distribution of the stress and displacement components along the radius of the structure [7]. This can be easily achieved by multiplying the potential Θ of each mode with the matrices of the stress and displacement components: SS and TT. Reshaping of the resulting vectors is done in the subroutine *radialprofile.m*. At the moment, the computation of displacement and stress profiles is implemented for an equal number of interpolation points in each layer. The profiles of all different modes for a fixed frequency can be displayed. Radial profiles can help us to understand better the physics of different modes propagating in elastic cylindrical structures.

EXAMPLES

In the software package we have included two examples. The first one is a fluid-filled borehole surrounded by an elastic formation. The medium parameters and the dimensions are given in Figure 5. For the computation of the dispersion the parameter file *DefineModelParams_1a.m* needs to be called in *ComputeDispersion.m*. The formation is modeled as a finite structure. It can be shown that for an outer radius 20 times bigger than the borehole radius, the tube wave dispersion is the same as for an unbounded formation. The result of the eigenvalue problem for a borehole surrounded by an elastic formation is illustrated in Figure 6. The dispersion of the tube wave is computed up to 10 kHz with a frequency step of 0.2 kHz. As we have chosen rigid surface boundary conditions, no extensional mode is observed. If we choose the surface boundary conditions to be stress free the dispersion of the tube wave will not be changed. The difference will be that an additional mode, the extensional or Young's modulus mode will be added and the cut-off frequencies of the higher order modes will be shifted towards slightly higher frequencies. As these modes are related to finite structures only, we do not consider this effect in our study.

We compare the results of the spectral method (red dots) with a dispersion curve obtained from root-finding (black line). The root-finding algorithm used to obtain
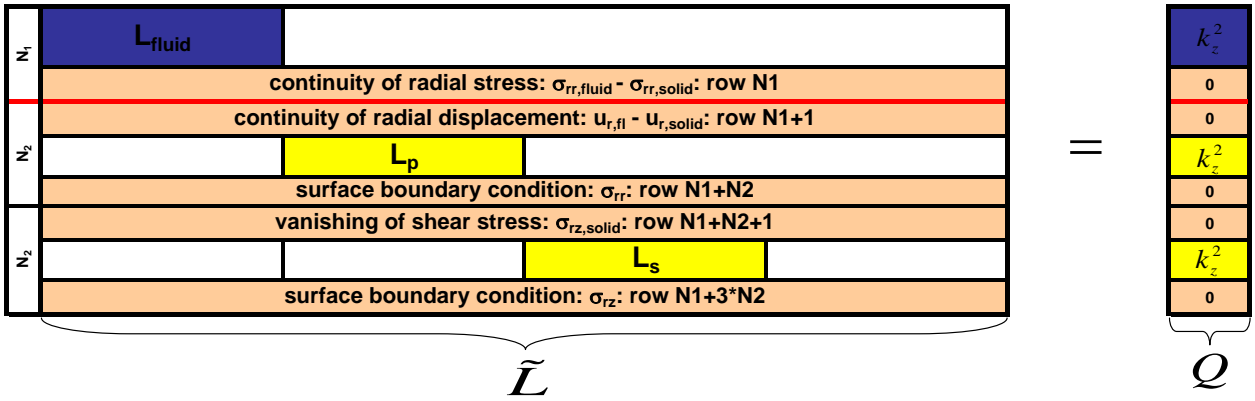
Figure 4: Structure of the matrices $\tilde{L}$ and Q for a borehole surrounded by an elastic formation. The $\tilde{L}$ matrix is built of the discretized differential operators of the Helmholtz equations arranged in a diagonal block matrix: fluid layer (blue) and solid layer (yellow); the differential operators of the stress and displacement components corresponding to the boundary conditions for the interface and the surface are set in the orange rows; the matrix Q is a diagonal matrix of the same size as $\tilde{L}$ where the elements corresponding to the boundary conditions are set equal to zero and the other diagonal elements contain the unknown squared axial wavenumber k_z^2.

the analytical results is from Sinha and Asvadurov (2004). Both results are in very good agreement. In addition to the tube wave, higher-order modes resulting from reflections on the outer surface of the structure are obtained. These modes are not shown here as they are not relevant for a borehole model. In order to account for an infinite structure and to avoid the higher-order modes, absorbing boundary conditions will have to be implemented in the future.

Figure 5: Schematic illustration of a borehole; the borehole is modeled as a finite structure where the outer boundary is 20 times the borehole radius; on the surface rigid boundary conditions are introduced.

Figure 6: Velocity dispersion of the tube wave computed with the parameters from the model in Figure 5.

For the fluid-filled borehole the displacement and stress profiles are displayed for 1.5 kHz (Figure 7). The radial distributions of the radial and axial displacement as well as the normal and shear stress along the radius are

shown. In this case the parameter file in *ComputeDispersion.m* needs to be named *DefineModelParams_1b.m*. These quantities are plotted as a function of r/a, where r is the radius vector and a the radius of the structure. All radial profiles are normalized by their maximum value. The dashed line indicates the borehole wall. All four plots show that the field quantities are almost zero at a distance of 20 borehole radii. This shows that the tube wave is not affected by the finite structure.

The second example is a four layer model shown in Figure 8. Here the parameter file in *ComputeDispersion.m* needs to be named *DefineModelParams_2.m*. Such geometry was used by Bakulin et al. (2008b) to simulate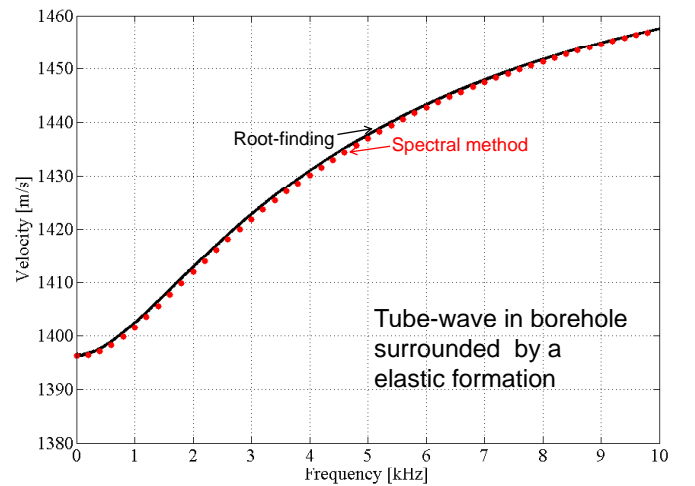 a well completion in a physical modeling experiment. In our computation we have taken the elastic parameters from Bakulin et al. (2008b). The resulting dispersion is displayed in Figure 9. Due to the presence of two fluid columns, two tube waves are supported by this configuration. The fast tube wave is supported mainly by the outer tube while the slow tube wave is supported by the inner tube. In contrast to the first example, we have chosen stress free surface boundary conditions. This adds two modes which propagate from zero frequency. These modes are called extensional, and propagate for low frequencies with the phase velocity of a bar $v_0 = \sqrt{\frac{E}{\rho}}$, where E is the Young's modulus of each solid layer. Radial profiles can be computed in the same manner as for the borehole case. It is a problem that for this example the low frequency - high velocity eigenvalues are unstable. Our attempts to overcome this artifact have so far been unsuccessful and it remains to be addressed. We think that the present results give reasonable estimates. As dispersion is very small up to 5 kHz, it is possible to extrapolate the results to the correct low frequency velocity.
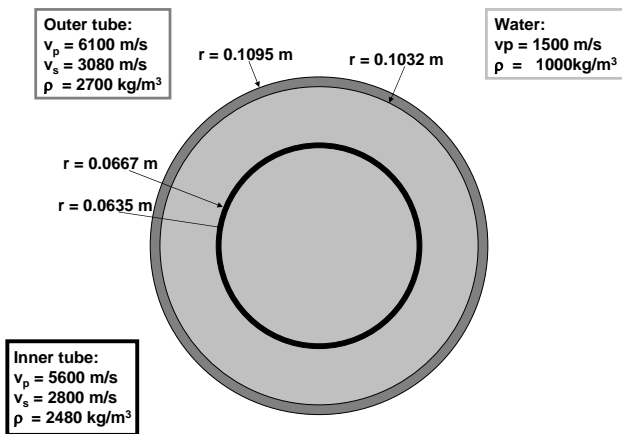

Figure 8: Geometry and elastic parameters of the four-layer model with stress free surface boundary conditions on the outer layer of the structure.

For both examples it is interesting to look at the number of discretization points. In the case of the borehole the structure is discretized with 10 points in the fluid layer
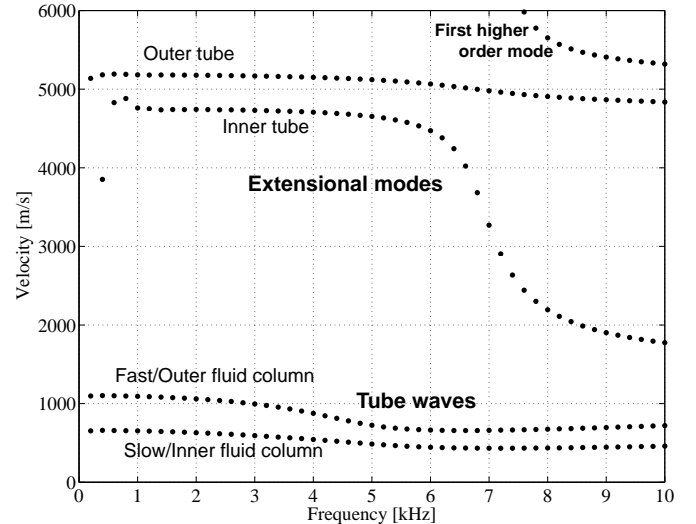

Figure 9: Dispersion of the two extensional modes and two tube waves.

and 40 in the formation. For the four-layer case the best result can be achieved for 8 points in the solid layers and 20 points in the fluid layers. Obviously more points are needed to model a borehole structure than a four layer tube. It is important to note here that the accuracy of the results can significantly decrease if the number of collocation points is increased. This is especially a problem for cases where some of the layers are very thin such as the four-layer example. Increasing the number of collocation points for this example by a factor of 2 or 3 will scatter the result especially for the higher order modes. This problem has to be considered while implementing new models as the right number of collocation points will most likely require several runs of the same model. In general, it can be said that for elastic modeling this is a minor issue as the computational time is in most cases smaller than 20 seconds.

DISCUSSION

In elasticity theory dispersion equations for guided waves are usually solved for a given wavenumber k_z with an unknown frequency ω (Ewing, 1957; Kolsky, 1963). The same approach can be used in the spectral method, where the equations of motion can be written for a given wavenumber k_z and the eigenvalues are squared frequencies ω or velocities $(\omega/k_z)^2$. A limitation of this approach is that it cannot be extended to more complex media where coefficients of the constitutive equations explicitly depend on frequency (such as poroelastic media discussed below). In order to design an algorithm which could potentially be extended to such media, we have reformulated the elastic problem in such a way that the eigenvalue problem is formulated with frequency ω as a (given) parameter and squared wavenumbers k_z^2 (or slownesses $(k_z/\omega)^2$) as eigenvalues.
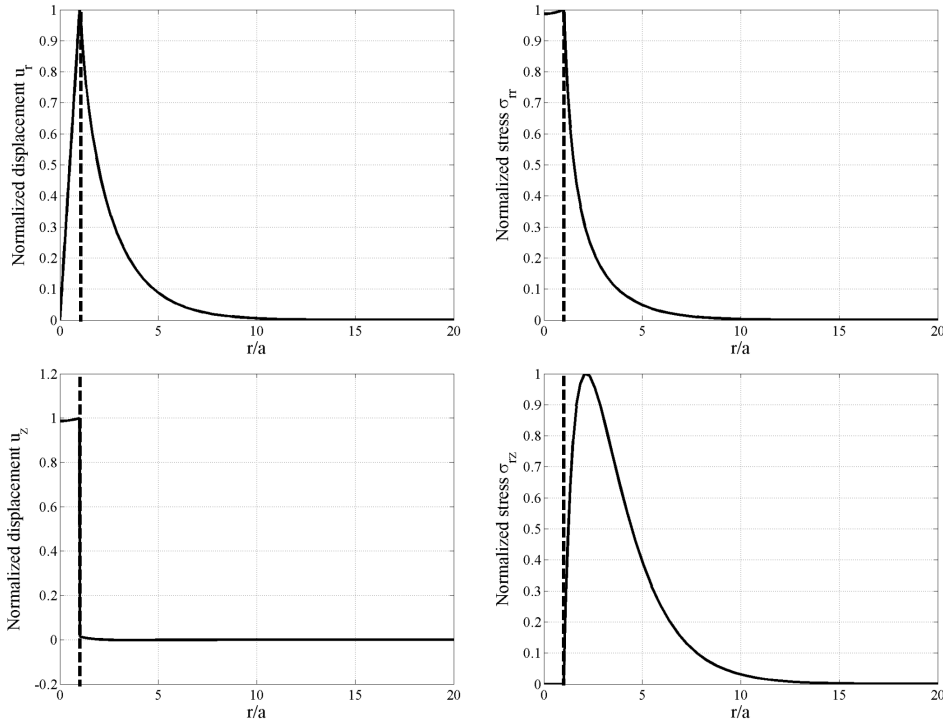
Figure 7: Radial profiles of the tube wave from Figure 6 computed at 1.5 kHz; The radial profiles are normalized by their maximum value of the displacements and stresses, respectively; r/a is the radial position r normalized by the radius of the structure a.

In an earlier work (Karpfinger et al., 2008a), the fluid was modeled as a limiting case of an elastic solid with a small shear velocity (say, $v_s = 1m/s$). This approach results in a number of additional spurious modes corresponding to fictitious shear waves in the fluid. This causes no difficulties when the problem is formulated for a given wavenumber k_z, because in this case the eigenvalues (squared velocities) corresponding to the spurious modes are very small and can be ignored. However, in the case of input frequency, the eigenvalues obtained are squared slownesses. For the spurious modes these slownesses are extremely high. This makes the eigenvalues of interest, which have a much smaller slowness, numerically unstable and thus difficult to recover. In order to obtain numerically more stable results, the equations for an ideal fluid (eqs. (A-7)-(A-10)) were implemented in the present algorithm, eliminating these spurious modes altogether. This also results in smaller matrices and hence faster computations.

In order to account for fluid flow across the layer boundaries we have recently extended the spectral method to poroelasticity (Karpfinger et al., 2008b). This allows us to model acoustic response of realistic situations such as a completed borehole surrounded by a formation with a radial variation of permeability. Such modeling may potentially be used to monitor reservoir production using permanent acoustic sensors (Bakulin et al., 2008a).

The algorithm presented here is limited to structures of finite radius. Infinite structures, such as a fluid filled borehole surrounded by an infinite formation are approximated by a finite structure with a large radius. The downside of this approach is that it produces higher-order modes corresponding to the reflection at the outer boundary of the structure. In order to avoid these higher order modes and to be able to model attenuated leaky modes, absorbing boundary conditions need to be introduced. This can be a subject of future work. The algorithm can also be extended to flexural waves and anisotropy.

CONCLUSIONS

In this work we have presented a new algorithm, based on spectral method, which computes wave propagation in elastic cylindrical structures with an arbitrary number of fluid and solid layers. We discretized the medium in the radial direction using Chebyshev points. We then approximated differential operators by Chebyshev differentiation matrices. The problem is then formulated as an algebraic generalized eigenvalue problem where the eigenvalues correspond to the axial wavenumbers and the eigenvectors to the displacement potentials. We have used the obtained displacement potentials to display radial profiles, which are the variation of displacement and stress along the radius of the structure. Creating an input file for multi-layered models is very straightforward and the results are very efficiently obtained. The algorithm is very fast due to the computational efficiency of the spectral method. It

is not straightforward to choose the optimum number of collocation points as there is no parameter that controls the accuracy. It will require some runs to get an optimal picture. The two examples in the paper give an idea how to choose the number of points. It is not so easy to give a general rule but after running the program for some examples a user will develop a certain feeling. The algorithm works for any number of layers and down to a layer thickness of 0.5% relative to the thickness of the structure. The drawbacks are that for an increasing number of layers the computational time increases significantly and for very thin layers the accuracy decreases. For most models of interest the algorithm works very efficiently and is easy to use.

CODE AVAILABILITY

A link to the complete MATLAB code of the algorithm, with examples, can be found on SEGs web site at

ACKNOWLEDGMENTS

REFERENCES

Adamou, A. T. I. and R. V. Craster, 2004, Spectral methods for modelling guided waves in elastic media: J. Acoust. Soc. Amer., **116**, 1524–1535.

Bakulin, A., F. Karpfinger, and B. Gurevich, 2008a, Understanding acoustic response of deepwater completions: The Leading Edge, **27**, 260–267.

Bakulin, A., A. Sidorov, B. Kashtan, and M. Jaaskelainen, 2008b, Real-time completion monitoring with acoustic waves: Geophysics, **73**, E15–E33.

Baltensperger, R. and M. R. Trummer, 2002, Spectral differencing with a twist: SIAM J. Sci. Comput., **24**, 1465–1487.

Boyd, J. P., 2001, Chebyshev and Fourier Spectral Methods: Dover, New York.

Canuto, C., M. Hussaini, A. Quarteroni, and T. Zang, 1988, Spectral methods in fluid dynamics: Springer Verlag, New York.

Carcione, J. M., G. C. Herman, and A. P. E. ten Kroode, 2002, Seismic modeling: Geophysics, **67**, 1304–1325.

Ewing, W. M., 1957, Elastic waves in layered media: McGraw Hill.

Fornberg, B., 1987, The pseudospectral method: Comparisons with finite differences for the elastic wave equation: Geophysics, **52**, 483–501.

Gazis, D. C., 1959a, Three-dimensional investigation of the propagation of waves in hollow circular cylinders. I. Analytical foundation: J. Acoust. Soc. Amer., **31**, 568–573.

——, 1959b, Three-dimensional investigation of the propagation of waves in hollow circular cylinders. II. Numerical results: J. Acoust. Soc. Amer., **31**, 573–578.

Karpfinger, F., B. Gurevich, and A. Bakulin, 2008a, Computation of wave propagation along cylindrical structures using the spectral method: J. Acoust. Soc. Amer., **124**, 859–865.

——, 2008b, Modeling of axisymmetric wave modes in a poroelastic cylinder using spectral method: J. Acoust. Soc. Amer., **124**, EL230–EL235.

Kolsky, H., 1963, Stress waves in solids: Dover, New York.

Kosloff, D., D. Kessler, A. Q. Filho, E. Tessmer, A. Behle, and R. Strahilevitz, 1990, Solution of the equations of dynamic elasticity by a Chebychev spectral method: Geophysics, **55**, 734–748.

Sinha, B. and S. Zeroug, 1997, Wiley encyclopedia of electrical and electronic engineers, chapter Geophysical prospecting using sonics and ultrasonics. Wiley, New York.

Sinha, B. K. and S. Asvadurov, 2004, Dispersion and radial depth of investigation of borehole modes: Geophysical Prospecting, **52**, 271–286.

Trefethen, L. N., 2000, Spectral Methods in MATLAB: SIAM.

Weideman, J. A. C. and S. C. Reddy, 2000, A MATLAB differentiation matrix suite: ACM Trans. Math. Softw., **26**, 465.

Zemanek, J., 1972, An experimental and theoretical investigation of elastic wave propagation in a cylinder: J. Acoust. Soc. Amer., **51**, 265–283.

APPENDIX A

UNDERLYING EQUATION

Equations for solid medium

The P and S wave Helmholtz equations for an isotropic elastic solid expressed in terms of displacement potentials are

$$\underbrace{\left(\partial_r^2 + r^{-1}\partial_r + \frac{\omega^2}{v_p^2}\right)}_{\mathfrak{L}_{v_p}}\Phi = k_z^2\Phi \quad, \quad \text{(A-1)}$$

$$\underbrace{\left(\frac{\partial^2}{\partial r^2} + \frac{1}{r}\frac{\partial}{\partial r} - \frac{1}{r^2} + \frac{\omega^2}{v_s^2}\right)}_{\mathfrak{L}_{v_s}}\Psi = k_z^2\Psi \quad. \quad \text{(A-2)}$$

The radial and axial displacement in such a medium can be expressed as

$$u_r = \partial_r\Phi - \hat{\Psi} \quad, \quad \text{(A-3)}$$

$$\hat{u}_z = \underbrace{-k_z^2\Phi}_{\mathfrak{L}_{v_p}\Phi} + \left(\partial_r + r^{-1}\right)\hat{\Psi} \quad, \quad \text{(A-4)}$$

where $\hat{\Phi} = ik_z\Phi$.

Tube wave signatures in cylindrically layered poroelastic media computed with spectral method

Tube wave signatures in cylindrically layered poroelastic media computed with spectral method

Florian Karpfinger, [1][⋆] Boris Gurevich, [1][†] [‡] Henri-Pierre Valero, [3][§] Andrey Bakulin [4][¶] and Bikash Sinha[3][‖]

[1] *Curtin University of Technology Department of Exploration Geophysics, GPO Box U1987, Perth, WA 6845, Australia*
[4] *WesternGeco, Houston, USA*
[3] *Schlumberger-Doll Research, Boston, USA*

SUMMARY
In this paper a new algorithm based on the spectral method is presented that computes the dispersion and attenuation of waves propagating in cylindrical structures composed of fluid, elastic and poroelastic layers. The medium is discretized along the radial axis using Chebyshev points and the differential operators of the underlying differential equations are approximated with spectral differentiation matrices. Thus the corresponding equations can be solved as a generalized algebraic eigenvalue problem. For a given frequency the eigenvalues correspond to the wavenumbers of different modes. The advantage of this approach is that problems with complicated structures, such as multiple fluid, solid and poroelastic layers, can be solved more easily and time efficiently than with conventional techniques such as *root-finding*. In this work the fundamental equations are discussed, followed by an outline of how they are implemented in the numerical spectral schema. The interface boundary conditions are then explained for fluid/porous, elastic/porous and porous interfaces. Finally, three examples from borehole acoustics are discussed.

Key words: poroelasticity, dispersion, cylindrical structures, tube wave, spectral method, borehole acoustics.

Introduction

Modeling propagation of various wave modes in a fluid-filled borehole is **an** important step in evaluating formation properties. Various modes are propagating in a fluid-filled borehole and are sensitive to different properties of the formation (White 1983; Paillet & Cheng 1991; Sinha & Zeroug 1997) One of the important aspects of the modeling of waves propagation in fluid-filled borehole concerns the wave propagation in poroelastic medium. This interest is strongly linked to the oil industry and the need to estimate the permeability of reservoirs. Beyond the scope of geophysical applications the understanding of wave propagation in cylindrical poroelastic structures is of great importance in the areas of non-destructive testing, mechanical engineering and civil engineering.

[⋆] florian.karpfinger@postgrad.curtin.edu.au
[†] boris.gurevich@geophy.curtin.edu.au
[‡] CSIRO Petroleum, Bentley, Western Australia
[§] hvalero@slb.com
[¶] abakulin@slb.com
[‖] sinha1@slb.com

Over the last three decades great effort has been made to investigate wave propagation in poroelastic cylindrical structures. The effects of dispersion and attenuation in cylindrically layered poroelastic structures were investigated theoretically as well as experimentally. We give a short literature review on the work done for geophysical applications.

The first fundamental work on this subject was done by Biot and now is known as Biot's equations of poroelasticity (Biot, 1956a,b, 1962). Then, framework for wave propagation in a fluid saturated poroelastic cylinder was provided by Gardner (1962) while the dispersion for the full range of frequencies for open and closed boundary conditions was studied by Berryman (1983). Later, White (1986) and Mörig & Burkhardt (1989) measured the dispersion of the extensional mode in laboratory experiments while Dunn (1986) wrote a review on extensional, torsional and flexural modes. Later, Berryman & Pride (2005) utilized torsional waves in order to estimate the effect of patchy saturation in a cylinder.

In addition to these general theoretical works, the need to estimate permeability of reservoir triggered studies on the so called tube wave or Stoneley wave which propagates in the fluid column of the hole. A special characteristic of tube

waves is their high sensitivity to the formation permeability. The dispersion of tube waves propagating in boreholes surrounded by a poroelastic formation was used to invert for the permeability (Rosenbaum 1974; Chang et al. 1988; Norris 1989; Schmitt et al. 1988) while Sinha et al. (2006) proposed an approach to estimate the radial distribution of permeability. In addition to these theoretical developments, some scale laboratory experiments have been conducted. This concept was modeled by using a hollow poroelastic cylinder submerged into a fluid (Liu 1988).

Even though significant work has been done to calculate wave dispersion in cylinders or boreholes, no poroelastic structures involving more than three layers have been studied. The problem is that the traditional *root-finding* technique for solving dispersion equations can become an extremely cumbersome task for structures with multiple poroelastic layers. The roots of such dispersion equations have to be traced in the complex plane and it can become very difficult to separate such roots (Berryman & Pride 2002, 2005).

In order to be able to study wave propagation in more complicated structures it would be a great benefit to be able to bypass the problems involved with *root-finding*. In this paper, we suggest the use of an alternative approach to model wave propagation in cylindrical structures based on the spectral method of Adamou & Craster (2004). The advantage of this approach is that it is faster and easier to implement than conventional *root-finding* methods, especially for attenuative, poroelastic or anisotropic structures.

Karpfinger et al. (2008a) expanded the spectral method to axisymmetric waves for an arbitrary number of fluid and solid layers while in this paper the same methodology is applied to the poroelastic case. First, poroelastic equations in cylindrical coordinates are introduced together with their formulation in spectral domain. Then boundary conditions for all possible poroelastic interfaces are discussed. Finally, three numerical examples are discussed. First, a borehole surrounded by a poroelastic formation with open and closed boundary conditions is used as a benchmark. The dispersion and attenuation are plotted for a range of permeabilities. In the second model, an additional elastic layer is introduced between the fluid and the poroelastic formation. This allows us to study the impact of the thickness of this layer on the dispersion of the tube wave. The third model illustrates the effect of an altered zone with a radial increase of the permeability.

1   THEORY

In this paper we study wave propagation in a fluid-filled borehole surrounded by a medium composed of fluid, elastic and poroelastic layers. Wave propagation in cylindrical, poroelastic structures is considered within the framework of Biot's theory of poroelasticity. In the next section Biot's theory for an infinite, poroelastic medium is reviewed. Fig. 1 illustrates a fluid-filled borehole case surrounded by a poroelastic medium. The structure is infinite in the axial direction while in the radial one any combination of fluid, elastic and poroelastic layers can be considered. A radially infinite medium is modeled by choosing the outer layer to be much bigger than the borehole radius. Due to the geometry of the problem we are going to solve, wave and constitutive equa-
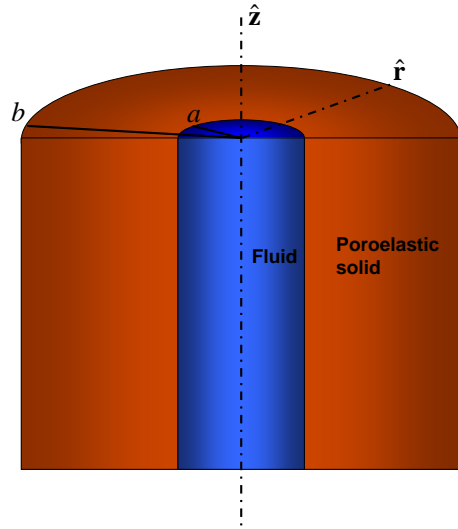

Figure 1. Example for a two layer cylindrical structure: hollow poroelastic cylinder filled with fluid.

tions will be expressed using a cylindrical coordinate system. In this study, the motion is independent of the angular displacement. Thus, the particle motion happens in the $r - z$ plane only, involving radial and axial displacement. The angular displacement is assumed to be zero. Throughout this paper the cylindrical coordinate system will be defined as follows: the z axis will be aligned with the axis of the cylinder while r is the radial coordinate (see Fig. 1).

In order to simulate propagating modes in such a system we assume that a plane wave front is propagating parallel to the axis of the cylinder. Under these assumptions, stress and displacement components can be estimated for a multilayered system composed of a combination of poroelastic, fluid and elastic layers.

1.1   Biot's theory of poroelasticity: Review

Waves propagating in an infinite poroelastic medium satisfy the following equations (Biot 1962):

$$\nabla \cdot \boldsymbol{\sigma} = -\omega^2(\rho \boldsymbol{u} + \rho_f \boldsymbol{w}), \tag{1}$$

$$\nabla p = \omega^2(\rho_f \boldsymbol{u} + q \boldsymbol{w}), \tag{2}$$

where the field variables are given as the bulk displacement $\boldsymbol{u}$ and the relative solid-fluid displacement $\boldsymbol{w} = \phi(\boldsymbol{U} - \boldsymbol{u})$ with ϕ being the porosity. $\boldsymbol{U}$ is the fluid displacement while ρ and ρ_f are respectively the density of porous material and the fluid. The frequency-dependent density term $q(\omega)$ is defined by Pride & Haartsen (1996) as

$$q(\omega) = \frac{i}{\omega} \frac{\eta}{k(\omega)}, \tag{3}$$

where η is the viscosity and $k(\omega)$ the frequency-dependent permeability (Johnson et al. 1987). This complex density is responsible for the viscous and inertial coupling between the solid and fluid phases (Biot 1956b). The total stress tensor $\boldsymbol{\sigma}$ and the fluid pressure p are related to the field vectors by

the constitutive equations

$$\boldsymbol{\sigma} = [(H - 2\mu)\nabla \cdot \boldsymbol{u} + \alpha M \nabla \cdot \boldsymbol{w}]\boldsymbol{I} + \mu[\nabla \boldsymbol{u} + \nabla \boldsymbol{u}^T], \quad (4)$$

$$p = -M\nabla \cdot \boldsymbol{w} - \alpha M \nabla \cdot \boldsymbol{u}. \quad (5)$$

In Eqs. (4) and (5) μ is the shear modulus of the solid frame while $\alpha = 1 - K/K_g$ is the Biot-Willis coefficient (Biot & Willis 1957). K is the drained bulk modulus and K_g is bulk modulus of the grain material. The so-called pore space modulus is defined as

$$M = \left[\frac{\alpha - \phi}{K_g} + \frac{\phi}{K_f} \right]^{-1}, \quad (6)$$

where K_f is the fluid bulk modulus.

The P-wave modulus H of the saturated poroelastic medium is defined as follows

$$H = K_{sat} + \frac{4}{3}\mu. \quad (7)$$

where K_{sat} is the bulk modulus of the saturated medium which is related to the drained modulus K by the (Gassmann 1951) equation

$$K_{sat} = K + \alpha^2 M. \quad (8)$$

Substituting the constitutive relations eqs. (4) and (5) into eqs. (1) and (2), we obtain two coupled wave equations. In order to decouple these equations into Helmholtz equations for the three bulk waves propagating in an isotropic poroelastic medium, the displacements is written in terms of scalar and vector potentials as

$$\boldsymbol{u} = \nabla\Upsilon + \nabla \times \boldsymbol{\beta}, \quad \boldsymbol{w} = \nabla\psi + \nabla \times \boldsymbol{\chi}, \quad (9)$$

where Υ, ψ and $\boldsymbol{\beta}, \boldsymbol{\chi}$ are respectively, scalar and vector potentials. Substituting eqs. (9) into the two coupled wave equations yields for the shear wave

$$(\nabla^2 + \omega^2 s_s^2)\boldsymbol{\beta} = 0, \quad \boldsymbol{\chi} = -\frac{\rho_f}{q}\boldsymbol{\beta}, \quad (10)$$

providing the expression for the shear wave slowness defined as

$$s_s^2 = \frac{\rho - \frac{\rho_f^2}{q}}{\mu}. \quad (11)$$

The wave equations for the two P-waves in an infinite poroelastic medium are

$$(\nabla^2 + \omega^2 s_\pm^2)A_\pm = 0, \quad (12)$$

where the fast and slow P-wave slownesses are defined as

$$2s_\pm^2 = \frac{\rho M + qH - 2\rho_f C}{MH - C^2} \pm$$
$$\sqrt{\left(\frac{\rho M + qH - 2\rho_f C}{(MH - C^2)} \right)^2 - \frac{4(q\rho - \rho_f^2)}{MH - C^2}}, \quad (13)$$

with the potential $A_\pm$ defined as

$$A_\pm = \Gamma_\pm \Upsilon + \psi, \quad (14)$$

where

$$\Gamma_\pm = \frac{\rho_f H - \rho C}{(MH - C^2)s_\pm^2 - (\rho M - \rho_f C)}. \quad (15)$$

C is a modulus defined as $C = \alpha M$. The equations derived above are valid for most kinds of coordinate systems.

1.2 Poroelastic equations in cylindrical coordinates

In order to apply Biot's theory for poroelastic media of cylindrical geometry it is more convenient to use cylindrical coordinates. For axisymmetric wave propagation, the subject of this work, the particle motion takes place solely in the $r - z$ plane. Thus the angular displacement u_θ equals zero. Under these assumptions, components of the stress-strain relations eq. (4) can be expressed as

$$\sigma_{rr} = (H - 2\mu)\Delta + 2\mu\frac{\partial u_r}{\partial_r} - \alpha M\zeta, \quad (16)$$

$$\sigma_{rz} = \mu\left(\frac{\partial u_r}{\partial_z} + \frac{\partial u_z}{\partial_r} \right), \quad (17)$$

where Δ is the dilation defined in cylindrical coordinates as

$$\Delta = \frac{\partial u_r}{\partial_r} + \frac{u_r}{r} + \frac{\partial u_z}{\partial_z}. \quad (18)$$

The fluid increment content is defined as $\zeta = -\nabla \cdot \boldsymbol{w}$. In order to distinguish between the torsional and extensional components of the wavefield, the potential $\boldsymbol{\beta}$ is further decomposed as

$$\boldsymbol{\beta} = \hat{\boldsymbol{z}}\beta_1 + \nabla \times (\hat{\boldsymbol{z}}\beta_2), \quad (19)$$

where $\hat{\boldsymbol{z}}$ is the unit vector in z-direction. Note that for axisymmetric modes only $\beta_2 \neq 0$. Eqs. (9)-(19) describe axisymmetric wave propagation in a poroelastic cylinder.

1.2.1 Helmholtz equations

Considering an infinite train of sinusoidal waves along the z axis of the cylinder, which is a harmonic function of z and t of the form

$$A(r)_\pm = a(r)_\pm e^{i(k_z z - \omega t)} \quad , \quad \beta(r)_2 = a(r)_s e^{i(k_z z - \omega t)}, \quad (20)$$

where ω is the angular frequency, k_z the axial wavenumber, and $a(r)_\pm$ and $a(r)_s$ are amplitude functions of r .

Using eqs. (20) the wave equations (eqs. 10 and 12) can be expressed in the $\omega - k_z$ domain as

$$\underbrace{\left(\partial_r^2 + r^{-1}\partial_r + \frac{\omega^2}{v_\pm^2} \right)}_{\mathfrak{L}_\pm} a_\pm = k_z^2 a_\pm \quad , \quad (21)$$

$$\underbrace{\left(\frac{\partial^2}{\partial r^2} + \frac{1}{r}\frac{\partial}{\partial r} - \frac{1}{r^2} + \frac{\omega^2}{v_s^2} \right)}_{\mathfrak{L}_s} a_s = k_z^2 a_s \quad . \quad (22)$$

The term $e^{i(k_z z - \omega t)}$ is omitted for clarity. The poroelastic Helmholtz equations are formulated similarly to the elastic case (Karpfinger et al. 2008a, Sec.1.B). Now the ordinary differential equations (eqs. 21-22) contain derivatives with only respect to r and coefficients depending on frequency ω and axial wavenumber k_z. In order to find a relation between ω and k_z eqs. (21)-(22) can be solved as an eigenvalue problem so that the wavenumber k_z^2 represents eigenvalues

and the potentials $a_\pm$ and a_s are the eigenvectors. For linear elasticity it is possible to find a k_z for a given ω or vice versa (Adamou & Craster 2004). However for poroelasticity it is advantageous to look for k_z as a function of ω as the bulk slowness (eq. (11 & 13) explicitly depend on ω.

The three Helmholtz equations of a poroelastic layer can be combined in a matrix equation and have the following form

$$
\underbrace{\begin{pmatrix} \mathfrak{L}_+ & 0 & 0 \\ 0 & \mathfrak{L}_{v_s} & 0 \\ 0 & 0 & \mathfrak{L}_- \end{pmatrix}}_{\mathfrak{L}_p} \underbrace{\begin{pmatrix} a_+ \\ a_s \\ a_- \end{pmatrix}}_{\boldsymbol{a_p}} = k_z^2 \begin{pmatrix} a_+ \\ a_s \\ a_- \end{pmatrix} \quad . \quad (23)
$$

In order to obtain the dispersion of propagating modes in multilayered cylindrical structures composed of poroelastic, elastic and fluid layers, eqs. (21)-(22) plus the equivalent equations for fluid and solid layers need to be solved. A solution for such a system can only be found if the appropriate interface conditions for such a system are set. In order to apply the boundary or interface conditions, the displacements and stress components have to be expressed independently of the axial wavenumber k_z.

1.2.2   Displacement components

Displacement components need to be expressed independently of k_z. In order to achieve this, eq. (19) with $\beta_1 = 0$ and the expressions

$$
\Upsilon = \frac{A_+ - A_-}{\Gamma_+ - \Gamma_-}, \qquad \psi = \frac{A_- \Gamma_+ - A_+ \Gamma_-}{\Gamma_+ - \Gamma_-}, \qquad (24)
$$

are used to express the solid displacement $\boldsymbol{u}$ (eq. 9) as

$$
\boldsymbol{u} = \underbrace{\frac{1}{\Gamma_+ - \Gamma_-}}_{\Gamma} \nabla A_+ - \underbrace{\frac{1}{\Gamma_+ - \Gamma_-}}_{\Gamma} \nabla A_- + \nabla \times (\nabla \times (\hat{z}\beta_2)). \quad (25)
$$

The relative displacement can be written in a similar form to eq. (25) as

$$
\boldsymbol{w} = -\Gamma_- \Gamma \nabla A_+ + \Gamma_+ \Gamma \nabla A_- - \frac{\rho_f}{q} \nabla \times (\nabla \times (\hat{z}\beta_2)). \quad (26)
$$

For three differential equations with three unknowns it is sufficient to use three displacement components: the radial u_r and axial u_z solid displacement components plus the radial w_r component of the relative displacement

$$
u_r = \Gamma \partial_r a_+ - a_s - \Gamma \partial_r a_-, \quad (27)
$$

$$
\bar{u}_z = -\Gamma \underbrace{k_z^2 a_+}_{\mathfrak{L}_+ a_+} + \left(\partial_r + \frac{1}{r} \right) a_s + \Gamma \underbrace{k_z^2 a_-}_{\mathfrak{L}_- a_-}, \quad (28)
$$

$$
w_r = -\Gamma_- \Gamma \partial_r a_+ + \frac{\rho_f}{q} a_s + \Gamma_+ \Gamma \partial_r a_-, \quad (29)
$$

where $a_s = ik_z a_s$ and $\bar{u}_z = ik_z u_z$. These equations reduce to elasticity for $a_- = 0$, $\Gamma = 1$ and $w_r = 0$ (see eqs. 13-14 and Karpfinger et al. (2008a)).

The displacement components of a poroelastic layer are combined in the following matrix equation

$$
\begin{pmatrix} u_r \\ u_z \\ w_r \end{pmatrix} = \underbrace{\begin{pmatrix} \mathfrak{T}_{u_r}^+ & \mathfrak{T}_{u_r}^s & \mathfrak{T}_{u_r}^- \\ \mathfrak{T}_{u_z}^+ & \mathfrak{T}_{u_z}^s & \mathfrak{T}_{u_z}^- \\ \mathfrak{T}_{u_r}^+ & \mathfrak{T}_{u_r}^s & \mathfrak{T}_{w_r}^- \end{pmatrix}}_{\mathfrak{T}_p} \cdot \begin{pmatrix} a_+ \\ a_s \\ a_- \end{pmatrix} \quad , \quad (30)
$$

where the matrix $\mathfrak{T}$ is composed of the coefficients of the displacement potential obtained from eqs. (27)-(29). These coefficients will be discretized using differentiation matrices as will be explain later on.

1.2.3   Stress components

Stress components σ_{rr}, σ_{rz} and the fluid pressure p can now be written as functions of the potentials $a_\pm$ and a_s. For the radial stress we get the following expression

$$
\begin{aligned}
\sigma_{rr} = &\ 2\mu\Gamma\partial_r^2 a_+ - (H - 2\mu)\Gamma\frac{\omega^2}{v_+^2}a_+ + C\Gamma\Gamma_-\frac{\omega^2}{v_+^2}a_+ - \\
&- 2G\partial_r a_s \\
&- 2\mu\Gamma\partial_r^2 a_- + (H - 2\mu)\Gamma\frac{\omega^2}{v_-^2}a_- - C\Gamma\Gamma_+\frac{\omega^2}{v_-^2}a_-. \quad (31)
\end{aligned}
$$

The shear stress is expressed as

$$
\begin{aligned}
\bar{\sigma}_{rz} = &\ -2\mu\Gamma\left(\partial_r^3 + \frac{1}{r}\partial_r^2 - \frac{1}{r^2}\partial_r + \partial_r\frac{\omega^2}{v_+^2} \right) a_+ + \\
&+ \left[2\mu\left(\partial_r^2 + \frac{1}{r}\partial_r - \frac{1}{r^2} \right) + \rho\omega^2 \right] a_s + \\
&+ 2\mu\Gamma\left(\partial_r^3 + \frac{1}{r}\partial_r^2 - \frac{1}{r^2}\partial_r + \partial_r\frac{\omega^2}{v_-^2} \right) a_-, \quad (32)
\end{aligned}
$$

while for the fluid pressure (compare eq. 5) we get

$$
\begin{aligned}
-p = &\ \left[-M\Gamma\Gamma_-\frac{\omega^2}{v_+^2} + C\Gamma\frac{\omega^2}{v_+^2} \right] a_+ + \\
&+ \left[M\Gamma\Gamma_+\frac{\omega^2}{v_-^2} - C\Gamma\frac{\omega^2}{v_-^2} \right] a_-, \quad (33)
\end{aligned}
$$

where $\bar{\sigma}_{rz} = ik_z\sigma_{rz}$. Note that eqs. (31)-(33) are derived from eq. (16),(17) and (5) by substituting the displacement components eqs. (27)-(29).

Stress components are expressed in matrix form similarly to the displacement components

$$
\begin{pmatrix} \sigma_{rr} \\ \sigma_{rz} \\ -p \end{pmatrix} = \underbrace{\begin{pmatrix} \mathfrak{S}_{\sigma_{rr}}^+ & \mathfrak{S}_{\sigma_{rr}}^s & \mathfrak{S}_{\sigma_{rr}}^- \\ \mathfrak{S}_{\sigma_{rz}}^+ & \mathfrak{S}_{\sigma_{rz}}^s & \mathfrak{S}_{\sigma_{rz}}^- \\ \mathfrak{S}_{-p}^+ & \mathfrak{S}_{-p}^s & \mathfrak{S}_{-p}^- \end{pmatrix}}_{\mathfrak{S}_p} \cdot \begin{pmatrix} a_+ \\ a_s \\ a_- \end{pmatrix} \quad , \quad (34)
$$

where $\mathfrak{S}_{-p}^s$ is zero as in the fluid as no shear stress exists.

The Helmholtz equations eqs. (21)-(23) together with the displacement eqs. (27)-(30) and stress eqs. (31)-(34) components describe the propagation of waves in a cylindrical, poroelastic layer. They are presented in a way that it is possible to formulate an eigenvalue problem which gives for a given frequency ω the axial wavenumber k_z as the eigenvalue. Presented in this form the displacement and stress components eqs. (27)-(34) can be utilized to incorporate any boundary and interface conditions for cylindrical poroelastic structures.

1.3 Boundary conditions on poroelastic interfaces

For finite cylindrical structures with arbitrary fluid, solid and poroelastic layers, conditions of continuity across the layer interfaces have to be introduced as well as boundary conditions on the free surface.

For poroelastic interfaces the relevant conditions to be discussed are (Deresiewicz & Skalak 1963; Gurevich & Schoenberg 1999):

(i) poroelastic/poroelastic $(p_1 - p_2)$,
(ii) poroelastic/solid $(p - s)$,
(iii) poroelastic/fluid $(p - f)$.

For case (i) $(p_1 - p_2)$ all stress and displacement components are assumed to be continuous therefore

$$u_r|_{p1} = u_r|_{p1}, \qquad u_z|_{p1} = u_z|_{p2}, \qquad w_r|_{p1} = w_r|_{p2}$$
$$\sigma_{rr}|_{p1} = \sigma_{rr}|_{p2}, \qquad \sigma_{rz}|_{p1} = \sigma_{rz}|_{p2}, \qquad p|_{p1} = p|_{p2}. \quad (35)$$

Case (ii) $(p - s)$ is governed by the following conditions:

$$u_r|_p = u_r|_s, \qquad u_z|_p = u_z|_s, \qquad w_r|_p = 0,$$
$$\sigma_{rr}|_p = \sigma_{rr}|_s, \qquad \sigma_{rz}|_p = \sigma_{rz}|_s. \quad (36)$$

All quantities are continuous across the interface except the relative displacement w_r which is zero in the solid.

For case (iii) $(p - f)$ two cases have to be considered. Either the pores are open and fluid freely moves across the interface (open pores) or they are closed and no fluid flow can exchange between both layers (closed pores). For both cases the continuity of radial stress and the radial displacement is required as well as the vanishing of the shear stress in the fluid

$$\sigma_{rr}|_p = \sigma_{rr}|_f, \qquad \sigma_{rz}|_p = 0, \qquad u_r|_p - w_r|_p = u|_f \quad (37)$$

The index f indicates a fluid layer. For the open pores case, the fluid pressure is continuous across the surface

$$p|_p = p|_f, \quad (38)$$

while in the closed pores case the relative displacement is zero in the fluid layer

$$w_r|_p = 0. \quad (39)$$

The conditions of interfaces between solid-solid, solid-fluid and fluid-fluid media are given in Karpfinger et al. (2008a).

In addition, surface boundary conditions on the outside layer of the cylindrical structure must be set. Open pore boundary conditions on the free surface of the cylinder $r = a$ are

$$\sigma_{rr}|_{r=a} = \sigma_{rz}|_{r=a} = -p_f|_{r=a} = 0. \quad (40)$$

In addition to the zero stress, the fluid pressure is zero on the surface and fluid can thus flow across the interface. For a closed surface, the boundary conditions become

$$\sigma_{rr}|_{r=a} = \sigma_{rz}|_{r=a} = 0 \quad , \quad w_r|_{r=a} = 0. \quad (41)$$

The pore pressure condition is replaced by the condition that relative motion of fluid with respect to solid is zero on the surface of the cylinder. For a single poroelastic cylinder these boundary conditions are discussed by Berryman (1983) and Karpfinger et al. (2008b).

2 SPECTRAL METHOD

The spectral method is an alternative numerical approach to obtain the dispersion and attenuation of modes propagating in cylindrical structures. This method was initially introduced for axisymmetric waves in elastic cylindrical structures by Karpfinger et al. (2008a). In this approach, the cylindrical structure is discretized globally using Chebyshev points while differential operators are computed using differentiation matrices (Adamou & Craster 2004; Weideman & Reddy 2000). The eqs. (21)-(23) have to be individually discretized for each poroelastic layer using Chebyshev points as well as differentiation matrices. For the case of a free poroelastic cylinder the dispersion of the axisymmetric modes has been presented by Karpfinger et al. (2008b). In this paper we extend this approach for an arbitrary number of fluid, elastic and poroelastic layers. In the following it is outlined how the generalized matrix eigenvalue problem is formulated for n-layers. Finally, the computation of the phase velocities and attenuation from the computed eigenvalues is explained.

2.1 Eigenvalue problem for multiple layers

The $\mathfrak{L}_p$-matrix equation (23) can be combined with the matrix equations of a fluid layer $\mathfrak{L}_f$ or a solid layer $\mathfrak{L}_s$ for any number n of layers in the following form

$$\underbrace{\begin{pmatrix} \mathfrak{L}_{\xi_1} & 0 & 0 & 0 \\ 0 & \mathfrak{L}_{\xi_2} & 0 & 0 \\ 0 & 0 & \ddots & 0 \\ 0 & 0 & 0 & \mathfrak{L}_{\xi_n} \end{pmatrix}}_{L} \underbrace{\begin{pmatrix} a_{\xi_1} \\ a_{\xi_2} \\ \vdots \\ a_{\xi_n} \end{pmatrix}}_{\Theta} = k_z^2 \begin{pmatrix} a_{\xi_1} \\ a_{\xi_2} \\ \vdots \\ a_{\xi_n} \end{pmatrix} \quad ,$$

$$(42)$$

where $\xi = p, f, s$ stands respectively for a poroelastic, fluid or solid layer.

The differential operators $\mathfrak{L}_{\xi_n}$ is discretized for each layer using the r vector as well as the differentiation matrices. The discretization of the differential operators is done as for the elastic case (Karpfinger et al. 2008a, Sec.III A).

In order to solve this eigenvalue problem the interface conditions eqs. (35)-(39) for each layer of the system are introduced, as well as open or closed pore boundary conditions on the surface of the structure.

2.2 Boundary conditions

The matrix for the stress S and the displacements T for a multi-layered system are constructed as presented in eq. (42). The boundary conditions for poroelastic interfaces discussed above are introduced into the eigenvalue problem eq. (42) in a similar manner to how they were introduced for fluid and elastic layers in Karpfinger et al. (2008a, Sec.IV). In Karpfinger et al. (2009) it is illustrated for the case of a fluid-filled borehole surrounded by a poroelastic formation how the interface boundary conditions are set.

Stress and displacement coefficient components corresponding to the boundary conditions are introduced in lines of eq. (42) which correspond to the collocation points of the inner and outer surfaces of each layer. A diagonal matrix Q is constructed where elements corresponding to lines with

boundary condition coefficients are set to zero. For more information regarding this construction, the reader can refer to Karpfinger et al. (2009) where it is explained in details how the boundary conditions are set for a fluid-poroelastic interface.

After setting all boundary conditions the following eigenvalue problem needs to be solved

$$\tilde{L}\boldsymbol{\Theta} = k_z^2 Q \boldsymbol{\Theta} \quad , \tag{43}$$

where $\tilde{L}$ is the L matrix from eq. (42) with coefficients of the boundary conditions introduced in the corresponding lines. Eigenvalues are the squared wavenumbers k_z^2 while phase velocities can be obtained from their real part as

$$v_{ph} = \frac{\omega}{\mathfrak{Re}(k_z)}. \tag{44}$$

The corresponding attenuation Q^{-1} is defined as

$$Q^{-1} = \frac{\mathfrak{Im}(k_z)}{\mathfrak{Re}(k_z)}. \tag{45}$$

Solving this generalized eigenvalue problem (eq. 43) for a range of frequencies allow the computation of the dispersion and attenuation of all modes propagating in the considered structure.

Eigenvectors corresponding to the displacement potentials $\boldsymbol{\Theta}$ can be used to compute the radial distribution of the displacement and stress components. This can be done by multiplying the potential vectors for each mode with the corresponding matrix coefficients of stresses S and displacements T.

3   APPLICATION TO BOREHOLE ACOUSTIC

In borehole acoustics it is of great importance to model dispersion of guided modes such as tube and flexural waves (Sinha & Asvadurov 2004; Schmitt 1988a). In this paper, our focus is on tube waves propagating in a fluid-filled borehole surrounded by a layered poroelastic formation. Tube wave signatures are sensitive to permeability of the surrounding formation (Chang et al. 1988; Liu 1988; Norris 1989).

In the following section three examples from borehole acoustic, computed with the spectral method are discussed. In all three models we have a layered poroelastic cylinder of radius $2m$, with a fluid-filled borehole in the center (radius: $0.1m$). Because the radius of the structure is 20 times the radius of the borehole, the tube signatures are the same as for infinite formation. The formation, borehole fluid and pore fluid parameters are described in Tab. 1. Note that the borehole fluid as well as the pore fluid are the same non-viscous fluid.

The first example discussed is a fluid-filled borehole surrounded by a poroelastic formation. This example is widely discussed in literature (Chang et al. 1988; Liu 1988; Norris 1989) and we use the well known results to benchmark the solution obtained with the spectral method. Dispersion and attenuation for closed and open pore boundary conditions are computed and displayed. The second example is a more complex three layer model with an elastic layer sandwiched between the fluid and the poroelastic formation. Due to the known problems with *root-finding* only few examples with three layered poroelastic structures are discussed in literature (Liu & Johnson 1997). Using the spectral method the

Grain Density	$\rho_{grain} = 2875 kg/m^3$
Shear modulus	$G = 8.85 GPa$
Drained bulk modulus	$K = 10.8 GPa$
Grain modulus	$K_g = 48 GPa$
Viscosity	$\eta = 10^{-3} Pa \cdot s$
Tortuosity	$a_\infty = 1.91$
Fluid density	$\rho_f = 1000 kg/m^3$
Porosity	$\phi = 0.2$
Fluid bulk modulus	$K_f = 2.3 GPa$
Permeability	$\kappa = 1D$

Table 1. Material parameters of the formation used for all discussed examples.

computation of waves propagating in a three layer model is straightforward. The third example considers an altered zone around the borehole which has an radius of to 2-3 borehole diameters. This zone will be modeled as layers with reduced permeability. This zone is altered by drilling process and thus has reduced permeability (Sinha et al. 2006). A similar model using a three layer model (fluid-altered zone - formation) has been already discussed by Schmitt (1988b). Here we consider a radial increase of the permeability by dividing the altered zone in up to eight sublayers. This requires to obtain the dispersion for a system with up to ten layers. With the spectral method no problems arise while it would be very difficult to solve this problem using a *root-finding* approach.

3.1   Fluid-filled borehole surrounded by poroelastic formation

First let us consider the dispersion and attenuation of a tube wave in a borehole surrounded by a poroelastic medium. An analytical low-frequency approximation as well as the exact solution are discussed in Chang et al. (1988) and Norris (1989). In Karpfinger et al. (2009) the exact solution is computed with the spectral method and is compared to the low frequency approximation proposed by Chang et al. (1988) in the case of open-pore boundary conditions. For the closed-pore boundary conditions case, numerical results were com-
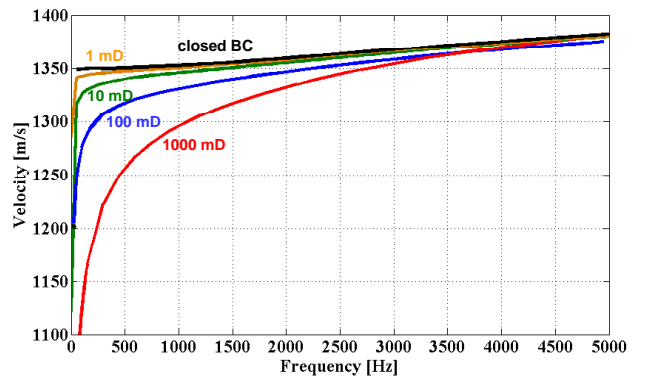

Figure 2. Tube-wave dispersion in a fluid-filled borehole surrounded by a poroelastic formation; top curve shows poroelastic formation with closed boundary conditions; other curves correspond to open boundary conditions with varying permeabilities.

Figure 3. Tube-wave attenuation in a fluid-filled borehole surrounded by a poroelastic formation; bottom curve shows poroelastic formation with closed boundary conditions; other curves correspond to open boundary conditions with varying permeabilities.
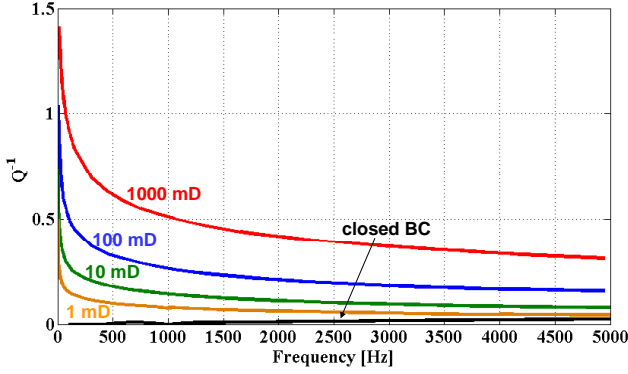

Figure 4. Tube-wave dispersion for an elastic layer with varying thickness sandwiched between the fluid and the poroelastic layer; top curve: two layer case fluid-poroelastic with close-pore boundary conditions on the interface; increasing thickness of sandwiched elastic layer show decrease of tube-wave velocity; for thicknesses bigger than $20cm$ the dispersion is only guided by the properties of the elastic layer.

pared to the equivalent Gassmann model obtained with the elastic spectral method (Karpfinger et al. 2008a). Here the influence of the formation permeability on the dispersion curve is illustrated. Fig. 2 presents dispersion curves computed for a range of permeabilities from $1mD$ to $1000mD$ and a frequency range from $1Hz$ to $5000Hz$. When the permeability is decreasing, the low frequencies part of the dispersion curve decreases and is, at $1mD$, almost indistinguishable from the closed boundary condition case.

For high frequencies, the dispersion curve for $1000mD$ has higher velocities compared to the one computed for lower permeabilities. For high enough frequencies tube wave for open pore boundary condition travels faster than the tube wave for the equivalent elastic medium (closed BC). Qualitatively it is observed that for increasing permeability the frequency where the elastic dispersion equals the poroelastic dispersion shifts towards lower frequencies. This result can be understood because the high-frequency limit of the tube wave in a poroelastic formation tends towards the Scholte velocity of a fluid-poroelastic interface which is faster than its elastic equivalent (Feng & Johnson 1983). In Fig. 3 the attenuation Q^{-1} as a function of frequency is plotted for the same model. Here it can be observed that for decreasing permeability the attenuation gets smaller. For closed boundary conditions the attenuation is zero.

3.2 Effect of an elastic layer between fluid and poroelastic formation

The second example investigates the effect of the thickness of an elastic layer sandwiched between the fluid-filled borehole and the poroelastic formation. For a very thin elastic layer the dispersion is equivalent to the case of closed pore boundary conditions. The pores on the borehole wall are effectively closed and no fluid flow can occur, therefore the dispersion is the same as for an equivalent elastic model. The dispersion due to closed-boundary conditions is compared to the dispersion with an elastic layer. Especially the effect of the thickness of the elastic layer is considered.

In Fig. 4 the dispersion of a tube wave propagating for such a model is illustrated. For the elastic layer the
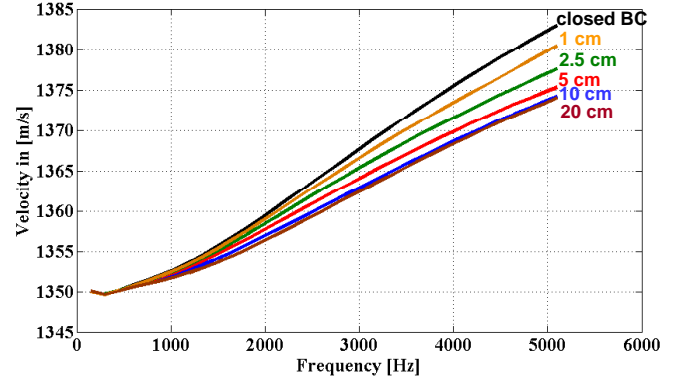
Gassmann velocities of the poroelastic formation are used. The thickness of the elastic layer ranges from $0cm$ (closed BCs) to $20cm$. At low frequencies all dispersion curves tend towards the same limit, i.e. the low-frequency limit of tube waves propagating in a borehole surrounded by an elastic formation. At high frequencies the thickness of the elastic layer causes a difference in the observed dispersion. For layer thicknesses of $5cm$ the difference to the closed boundary conditions case is approximately $8m/s$. As the thickness of the elastic layer becomes bigger than $5cm$ the tube wave signatures do not significantly change anymore and is therefore not influenced by the surrounding poroelastic formation.

3.3 Effect of an altered zone between fluid and poroelastic formation

Reservoir engineers know well that altered zone around borehole often experiences "formation damage" (i.e. permeability reduction). In some cases an altered zone can have distinct mechanical properties, but almost always it suffers from a permeability reduction due to mechanical and chemical factors caused by well drilling and completion processes. Permeability reduction causes problems when extracting oil and gas from hydrocarbon reservoirs. The problem of an altered zone with reduced permeability has been discussed by various authors (Sinha et al. 2006; Schmitt 1988b).

The last example considerers a borehole surrounded by such an altered zone. The geometry is illustrated Fig. 5 where the altered zone has a thickness of $0.24m$. In order to consider the effect of the reduced permeability on the tube wave signatures a radial change in permeability is included. In Fig. 6 the black curve represents the dispersion of a tube wave in a borehole surrounded by an unaltered formation with a permeability of $1000mD$.

The curves in magenta, green and red take the effect of the altered zone into account with different radial permeability profiles. The magenta curve is the dispersion considering an altered zone as a single layer with a permeability of $200mD$. The green dispersion
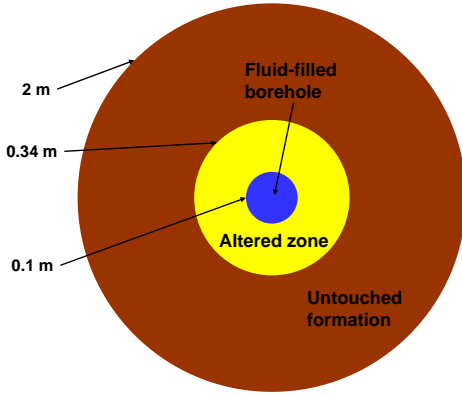
Figure 5. Geometry of the model of a borehole surrounded by a invaded zone of reduced permeability and an untouched formation.

Figure 7. Same as Fig. 6 but zoomed in for low frequencies; displayed is here an invaded zone with a single sublayer (violet) and eight (red) sublayers; the effect of the sublayers is most significant for frequencies between $100Hz$ and $400Hz$; in all cases the permeability of the inner layer is $200mD$.

curve was computed for an invaded zone composed of 4 layers of $6cm$ thickness with a permeability increasing stepwise $(200mD, 400mD, 600mD, 800mD)$. The red line separates the invaded zone into 8 layers of $3cm$ thickness where the radial change in permeability is $(200mD, 300mD, 400mD, 500mD, 600mD, 800mD, 900mD)$.

As one can see, there is a significant change in dispersion from no invaded to invaded zone with one layer and a permeability reduced to $200mD$. However, for a radial permeability change within the invaded zone the difference between one and eight layers is not significant. The fluid flow causing the tube wave dispersion mostly depends on the permeability of the layer adjacent to the borehole, therefore the flow between the different poroelastic layers does not significantly influence the tube wave dispersion.

In Fig. 7 the dispersion curve for an altered zone with one internal layer is compared to the eight layer case. On a smaller scale it becomes obvious that for a frequency range from $100Hz - 400Hz$ the difference is up to $10m/s$. It might be possible to use this low frequency range to invert for the radial distribution of the permeability.

CONCLUSIONS

In this study the spectral method was applied to a fluid-filled borehole surrounded by a cylindrically layered poroelastic formation. The fundamental equations for cylindrical poroelastic structures are derived on the basis of Biot's theory and presented in the context of the spectral method. It is outlined how these equations are used to construct a generalized matrix eigenvalue problem for an arbitrary number of fluid, elastic and poroelastic layers. In order to illustrate the numerical scheme we discuss three examples from borehole acoustics. First we validated spectral method on a well-kown example of fluid-filled borehole surrounded by a poroelastic medium. Two remaining examples illustrate cases with additional cylindrical layering of up to 10 layers. These multi-layered cases would be hard to handle with *root-finding*.

The spectral method allows successfully to obtain the dispersion for all examples easily and time efficiently. It could be shown that the spectral method is a very powerful tool for the computation of wave propagation in complicated poroelastic structures. This gives us a chance to obtain more accurate description of realistic borehole conditions and thus achieve a better characterization of petrophysical properties of subsurface formations.

Future work can be focused on the implementation of absorbing boundary conditions in order to model a real infinite medium. This will allow to also obtain the dispersion of leaky modes and eliminates higher order modes which only propagate in finite structures. Absorbing boundary conditions will also help to reduce the number of collocation points In the example with the altered zone only one parameter, the permeability, was changed. It would be of interest to see how the dispersion would be influenced if various parameters were changed such as, for example, the shear modulus. This, as well as, for example, the effect of anisotropic media can be considered in the future.
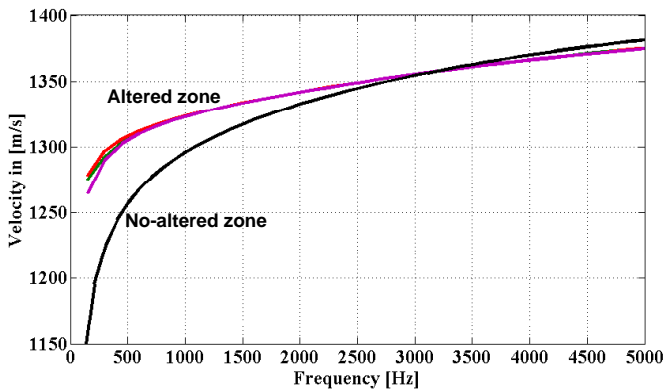

Figure 6. Tube-wave dispersion of a borehole surrounded by an invaded zone of reduced permeability and an untouched formation; altered zone has thickness of $24cm$; we consider several models which consist of no (black), single (violet), four (green) and eight (red) sublayers of equal thickness; in all cases the permeability of the inner layer is $200mD$.
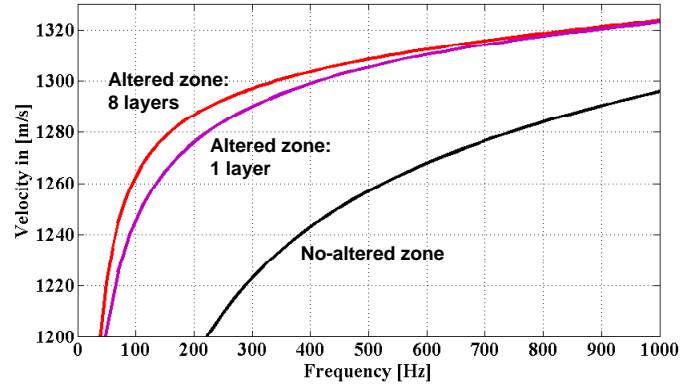
ACKNOWLEDGMENTS

REFERENCES

Adamou, A. T. I. & Craster, R. V., 2004. Spectral methods for modelling guided waves in elastic media, *J. Acoust. Soc. Amer.*, **116**(3), 1524–1535.

Berryman, J. & Pride, S., 2002. *Poromechanics II: Proceedings of the 2nd Biot Conference on Poromechanics*, chap. Dispersion of extensional and torsional waves in porous cylinders with patchy saturation, pp. 613–618, Taylor & Francis.

Berryman, J. G., 1983. Dispersion of extensional waves in fluid-saturated porous cylinders at ultrasonic frequencies, *J. Acoust. Soc. Amer.*, **74**(6), 1805 – 1812.

Berryman, J. G. & Pride, S. R., 2005. Dispersion of waves in porous cylinders with patchy saturation: Formulation and torsional waves, *The Journal of the Acoustical Society of America*, **117**(4), 1785–1795.

Biot, M. A., 1956a. Theory of propagation of elastic waves in a fluid-saturated porous solid. I. Low-frequency range, *J. Acoust. Soc. Amer.*, **28**, 168–178.

Biot, M. A., 1956b. Theory of propagation of elastic waves in a fluid-saturated porous solid. II. Higher frequency range, *J. Acoust. Soc. Amer.*, **28**, 179–191.

Biot, M. A., 1962. Generalized theory of acoustic propagation in porous dissipative media, *J. Acoust. Soc. Amer.*, **34**(5), 1254 – 1264.

Biot, M. A. & Willis, D. G., 1957. The elastic co-efficients of the theory of consolidation, *J. App. Mech.*, **24**, 594–601.

Chang, S. K., Liu, H. L., & Johnson, D. L., 1988. Low-frequency tube waves in permeable rocks, *Geophysics*, **53**(4), 519 – 527.

Deresiewicz, H. & Skalak, R., 1963. On uniqueness in dynamic poroelasicity, *Bull. Seismol. Soc. Amer.*, **53**, 783–788.

Dunn, K.-J., 1986. Acoustic attenuation in fluid-saturated porous cylinders at low frequencies, *The Journal of the Acoustical Society of America*, **79**(6), 1709–1721.

Feng, S. & Johnson, D. L., 1983. High-frequency acoustic properties of a fluid/porous solid interface. i. new surface mode, *J. Acoust. Soc. Amer.*, **74**(3), 906–914.

Gardner, G. H. F., 1962. Extensional waves in fluid-saturated porous cylinders, *J. Acoust. Soc. Amer.*, **34**(1), 36–39.

Gassmann, F., 1951. Über die elastizität poröser medien, *Viertel. Naturforsch. Ges. Zürich*, **96**, 1–23.

Gurevich, B. & Schoenberg, M., 1999. Interface conditions for biot's equations of poroelasticity, *J. Acoust. Soc. Amer.*, **105**, 2585–2589.

Johnson, D. L., Koplik, J., & Dashen, R., 1987. Theory of dynamic permeability and tortuosity in fluid-saturated porous media, *Journal of Fluid Mechanics*, **176**, 379–402.

Karpfinger, F., Gurevich, B., & Bakulin, A., 2008a. Computation of wave propagation along cylindrical structures using the spectral method, *J. Acoust. Soc. Amer.*, **124**(2), 859–865.

Karpfinger, F., Gurevich, B., & Bakulin, A., 2008b. Modeling of axisymmetric wave modes in a poroelastic cylinder using spectral method, *J. Acoust. Soc. Amer.*, **124**(4), EL230–EL235.

Karpfinger, F., Gurevich, B., & Bakulin, A., 2009. *Poromechanics IV: Proceedings of the 4th Biot Conference on Poromechanics*, chap. Axisymetric waves in fluid saturated porous structures, p. accepted, DEStech Publications.

Liu, H.-L., 1988. Borehole modes in a cylindrical fluid-saturated permeable medium, *J. Acoust. Soc. Amer.*, **84**(1), 424–431.

Liu, H.-L. & Johnson, D. L., 1997. Effects of an elastic membrane on tube waves in permeable formations, *The Journal of the Acoustical Society of America*, **101**(6), 3322–3329.

Mörig, R. & Burkhardt, H., 1989. Experimental evidence for the Biot-Gardner theory, *Geophysics*, **54**(4), 524–527.

Norris, A. N., 1989. Stoneley-wave attenuation and dispersion in permeable formations, *Geophysics*, **54**(3), 330 – 341.

Paillet, F. L. & Cheng, C. H., 1991. *Acoustic waves in boreholes*, Boca Raton, CRC Press.

Pride, S. R. & Haartsen, M. W., 1996. Electroseismic wave properties, *J. Acoustic. Soc. Am.*, **100**(3), 1301–1315.

Rosenbaum, J. H., 1974. Synthetic microseismograms: Logging in porous formations, *Geophysics*, **39**, 14–32.

Schmitt, D. P., 1988a. Shear wave logging in elastic formations, *The Journal of the Acoustical Society of America*, **84**(6), 2215–2229.

Schmitt, D. P., 1988b. Effects of radial layering when logging in saturated porous formations, *The Journal of the Acoustical Society of America*, **84**(6), 2200–2214.

Schmitt, D. P., Zhu, Y., & Cheng, C. H., 1988. Shear wave logging in semi-infinite saturated porous formations, *The Journal of the Acoustical Society of America*, **84**(6), 2230–2244.

Sinha, B. & Zeroug, S., 1997. *Wiley Encyclopedia of Electrical and Electronic Engineers*, chap. Geophysical prospecting using sonics and ultrasonics, Wiley, New York.

Sinha, B. K. & Asvadurov, S., 2004. Dispersion and radial depth of investigation of borehole modes, *Geophysical Prospecting*, **52**(4), 271–286.

Sinha, B. K., Vissapragada, B., Renlie, L., & Tysse, S., 2006. Radial profiling of the three formation shear moduli and its application to well completions, *Geophysics*, **71**(6), E65–E77.

Weideman, J. A. C. & Reddy, S. C., 2000. A MATLAB differentiation matrix suite, *ACM Trans. Math. Softw.*, **26**, 465.

White, J. E., 1983. *Underground sound - Application of seismic waves*, New York,Elsevier.

White, J. E., 1986. Biot-Gardner theory of extensional waves in porous rods, *Geophysics*, **51**(3), 742–745.

Equations for waves in cylindrical solid structures

For the case of wave propagation in a solid bar we follow the approach in Armenakas et al. (1969). Solutions of the wave equations in terms of potentials are provided there (eq. 7) in the following form

$$\phi = f(r)\cos n\theta \cos(\omega t + k_z z) \tag{E.0.1}$$

$$\psi_r = h(r)_r \sin n\theta \sin(\omega t + k_z z) \tag{E.0.2}$$

$$\psi_\theta = h(r)_\theta \cos n\theta \sin(\omega t + k_z z) \tag{E.0.3}$$

$$\psi_z = h(r)_z \sin n\theta \cos(\omega t + k_z z) \tag{E.0.4}$$

Based on eqs. (F.0.1-F.0.4) the wave equations in cylindrical coordinates (Achenbach, eqs. 2.135-2.139) can be solved in the following form

The differential equation for the scalar potential f becomes:

$$\left(\partial_r^2 + \frac{1}{r}\partial_r - \frac{n^2}{r^2} + \frac{\omega^2}{v_p^2}\right) f = k_z^2 f \tag{E.0.5}$$

and for h_z:

$$\left(\partial_r^2 + \frac{1}{r}\partial_r - \frac{n^2}{r^2} + \frac{\omega^2}{v_s^2}\right)h_z = k_z^2 h_z \qquad (\text{E.0.6})$$

The equations for h_r and h_θ are coupled:

$$\left(\partial_r^2 + \frac{1}{r}\partial_r - \frac{n^2}{r^2} - \frac{1}{r^2} + \frac{\omega^2}{v_s^2}\right)h_r + \frac{2n}{r^2}h_\theta = k_z^2 h_r \qquad (\text{E.0.7})$$

$$\left(\partial_r^2 + \frac{1}{r}\partial_r - \frac{n^2}{r^2} - \frac{1}{r^2} + \frac{\omega^2}{v_s^2}\right)h_\theta + \frac{2n}{r^2}h_r = k_z^2 h_\theta \qquad (\text{E.0.8})$$

It can be shown that

$$h_r = -h_\theta. \qquad (\text{E.0.9})$$

Using this we get from eqs. (E.0.7) - (E.0.8) :

$$\left(\partial_r^2 + \frac{1}{r}\partial_r - \frac{(n+1)^2}{r^2} + \frac{\omega^2}{v_s^2}\right)h_\theta = k_z^2 h_\theta \qquad (\text{E.0.10})$$

The eqs. (F.0.19, F.0.20 and E.0.33) are utilized to solve axisymmetric and non-symmetric wave propagation in cylindrical elastic structures.

The displacement components

In Achenbach the displacement components are given in terms of potentials as (Achenbach eqs. 2.132-2.135):

$$u_r = \left(\partial_r\phi + \frac{1}{r}\partial_\theta\psi_z - \partial_z\psi_\theta\right) \qquad (\text{E.0.11})$$

$$u_\theta = \left(\frac{1}{r}\partial_\theta\phi + \partial_z\psi_r - \partial_r\psi_z\right) \qquad (\text{E.0.12})$$

$$u_z = \left(\partial_z\phi + \partial_r\psi_\theta + \frac{1}{r}\psi_\theta - \frac{1}{r}\partial_\theta\psi_r\right) \qquad (\text{E.0.13})$$

Using eqs. (F.0.1-F.0.4) and the assumption eq. (E.0.9) we get

$$u_r = \left(\partial_r f + \frac{n}{r}h_z - k_z h_\theta\right)\cos n\theta \cos(\omega t + k_z z) \qquad (\text{E.0.14})$$

$$u_\theta = \left(-\frac{n}{r}f - k_z h_\theta - \partial_r h_z\right)\sin n\theta \cos(\omega t + k_z z) \qquad (\text{E.0.15})$$

$$u_z = \left(-k_z f + \partial_r h_\theta + \frac{1}{r}h_\theta + \frac{n}{r}h_\theta\right)\cos n\theta \sin(\omega t + k_z z) \quad (\text{E.0.16})$$

For the spectral method it is of importance to have equations wich do not depend on the wavenumber k_z. In order to achieve that we substitute $k_z h_\theta = \bar{h}_\theta$

$$u_r = \left(\partial_r f + \frac{n}{r} h_z - \bar{h}_\theta \right) \cos n\theta \cos(\omega t + k_z z) \tag{E.0.17}$$

$$u_\theta = \left(-\frac{n}{r} f - \bar{h}_\theta - \partial_r h_z \right) \sin n\theta \cos(\omega t + k_z z) \tag{E.0.18}$$

$$\bar{u}_z = \left\{ -k_z^2 f + \left(\partial_r + \frac{1}{r} + \frac{n}{r} \right) \bar{h}_\theta \right\} \cos n\theta \sin(\omega t + k_z z) \tag{E.0.19}$$

In order to write the displacement component u_z without k_z dependence the whole equation is multiplied with k_z. Consequently u_z becomes $k_z u_z = \bar{u}_z$. For the expression $k_z^2 f$ we can substitute eq. (F.0.19).

The stress components

The stress components σ_{rr} and $\sigma_{r\theta}$ can be used straightforward in the following form.

The radial stress σ_{rr}

$$\sigma_{rr} = \lambda \left(\partial_r u_r + \frac{u_r}{r} + \frac{1}{r} \partial_\theta u_\theta + \partial_z u_z \right) + 2\mu \partial_r u_r \tag{E.0.20}$$

$$\lambda \underbrace{\left(\partial_r^2 + \frac{1}{r} \partial_r - \frac{n^2}{r^2} - k_z^2 \right) f}_{=-\omega^2 / v_p^2} +$$

$$2\mu \left(\partial_r^2 f - k_z \partial_r h_\theta + \frac{n}{r} \left(\partial_r - \frac{1}{r} \right) h_z \right) \tag{E.0.21}$$

$$= \left(2\mu \partial_r^2 - \lambda \frac{\omega^2}{v_p^2} \right) f - 2\mu \partial_r \underbrace{k_z h_\theta}_{\bar{h}_\theta} + 2\mu \frac{n}{r} \left(\partial_r - \frac{1}{r} \right) h_z \tag{E.0.22}$$

$$= \left(2\mu \partial_r^2 - \lambda \frac{\omega^2}{v_p^2} \right) f - 2\mu \partial_r \bar{h}_\theta + 2\mu \frac{n}{r} \left(\partial_r - \frac{1}{r} \right) h_z \tag{E.0.23}$$

The shear stress $\sigma_{r\theta}$

$$
\begin{aligned}
\sigma_{r\theta} &= \mu \left(\partial_r u_\theta - \frac{u_\theta}{r} + \frac{1}{r}\partial_\theta u_r \right) & \text{(E.0.24)} \\
&= -\mu \frac{2n}{r} \left(\partial_r - \frac{1}{r} \right) f \\
&\quad + \mu \left(\frac{n+1}{r} - \partial_r \right) \underbrace{k_z h_\theta}_{\bar{h}_\theta} \\
&\quad \mu \left(-\partial_r^2 + \frac{1}{r}\partial_r - \frac{n^2}{r^2} \right) h_z & \text{(E.0.25)}
\end{aligned}
$$

The shear stress σ_{rz}

$$
\begin{aligned}
\sigma_{rz} &= \mu \left(\partial_r u_z + \partial_z u_r \right) & \text{(E.0.26)} \\
&= \mu \left(\partial_r u_z - k_z u_r \right) & \text{(E.0.27)} \\
&= -2\mu k_z \partial_r f + \\
&\quad \mu \left(\partial_r^2 + \frac{1+n}{r}\partial_r - \frac{1+n}{r^2} + k_z^2 \right) h_\theta \\
&\quad -\mu \frac{n}{r} k_z h_z & \text{(E.0.28)}
\end{aligned}
$$

The radial shear stress has to be slightly manipulated in order to eliminate the dependance on k_z. In order to achieve that the whole expression will

be multiplied with k_z.

$$k_z \sigma_{rz} = -2\mu k_z^2 \partial_r f +$$
$$\mu \left(\partial_r^2 + \frac{1+n}{r} \partial_r - \frac{1+n}{r^2} + k_z^2 \right) k_z h_\theta$$
$$-\mu \frac{n}{r} k_z^2 h_z \tag{E.0.29}$$

$$\bar{\sigma}_{rz} = -2\mu \partial_r k_z^2 f +$$
$$\mu \left(\partial_r^2 + \frac{1+n}{r} \partial_r - \frac{1+n}{r^2} + k_z^2 \right) \bar{h}_\theta$$
$$-\mu \frac{n}{r} k_z^2 h_z \tag{E.0.30}$$

$$\bar{\sigma}_{rz} = -2\mu \left(\partial_r^3 + \frac{1}{r} \partial_r^2 - \frac{1+n^2}{r^2} \partial_r + \frac{2n^2}{r^3} + \frac{\omega^2}{v_p^2} \partial_r \right) f +$$
$$\mu \left(\partial_r^2 + \frac{1+n}{r} \partial_r - \frac{1+n}{r^2} + k_z^2 \right) \bar{h}_\theta$$
$$-\mu \frac{n}{r} k_z^2 h_z \tag{E.0.31}$$

Consequently σ_{rz} becomes $k_z \sigma_{rz} = \bar{\sigma}_{rz}$ and $k_z h_\theta = \bar{h}_\theta$. The expression $k_z^2 f$ and $k_z^2 h_z$ can be subsequently substitute using the eq. (F.0.19-E.0.8).

Axisymmetric modes

For axisymmetric wave propagation the underlying equations do not dependent on the angle θ. Consequently $n = 0$ and the problem can be solved with two wave equations. The P-wave equation (eq. (F.0.19)) and one S-wave equation (E.0.33) which reduce to:

$$\left(\partial_r^2 + \frac{1}{r} \partial_r + \frac{\omega^2}{v_p^2} \right) f = k_z^2 f \tag{E.0.32}$$

$$\left(\partial_r^2 + \frac{1}{r} \partial_r - \frac{1}{r^2} + \frac{\omega^2}{v_s^2} \right) h_\theta = k_z^2 h_\theta \tag{E.0.33}$$

For axisymmetric wave propagation the displacement and stress components required to fulfill boundary conditions are the radial, axial displace-

ment (u_r, u_z) as well as the radial and normal shear stress (σ_{rr}, σ_{rz}). The displacement components become for $n = 0$:

$$u_r = (\partial_r f - k_z h_\theta) \cos(\omega t + k_z z) \tag{E.0.34}$$

$$u_z = \left(-k_z f + \partial_r h_\theta + \frac{1}{r} h_\theta\right) \sin(\omega t + k_z z) \tag{E.0.35}$$

The cosine and sine terms can be discarded.

For the radial stress we obtain

$$\sigma_{rr} = \left(2\mu\partial_r^2 - \lambda\frac{\omega^2}{v_p^2}\right) f - 2\mu\partial_r \bar{h}_\theta \tag{E.0.36}$$

while the normal shear becomes

$$\bar{\sigma}_{rz} = -2\mu\left(\partial_r^3 + \frac{1}{r}\partial_r^2 - \frac{1}{r^2}\partial_r + \frac{\omega^2}{v_p^2}\partial_r\right) f +$$

$$\mu\left(\partial_r^2 + \frac{1}{r}\partial_r - \frac{1}{r^2} + k_z^2\right) \bar{h}_\theta \tag{E.0.37}$$

Interface boundary conditions are either fluid-fluid, fluid-solid or solid-solid. For a fluid-fluid interface the continuity of radial stress and displacement have to be fulfilled

$$\sigma_{rr}^{fl_1} = \sigma_{rr}^{fl_2} \tag{E.0.38}$$

$$u_r^{fl_1} = u_r^{fl_2} \tag{E.0.39}$$

A fluid-solid interface requires

$$\sigma_{rr}^{fl} = \sigma_{rr}^s \tag{E.0.40}$$

$$u_r^{fl} = u_r^s \tag{E.0.41}$$

$$0 = \sigma_{rz}^s \tag{E.0.42}$$

where in addition to the continuity conditions the shear stress vanishes in the fluid. For solid-solid continuity of all displacement and stress compo-

nents is required

$$\sigma_{rr}^{s1} = \sigma_{rr}^{s2} \tag{E.0.43}$$

$$u_r^{s1} = u_r^{s2} \tag{E.0.44}$$

$$\sigma_{rz}^{s1} = \sigma_{rz}^{s2} \tag{E.0.45}$$

$$u_z^{s1} = u_z^{s2} \tag{E.0.46}$$

How these equations are utilized for the spectral method schema is shown in Karpfinger et al. (2008a). Here the results for a fluid filled borehole and a four layer case are shown

Dipole, Quadrupole etc

The dispersion of dipole or quadrupole or even higher order modes depends on the angle θ. Dipole modes can be obtained for $n = 1$ and quadrupole for $n = 2$ etc. Summarized from section one here again are all the equations required

Helmholtz equations

$$\left(\partial_r^2 + \frac{1}{r} \partial_r - \frac{n^2}{r^2} + \frac{\omega^2}{v_p^2} \right) f = k_z^2 f \tag{E.0.47}$$

$$\left(\partial_r^2 + \frac{1}{r} \partial_r - \frac{n^2}{r^2} + \frac{\omega^2}{v_s^2} \right) h_z = k_z^2 h_z \tag{E.0.48}$$

$$\left(\partial_r^2 + \frac{1}{r} \partial_r - \frac{(n+1)^2}{r^2} + \frac{\omega^2}{v_s^2} \right) h_\theta = k_z^2 h_\theta \tag{E.0.49}$$

Displacement components

$$u_r = \left(\partial_r f + \frac{n}{r} h_z - \bar{h}_\theta\right) \cos n\theta \cos(\omega t + k_z z) \tag{E.0.50}$$

$$u_\theta = \left(-\frac{n}{r} f - \bar{h}_\theta - \partial_r h_z\right) \sin n\theta \cos(\omega t + k_z z) \tag{E.0.51}$$

$$\bar{u}_z = \left\{-k_z^2 f + \left(\partial_r + \frac{1}{r} + \frac{n}{r}\right) \bar{h}_\theta\right\} \cos n\theta \sin(\omega t + k_z z) \tag{E.0.52}$$

Stress components

$$\sigma_{rr} = \left(2\mu\partial_r^2 - \lambda\frac{\omega^2}{v_p^2}\right) f - 2\mu\partial_r \bar{h}_\theta + 2\mu\frac{n}{r}\left(\partial_r - \frac{1}{r}\right) h_z \tag{E.0.53}$$

$$\sigma_{r\theta} = -\mu\frac{2n}{r}\left(\partial_r - \frac{1}{r}\right) f + \mu\left(\frac{n+1}{r} - \partial_r\right) \bar{h}_\theta$$

$$\quad - \mu\left(\partial_r^2 - \frac{1}{r}\partial_r + \frac{n^2}{r^2}\right) h_z \tag{E.0.54}$$

$$\bar{\sigma}_{rz} = -2\mu\left(\partial_r^3 + \frac{1}{r}\partial_r^2 - \frac{1+n^2}{r^2}\partial_r + \frac{2n^2}{r^3} + \frac{\omega^2}{v_p^2}\partial_r\right) f +$$

$$\quad \mu\left(\partial_r^2 + \frac{1+n}{r}\partial_r - \frac{1+n}{r^2} + k_z^2\right) \bar{h}_\theta - \mu\frac{n}{r} k_z^2 h_z \tag{E.0.55}$$

Boundary conditions

The same boundary conditions as for axisymmetric modes apply. In addition for a fluid-solid interface the angular shear stress vanishes in the fluid

$$0 = \sigma_{r\theta}^s \tag{E.0.56}$$

and is continuous for a solid-solid interface

$$\sigma_{r\theta}^{s_1} = \sigma_{r\theta}^{s_2} \tag{E.0.57}$$

Equations for waves in cylindrical poroelastic structures

In order to solve wave propagation in poroelastic structures the following plane wave solution of the potentials are assumed

$$A_{\pm} = a_{\pm}(r)\cos n\theta \cos(\omega t + k_z z) \tag{F.0.1}$$

$$\beta_r = h(r)_r \sin n\theta \sin(\omega t + k_z z) \tag{F.0.2}$$

$$\beta_\theta = h(r)_\theta \cos n\theta \sin(\omega t + k_z z) \tag{F.0.3}$$

$$\beta_z = h(r)_z \sin n\theta \cos(\omega t + k_z z) \tag{F.0.4}$$

Displacement components

For poroelastic structures two displacements exist. The average solid displacement u and the relative displacement $w = \phi(U - u)$, where ϕ is the porosity and U is the fluid displacement. The displacements can be decomposed in terms of potentials as:

$$u = \nabla Y + \nabla \times \beta \qquad w = \nabla \psi + \nabla \times \chi \tag{F.0.5}$$

The solid displacement u separated into its components can be written as follows

$$u_r = \partial_r Y + \frac{1}{r}\partial_\theta \beta_z - \partial_z \beta_\theta \tag{F.0.6}$$

$$u_\theta = \partial_\theta \frac{1}{r} Y + \partial_z \beta_r - \partial_r \beta_z \tag{F.0.7}$$

$$u_z = \partial_z Y + \frac{1}{r}\beta_\theta + \partial_r \beta_\theta - \partial_\theta \frac{1}{r}\beta_r \tag{F.0.8}$$

Using the definition $Y = A_+ \Xi - A_- \Xi$, where $\Xi = \frac{1}{\Gamma_+ - \Gamma_-}$, which decomposes the scalar potential *Upsilon* into its fast $(+)$ and slow $(-)$ P-wave contribution yields

$$u_r = \partial_r A_+ \Xi - \partial_r A_- \Xi + \frac{1}{r}\partial_\theta \beta_z - \partial_z \beta_\theta \tag{F.0.9}$$

$$u_\theta = \partial_\theta \frac{1}{r} A_+ \Xi - \partial_\theta \frac{1}{r} A_- \Xi + \partial_z \beta_r - \partial_r \beta_z \tag{F.0.10}$$

$$u_z = \partial_z A_+ \Xi - \partial_z A_- \Xi + \frac{1}{r}\beta_\theta + \partial_r \beta_\theta - \partial_\theta \frac{1}{r}\beta_r \tag{F.0.11}$$

For the relative displacement the following equation introduces the β potential: $\chi = -\frac{\rho_f}{q}\beta$

Solving the displacements

Applying eqs. (F.0.1-F.0.4) to eqs (F.0.53-F.0.52) the following equations are obtained. The sine and cosine terms are discarded.

$$u_r = \Xi \partial_r a_+ - \Xi \partial_r a_- + \frac{n}{r} h_z - k_z h_\theta \tag{F.0.12}$$

$$u_\theta = -\Xi \frac{n}{r} a_+ + \Xi \frac{n}{r} a_- - k_z h_\theta - \partial_r h_z \tag{F.0.13}$$

$$u_z = -\Xi k_z a_+ + \Xi k_z a_- + \partial_r h_\theta + \frac{1}{r} h_\theta + \frac{n}{r} h_\theta \tag{F.0.14}$$

For the relative displacement the following equation introduces the β potential: $\chi = -\frac{\rho_f}{q}\beta$

The four components required to fulfill the boundary conditions are

$$u_r = \Xi \partial_r a_+ - \Xi \partial_r a_- + \frac{n}{r} h_z - \tilde{h}_\theta \tag{F.0.15}$$

$$u_\theta = -\Xi \frac{n}{r} a_+ + \Xi \frac{n}{r} a_- - \tilde{h}_\theta - \partial_r h_z \tag{F.0.16}$$

$$\tilde{u}_z = -\Xi k_z^2 a_+ + \Xi k_z^2 a_- + \partial_r \tilde{h}_\theta + \frac{1}{r} \tilde{h}_\theta + \frac{n}{r} \tilde{h}_\theta \tag{F.0.17}$$

$$w_r = -\Xi \partial_r a_+ + \Xi \partial_r a_- - \frac{\rho_f}{q} \frac{n}{r} h_z + \frac{\rho_f}{q} \tilde{h}_\theta \tag{F.0.18}$$

Wave equations

In poroelasticity there are two P-wave equations:

$$\left(\nabla^2 + \frac{\omega^2}{v_\pm^2} \right) A_\pm = 0 \tag{F.0.19}$$

equation is the same as for elastic except that there are two and the definition of the bulk velocities is different.

The shear wave equation decomposes in the same way as for elastic. For solving the eigenvalue problem we need two S-wave equations. The equation for β_θ and β_z will be used:

$$\left(\nabla^2 - \frac{1}{r^2} - \frac{2}{r^2} \partial_\theta + \frac{\omega^2}{v_s^2} \right) \beta_\theta = 0 \tag{F.0.20}$$

$$\left(\nabla^2 + \frac{\omega^2}{v_s^2} \right) \beta_z = 0 \tag{F.0.21}$$

Solving the wave equations

Solving the wave equations (eqs. F.0.19-F.0.21) by introducing the definition of the Laplace operator

$$\nabla^2 = \partial_r^2 + \frac{1}{r} \partial_r + \frac{1}{r^2} \partial_\theta^2 + \partial_z^2 \tag{F.0.22}$$

yields

$$\left(\partial_r^2 + \frac{1}{r}\partial_r - \frac{n^2}{r^2} + \frac{\omega^2}{v_\pm^2} \right) a_\pm = k_z^2 a_\pm \tag{F.0.23}$$

$$\left(\partial_r^2 + \frac{1}{r}\partial_r - \frac{(n+1)^2}{r^2} + \frac{\omega^2}{v_s^2} \right) h_\theta = k_z^2 h_\theta \tag{F.0.24}$$

$$\left(\partial_r^2 + \frac{1}{r}\partial_r - \frac{n^2}{r^2} + \frac{\omega^2}{v_s^2} \right) h_z = k_z^2 h_z \tag{F.0.25}$$

Stress components

For poroelastic media the radial and normal shear stress have the same structure as for elastic:

$$\sigma_{r\theta} = \mu \left(\partial_r u_\theta - \frac{u_\theta}{r} + \frac{1}{r}\partial_\theta u_r \right) \tag{F.0.26}$$

$$= -\mu \Xi \frac{2n}{r} \left(\partial_r - \frac{1}{r} \right) a_+ + \mu \Xi \frac{2n}{r} \left(\partial_r - \frac{1}{r} \right) a_-$$

$$+ \mu \left(\frac{n+1}{r} - \partial_r \right) \bar{h}_\theta - \mu \left(\partial_r^2 - \frac{1}{r}\partial_r + \frac{n^2}{r^2} \right) h_z \tag{F.0.27}$$

$$\sigma_{rz} = \mu \left(\partial_z u_r + \partial_r u_z \right) \tag{F.0.28}$$

$$-2\mu \Xi \left(\partial_r^3 + \frac{1}{r}\partial_r^2 - \frac{1+n^2}{r^2}\partial_r + \frac{2n^2}{r^3} + \frac{\omega^2}{v_p^2}\partial_r \right) a_+ +$$

$$+2\mu \Xi \left(\partial_r^3 + \frac{1}{r}\partial_r^2 - \frac{1+n^2}{r^2}\partial_r + \frac{2n^2}{r^3} + \frac{\omega^2}{v_p^2}\partial_r \right) a_- +$$

$$\mu \left(\partial_r^2 + \frac{1+n}{r}\partial_r - \frac{1+n}{r^2} + k_z^2 \right) \bar{h}_\theta - \mu \frac{n}{r} k_z^2 h_z \tag{F.0.29}$$

where delta is the dilatation which becomes $\Delta = -\frac{\omega^2}{v_\pm^2}\Upsilon$.

The radial stress for poroelastic media is:

$$\sigma_{rr} = \lambda_{sat}\Delta + 2\mu\partial_r u_r - C\xi \tag{F.0.30}$$

$$= \Xi\left(2\mu\partial_r^2 - (C\Gamma_- - \lambda)\frac{\omega^2}{v_+^2}\right)a_+ - \Xi\left(2\mu\partial_r^2 - (C\Gamma_+ - \lambda)\frac{\omega^2}{v_-^2}\right)a_-$$

$$-2\mu\partial_r\bar{h}_\theta + 2\mu\frac{n}{r}\left(\partial_r - \frac{1}{r}\right)h_z \tag{F.0.31}$$

$$\tag{F.0.32}$$

The first two terms are similar to elastic terms and the third term, which considers the fluid pressure, is scalar and consequently independent of θ.

The equation for the fluid pressure will be the same for axisymmetric and for flexural wave propagation as it is a scalar equation:

$$p = M\xi - C\Delta \tag{F.0.33}$$

$$p_f = -\Xi\left[M\Gamma_- - C\right]\frac{\omega^2}{v_+^2}A_+ +$$

$$+\Xi\left[M\Gamma_+ - C\right]\frac{\omega^2}{v_-^2}A_- \tag{F.0.34}$$

Monopole modes

For axisymmetric wave propagation the underlying equations do not dependent on the angle θ. Consequently $n = 0$ and the problem can be solved with two wave equations. The P-wave equation (eq. (F.0.47)) and one S-wave equation (F.0.48) which reduce to:

$$\left(\partial_r^2 + \frac{1}{r}\partial_r + \frac{\omega^2}{v_\pm^2}\right)a_\pm = k_z^2 a_\pm \tag{F.0.35}$$

$$\left(\partial_r^2 + \frac{1}{r}\partial_r - \frac{1^2}{r^2} + \frac{\omega^2}{v_s^2}\right)h_\theta = k_z^2 h_\theta \tag{F.0.36}$$

The displacement components reduce to

$$u_r = \Xi \partial_r a_+ - \Xi \partial_r a_- - \tilde{h}_\theta \tag{F.0.37}$$

$$\tilde{u}_z = -\Xi k_z^2 a_+ + \Xi k_z^2 a_- + \partial_r \tilde{h}_\theta + \frac{1}{r} \tilde{h}_\theta + \tag{F.0.38}$$

$$w_r = -\Xi \partial_r a_+ + \Xi \partial_r a_- h_z + \frac{\rho_f}{q} \tilde{h}_\theta \tag{F.0.39}$$

and the stress becomes

$$\sigma_{rr} = \Xi \left(2\mu \partial_r^2 - (C\Gamma_- - \lambda) \frac{\omega^2}{v_+^2} \right) a_+ - \Xi \left(2\mu \partial_r^2 - (C\Gamma_+ - \lambda) \frac{\omega^2}{v_-^2} \right) a_-$$
$$- 2\mu \partial_r \bar{h}_\theta \tag{F.0.40}$$

$$\sigma_{rz} \quad -2\mu \Xi \left(\partial_r^3 + \frac{1}{r} \partial_r^2 - \frac{1}{r^2} \partial_r + \frac{\omega^2}{v_p^2} \partial_r \right) a_+ +$$

$$+2\mu \Xi \left(\partial_r^3 + \frac{1}{r} \partial_r^2 - \frac{1}{r^2} \partial_r + \frac{\omega^2}{v_p^2} \partial_r \right) a_- +$$

$$\mu \left(\partial_r^2 + \frac{1}{r} \partial_r - \frac{1}{r^2} + k_z^2 \right) \bar{h}_\theta \tag{F.0.41}$$

$$p = -\Xi \left[M\Gamma_- - C \right] \frac{\omega^2}{v_+^2} A_+ + \Xi \left[M\Gamma_+ - C \right] \frac{\omega^2}{v_-^2} A_- \tag{F.0.42}$$

Solving these equations certain boundary conditions have to be applied. For a fluid-porous interface the following boundary conditions have to be imposed

$$\sigma_{rr}^{fl} = \sigma_{rr}^{p} \tag{F.0.43}$$

$$u_r^{fl} = u_r^{p} + w_r^{p} \tag{F.0.44}$$

$$0 = \sigma_{rz}^{s} \tag{F.0.45}$$

$$-\sigma_{rr}^{fl} = p^{p} + W_{mc} w_r^{p} \tag{F.0.46}$$

The first three are analogous to fluid-solid while the fourth term takes account of the fluid flow across the interface. For a fluid-porous interface two limiting cases can be considered. Either the term W_{mc} is zero which results in the continuity of fluid pressure across the interface: open pore

case. The other extrem is if $W_{mc} \to \infty$. This results in $0 = w_r^p$ describing a sealed interface. For all values in between W_{mc} is a membrane which can flex in and out of the pore space and thus takes into account partially sealed pores. This is the most realistic case as the pores on the borehole wall are very often sealed by clay particles from the mud. Such a layer is called mudcake and was described by Liu et al..

Dipole, Quadrupole modes etc

$$\left(\partial_r^2 + \frac{1}{r}\partial_r - \frac{n^2}{r^2} + \frac{\omega^2}{v_\pm^2} \right) a_\pm = k_z^2 a_\pm \qquad \text{(F.0.47)}$$

$$\left(\partial_r^2 + \frac{1}{r}\partial_r - \frac{(n+1)^2}{r^2} + \frac{\omega^2}{v_s^2} \right) h_\theta = k_z^2 h_\theta \qquad \text{(F.0.48)}$$

$$\left(\partial_r^2 + \frac{1}{r}\partial_r - \frac{n^2}{r^2} + \frac{\omega^2}{v_s^2} \right) h_z = k_z^2 h_z \qquad \text{(F.0.49)}$$

$$u_r = \Xi\partial_r a_+ - \Xi\partial_r a_- + \frac{n}{r}h_z - \tilde{h}_\theta \qquad \text{(F.0.50)}$$

$$u_\theta = -\Xi\frac{n}{r}a_+ + \Xi\frac{n}{r}a_- - \tilde{h}_\theta - \partial_r h_z \qquad \text{(F.0.51)}$$

$$\tilde{u}_z = -\Xi k_z^2 a_+ + \Xi k_z^2 a_- + \partial_r\tilde{h}_\theta + \frac{1}{r}\tilde{h}_\theta + \frac{n}{r}\tilde{h}_\theta \qquad \text{(F.0.52)}$$

$$w_r = -\Xi\partial_r a_+ + \Xi\partial_r a_- - \frac{\rho_f}{q}\frac{n}{r}h_z + \frac{\rho_f}{q}\tilde{h}_\theta \qquad \text{(F.0.53)}$$

$$\sigma_{rr} = \Xi\left(2\mu\partial_r^2 - (C\Gamma_- - \lambda)\frac{\omega^2}{v_+^2} \right) a_+ - \Xi\left(2\mu\partial_r^2 - (C\Gamma_+ - \lambda)\frac{\omega^2}{v_-^2} \right) a_-$$
$$- 2\mu\partial_r\bar{h}_\theta + 2\mu\frac{n}{r}\left(\partial_r - \frac{1}{r} \right) h_z \qquad \text{(F.0.54)}$$

$$\sigma_{r\theta} = -\mu\Xi\frac{2n}{r}\left(\partial_r - \frac{1}{r}\right)a_+ + \mu\Xi\frac{2n}{r}\left(\partial_r - \frac{1}{r}\right)a_-$$
$$+\mu\left(\frac{n+1}{r} - \partial_r\right)\bar{h}_\theta - \mu\left(\partial_r^2 - \frac{1}{r}\partial_r + \frac{n^2}{r^2}\right)h_z \quad \text{(F.0.55)}$$

$$\sigma_{rz} = -2\mu\Xi\left(\partial_r^3 + \frac{1}{r}\partial_r^2 - \frac{1+n^2}{r^2}\partial_r + \frac{2n^2}{r^3} + \frac{\omega^2}{v_p^2}\partial_r\right)a_+ +$$
$$+2\mu\Xi\left(\partial_r^3 + \frac{1}{r}\partial_r^2 - \frac{1+n^2}{r^2}\partial_r + \frac{2n^2}{r^3} + \frac{\omega^2}{v_p^2}\partial_r\right)a_- +$$
$$\mu\left(\partial_r^2 + \frac{1+n}{r}\partial_r - \frac{1+n}{r^2} + k_z^2\right)\bar{h}_\theta - \mu\frac{n}{r}k_z^2 h_z \quad \text{(F.0.56)}$$

$$p = -\Xi\left[M\Gamma_- - C\right]\frac{\omega^2}{v_+^2}A_+ + \Xi\left[M\Gamma_+ - C\right]\frac{\omega^2}{v_-^2}A_- \quad \text{(F.0.57)}$$

For dipole, quadupole etc the only new boundary condition, in addition to the boundary conditions for monopole, is the angular shear component For a fluid-porous interface the shear stress vanishes in the fluid:

$$0 = \sigma_{r\theta}^p \quad \text{(F.0.58)}$$

while for a solid-porous or porous-porous interface the shear stress is continuous

$$\sigma_{r\theta}^{s,p} = \sigma_{r\theta}^p \quad \text{(F.0.59)}$$

APPENDIX G

MATLAB code for fluid and elastic structures

ComputeDispersion.m

```
0001 function ComputeDispersion
0002 % Name: ComputeDispersion
0003 %
0004 %Purpose:
0005 %        Main Program to compute dispersion and attenuation curves as well as mode shapes
0006 %        for finite cylindrical structures with arbitrary elastic solid and fluid
0007 %        layers
0008 %
0009 %Outputs:
0010 %        - F             : matrix with all the phasevelocities for all modes
0011 %                           and frequencies
0012 %        - G             : matrix with the attenuation for all modes
0013 %                           and frequencies
0014 %
0015 %Author: Florian Karpfinger 01/09
0016
0017 clc;
0018 h = waitbar(0,'Please wait...');
0019
0020 tic
0021
0022 % Read Input File
0023 [Par] = ReadInputFile_1;  %type 1 for example 1 and 2 for example 2
0024
0025 % Set parameters
0026 [Par,matop,BCO]=SetStructureParameters(Par);
0027
0028 n = 1;
0029 for w = Par.wmin:Par.wstep:Par.wmax
0030     [vel,q,ModeSh] = eigen(Par,matop,BCO,w);
0031     F(1:length(vel),n) = vel;
0032     G(1:length(q),n) = q;
0033     waitbar(w/(Par.wmax),h)
0034     n = n+1;
0035 end
0036
0037 close(h);
0038
0039 F(F==0) = NaN;
0040 G(G==0) = NaN;
0041
0042 % Plotting
0043 PlotDispersion(F,G,Par,ModeSh);
0044
0045 t=toc
```

DefineModelParams_1.m

Matlab, The Mathworks, Inc.

June 24, 2009

```
0001 function [Par]=DefineModelParams_1;
0002 %
0003 % Purpose:
0004 %        Definition of input parameters for Example 1: fluid filled
0005 %        boerhole surrounded by an elastic formation;
0006 % Inputs:
0007 %        -Par: Structure containing all parameters defining elastic and geometric
0008 %              parameters as well as all calculations independent of
0009 %              frequency:
0010 %        - N           : number of discretization points for each layer
0011 %        - vpf         : The P-wave velocity of each layer
0012 %        - vs          : The shear wave velocity for each layer
0013 %        - rho         : The bulk density for each layer
0014 %        - qp          : Q-factor for P-waves
0015 %        - qs          : Q-factor for S-waves
0016 %        - A           : the inner radii of the cylindrical layers
0017 %        - wstep       : frequency intervall
0018 %        - wmin        : minimum frequency
0019 %        - wmax        : maximum frequency
0020 %        - SelectminVel : smallest phase velocity displayed
0021 %        - SelectmaxVel : highest phase velocity displayed
0022 %        - s           : choose surface BC
0023 %        - comp        : choose if dispersion or mode shapes are computed
0024 %        - deriv       : max rank of differentation matrices computed
```

```
0025 %         - wstep      : frequency step
0026 %         - wmin       : minimum frequency
0027 %         - wmax       : maximum frequency
0028 %         - w          : single frequency for which modeshpes are computed
0029 % Author: Florian Karpfinger 01/09
0030
0031 %Two layer model
0032 Par.N=[160,160];           %Number of Chebychev points; must be the same number of points for modeshpaes
0033 Par.vpf=[1500,4878];       %P-wave velocities in [m/s]
0034 Par.vs=[0,2600];           %S-wave velocity in [m/s]
0035 Par.rho=[1000,2160];       %Densities in [kg/m^3]
0036 Par.A=[1e-4,0.1,2];        %Radii in [m]
0037 %radii of each layer in [m] (the first value corresponds
0038 %to the center which can not be set equal to zero due to the singularity in cylindrical
0039 %coordinates: 1/r)
0040 Par.SelectminVel = 1750;   %smallest displayed velocity in [m/s]
0041 Par.SelectmaxVel = 1850;   %highest displayed velocity in [m/s]
0042 %Surface boundary conditions
0043 Par.s=0;         %0= stress free boundary conditions on the surface
0044                  %1= rigid boundary conditition on surface
0045 Par.comp =2;     %1= dispersion for a whole frequency intervall is computed
0046                  %2= modeshapes (distribution of displacement and stress along the radius of the structure)
0047                  %for one frequency are computed
0048 Par.deriv = 3; %number of derivatives computed
0049
0050 if Par.comp == 1
0051    Par.wmin=925*2*pi; Par.wstep=925*2*pi; Par.wmax=925*2*pi;        %Frequency Range in [Hz] for dispersion
0052     %%%%%%%%%%%%%%%%%%%%%%%%%%%%%%%%%%%%%%%%%%%%%%%%%%%%%%%%%%%
0053 elseif Par.comp == 2
0054    Par.w= 15000*2*pi;           % single frequency in [Hz] for modeshapes
0055    Par.wstep = Par.w;
0056    Par.wmin  = Par.w;
0057    Par.wmax  = Par.w;
0058 end
```

2

DefineModelParams_2.m

Matlab, The Mathworks, Inc.

June 24, 2009

```matlab
0001 function [Par]=DefineModelParams_2;
0002 % Purpose:
0003 %         Definition of all the input parameters
0004 % Inputs:
0005 %         -Par: Structure containing all parameters defining elastic and geometric
0006 %               parameters as well as all calculations independent of
0007 %               frequency:
0008 %         - N           : number of discretization points for each layer
0009 %         - vpf         : The P-wave velocity of each layer
0010 %         - vs          : The shear wave velocity for each layer
0011 %         - rho         : The bulk density for each layer
0012 %         - qp          : Q-factor for P-waves
0013 %         - qs          : Q-factor for S-waves
0014 %         - A           : the inner radii of the cylindrical layers
0015 %         - wstep       : frequency intervall
0016 %         - wmin        : minimum frequency
0017 %         - wmax        : maximum frequency
0018 %         - SelectminVel : smallest phase velocity displayed
0019 %         - SelectmaxVel : highest phase velocity displayed
0020 %         - s           : choose surface BC
0021 %         - comp        : choose if dispersion or mode shapes are computed
0022 %         - deriv       : max rank of differentation matrices computed
0023 %         - wstep       : frequency step
0024 %         - wmin        : minimum frequency
```

```matlab
0025 %          - wmax          : maximum frequency
0026 %          - w             : single frequency for which modeshpes are computed
0027 % Author: Florian Karpfinger 01/09
0028
0029 %%%%%%%%%%%%%%%%%%
0030 % Four layer model%
0031 %%%%%%%%%%%%%%%%%%%%
0032 Par.N=[20,8,20,8];              %Number of Chebychev points; must be the same number of points for modeshpaes
0033 Par.vpf=[1500,5600,1500,6100];      %P-wave velocities in [m/s]
0034 Par.vs=[0,2800,0,3080];          %S-wave velocity in [m/s]
0035 Par.rho=[1000,2480,1000,2700];      %Densities in [kg/m^3]
0036 Par.A=[1e-4,0.0635,0.0667,0.1032,0.1095];      %Radii in [m]
0037
0038 %radii of each layer in [m] (the first value corresponds
0039 %to the center which can not be set equal to zero due to the singularity in cylindrical
0040 %coordinates: 1/r)
0041 Par.SelectminVel =200;        %smallest displayed velocity in [m/s]
0042 Par.SelectmaxVel = 6000;     %highest displayed velocity in [m/s]
0043 %Surface boundary conditions
0044 Par.s=0;        %0= stress free boundary conditions on the surface
0045                 %1= rigid boundary condititions on surface
0046 Par.comp =1;    %1= dispersion for a whole frequency intervall is computed
0047                 %2= modeshapes (distribution of displacement and stress along the radius of the structure)
0048                 %for one frequency are computed
0049 Par.deriv = 3; %number of derivatives computed
0050
0051 if Par.comp == 1
0052    Par.wmin=200*2*pi; Par.wstep=200*2*pi; Par.wmax=10010*2*pi;          %Frequency Range
0053    %%%%%%%%%%%%%%%%%%%%%%%%%%%%%%%%%%%%%%%%%%%%%%%%%%%%%%
0054 elseif Par.comp == 2
0055    Par.w= 1500*2*pi;
0056    Par.wstep = Par.w;
0057    Par.wmin  = Par.w;
0058    Par.wmax  = Par.w;
0059 end
```

2

SetStructureParameters.m

```
0001 function [Par,matop,BCO]=SetStructureParameters(Par)
0002 %
0003 %Purpose:
0004 %       Computation of all frequency independent parameters
0005 %Input:
0006 %       -Par: Structure containing all parameters defining elastic and geometric
0007 %             parameters as well as all calculations independent of
0008 %             frequency
0009 %
0010 %Outputs:
0011 %       -Par: additional frequency independent computations for Par
0012 %             vs2   :  squared shear velocity
0013 %             vpf2  :  squared P-wave velocity
0014 %             MU_2  :  two times shear modulus
0015 %             LAMBDA:  Lame parameter Lambda
0016 %             aa    :  radius vector for the whole structure to plot modeshpaes
0017 %             NA,cc,dd,ee,gg,ff,hh etc: indices which compute the lines where to
0018 %             set BCs in the K matrix => see eigen function
0019 %       -matop: structure containing all frequency independent matrix
0020 %       operators
0021 %             Zeromatrix: conataining Zeromatrices for each layer
0022 %             Identity  : conataining Identitymatrices for each layer
0023 %             D1        : differentiation matrix for first radial derivative for each layer
0024 %             D2        : differentiation matrix for second radial derivative for each layer
0025 %             D3        : differentiation matrix for third radial derivative for each layer
0026 %             radius_vector: radius vector for each layer
0027 %             rd1       : inverse of radius vector for each layer
0028 %             rd2       : squared inverse radius vector for each layer
0029 %             Laplacian : Laplace operator for each layer
0030 %       -BCO: the preallocated structure BCO
0031 % Author: Florian Karpfinger  01/09
0032
0033
0034 %precompomputation
0035 %%%%%%%%%%%%%%%%%%%%%%%%%%%%%%%%%%%%%%%%%%%%%%%%%%%%%%%%%%%%%%%
0036 %equations
0037 h = diff(Par.A);      %thicknesses of layers
0038 tempo_var  = -2./h;
0039 tempo_var2 = tempo_var.*tempo_var;
0040 tempo_var3 = tempo_var2.*tempo_var;
0041
0042 Par.vs2 = Par.vs.*Par.vs;      %squared shear velocity
0043 Par.vpf2= Par.vpf.*Par.vpf;    %squared P-wave velocity
0044
0045 % shear modulus times two for each layer
```

```
0046 Par.MU_2  = 2*Par.rho.*Par.vs2;
0047
0048 %LAMBDA for each layer
0049 Par.LAMBDA   = Par.rho.*(Par.vpf2-2*Par.vs2);
0050
0051
0052
0053 %Differentiation matrices and radius vector for all layers
0054 for jj=1:length(Par.N);
0055
0056     matop(jj).Zeromatrix = zeros(Par.N(jj));
0057     matop(jj).Identity   = eye(Par.N(jj));
0058
0059     s = Par.A(jj)   + Par.A(jj+1);     %sums of borders
0060     [x,D] = chebdif(Par.N(jj),Par.deriv);
0061
0062     matop(jj).radius_vector  =  (-h(jj).*x+s)*0.5;
0063     matop(jj).D1    =  tempo_var(jj) *D(:,:,1);
0064     matop(jj).D2    =  tempo_var2(jj)*D(:,:,2);
0065     matop(jj).D3    =  tempo_var3(jj)*D(:,:,3);
0066
0067     matop(jj).rd1 =  diag(1./matop(jj).radius_vector);
0068     matop(jj).rd2 =  matop(jj).rd1.*matop(jj).rd1;
0069
0070      % LAPLACIAN
0071     matop(jj).Laplacian = matop(jj).D2 + matop(jj).rd1*matop(jj).D1;
0072
0073     BCO(jj).Lf = zeros(size(matop(jj)));
0074     BCO(jj).Sf = zeros(size(matop(jj)));
0075     BCO(jj).Tf = zeros(size(matop(jj)));
0076 end
0077
0078 if Par.comp ~= 1
0079     %radius vector for plotting modeshapes
0080     ll=1;
0081     for  mm=1:Par.N(ll):sum(Par.N)
0082         Par.aa(mm:sum(Par.N(1:ll)))=matop(ll).radius_vector(1:length(matop(jj).radius_vector));
0083         ll=ll+1;
0084     end
0085 end
0086
0087 %%%%%%%%%%%%%%%%%%%%%%%%%%%%%%%%%%%%
0088 %Indices for introduction of BCs%
0089 %%%%%%%%%%%%%%%%%%%%%%%%%%%%%%%%%%%%
0090
0091 Par.nlayers=length(Par.N);
0092 flag = zeros(1,Par.nlayers);
0093
0094 [Par.rowf, Par.colf] = find(Par.vs == 0);
0095 [Par.rows, Par.cols] = find(Par.vs ~= 0);
0096
0097 if Par.comp >1
0098     flag = Par.comp*ones(1,Par.nlayers);
0099 else
0100     flag(Par.cols) = 1;
0101     flag = flag + 1; % 1-> fluid 2->solid
```

```matlab
0102 end
0103
0104 Par.NA = zeros(1,Par.nlayers);
0105 NAA = cumsum(flag .* Par.N);
0106 Par.NA(2:Par.nlayers) = NAA(1:Par.nlayers-1);
0107
0108 Par.sbca = 2*Par.N(Par.nlayers);
0109 Par.sbcb = Par.N(Par.nlayers);
0110 Par.sbcc = Par.NA(Par.nlayers);
0111
0112 %%%%%%%%%%%%%%%%%%%%
0113 %Loop on interface%
0114 %%%%%%%%%%%%%%%%%%%%
0115
0116 for jj=1:Par.nlayers-1
0117     Par.cc(jj) = Par.NA(jj) + Par.N(jj);
0118     Par.dd(jj) = Par.NA(jj) + Par.N(jj)*Par.comp+1;
0119     Par.ee(jj) = Par.dd(jj) + Par.N(jj+1);
0120     Par.gg(jj) = Par.cc(jj) + Par.N(jj) + 1;
0121     Par.ff(jj) = Par.gg(jj) - 1;
0122     Par.hh(jj) = Par.gg(jj) + Par.N(jj+1);
0123 end
```

eigen.m

Matlab, The Mathworks, Inc.

February 26, 2009

```matlab
0001 function [vel,q,ModeSh] = eigen(Par,matop,BCO,w)
0002 % Name: eigen
0003 %
0004 % Purpose:
0005 %         The corresponding stress and displacement components are
0006 %         introduced in the Helmholtz equation matrix and appropriate
0007 %         boundary conditions are set. At the end the Eigenvalue problem is
0008 %         solved and the Eigenvalues which are of interest are selected
0009 % Inputs:
0010 %         -Par: Structure containing all parameters defining elastic and geometric
0011 %               parameters as well as all calculations independent of
0012 %               frequency
0013 %         -matop: structure containing all frequency independent matrix operators
0014 %         -BCO: the preallocated structure BCO
0015 %         -w: frequency
0016 %
0017 % Outputs:
0018 %         - vel            :phase velocities corresponding to the frequency w
0019 %
0020 %         - q              : values of Q-1  corresponding to the frequency w
0021 %         -ModeSh          : Structure containing all the modeshapes for all
0022 %                            modes corresponding to frequency w
0023 %
0024 % Author: Florian Karpfinger 01/09
0025
0026 %Calculates stress, displacement components and Helmholtz equations for
0027 %each layer
0028
0029 [SS,TT,K,M] = matrices(Par,matop,BCO,w);
0030
0031
0032 %%%%%%%%%%%%%%%%%%%%%%%%%%%%%%%%%%%
0033 %Interface Boundary Conditions%
0034 %%%%%%%%%%%%%%%%%%%%%%%%%%%%%%%%%%%
0035
0036 if Par.nlayers>1
0037
0038     %%%%%%%%%%%%%%%%%%%%%%%%%%%%%%%%%%%%%%%%%%%%%%%%%%%%%%
0039     %Boundary conditions for:                         %
0040     %first layer: fluid next layer: fluid or solid%
0041     %%%%%%%%%%%%%%%%%%%%%%%%%%%%%%%%%%%%%%%%%%%%%%%%%%%%%%
0042
0043         %%%%%%%%%%%%%%%
0044         %fluid/fluid%
0045         %%%%%%%%%%%%%%%
```

```
0046
0047      %BC1: continuity of radial stress for f-f or f-s
0048      K(Par.cc(Par.colf),:)     = SS(Par.cc(Par.colf),:)-SS(Par.dd(Par.colf),:);
0049      M(Par.cc(Par.colf),Par.cc(Par.colf)) = 0;
0050      %BC2: continuity of radial displacement for f-f or f-s
0051      K(Par.dd(Par.colf),:)     = TT(Par.cc(Par.colf),:)- TT(Par.dd(Par.colf),:);
0052      M(Par.dd(Par.colf),Par.dd(Par.colf)) = 0;
0053
0054          %%%%%%%%%%%%
0055          %fluid/solid%
0056          %%%%%%%%%%%%
0057
0058      arrayf = Par.vs(Par.colf+1);  %finds the shear velocity of every layer after a fluid layer
0059      [a b]= find(arrayf > 0);      %finds if these layers are solid (shear velocity bigger
than zero)
0060
0061      %if the next layer is a solid layer in addition to BC1 and BC2
0062      %the shear stress on the fluid solid interface has to vanish
0063
0064      %BC3: vanishing of shear stress for f-s
0065      K(Par.ee(Par.colf(b)),:)    = SS(Par.ee(Par.colf(b)),:);
0066      M(Par.ee(Par.colf(b)),Par.ee(Par.colf(b))) = 0;
0067
0068      %%%%%%%%%%%%%%%%%%%%%%%%%%%%%%%%%%%%%%%%%%%%%%%%
0069      %Boundary conditions for:                      %
0070      %first layer: solid next layer: fluid or solid%
0071      %%%%%%%%%%%%%%%%%%%%%%%%%%%%%%%%%%%%%%%%%%%%%%%%
0072
0073      Par.cols = Par.cols(1:end-1);
0074      %in any case the the continuity of radial stress and displacement have
0075      %to fulfilled:
0076      %BC4: continuity of radial stress for s-f or s-s
0077      K(Par.cc(Par.cols),:)  = (SS(Par.gg(Par.cols),:)-SS(Par.cc(Par.cols),:));
0078      M(Par.cc(Par.cols),Par.cc(Par.cols)) = 0;
0079      %BC5: continuity of radial displacement for s-f or s-s
0080      K(Par.ff(Par.cols),:)  = (TT(Par.gg(Par.cols),:)-TT(Par.cc(Par.cols),:));
0081      M(Par.ff(Par.cols),Par.ff(Par.cols)) = 0;
0082
0083      M(Par.gg(Par.cols),Par.gg(Par.cols)) = 0;
0084
0085      arrays = Par.vs(Par.cols+1); %finds the shear velocity of every layer after a solid layer
0086      [c d]= find(arrays > 0); %finds if these layers are solid (shear velocity bigger than zero)
0087      [e f]= find(arrays == 0); %finds if these layers are fluid (shear velocity equal to zero)
0088
0089          %%%%%%%%%%%%
0090          %solid/solid%
0091          %%%%%%%%%%%%
0092
0093      %if the subsequent layer is a solid: BC4 + BC5 plus =>
0094      %BC6: continuity of normal displacement for s-s
0095      K(Par.gg(Par.cols(d)),:)  = TT(Par.ff(Par.cols(d)),:)-TT(Par.hh(Par.cols(d)),:);
0096      M(Par.gg(Par.cols),Par.gg(Par.cols)) = 0;
0097
0098      %BC7: continuity of shear stress for s-s
0099      K(Par.hh(Par.cols(d)),:)   = SS(Par.ff(Par.cols(d)),:)-SS(Par.hh(Par.cols(d)),:);
0100      M(Par.hh(Par.cols(d)),Par.hh(Par.cols(d))) = 0;
```

```matlab
0101
0102                %%%%%%%%%%%%%
0103                %solid/fluid%
0104                %%%%%%%%%%%%%
0105
0106        %if the subsequent layer is a solid: BC4 + BC5 plus =>
0107        %BC8: vanishing of shear stress for s-f
0108        K(Par.gg(Par.cols(f)),:)    = SS(Par.ff(Par.cols(f)),:);
0109
0110 end
0111
0112 %%%%%%%%%%%%%%%%%%%%%%%%%%%%%%%%
0113 %Surface Boundary Conditions%
0114 %%%%%%%%%%%%%%%%%%%%%%%%%%%%%%%%
0115
0116
0117 M(Par.sbcc + Par.sbcb,Par.sbcc + Par.sbcb) = 0;
0118 M(Par.sbcc + Par.sbca,Par.sbcc + Par.sbca) = 0;
0119
0120 if Par.s > 0  %Rigid surface: radial and normal displacement
are zero on the outer surface of the structure
0121       K(Par.sbcc + Par.sbcb,:)  = TT(Par.sbcc + Par.sbcb,:);
0122       K(Par.sbcc + Par.sbca,:)  = TT(Par.sbcc + Par.sbca,:);
0123 else            %Stress free surface: radial and shear stress
are zero on the outer surface of the structure
0124      K(Par.sbcc + Par.sbcb,:)   = SS(Par.sbcc + Par.sbcb,:);
0125      K(Par.sbcc + Par.sbca,:)   = SS(Par.sbcc + Par.sbca,:);
0126 end
0127
0128 %========================================================================
0129 % Solve eignevalue problem
0130 [U,E]=eig(K,M);
0131
0132 % Velocity computation
0133 vel=sqrt(1./(diag(E)));
0134
0135 % selection of useful eigenvalues
0136 aa = real(vel)>0 & real(vel)>abs(imag(vel)) & imag(vel)==0 & real(vel)> Par.SelectminVel
& real(vel) < Par.SelectmaxVel;
0137 vel =sort(vel(aa),'ascend');
0138
0139 % Compute attenuation
0140 q=imag(vel)./real(vel);
0141
0142 %%%%%%%%%%%%%%%%%%%%%%%%%%%%%%%%%%%%%%%
0143 ModeSh = [];
0144 if Par.comp > 1
0145     %Mode Shapes
0146     U=U(:,aa);
0147     [ModeSh] = displacement(Par,w,U,vel,SS,TT);
0148 end
```

matrices.m

MATLAB, The Mathworks, Inc.

February 26, 2009

```matlab
0001 function [SS,TT,K,M] = matrices(Par,matop,BCO,w)
0002 % Name: matrices
0003 %
0004 % Purpose:
0005 %        This function computes the coeficients of the Helmholtz equations,
0006 %        displacementand stress components for each layer and combines each
0007 %        of them in one big matrix. Each matrix is normalized by its
0008 %        maximum value.
0009 % Inputs:
0010 %        -Par: Structure containing all parameters defining elastic and geometric
0011 %              parameters as well as all calculations independent of
0012 %              frequency
0013 %        -matop: structure containing all frequency independent matrix operators
0014 %        -BCO: the preallocated structure BCO
0015 %        -w: frequency
0016 % Outputs:
0017 %        -SS: The normalized matrix containing all stress coeficients for all layers
0018 %        -TT: The normalized matrix containing all displacement coeficients for all layers
0019 %        -K: The normalized matrix containing all Helmholtz equation coeficients for all layers
0020 %        -M: diagonal matrix multiplied with w^2 and normalized in the same
0021 %              way as K => this matrix will be used subsequently to set
0022 %              boundary conditions
0023 % Author: Florian Karpfinger 01/09
0024
0025 w2 =w^2;
0026
0027 for jj=1:length(Par.N);
0028
0029     Idw2 = matop(jj).Identity.*w2;
0030     kp = Idw2./Par.vpf2(jj);
0031     ks = Idw2./Par.vs2(jj);
0032
0033 %%%%%%
0034 %FLUID%
0035 %%%%%%
0036
0037     % HELMOTZ EQUATION
0038     BCO(jj).Lf  =  matop(jj).Laplacian + kp;
0039
0040     % Fluid Pressure
0041     BCO(jj).Sf  = -w2*Par.rho(jj)* matop(jj).Identity;
0042
0043     % Fluid Displacement
0044     BCO(jj).Tf  =  matop(jj).D1;
0045     BCO(jj).Tfz = -BCO(jj).Lf ;
```

```matlab
0046
0047     if Par.comp > 1
0048          BCO(jj).Lf = [BCO(jj).Lf,matop(jj).Zeromatrix;...
0049              matop(jj).Zeromatrix,matop(jj).Zeromatrix];
0050          BCO(jj).Sf = [BCO(jj).Sf,matop(jj).Zeromatrix;...
0051              matop(jj).Zeromatrix,matop(jj).Zeromatrix];
0052          BCO(jj).Tf = [BCO(jj).Tf,matop(jj).Zeromatrix;...
0053              BCO(jj).Tfz,matop(jj).Zeromatrix];
0054     end
0055
0056 %%%%%%%
0057 %SOLID%
0058 %%%%%%%
0059
0060     %HELMOTZ EQUATIONS
0061
0062          %P-wave equation
0063     L1 = matop(jj).Laplacian + kp;
0064          %shear wave equation
0065     L2 = matop(jj).Laplacian + ks - matop(jj).rd2;
0066
0067          %compination of components in one matrix
0068     BCO(jj).LL = [L1,matop(jj).Zeromatrix;...
0069              matop(jj).Zeromatrix,L2];
0070
0071     %STRESS COEFFICIENTS
0072          %radial components
0073     rrs1 = -kp*Par.LAMBDA(jj)*matop(jj).Identity + Par.MU_2(jj)*matop(jj).D2;
0074     rrs2 = -Par.MU_2(jj)*matop(jj).D1;
0075          %shear components
0076     rzs1 = -Par.MU_2(jj)*(matop(jj).D3 + matop(jj).rd1*matop(jj).D2 - ...
matop(jj).rd2*matop(jj).D1 + kp*matop(jj).D1);
0077     rzs2 =  Par.MU_2(jj)*(matop(jj).Laplacian - matop(jj).rd2 + 0.5*ks);
0078
0079     %compination of components in one matrix
0080     BCO(jj).Ss=[rrs1,rrs2;rzs1,rzs2];
0081
0082     %DISPLACEMENT COEFFICIENTS
0083          %radial components
0084     urs1 =  matop(jj).D1;
0085     urs2 = -matop(jj).Identity;
0086          %normal components
0087     uzs1 = -matop(jj).Laplacian - kp;
0088     uzs2 =  matop(jj).D1 + matop(jj).rd1;
0089
0090     %compination of components in one matrix
0091     BCO(jj).Ts=[urs1,urs2;uzs1,uzs2];
0092
0093 end
0094
0095 %distributes fluid matrices on the positions where fluid layers are in the
0096 %structure
0097 [BCO(Par.colf).L] = deal(BCO(Par.colf).Lf);
0098 [BCO(Par.colf).S] = deal(BCO(Par.colf).Sf);
0099 [BCO(Par.colf).T] = deal(BCO(Par.colf).Tf);
0100
```

```matlab
0101 %distributes solid matrices on the positions where solid layers are in the
0102 %structure
0103 [BCO(Par.cols).L] = deal(BCO(Par.cols).LL);
0104 [BCO(Par.cols).S] = deal(BCO(Par.cols).Ss);
0105 [BCO(Par.cols).T] = deal(BCO(Par.cols).Ts);
0106
0107 %compute zero matrices which will contain all matrices for the whole
0108 %stucture
0109 size_matrix = (Par.comp*sum(Par.N(Par.colf)) + 2*sum(Par.N(Par.cols)));
0110 K  = zeros(size_matrix);
0111 SS = zeros(size_matrix);
0112 TT = zeros(size_matrix);
0113
0114 %compine all matrices in the big matrices
0115 kk=1;
0116 for hh=1:length(Par.N);
0117     ff = kk+length(BCO(hh).S)-1;
0118     K(kk:ff,kk:ff)=BCO(hh).L;
0119     SS(kk:ff,kk:ff)=BCO(hh).S;
0120     TT(kk:ff,kk:ff)=BCO(hh).T;
0121     kk=kk+size(BCO(hh).S);
0122 end
0123
0124 %Normalize each matrix with its maximum value
0125 rr = abs(K)>0;
0126 pL = max(abs(K(rr)));
0127 K=K/pL;
0128 M = eye(size(K))*w^2/pL;
0129
0130 rr = abs(SS)>0;
0131 pS = max(abs(SS(rr))) ;
0132 SS=SS/pS;
0133
0134 rr = abs(TT)>0;
0135 pT = max(abs(TT(rr))) ;
0136 TT=TT/pT;
0137
0138
0139
0140
0141
0142
```

displacement.m

Matlab, The Mathworks, Inc.

February 26, 2009

```
0001 function [ModeSh] = displacement(Par,w,U,vel,SS,TT)
0002
0003 % Name: displacement
0004 %
0005 %Purpose:
0006 %        Computes the radial change of stress and displacement components
0007 %        for a given frequency
0008 %
0009 %Outputs:
0010 %        - ModeSh            : contains the modeshapes for all modes of a
0011 %                                  given frequency
0012
0013 %Author: Florian Karpfinger 01/09
0014
0015 for jj=1:size(U,2)
0016     ModeSh.u(:,jj)=TT*U(:,jj);        %Multiply the displacement
coefficient with the Eigenvectors
0017     ModeSh.s(:,jj)=SS*U(:,jj);        %Multiply the stress coefficient
with the Eigenvectors
0018 end
0019 %DISPLACEMENT%%%%%%
0020 ModeSh.u = reshape(ModeSh.u,size(ModeSh.u,1)/length(Par.N),size(ModeSh.u,2)*length(Par.N));
0021
0022 ModeSh.ur = ModeSh.u(1:size(ModeSh.u,1)*0.5,:);
0023 ModeSh.uz = ModeSh.u(size(ModeSh.u,1)*0.5+1:size(ModeSh.u,1),:);
0024
0025 ModeSh.ur  = reshape(ModeSh.ur,[],length(vel));
0026 ModeSh.uz  = reshape(ModeSh.uz,[],length(vel));
0027
0028 %STRESSES%%%%%%%%%%
0029 ModeSh.s = reshape(ModeSh.s,size(ModeSh.s,1)/length(Par.N),size(ModeSh.s,2)*length(Par.N));
0030
0031 ModeSh.srr = ModeSh.s(1:size(ModeSh.s,1)*.5,:);
0032 ModeSh.srz = ModeSh.s(size(ModeSh.s,1)*.5+1:size(ModeSh.s,1),:);
0033
0034 ModeSh.srr = reshape(ModeSh.srr,[],length(vel));
0035 ModeSh.srz = reshape(ModeSh.srz,[],length(vel));
0036
0037
0038 for m=1:size(ModeSh.uz,2)
0039     ModeSh.uz(:,m) = ModeSh.uz(:,m)/(i*(w/vel(m)));
0040     ModeSh.srz(:,m) = ModeSh.srz(:,m)/(i*(w/vel(m)));
0041
0042     msr(m)=max(abs(ModeSh.srz(:,m)));
0043     muz(m)=max(abs(ModeSh.uz(:,m)));
```

```
0044
0045      ModeSh.ur(:,m)=ModeSh.ur(:,m)/muz(m);
0046      ModeSh.uz(:,m)=ModeSh.uz(:,m)/muz(m);
0047
0048      ModeSh.srr(:,m) = ModeSh.srr(:,m)/msr(m);
0049      ModeSh.srz(:,m) = ModeSh.srz(:,m)/msr(m);
0050 end
0051
```

PlotDispersion.m

MATLAB, The Mathworks, Inc.

February 26, 2009

```matlab
0001 function PlotDispersion(F,G,Par,ModeSh)
0002 %Name: PlotDispersion
0003 %
0004 %Purpose:
0005 %        Here the dispersion curves and the attenuation are plotted
0006 % Inputs:
0007 %        - F            : matrix with all the phasevelocities for all modes
0008 %                          and frequencies
0009 %        - G            : matrix with the attenuation for all modes
0010 %                          and frequencies
0011 %        -Par: Structure containing all parameters defining elastic and geometric
0012 %             parameters as well as all calculations independent of
0013 %             frequency
0014 % Author: Florian Karpfinger 01/09
0015
0016 w= Par.wmin:Par.wstep:Par.wmax;
0017
0018 % Plot dispersion in velocity [m/s]
0019 %  figure;
0020 for n = 1:size(F,1)
0021     plot((w/(2*pi))/1000,((F(n,:))),'*','color','magenta','markersize',15)
0022     hold on
0023 end
0024 grid on;
```

```
0025 set(gca,'FontSize',18,'FontName','Times', 'FontWeight','Bold', 'FontAngle', 'normal');
0026 xlabel('Frequency [kHz]')
0027 ylabel('Velocity in [m/s]')
0028 set(gcf,'Color','white')
0029
0030 if Par.comp == 2
0031     mode_num=1;
0032     %PLOT DISPLACEMENT
0033     for kk = 1:mode_num;
0034         figure('Name','u_r displacement','NumberTitle','on');
0035         plot(Par(1).aa./0.1,abs(ModeSh.ur(:,kk))./max(abs(ModeSh.ur(:,kk))),'-','color','green','LineWidth',2)
0036         set(gca,'FontSize',18,'FontName','Times', 'FontWeight','Bold', 'FontAngle', 'normal');
0037         xlabel('r/a','FontSize',24);
0038         ylabel('Amp. u_r','FontSize',24);
0039         set(gcf,'Color','white');
0040         grid on
0041         figure('Name','u_z displacement','NumberTitle','on');
0042         plot(Par(1).aa./0.1,(ModeSh.ur(:,kk)).*(imag(ModeSh.uz(:,kk)./ModeSh.ur(:,kk))),'-','color','red','LineWidth',2)
0043         grid on;
0044         set(gca,'FontSize',18,'FontName','Times', 'FontWeight','Bold', 'FontAngle', 'normal');
0045         xlabel('r/a','FontSize',24);
0046         ylabel('Amp. u_z','FontSize',24);
0047         set(gcf,'Color','white');
0048         grid on;
0049     end
0050
0051     %PLOT STRESS COMPONENTS
0052
0053     for kk = 1:mode_num;
0054         figure('Name','radial stress','NumberTitle','on');
0055         plot(Par(1).aa./0.1,abs(ModeSh.srr(:,kk)),'-','color','green','LineWidth',2)
0056         set(gca,'FontSize',18,'FontName','Times', 'FontWeight','Bold', 'FontAngle', 'normal');
0057         xlabel('r/a','FontSize',24);
0058         ylabel('Amp. \sigma_{rr}','FontSize',24);
0059         set(gcf,'Color','white');
```

```matlab
0060        grid on
0061        figure('Name','shear stress','NumberTitle','on');
0062        plot(Par(1).aa./0.1,(ModeSh.srr(:,kk)).*(imag(ModeSh.srz(:,kk)./ModeSh.srr(:,kk))),'-','color','red','LineWidth',2)
0063        grid on;
0064        set(gca,'FontSize',18,'FontName','Times', 'FontWeight','Bold', 'FontAngle', 'normal');
0065        xlabel('r/a','FontSize',24);
0066        ylabel('Amp.  \sigma_{rz}','FontSize',24);
0067        set(gcf,'Color','white');
0068        grid on;
0069    end
0070
0071  end
0072
0073
```

chebdif.m

Matlab, The Mathworks, Inc.

February 26, 2009

```
0001 function [x, DM] = chebdif(N, M)
0002
0003 %  The function [x, DM] =  chebdif(N,M) computes the differentiation
0004 %  matrices D1, D2, ..., DM on Chebyshev nodes.
0005 %
0006 %  Input:
0007 %  N:        Size of differentiation matrix.
0008 %  M:        Number of derivatives required (integer).
0009 %  Note:     0 < M <= N-1.
0010 %
0011 %  Output:
0012 %  DM:       DM(1:N,1:N,ell) contains ell-th derivative matrix, ell=1..M.
0013 %
0014 %  The code implements two strategies for enhanced
0015 %  accuracy suggested by W. Don and S. Solomonoff in
0016 %  SIAM J. Sci. Comp. Vol. 6, pp. 1253--1268 (1994).
0017 %  The two strategies are (a) the use of trigonometric
0018 %  identities to avoid the computation of differences
0019 %  x(k)-x(j) and (b) the use of the "flipping trick"
0020 %  which is necessary since sin t can be computed to high
0021 %  relative precision when t is small whereas sin (pi-t) cannot.
0022 %  Note added May 2003:  It may, in fact, be slightly better not to
0023 %  implement the strategies (a) and (b).   Please consult the following
0024 %  paper for details:   "Spectral Differencing with a Twist", by
0025 %  R. Baltensperger and M.R. Trummer, to appear in SIAM J. Sci. Comp.
0026
0027 %  J.A.C. Weideman, S.C. Reddy 1998.  Help notes modified by
0028 %  JACW, May 2003.
0029
0030 I = eye(N);                          % Identity matrix.
0031 L = logical(I);                      % Logical identity matrix.
0032
0033 n1 = floor(N/2); n2  = ceil(N/2);    % Indices used for flipping trick.
0034
0035 k = [0:N-1]';                        % Compute theta vector.
0036 th = k*pi/(N-1);
0037
0038 x = sin(pi*[N-1:-2:1-N]'/(2*(N-1))); % Compute Chebyshev points.
0039
0040 T = repmat(th/2,1,N);
0041 DX = 2*sin(T'+T).*sin(T'-T);         % Trigonometric identity.
0042 DX = [DX(1:n1,:); -flipud(fliplr(DX(1:n2,:)))];   % Flipping trick.
0043 DX(L) = ones(N,1);                   % Put 1's on the main diagonal of DX.
0044
0045 C = toeplitz((-1).^k);               % C is the matrix with
```

```
0046 C(1,:) = C(1,:)*2; C(N,:) = C(N,:)*2;      % entries c(k)/c(j)
0047 C(:,1) = C(:,1)/2; C(:,N) = C(:,N)/2;
0048
0049 Z = 1./DX;                                 % Z contains entries 1/(x(k)-x(j))
0050 Z(L) = zeros(N,1);                          % with zeros on the diagonal.
0051
0052 D = eye(N);                                % D contains diff. matrices.
0053
0054 for ell = 1:M
0055     D = ell*Z.*(C.*repmat(diag(D),1,N) - D); % Off-diagonals
0056     D(L) = -sum(D');                                % Correct main diagonal of D
0057     DM(:,:,ell) = D;                                 % Store current D in DM
0058 end
```

2

APPENDIX H

MATLAB code for fluid, elastic and poroelastic structures

ComputeDispersionporoelastic.m

```matlab
0001 function ComputeDispersionporoelastic
0002 % Name: ComputeDispersionporoelastic
0003 %
0004 % Purpose:
0005 %        The main function which gives us the dispersion and attenuation
0006 %        for cylindrically layered structures built of an arbitrary number
0007 %        of  fluid, elastic and poroelastic layeres for each frequency
0008 % Author: Florian Karpfinger 03/09
0009
0010
0011 % Clean screen
0012 clc;
0013 h = waitbar(0,'Please wait...');
0014 tic
0015
0016 % Read Input File
0017 [Par] = ReadInputFile;
0018
0019
0020 % Set parameters
0021 [Par,Velo,matop]=SetStructureParameters(Par);
0022
0023
0024
0025 n = 1;
0026 for w = Par.wmin:Par.wstep:Par.wmax
0027     [Par,Velo] = velocity(Par,Velo,w);
0028     [vel,q,ModeSh] = eigen(Par,Velo,matop,w);
0029     F(1:length(vel),n) = vel
0030     G(1:length(q),n) = q;
0031     waitbar(w/(Par.wmax),h)
0032     n = n+1
0033 end
0034 close(h)
0035 % Check consistency of the solution
0036 F(F==0) = NaN;
0037 G(G==0) = NaN;
0038
0039 % Plotting
0040 PlotDispersion(F,G,Par,ModeSh);
0041
0042 t=toc
```

ReadInputFile.m

Matlab, The Mathworks, Inc.

March 13, 2009

```matlab
0001 function [Par]=ReadInputFile
0002 %
0003 % Purpose:
0004 %         Definition of all the input parameters
0005 % Inputs:
0006 %         Par: field containing all input parameters
0007 %         - N              : number of discretization points for each layer
0008 %         - A              : the inner radii of the cylindrical layers
0009 %         Fluid parameters:
0010 %         - rof          : Fluid density
0011 %         - eta          : Viscosity
0012 %         - Kf           : Bulk Modulus fluid
0013 %         Frame parameters:
0014 %         - rog          : grain-density
0015 %         - G            : shear modulus
0016 %         - Kd           : Bulk Modulus drained
0017 %         - Kg           : Bulk Modulus grain
0018 %         Poroelastic parameters
0019 %         - phi          : Porosity
0020 %         - k0           : Permeability
0021 %         - T0           : Tortusity
0022 %         - WMC          : Membrane Stiffness
0023 %         - wstep        : frequency intervall
0024 %         - wmin         : minimum frequency
0025 %         - wmax         : maximum frequency
0026 %
0027 % Author: Florian Karpfinger 03/09
0028
0029 %%%%%%%%%%%%%%%%%%%%%%%%%%%%%%%%%%%%%%%%%%%%%%%%%%%%%%%%%%%%%%%%%%%%%%%
0030 %Model of a borehole surrounded by a poroelastic formation%
0031 %%%%%%%%%%%%%%%%%%%%%%%%%%%%%%%%%%%%%%%%%%%%%%%%%%%%%%%%%%%%%%%%%
0032
0033 Par.N   = [60,60];              % number of discretization points for each layer
0034 Par.A   = [1e-4,.1,2];         % the inner radii of the cylindrical layers in [m]
0035 % Fluid parameters:
0036 Par.rof = [1000,1000];         % Fluid density in [kg/m^3]
0037 Par.eta = [1e-3,1e-3];         % Viscosity in [Pa s]
0038 Par.Kf  = [2.3*1e9,2.3*1e9];  % Bulk Modulus fluid in [Pa]
0039 % Frame parameters:
0040 Par.rog = [0,2875];            % Grain density in [kg/m^3]
0041 Par.G   = [0,8.85e9];          % Shear modulus in [Pa]
0042 Par.Kd  = [0,10.8e9];          % Bulk Modulus drained in [Pa]
0043 Par.Kg  = [0,48e9];            % Bulk Modulus grain in [Pa]
0044 % Poroelastic parameters:
0045 Par.phi = [0,0.2];             % Porosity
```

```
0046 Par.k0  = [0,1e-12];          % Permeability in [m^2]
0047 Par.T0  = [0,1.91];           % Tortusity
0048 Par.WMC = 0;                  % Membrane Stiffness
0049
0050
0051
0052 Par.SelectminVel =1200;     %smallest displayed velocity in [m/s]
0053 Par.SelectmaxVel = 1350;    %highest displayed velocity in [m/s]
0054
0055 %%%%%%%%%%%%%%%%%%%%%%%%%%%%%%%%%%%%%%%%%%%%%%%%%%%%%%%%%%%%%%%%%%%%%%%%%
0056 %surface boundary conditions
0057 Par.s=1;          %0= stress free boundary conditions on the surface
0058                   %1= rigid boundary conditions on surface
0059 Par.deriv = 3;    %1= dispersion for a whole frequency intervall is computed
0060                   %3= modeshapes (distribution of displacement and stress
0061                   %along the radius of the structure)
0062 Par.comp = 1;     % choose 1 to compute dispersion and 3 to compute modeshapes
0063
0064 if Par.comp == 1
0065 Par.wmin=50*2*pi; Par.wstep=150*2*pi; Par.wmax=5000*2*pi;
 %Frequency Range in [Hz] for dispersion
0066 %%%%%%%%%%%%%%%%%%%%%%%%%%%%%%%%%%%%%%%%%%%%%%%%%%%%%%%%%%
0067 elseif Par.comp == 3
0068     Par.w=500*2*pi;          % single frequency in [Hz] for modeshapes
0069
0070     Par.wstep = Par.w;
0071     Par.wmin  = Par.w;
0072     Par.wmax  = Par.w
0073 end
```

```
0001 function [Par,Velo,matop]=SetStructureParameters(Par)
0002 %
0003 %% Purpose:
0004 %       Definition of all the input parameters
0005 % Inputs:
0006 %       Par: field containing all input parameters
0007 %        - N            : number of discretization points for each layer
0008 %        - A            : the inner radii of the cylindrical layers
0009 %       Fluid parameters:
0010 %        - rof          : Fluid density
0011 %        - eta          : Viscosity
0012 %        - Kf           : Bulk Modulus fluid
0013 %       Frame parameters:
0014 %        - rog          : grain-density
0015 %        - G            : shear modulus
0016 %        - Kd           : Bulk Modulus drained
0017 %        - Kg           : Bulk Modulus grain
0018 %       Poroelastic parameters
0019 %        - phi          : Porosity
0020 %        - k0           : Permeability
0021 %        - T0           : Tortusity
0022 %        - WMC          : Membrane Stiffness
0023 %        - wstep        : frequency intervall
0024 %        - wmin         : minimum frequency
0025 %        - wmax         : maximum frequency
0026 %Outputs:
0027 %       -Par: additional frequency independent computations for Par
0028 %             MU_2  :  two times shear modulus
0029 %             aa    :  radius vector for the whole structure to plot modeshpaes
0030 %             NA,cc,dd,ee,gg,ff,hh etc: indices which compute the lines where to
0031 %             set BCs in the K matrix => see BC function
0032 %       -Velo: contains all velocity related computations (in this function only the frequency
0033 %              fluid and elastic)
0034 %
0035 %        -matop: structure containing all frequency independent matrix
0036 %        operators
0037 %             Zeromatrix: conataining Zeromatrices for each layer
0038 %             Identity  : conataining Identitymatrices for each layer
0039 %             D1        : differentiation matrix for first radial derivative for each layer
0040 %             D2        : differentiation matrix for second radial derivative for each layer
0041 %             D3        : differentiation matrix for third radial derivative for each layer
0042 %             radius_vector: radius vector for each layer
0043 %             rd1       : inverse of radius vector for each layer
0044 %             rd2       : squared inverse radius vector for each layer
0045 %             Laplacian : Laplace operator for each layer
```

```
0046 % Author: Florian Karpfinger 03/09
0047
0048
0049
0050
0051 Par.MU_2    = 2*Par.G;
0052
0053 h = diff(Par.A);        %thicknesses of layers
0054 tempo_var  = -2./h;
0055 tempo_var2 =  tempo_var.*tempo_var;
0056 tempo_var3 =  tempo_var2.*tempo_var;
0057
0058
0059
0060 for jj=1:length(Par.N);
0061
0062     matop(jj).Zeromatrix = zeros(Par.N(jj));
0063     matop(jj).Identity =eye(Par.N(jj));
0064
0065     s = Par.A(jj)   + Par.A(jj+1);    %sums of borders
0066     [x,D] = chebdif(Par.N(jj),Par.deriv);
0067
0068     matop(jj).radius_vector    =  (-h(jj).*x+s)*0.5;
0069     matop(jj).D1    =  tempo_var(jj)*D(:,:,1);
0070     matop(jj).D2    =  tempo_var2(jj)*D(:,:,2);
0071     matop(jj).D3    =  tempo_var3(jj)*D(:,:,3);
0072
0073     matop(jj).rd1 =   diag(1./matop(jj).radius_vector);
0074     matop(jj).rd2 =   matop(jj).rd1.*matop(jj).rd1;
0075
0076     matop(jj).Laplacian = matop(jj).D2 + matop(jj).rd1*matop(jj).D1;
0077matop(jj).rz_diff=  matop(jj).D3 + matop(jj).rd1*matop(jj).D2 - matop(jj).rd2*matop(jj).D1;
0078 end
0079
0080 if Par.comp ~= 1
0081     %radius vector for plotting modeshapes
0082     ll=1;
0083     for  mm=1:Par.N(ll):sum(Par.N)
0084Par.aa(mm:sum(Par.N(1:ll)))=matop(ll).radius_vector(1:length(matop(jj).radius_vector));
0085         ll=ll+1;
0086     end
0087 end
0088
0089 %%%%%%%%%%%%%%%%%%%%%%%%%%%%%%%%%%%%%%%%%%%%%%%%%%%%%
0090 %Computation of all indeces where BCs are set%
0091 %%%%%%%%%%%%%%%%%%%%%%%%%%%%%%%%%%%%%%%%%%%%%%%%%%%%%
0092 Par.nlayers=length(Par.N);
0093 flag = zeros(1,Par.nlayers);
0094
0095 [Par.rowf, Par.colf] = find(Par.G == 0 & Par.TO == 0);
0096 [Par.rows, Par.cols] = find(Par.G ~= 0 & Par.TO == 0);
0097 [Par.rowp, Par.colp] = find(Par.G ~= 0 & Par.TO ~= 0);
0098
0099 if Par.comp >1
0100     flag = Par.comp*ones(1,Par.nlayers);
0101 else
```

```matlab
0102     flag(Par.colf) = 1;
0103     flag(Par.cols) = 2;
0104     flag(Par.colp) = 3; % 1-> fluid 2->solid 3->porous
0105
0106 end
0107
0108 Par.NA = zeros(1,Par.nlayers);
0109 NAA = cumsum(flag .* Par.N);
0110 Par.NA(2:Par.nlayers) = NAA(1:Par.nlayers-1);
0111
0112 Par.sbca = 2*Par.N(Par.nlayers);
0113 Par.sbcd = 3*Par.N(Par.nlayers);
0114 Par.sbcb = Par.N(Par.nlayers);
0115 Par.sbcc = Par.NA(Par.nlayers);
0116
0117 %%%%%%%%%%%%%%%%%%%%
0118 %Loop on interface%
0119 %%%%%%%%%%%%%%%%%%%%
0120
0121 for jj=1:Par.nlayers-1
0122     Par.cc(jj) = Par.NA(jj) + Par.N(jj);
0123     Par.dd(jj) = Par.NA(jj) + Par.N(jj)*Par.comp + 1;
0124     Par.ee(jj) = Par.dd(jj) + Par.N(jj+1);
0125     Par.q1(jj) = Par.ee(jj) + Par.N(jj+1);
0126     Par.gg(jj) = Par.cc(jj) + Par.N(jj) + 1;
0127     Par.ff(jj) = Par.gg(jj) - 1;
0128     Par.mm(jj) = Par.ff(jj) + Par.N(jj);
0129     Par.pp(jj) = Par.mm(jj) + 1;
0130     Par.q2(jj) = Par.mm(jj) + 1 + Par.N(jj+1);
0131     Par.rr(jj) = Par.mm(jj) + 1 + 2*Par.N(jj+1);
0132     Par.hh(jj) = Par.gg(jj) + Par.N(jj+1);
0133     Par.nn(jj) = Par.gg(jj) + 2*Par.N(jj+1);
0134 end
0135
0136 for ii=1:length(Par.N)
0137
0138     if Par.Kg(ii)==0
0139         %%%%%%%
0140         %FLUID%
0141         %%%%%%%
0142
0143         Velo.vpf(ii) = sqrt(Par.Kf(ii)/Par.rof(ii));  %fluid velocity
0144         Velo.vpf2(ii) = Velo.vpf(ii).*Velo.vpf(ii);   %squared fluid velocity
0145         Par.rho(ii) = Par.rof(ii);                    %fluid density
0146         Velo.vps(ii) = 0;                             %Biot slow wave is zero
0147         Velo.vs(ii)  = 0;                             %shear velocity is zero
0148
0149     elseif Par.TO(ii)==0
0150
0151         %%%%%%%%%%%%%%%%
0152         %Elastic Solid%
0153         %%%%%%%%%%%%%%%%
0154         Par.rho(ii) = Par.phi(ii)*Par.rof(ii)+(1-Par.phi(ii))*Par.rog(ii);    %bulk density
0155
0156         %%%%%%%%%%%%%%%%%
0157         %Elastic moduli%
```

```matlab
0158            %%%%%%%%%%%%%%%%%
0159            Velo.H(ii) = Par.Kd(ii) +(4/3)*Par.G(ii);    %P-wave modulus
0160            Velo.lam(ii) = Velo.H(ii)-2*Par.G(ii);       % Lame parameter
0161
0162            %%%%%%%%%%%%%%%%%%%%%%
0163            %Elastic velocities%
0164            %%%%%%%%%%%%%%%%%%%%%%
0165            Velo.vs(ii) = sqrt(Par.G(ii)/Par.rho(ii));    %shear velocity
0166            Velo.vs2(ii) = Velo.vs(ii).*Velo.vs(ii);      %squared shear velocity
0167            Velo.vpf(ii) = sqrt((Velo.H(ii))/Par.rho(ii)); %P-wave velocity
0168            Velo.vpf2(ii) = Velo.vpf(ii).*Velo.vpf(ii);   %squared P-wave velocity
0169
0170            Velo.vps(ii)=0;                                %Biot slow wave is zero
0171            Velo.gps(ii)=0;
0172            Velo.gpf(ii)=0;
0173            Velo.rr(ii)=0;
0174        end
0175 end
```

4

velocity.m

Matlab, The Mathworks, Inc.

March 13, 2009

```matlab
0001 function [Par,Velo] = velocity(Par,Velo,w)
0002
0003 % Author: Florian Karpfinger 03/09
0004
0005 [jj ii] = find(Par.TO>0);
0006 %%%%%%%%%%%%
0007 %POROELASTIC%
0008 %%%%%%%%%%%%
0009
0010 %%%%%%%%%%%%%%%%%%%%%%%%%%%%%%%%%%%%%%%%%%%%%%
0011 % Permeability Model (Johnson et al., 1987)%
0012 %%%%%%%%%%%%%%%%%%%%%%%%%%%%%%%%%%%%%%%%%%%%%%
0013
0014
0015 m=1;  %Pore geometry number
0016
0017 %transition frequency: seperating low frequency viscous flow and
0018 %high frequency inertial flow
0019
0020 wt = (Par.phi(ii).*Par.eta(ii))./(Par.TO(ii).*Par.k0(ii).*Par.rof(ii));
0021
0022 %frequency depndent permeability
0023
0024 kw = Par.k0(ii)./(sqrt(1 - (i*w*4)./(wt*m)) - i*w./wt);
0025
0026 %%%%%%%%%%%
0027 %DENSITIES%
0028 %%%%%%%%%%%
0029
0030 %Effective Density of fluid in relative motion (Pride & Haartsen, 1996 eq. 77)
0031
0032 Par.q(ii) = (i/w)*(Par.eta(ii)./kw);
0033
0034 %Bulk density
0035
0036 Par.rho(ii) = Par.phi(ii).*Par.rof(ii) + (1-Par.phi(ii)).*Par.rog(ii) ;   %Bulk Density
0037
0038
0039 Velo.rr(ii) = Par.rof(ii)./Par.q(ii);
0040
0041 %%%%%%%%%%%%%%%%%%%%%
0042 %Gassmann equations%
0043 %%%%%%%%%%%%%%%%%%%%%
0044
0045 alpha = 1 - Par.Kd(ii)./Par.Kg(ii);
```

```
0046
0047 Velo.M(ii) = 1./((alpha-Par.phi(ii))./Par.Kg(ii) + Par.phi(ii)./Par.Kf(ii));
0048
0049 Velo.H(ii) = Par.Kd(ii) +(4/3)*Par.G(ii) + alpha.^2.*Velo.M(ii);
0050
0051 Velo.C(ii) = alpha.*Velo.M(ii);
0052
0053 Velo.lam(ii) = Velo.H(ii)-2*Par.G(ii);
0054
0055 %%%%%%%%%%%%%%%%%%%%%%%%%%%%%%%%%%%%%%%%%%%%%%%%%%%%%%%%%%%%%%%%%%%%%%%%%
0056 %Computation of wavenumbers for poroelasticity (Berryman, JASA, 1983)%
0057 %%%%%%%%%%%%%%%%%%%%%%%%%%%%%%%%%%%%%%%%%%%%%%%%%%%%%%%%%%%%%%%%%%%%%%%%%
0058
0059 delta = Velo.M(ii).*Velo.H(ii) - Velo.C(ii).^2;   %BE:29
0060
0061 b = w^2*(Par.rho(ii).*Velo.M(ii) - Par.rof(ii).*Velo.C(ii))./delta;    %BE:28
0062
0063 c = w^2*(Par.rof(ii).*Velo.M(ii) - Par.q(ii).*Velo.C(ii))./delta;      %BE:28
0064
0065 d = w^2*(Par.rof(ii).*Velo.H(ii) - Par.rho(ii).*Velo.C(ii))./delta;    %BE:28
0066
0067 f = w^2*(Par.q(ii).*Velo.H(ii) - Par.rof(ii).*Velo.C(ii))./delta;      %BE:28
0068
0069
0070 %S-wave velocity
0071
0072 Velo.ks(ii) =  w^2*(Par.rho(ii) - Par.rof(ii).^2./Par.q(ii))./Par.G(ii); %shear-wave wavenumber
0073 Velo.vs(ii) =  sqrt(w^2./Velo.ks(ii));
0074
0075 %P-wave velocities
0076
0077 Velo.kpf(ii) =  0.5*(b + f - sqrt((b-f).^2 + 4*c.*d)); %fast P-wave wavenumber BE:27
0078 Velo.kps(ii) =  0.5*(b + f + sqrt((b-f).^2 + 4*c.*d)); %slow P-wave wavenumber BE:27
0079
0080 Velo.vpf(ii) = sqrt(w^2./Velo.kpf(ii));
0081 Velo.vps(ii) = sqrt(w^2./Velo.kps(ii));
0082
0083 Velo.vpf2(ii) = Velo.vpf(ii).*Velo.vpf(ii);
0084 Velo.vps2(ii) = Velo.vps(ii).*Velo.vps(ii);
0085 Velo.vs2(ii)  = Velo.vs(ii).*Velo.vs(ii);
0086
0087 %%%%%%%%%%%%%%%%%%%%%%%%
0088 %The Scalar potential%
0089 %%%%%%%%%%%%%%%%%%%%%%%%
0090
0091 Velo.gpf(ii) = d./(Velo.kpf(ii)-b);
0092
0093 Velo.gps(ii) = d./(Velo.kps(ii)-b);
0094
0095 Velo.o1(ii) = 1./(Velo.gpf(ii) - Velo.gps(ii)) ;                %BE:45
```

eigen.m

Matlab, The Mathworks, Inc.

March 13, 2009

```matlab
0001 function [vel,q,ModeSh] = eigen(Par,Velo,matop,w)
0002 % Name: Eigen
0003 %
0004 % Purpose:
0005 %       After all underlying equations are discretized and the boundary
0006 %       conditions are introduced the matrix eigenvalue problem is solved
0007 %       and the phase velocities and attenuation Q^-1 are obtained
0008 % Inputs:
0009 %         -Par: Structure containing all parameters defining elastic and geometric
0010 %               parameters as well as all calculations independent of
0011 %               frequency
0012 %         -Velo: Structure with all velocitiy related parameters
0013 %         -matop: structure containing all frequency independent matrix
0014 %         operators
0015 %         -w: frequency
0016 %
0017 % Outputs:
0018 %         - vel            :phase velocities corresponding to the frequency w
0019 %
0020 %         - q              : values of Q-1  corresponding to the frequency w
0021 %         -ModeSh          : Structure containing all the modeshapes for all
0022 %                            modes corresponding to frequency w
0023 % Author: Florian Karpfinger 03/09
0024
0025 %Calculates stress and displacement components
0026 [SS,TT,K,M,Par] = matrices(Par,Velo,matop,w);
0027
0028 %Sets interface and surface boundary conditions
0029 [K,M] = BC(Par,Velo,SS,TT,K,M,w);
0030
0031
0032 % Solve eignevalue problem
0033 [U,E]=eig(K,M);
0034
0035 % Velocity computation
0036 % kz = sqrt(real(diag(E)));
0037 slow = sqrt((diag(E)));
0038 %selection of the eigenvalues which are of interest
0039 aa = real(slow)>0  & real(slow)>abs(imag(slow)) & real(1./slow) > Par.SelectminVel
          ...& real(1./slow) < Par.SelectmaxVel;
0040
0041 %Phase velocity
0042 vph = 1./(real(slow(aa)));
0043
0044 vel = sort(vph,'ascend') ;
```

```matlab
0045
0046 %Compute attenuation
0047  q=2*(sqrt(imag(slow(aa)))./sqrt(real(slow(aa))));
0048 %%%%%%%%%%%%%%%%%%%%%%%%%%%%%%%%%%%%
0049 ModeSh = [];
0050 if Par.comp > 2
0051 %Mode Shapes
0052 U=U(:,aa);
0053 [ModeSh] = displacement(Par,w,U,vel,SS,TT);
0054 end
0055
0056
0057
0058
0059
0060
0061
0062
```

matrices.m

MATLAB, The Mathworks, Inc.

March 13, 2009

```matlab
0001 function [SS,TT,K,M,Par] = matrices(Par,Velo,matop,w)
0002 % Name: BC
0003 %
0004 % Purpose:
0005 %        This function computes the coefficients of the displacement and
0006 %        stress components for each layer and combines them in one matrix
0007 %        for the stress (S) and in one matrix for the displacement (T)
0008 %
0009 % Author: Florian Karpfinger 03/09
0010 w2 =w^2;
0011
0012 for jj=1:length(Par.N);
0013     Idw2 = matop(jj).Identity.*w2;
0014     kpf = Idw2./Velo.vpf2(jj);
0015     kps = Idw2./Velo.vps2(jj);
0016     ks = Idw2./Velo.vs2(jj);
0017     %%%%%%
0018     %FLUID%
0019     %%%%%%
0020     % HELMOTZ EQUATION
0021     BCO(jj).Lf = matop(jj).Laplacian + kpf;
0022
0023     % Fluid Pressure
0024     BCO(jj).Sf   = -w2*Par.rho(jj)* matop(jj).Identity;
0025
0026     % Fluid Displacement
0027     BCO(jj).Tf   =  matop(jj).D1;
0028     BCO(jj).Tfz  =  matop(jj).Laplacian + kpf;
0029
0030     if Par.comp == 2
0031        BCO(jj).Lf = [BCO(jj).Lf,matop(jj).Zeromatrix;...
0032            matop(jj).Zeromatrix,matop(jj).Zeromatrix];
0033        BCO(jj).Sf = [BCO(jj).Sf,matop(jj).Zeromatrix;...
0034            matop(jj).Zeromatrix,matop(jj).Zeromatrix];
0035        BCO(jj).Tf = [BCO(jj).Tf,matop(jj).Zeromatrix;...
0036            BCO(jj).Tfz,matop(jj).Zeromatrix];
0037     elseif Par.comp == 3
0038        BCO(jj).Lf = [BCO(jj).Lf,matop(jj).Zeromatrix,matop(jj).Zeromatrix;...
0039            matop(jj).Zeromatrix,matop(jj).Zeromatrix,matop(jj).Zeromatrix;...
0040            matop(jj).Zeromatrix,matop(jj).Zeromatrix,matop(jj).Zeromatrix];
0041        BCO(jj).Sf = [BCO(jj).Sf,matop(jj).Zeromatrix,matop(jj).Zeromatrix;...
0042            matop(jj).Zeromatrix,matop(jj).Zeromatrix,matop(jj).Zeromatrix;...
0043            matop(jj).Zeromatrix,matop(jj).Zeromatrix,matop(jj).Zeromatrix];
0044        BCO(jj).Tf = [BCO(jj).Tf,matop(jj).Zeromatrix,matop(jj).Zeromatrix;...
0045            matop(jj).Zeromatrix,matop(jj).Zeromatrix,matop(jj).Zeromatrix;...
```

```matlab
0046                matop(jj).Zeromatrix,matop(jj).Zeromatrix,matop(jj).Zeromatrix];
0047      end
0048
0049      %%%%%%%%%
0050      %ELASTIC%
0051      %%%%%%%%%
0052
0053      % HELMOTZ EQUATION
0054      LS = matop(jj).Laplacian  - matop(jj).rd2 + ks;
0055      BCO(jj).LP = matop(jj).Laplacian + kpf;
0056      BCO(jj).LL = [BCO(jj).LP,matop(jj).Zeromatrix;matop(jj).Zeromatrix,LS];
0057
0058      %Stress Matrix
0059      As = -kpf*Velo.lam(jj) + Par.MU_2(jj)*matop(jj).D2;
0060      Bs = -Par.MU_2(jj)*matop(jj).D1;
0061      Cs = -Par.MU_2(jj)*(matop(jj).rz_diff + kpf*matop(jj).D1);
0062      Ds =  Par.MU_2(jj)*(matop(jj).Laplacian - matop(jj).rd2 + 0.5*ks);
0063
0064      BCO(jj).Ss=[As,Bs;Cs,Ds];
0065
0066      %Solid displacement
0067      Es =   matop(jj).D1;
0068      Hs = -(matop(jj).Laplacian + kpf);
0069      Is =  (matop(jj).D1 + matop(jj).rd1);
0070
0071      BCO(jj).Ts=[Es,-matop(jj).Identity;Hs,Is];
0072  if Par.comp == 3
0073       BCO(jj).LL = [BCO(jj).LP,matop(jj).Zeromatrix,matop(jj).Zeromatrix;
0074                    matop(jj).Zeromatrix,LS,matop(jj).Zeromatrix;
0075                    matop(jj).Zeromatrix,matop(jj).Zeromatrix,matop(jj).Zeromatrix];
0076       BCO(jj).Ss=[As,Bs,matop(jj).Zeromatrix;
0077                   Cs,Ds,matop(jj).Zeromatrix;
0078                    matop(jj).Zeromatrix,matop(jj).Zeromatrix,matop(jj).Zeromatrix];
0079             BCO(jj).Ts=[Es,-matop(jj).Identity,matop(jj).Zeromatrix;
0080                 Hs,Is,matop(jj).Zeromatrix;
0081                  matop(jj).Zeromatrix,matop(jj).Zeromatrix,matop(jj).Zeromatrix];
0082  end
0083      %%%%%%%%%%%%%
0084      %POROELASTIC%
0085      %%%%%%%%%%%%%
0086
0087      % HELMOTZ EQUATION
0088      LPS = matop(jj).Laplacian + kps;
0089
0090      BCO(jj).LS = [BCO(jj).LP,matop(jj).Zeromatrix,matop(jj).Zeromatrix;...
0091          matop(jj).Zeromatrix,LS,matop(jj).Zeromatrix;...
0092          matop(jj).Zeromatrix,matop(jj).Zeromatrix,LPS];
0093
0094      %radial stress
0095      Ap      =   (Par.MU_2(jj)*matop(jj).D2 + (Velo.C(jj)*Velo.gps(jj) - Velo.lam(jj))*kpf);
0096      Bp      =  -Par.MU_2(jj)*matop(jj).D1;
0097      Cp      =  -(Par.MU_2(jj)*matop(jj).D2 + (Velo.C(jj)*Velo.gpf(jj) - Velo.lam(jj))*kps);
0098
0099
0100      %shear stress
0101      Dp      =  -Par.MU_2(jj)*(matop(jj).rz_diff + kpf*matop(jj).D1);
```

2

```matlab
0102     Ep        =     Par.MU_2(jj)*(matop(jj).Laplacian- matop(jj).rd2 + 0.5*ks);
0103     Fp        =     Par.MU_2(jj)*(matop(jj).rz_diff + kps*matop(jj).D1);
0104
0105
0106     %fluid pressure p
0107     Gp        =     (Velo.C(jj) - Velo.M(jj)*Velo.gps(jj))* kpf;
0108     Hp        =     zeros(Par.N(jj));
0109     Ip        =    -(Velo.C(jj) - Velo.M(jj)*Velo.gpf(jj))* kps;
0110
0111     BCO(jj).Sp = [Ap,Bp,Cp;Dp,Ep,Fp;Gp,Hp,Ip];
0112
0113     %ur
0114     Ip        =     matop(jj).D1;
0115     Jp        =    -eye(Par.N(jj));
0116     Kp        =    -matop(jj).D1;
0117
0118     %uz
0119     Lp        =    -(matop(jj).Laplacian + kpf);
0120     Mp        =     matop(jj).D1 + matop(jj).rd1;
0121     Np        =     (matop(jj).Laplacian + kps);
0122
0123     %wr
0124     Op        =     -Velo.gps(jj)*matop(jj).D1;
0125     Pp        =      Velo.rr(jj)*eye(Par.N(jj));
0126     Qp        =      Velo.gpf(jj)*matop(jj).D1;
0127
0128     BCO(jj).Tp= [Ip,Jp,Kp;Lp,Mp,Np;Op,Pp,Qp];
0129 end
0130
0131 %Sort the fluid matrices
0132 [BCO(Par.colf).S] = deal(BCO(Par.colf).Sf);
0133 [BCO(Par.colf).T] = deal(BCO(Par.colf).Tf);
0134 [BCO(Par.colf).L] = deal(BCO(Par.colf).Lf);
0135 %Sort the elastic matrices
0136 [BCO(Par.cols).S] = deal(BCO(Par.cols).Ss);
0137 [BCO(Par.cols).T] = deal(BCO(Par.cols).Ts);
0138 [BCO(Par.cols).L] = deal(BCO(Par.cols).LL);
0139 %Sort the porous matrices
0140 [BCO(Par.colp).S] = deal(BCO(Par.colp).Sp);
0141 [BCO(Par.colp).T] = deal(BCO(Par.colp).Tp);
0142 [BCO(Par.colp).L] = deal(BCO(Par.colp).LS);
0143
0144 %Intialize matrices
0145 size_matrix = 0;
0146 for jj=1:length(Par.N);
0147     size_matrix = sum(size(BCO(jj).S,1)) + size_matrix;
0148 end
0149
0150 K  = zeros(size_matrix);
0151 SS = zeros(size_matrix);
0152 TT = zeros(size_matrix);
0153
0154 kk=1;
0155 for hh=1:length(Par.N);
0156     ff = kk+length(BCO(hh).S)-1;
0157     SS(kk:ff,kk:ff)=BCO(hh).S;
```

```
0158      TT(kk:ff,kk:ff)=BCO(hh).T;
0159      K(kk:ff,kk:ff)=BCO(hh).L;
0160      kk=kk+size(BCO(hh).S);
0161 end
0162
0163 %%%%%%%%%%%%%%
0164 %Normalization%
0165 %%%%%%%%%%%%%%
0166
0167 rr = abs(K)>0;
0168 pL = max(abs(K(rr)));
0169
0170 rr = abs(SS)>0;
0171 pS = max(abs(SS(rr))) ;
0172
0173 rr = abs(TT)>0;
0174 pT = max(abs(TT(rr))) ;
0175
0176 SS = SS/pS;
0177
0178 TT = TT/pT;
0179 K  = K/pL;
0180
0181 M = eye(size(K))*w^2/pL;
0182
0183
```

BC.m

```
0001 function [K,M] = BC(Par,Velo,SS,TT,K,M,w);
0002 % Name: BC
0003 %
0004 % Purpose:
0005 %         The interface and surface conditions are introduced in the
0006 %         appropriate lines of the matrix K and they are set equal to zero
0007 %         in the corresponding lines of the unit matrix M
0008 % Inputs:
0009 %       -Par: Structure containing all parameters defining elastic and geometric
0010 %             parameters as well as all calculations independent of
0011 %             frequency
0012 %       -Velo: Structure with all velocitiy related parameters
0013
0014 %       -w: angular frequency
0015 %
0016 % Outputs:
0017
0018 % Author: Florian Karpfinger 03/09
0019
0020
0021 %%%%%%%%%%%%%%%%%%%%%%%%%%%%%%%%
0022 %Interface Boundary Conditions%
0023 %%%%%%%%%%%%%%%%%%%%%%%%%%%%%%%%
0024
```

```matlab
0025    %%%%%%%%%%%%%%%%%%%%%%%%%%%%%%%%%%%%%%%%%%%%%%%%%%%%%%%%%%%%
0026    %Boundary conditions for:                                %
0027    %first layer: fluid next layer: fluid,solid or porous%
0028    %%%%%%%%%%%%%%%%%%%%%%%%%%%%%%%%%%%%%%%%%%%%%%%%%%%%%%%%%%%%
0029
0030
0031        %%%%%%%%%%%%%
0032        %fluid/fluid%
0033        %%%%%%%%%%%%%%
0034 %BC1: continuity of radial stress for f-f f-s or f-p
0035 K(Par.cc(Par.colf),:) = SS(Par.cc(Par.colf),:)- SS(Par.dd(Par.colf),:);
0036 M(Par.cc(Par.colf),Par.cc(Par.colf)) = 0;
0037  %BC2: continuity of radial displacement for f-f f-s or f-p
0038 K(Par.dd(Par.colf),:) = TT(Par.cc(Par.colf),:)- TT(Par.dd(Par.colf),:); %continuity of radial displacement plus relativ displacement
0039 M(Par.dd(Par.colf),Par.dd(Par.colf)) = 0;
0040
0041
0042
0043        %%%%%%%%%%%%%
0044        %fluid/solid%
0045        %%%%%%%%%%%%%%
0046 arrayf1 = Par.G(Par.colf+1);   %finds the shear modulus of every layer after a fluid layer
0047 [a b]= find(arrayf1 >0);       %finds if these layers are solid (shear velocity bigger than zero)
0048
0049 %if the next layer is a solid pr porous layer in addition to BC1 and BC2
0050 %the shear stress on the fluid solid interface has to vanish
0051
0052 %BC3: vanishing of shear stress for f-s or f-p
0053 K(Par.ee(Par.colf(b)),:) = SS(Par.ee(Par.colf(b)),:);
0054 M(Par.ee(Par.colf(b)),Par.ee(Par.colf(b))) = 0;
0055
0056        %%%%%%%%%%%%%%
0057        %fluid/porous%
0058        %%%%%%%%%%%%%%%
0059 arrayf2 = Par.TO(Par.colf+1);  %finds the tortuosity  of every layer after a fluid layer
```

```
0060 [c d]= find(arrayf1 > 0 & arrayf2 > 0);  %finds if these layers are porous (shear velocity bigger than zero and tortuosity bigger than zero)
0061
0062 %BC4: continuity of radial displacement for f-p
0063 K(Par.dd(Par.colf(d)),:) = TT(Par.cc(Par.colf(d)),:)- TT(Par.dd(Par.colf(d)),:) - TT(Par.q1(Par.colf(d)),:);
%continuity of radial displacement plus relativ displacement
0064 M(Par.dd(Par.colf(d)),Par.dd(Par.colf(d))) = 0;
0065
0066 %BC5: continuity of fluid pressure plus membrane stiffness for mudcake for f-p
0067 %WMC is zero=> open formation
0068 %WMC is infinite => closed formation
0069 %WMC intermediat values consider mudcake effect
0070 K(Par.q1(Par.colf(d)),:) = SS(Par.cc(Par.colf(d)),:) + SS(Par.q1(Par.colf(d)),:)+ Par.WMC*TT(Par.q1(Par.colf(d)),:);
0071 M(Par.q1(Par.colf(d)),Par.q1(Par.colf(d))) = 0;
0072
0073     %%%%%%%%%%%%%%%%%%%%%%%%%%%%%%%%%%%%%%%%%%%%%%%%%%%%%%%%
0074     %Boundary conditions for:                            %
0075     %first layer: solid next layer: fluid,solid or porous%
0076     %%%%%%%%%%%%%%%%%%%%%%%%%%%%%%%%%%%%%%%%%%%%%%%%%%%%%%%%
0077
0078
0079 %BC6: continuity of radial stress for f-f f-s or f-p
0080 K(Par.cc(Par.cols),:)  = (SS(Par.cc(Par.cols),:) - SS(Par.gg(Par.cols),:));
0081 M(Par.cc(Par.cols),Par.cc(Par.cols)) = 0;
0082
0083 %BC7: continuity of radial displacement for f-f f-s or f-p
0084 K(Par.ff(Par.cols),:)  = (TT(Par.cc(Par.cols),:) - TT(Par.gg(Par.cols),:));
0085 M(Par.ff(Par.cols),Par.ff(Par.cols)) = 0;
0086
0087     %%%%%%%%%%%%%
0088     %solid/fluid%
0089     %%%%%%%%%%%%%
0090 M(Par.gg(Par.cols),Par.gg(Par.cols)) = 0;
0091 arrays1 = Par.G(Par.cols+1);
0092 [a b]= find(arrays1 ==0); % in case 2 consecutives layers are fluid....
0093
```

3

```
0094 %BC8: vanishing of shear stress for f-s or f-p
0095 K(Par.gg(Par.cols(b)),:)     = SS(Par.ff(Par.cols(b)),:);
0096
0097        %%%%%%%%%%%%
0098        %solid/solid%
0099        %%%%%%%%%%%%
0100
0101 arrays2 = Par.TO(Par.cols+1);
0102 [c d]= find(arrays1 >0  & arrays2 == 0); % in case 2 consecutives layers are solid....
0103 %BC9:  continuity of radial displacement for f-f f-s or f-p
0104 K(Par.gg(Par.cols(d)),:)  = TT(Par.ff(Par.cols(d)),:)-TT(Par.hh(Par.cols(d)),:);
0105 %BC10:  continuity of radial stress for f-f f-s or f-p
0106 K(Par.hh(Par.cols(d)),:)  = SS(Par.ff(Par.cols(d)),:)-SS(Par.hh(Par.cols(d)),:);
0107 M(Par.hh(Par.cols(d)),Par.hh(Par.cols(d))) = 0;
0108
0109        %%%%%%%%%%%%%
0110        %solid/porous%
0111        %%%%%%%%%%%%%%
0112 [e f]= find(arrays2 > 0); % in case 2 consecutives layers are porous...
0113
0114 %BC11: continuity of radial displacement for f-p
0115 K(Par.ff(Par.cols(f)),:)         = TT(Par.cc(Par.cols(f)),:) - TT(Par.gg(Par.cols(f)),:) - TT(Par.nn(Par.cols(f)),:);
0116 M(Par.ff(Par.cols(f)),Par.ff(Par.cols(f))) = 0;
0117 %BC12: continuity of normal shear stress for f-p
0118 K(Par.gg(Par.cols(f)),:)         = SS(Par.ff(Par.cols(f)),:) - SS(Par.hh(Par.cols(f)),:);
0119 M(Par.gg(Par.cols(f)),Par.gg(Par.cols(f))) = 0;
0120 %BC13: continuity of axial displacement for f-p
0121 K(Par.hh(Par.cols(f)),:)         = TT(Par.ff(Par.cols(f)),:) - TT(Par.hh(Par.cols(f)),:);
0122 M(Par.hh(Par.cols(f)),Par.hh(Par.cols(f))) = 0;
0123 %BC14: vanishing of relativ displacement
0124 K(Par.nn(Par.cols(f)),:)         = TT(Par.nn(Par.cols(f)),:);
0125 M(Par.nn(Par.cols(f)),Par.nn(Par.cols(f))) = 0;
0126
0127
0128      %%%%%%%%%%%%%%%%%%%%%%%%%%%%%%%%%%%%%%%%%%%%%%%%%%%%%%%%%%
```

```
0129    %Boundary conditions for:                        %
0130    %first layer: porous next layer: fluid,solid or porous%
0131    %%%%%%%%%%%%%%%%%%%%%%%%%%%%%%%%%%%%%%%%%%%%%%%%%%%%%%%%%%
0132
0133 Par.colp = Par.colp(1:end-1);
0134 arrayp1 = Par.G(Par.colp+1);
0135 arrayp2 = Par.TO(Par.colp+1);
0136 [g h]= find(arrayp2 > 0); % in case 2 consecutives layers are porous....
0137        %%%%%%%%%%%%%%%%
0138        %porous/porous%
0139        %%%%%%%%%%%%%%%%
0140 %BC15: continuity of  radial stress
0141 K(Par.cc(Par.colp(h)),:) = SS(Par.cc(Par.colp(h)),:)-SS(Par.pp(Par.colp(h)),:);
0142 M(Par.cc(Par.colp(h)),Par.cc(Par.colp(h))) = 0;
0143 %BC16: continuity of  radial displacement
0144 K(Par.ff(Par.colp(h)),:) = TT(Par.cc(Par.colp(h)),:)- TT(Par.pp(Par.colp(h)),:);
0145 M(Par.ff(Par.colp(h)),Par.ff(Par.colp(h))) = 0;
0146 %BC17: continuity of  continuity of normal shear stress
0147 K(Par.mm(Par.colp(h)),:) = SS(Par.ff(Par.colp(h)),:)-SS(Par.q2(Par.colp(h)),:);
0148 M(Par.mm(Par.colp(h)),Par.mm(Par.colp(h))) = 0;
0149 %BC18: continuity of  continuity of axial displacement
0150 K(Par.pp(Par.colp(h)),:) = TT(Par.ff(Par.colp(h)),:)-TT(Par.q2(Par.colp(h)),:);
0151 M(Par.pp(Par.colp(h)),Par.pp(Par.colp(h))) = 0;
0152 %BC19: continuity of  fluid pressure
0153 K(Par.q2(Par.colp(h)),:) = SS(Par.mm(Par.colp(h)),:)-SS(Par.rr(Par.colp(h)),:);
0154 M(Par.q2(Par.colp(h)),Par.q2(Par.colp(h))) = 0;
0155 %BC20: continuity of  continuity ofrelative displacement
0156 K(Par.rr(Par.colp(h)),:) = TT(Par.mm(Par.colp(h)),:)-TT(Par.rr(Par.colp(h)),:);
0157 M(Par.rr(Par.colp(h)),Par.rr(Par.colp(h))) = 0;
0158
0159        %%%%%%%%%%%%%%%
0160        %porous/solid%
0161        %%%%%%%%%%%%%%%
0162
0163 [v b1]= find(arrayp1 > 0  & arrayp2 == 0); % in case 2 consecutives layers are solid....
```

```
0164 %BC21: continuity of  radial stress
0165 K(Par.cc(Par.colp(b1)),:)            = SS(Par.cc(Par.colp(b1)),:)-SS(Par.pp(Par.colp(b1)),:);
0166 M(Par.cc(Par.colp(b1)),Par.cc(Par.colp(b1))) = 0;
0167 %BC22: continuity of  radial displacement
0168 K(Par.ff(Par.colp(b1)),:)           = TT(Par.cc(Par.colp(b1)),:) + TT(Par.mm(Par.colp(b1)),:)- TT(Par.pp(Par.colp(b1)),:);
0169 M(Par.ff(Par.colp(b1)),Par.ff(Par.colp(b1))) = 0;
0170 %BC23: continuity of  continuity of normal shear stress
0171 K(Par.mm(Par.colp(b1)),:)           = SS(Par.ff(Par.colp(b1)),:)-SS(Par.q2(Par.colp(b1)),:);
0172 M(Par.mm(Par.colp(b1)),Par.mm(Par.colp(b1))) = 0;
0173 %BC24: continuity of  continuity of axial displacement
0174 K(Par.pp(Par.colp(b1)),:)        = TT(Par.ff(Par.colp(b1)),:)-TT(Par.q2(Par.colp(b1)),:);
0175 M(Par.pp(Par.colp(b1)),Par.pp(Par.colp(b1))) = 0;
0176 %BC25: vanishing of relative displacement
0177 K(Par.q2(Par.colp(b1)),:)  = TT(Par.mm(Par.colp(b1)),:);
0178 M(Par.q2(Par.colp(b1)),Par.q2(Par.colp(b1))) = 0;
0179
0180
0181         %%%%%%%%%%%%%%
0182         %porous/fluid%
0183         %%%%%%%%%%%%%%
0184 [d e]= find(arrayp1== 0 ); % in case 2 consecutives layers are fluid....
0185 %BC26: continuity of  radial stress
0186 K(Par.cc(Par.colp(e)),:)            = SS(Par.pp(Par.colp(e)),:)- SS(Par.cc(Par.colp(e)),:);
0187 M(Par.cc(Par.colp(e)),Par.cc(Par.colp(e)))      = 0;
0188 %BC27:continuity of  radial displacement
0189 K(Par.ff(Par.colp(e)),:)         = TT(Par.pp(Par.colp(e)),:)- TT(Par.cc(Par.colp(e)),:) - TT(Par.mm(Par.colp(e)),:) ;
0190 M(Par.ff(Par.colp(e)),Par.ff(Par.colp(e))) = 0;
0191 %BC28: vanishing of shear stress
0192 K(Par.mm(Par.colp(e)),:)         = SS(Par.ff(Par.colp(e)),:);
0193 M(Par.mm(Par.colp(e)),Par.mm(Par.colp(e))) = 0;
0194 %BC29: continuity of fluid pressure
0195 K(Par.pp(Par.colp(e)),:)       = SS(Par.pp(Par.colp(e)),:) + SS(Par.mm(Par.colp(e)),:);
0196 M(Par.pp(Par.colp(e)),Par.pp(Par.colp(e))) = 0;
0197
0198 %%%%%%%%%%%%%%%%%%%%%%%%%%%%
```

```matlab
0199 %Surface Boundary Conditions%
0200 %%%%%%%%%%%%%%%%%%%%%%%%%%%%%%
0201
0202
0203 M(Par.sbcc + Par.sbcb,Par.sbcc + Par.sbcb) = 0;
0204 M(Par.sbcc + Par.sbca,Par.sbcc + Par.sbca) = 0;
0205
0206 if Par.s > 0    %rigid surface
0207     K(Par.sbcc + Par.sbcb,:)  = TT(Par.sbcc + Par.sbcb,:);
0208     K(Par.sbcc + Par.sbca,:)  = TT(Par.sbcc + Par.sbca,:);
0209 else            %stress free surface
0210     K(Par.sbcc + Par.sbcb,:)   = SS(Par.sbcc + Par.sbcb,:);
0211     K(Par.sbcc + Par.sbca,:)   = SS(Par.sbcc + Par.sbca,:);
0212 end
0213
0214 if Velo.vps(length(Par.N))~=0;   %condition for poroelastic surface (either rigid or stress free)
0215     K(Par.sbcc+Par.sbcd,:)        = SS(Par.sbcc+Par.sbcd,:);
0216     M(Par.sbcc+Par.sbcd,Par.sbcc+Par.sbcd) = 0;
0217 end
```

displacement.m

Matlab, The Mathworks, Inc.

March 13, 2009

```matlab
0001 function [ModeSh] = displacement(Par,w,U,vel,SS,TT)
0002 % Name: displacement
0003
0004  %Purpose:
0005  % Computes the radial change of stress and displacement components
0006  % for a given frequency
0007  %
0008 %Outputs:
0009  % - ModeSh : contains the modeshapes for all modes of a
0010  % given frequency
0011
0012 %Author: Florian Karpfinger 03/09
0013
0014
0015 for jj=1:size(U,2)
0016     ModeSh.u(:,jj)=TT*U(:,jj);                 %Multiply the displacement coefficient with the Eigenvectors
0017     ModeSh.s(:,jj)=SS*U(:,jj);                 %Multiply the stress coefficient with the Eigenvectors
0018 end
0019 %DISPLACEMENT%%%%%
0020 ModeSh.u = reshape(ModeSh.u,size(ModeSh.u,1)/length(Par.N),size(ModeSh.u,2)*length(Par.N));
0021
0022 ModeSh.ur=[ModeSh.u(1:size(ModeSh.u,1)/3,:)];
0023 ModeSh.uz = [ModeSh.u(size(ModeSh.u,1)/3+1:2*size(ModeSh.u,1)/3,:)];
0024 ModeSh.wr = [ModeSh.u(2*size(ModeSh.u,1)/3+1:size(ModeSh.u,1),:)];
```

```matlab
%STRESSES%%%%%%%%%%
ModeSh.s = reshape(ModeSh.s,size(ModeSh.s,1)/length(Par.N),size(ModeSh.s,2)*length(Par.N));

ModeSh.srr =[ModeSh.s(1:size(ModeSh.s,1)/3,:)];
ModeSh.srz = [ModeSh.s(size(ModeSh.s,1)/3+1:2*size(ModeSh.s,1)/3,:)];
ModeSh.p = [ModeSh.s(2*size(ModeSh.s,1)/3+1:size(ModeSh.s,1),:)];

ModeSh.ur  = reshape(ModeSh.ur,[],length(vel));
ModeSh.uz  = reshape(ModeSh.uz,[],length(vel));
ModeSh.wr  = reshape(ModeSh.wr,[],length(vel));
ModeSh.srr = reshape(ModeSh.srr,[],length(vel));
ModeSh.srz = reshape(ModeSh.srz,[],length(vel));
ModeSh.p  = reshape(ModeSh.p,[],length(vel));

for jj=1:size(ModeSh.uz,2)
    ModeSh.uz(:,jj) = ModeSh.uz(:,jj)/(i*(w/vel(jj)));
    ModeSh.srz(:,jj) = ModeSh.srz(:,jj)/(i*(w/vel(jj)));
end


for m=1:size(ModeSh.uz,2)
    mur(m)=max((ModeSh.ur(:,m)));
    muz(m)=max((ModeSh.uz(:,m)));
    msz(m)=max((ModeSh.srz(:,m)));
    msr(m)=max((ModeSh.srr(:,m)))
end

for m=1:size(ModeSh.uz,2);
    ModeSh.ur(:,m)=ModeSh.ur(:,m)/mur(m);
    ModeSh.wr(:,m)=ModeSh.wr(:,m)/mur(m);
    ModeSh.uz(:,m)=ModeSh.uz(:,m)/muz(m);
    ModeSh.srr(:,m) = ModeSh.srr(:,m)./msr(m);
    ModeSh.srz(:,m) = ModeSh.srz(:,m)/msz(m);
    ModeSh.p(:,m)=ModeSh.p(:,m)/msr(m);
end
```

2

PlotDispersion.m

Matlab, The Mathworks, Inc.

February 26, 2009

```matlab
0001 function PlotDispersion(F,G,Par,ModeSh)
0002 %Name: PlotDispersion
0003 %
0004 %Purpose:
0005 %        Here the dispersion curves and the attenuation are plotted
0006 % Inputs:
0007 %        - F             : matrix with all the phasevelocities for all modes
0008 %                          and frequencies
0009 %        - G             : matrix with the attenuation for all modes
0010 %                          and frequencies
0011 %        -Par: Structure containing all parameters defining elastic and geometric
0012 %              parameters as well as all calculations independent of
0013 %              frequency
0014 % Author: Florian Karpfinger 01/09
0015
0016 w= Par.wmin:Par.wstep:Par.wmax;
0017
0018 % Plot dispersion in velocity [m/s]
0019 %  figure;
0020 for n = 1:size(F,1)
0021     plot((w/(2*pi))/1000,((F(n,:))),'*','color','magenta','markersize',15)
0022     hold on
0023 end
0024 grid on;
```

```matlab
0025 set(gca,'FontSize',18,'FontName','Times', 'FontWeight','Bold', 'FontAngle', 'normal');
0026 xlabel('Frequency [kHz]')
0027 ylabel('Velocity in [m/s]')
0028 set(gcf,'Color','white')
0029
0030 if Par.comp == 2
0031     mode_num=1;
0032     %PLOT DISPLACEMENT
0033     for kk = 1:mode_num;
0034         figure('Name','u_r displacement','NumberTitle','on');
0035         plot(Par(1).aa./0.1,abs(ModeSh.ur(:,kk))./max(abs(ModeSh.ur(:,kk))),'-','color','green','LineWidth',2)
0036         set(gca,'FontSize',18,'FontName','Times', 'FontWeight','Bold', 'FontAngle', 'normal');
0037         xlabel('r/a','FontSize',24);
0038         ylabel('Amp. u_r','FontSize',24);
0039         set(gcf,'Color','white');
0040         grid on
0041         figure('Name','u_z displacement','NumberTitle','on');
0042         plot(Par(1).aa./0.1,(ModeSh.ur(:,kk)).*(imag(ModeSh.uz(:,kk)./ModeSh.ur(:,kk))),'-','color','red','LineWidth',2)
0043         grid on;
0044         set(gca,'FontSize',18,'FontName','Times', 'FontWeight','Bold', 'FontAngle', 'normal');
0045         xlabel('r/a','FontSize',24);
0046         ylabel('Amp. u_z','FontSize',24);
0047         set(gcf,'Color','white');
0048         grid on;
0049     end
0050
0051     %PLOT STRESS COMPONENTS
0052
0053     for kk = 1:mode_num;
0054         figure('Name','radial stress','NumberTitle','on');
0055         plot(Par(1).aa./0.1,abs(ModeSh.srr(:,kk)),'-','color','green','LineWidth',2)
0056         set(gca,'FontSize',18,'FontName','Times', 'FontWeight','Bold', 'FontAngle', 'normal');
0057         xlabel('r/a','FontSize',24);
0058         ylabel('Amp. \sigma_{rr}','FontSize',24);
0059         set(gcf,'Color','white');
```

```matlab
0060        grid on
0061        figure('Name','shear stress','NumberTitle','on');
0062        plot(Par(1).aa./0.1,(ModeSh.srr(:,kk)).*(imag(ModeSh.srz(:,kk)./ModeSh.srr(:,kk))),'-','color','red','LineWidth',2)
0063        grid on;
0064        set(gca,'FontSize',18,'FontName','Times', 'FontWeight','Bold', 'FontAngle', 'normal');
0065        xlabel('r/a','FontSize',24);
0066        ylabel('Amp.  \sigma_{rz}','FontSize',24);
0067        set(gcf,'Color','white');
0068        grid on;
0069    end
0070
0071  end
0072
0073
```